Test Cell Design for the Development of a Hydrogen Internal Combustion Engine

Risk Mitigation of Hydrogen Leakages in a 20-feet Container

W. Frijters

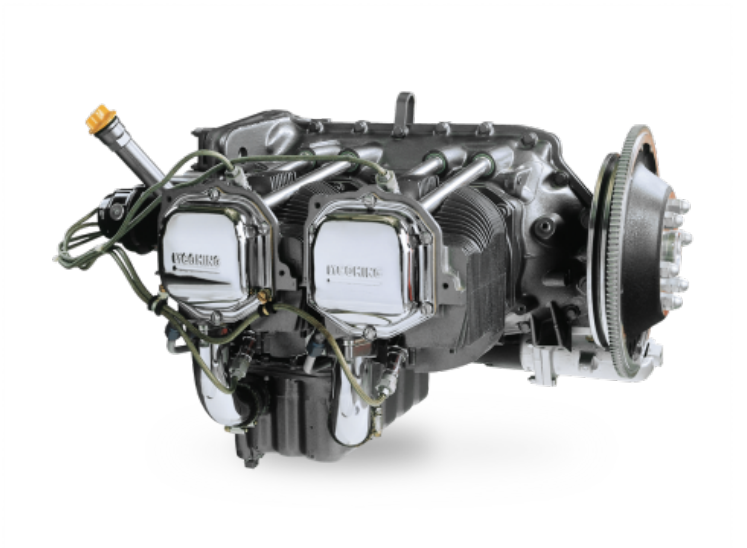

TU Delft Delft University of Technology

"All models are wrong, but some are useful."

$\sim$ *George E.P. Box*

[1]

[1]Cover page figure source: `https://www.lycoming.com/node/16868` [Retrieved 5.04.2020]

Test Cell Design for the Development of a Hydrogen Internal Combustion Engine

Risk Mitigation of Hydrogen Leakages in a 20-feet Container

Master Thesis

by

Wout Frijters

at the Delft University of Technology

Student number:	4481305	
Date:	May 26, 2021	
Supervisors:	Ir. J. A. Melkert	TU Delft
	Prof. dr. ir. L.L.M. Veldhuis	TU Delft
Advisor:	V. Klein	Deltion College

TU Delft

Preface

This MSc. thesis marks the end of a five and half year journey at the TU Delft. I want to extend my gratitude to my supervisors, family and close friends.

Thank you Joris, Leo and Victor for always being available. You were eager to teach me new material and to give more insight in the project. Having enthusiastic supervisors is something every student may only wish for.

I have to thank my family, Gudie, Annemie, Kaat, Tim and Miek for continuously supporting me throughout my study. Having a family to rely on and one which keeps encouraging you, eases the journey. I also want to thank the rest of my family, who I sadly enough due to the pandemic could not see much, for supporting me.

Finally, I have to thank my friends for making my time as a student enjoyable. Thank you Sven, Killian, Lina, Jeff, Edward, Bente, Bart, Maarten, Tuur, Jordi, Robin, Karl and Romuald for the great memories. A special thanks goes to my roommates who not only during this pandemic managed to continuously brighten my day but also provided me with valuable input for my master's thesis. Thank you Bram, Tine, Tim, Fréderic and Emiel.

Wout Frijters
Delft, May 2021

Abstract

Hydrogen is an energy carrier which may take part in reducing greenhouse gas emissions in aviation. A collaborative group comprising of the TU Delft, Deltion College and Dutch Electric Aviation Centre aim to develop a flying test bed for sustainable aviation.

The collaborative group has acquired a Cessna 337F Skymaster with the intent to replace one of the engines with a retrofit hydrogen internal combustion engine. An ancillary engine will serve as test unit prior to modifying one of the engines of the Cessna 337F Skymaster.

The project includes a logistical challenge since the three organisations are situated in different areas of the Netherlands. The solution is to build a portable test cell in a 20-feet container. Subsequently, a certification is required to be permitted to experiment with hydrogen.

Experimenting with hydrogen is heavily regulated as the element is characterised by a low minimum activation energy. Hydrogen may leak from a fuel pipe or through a fuel injector from the engine, consequently hydrogen may accumulate in the enclosed testing environment and a detonation occurs. One must further note aircraft piston engines are air-cooled and entail high thermal loads. A fan will push cold air over the engine to cool the cylinders, consequently the temperature in the 20-feet container will rapidly rise without adequate ventilation.

Furthermore, it must be noted the engine cylinders must be cooled from above. Therefore, hydrogen will be pushed downwards if a leak occurs near the engine. Hydrogen might accumulate in the test cell despite the container being well-ventilated. The accumulation of hydrogen imposes a large hazard and a solution requires to be sought. A CFD model is requested by hydrogen safety experts to simulate the flow field, heat balance and diffusion of hydrogen in the 20-feet container. The purpose of the CFD simulation is to minimise the risk of detonation and subsequently to obtain a certification.

CFD models of the test cell are simulated in ANSYS fluent. One may conclude that heat and hydrogen can be disposed of well, providing an optimal placement of the ventilation system and test cell elements. An essential observation is that the internal combustion engine must be compartmentalised from the remainder of the test set-up to prevent hydrogen flowing over electric wires and ignition surfaces.

Additional safety measures are discussed as well to further minimise the risk such as optimal placement of sensors and grounding of all the test cell elements.

Contents

List of Figures

List of Tables

Nomenclature

Acronyms

A/F	Air to fuel ratio
ANSYS	Analysis Systems
ATEX	Atmosphere Explosible
CAD	Computer-aided design
CFD	Computational fluid dynamics
DEAC	Dutch Electric Aviation Centre
DFI	Direct fuel injection
ECU	Electronic control unit
fmean	Mean mixture fraction
fvar	Mixture fraction variance
GHG	Greenhouse gas
H_2	Hydrogen
H_2O	Water vapour
HVAC	Heat, ventilation & air conditioning
ISA	International Standard Atmosphere
ISO	International Standardisation Organisation
LEL	Lower explosion limit
LFL	Lower flammability limit
LHV	Lower heating value
LNG	Liquid natural gas
LPG	Liquefied petroleum gas
NO_2	Nitrogen
NO_x	Nitrogen oxides
O_2	Oxygen
PFI	Port fuel injection
RON	Research octane number
rpm	Rotations per minute

TAS	True airspeed	

Greek Symbols

β	Fin parameter	–
χ	Fin parameter two	–
ΔT	Pseudo-time step	–
ϵ	Dissipation rate of turbulent kinetic energy	m^2/s^3
ϵ_{engine}	Emissivity coefficient of engine	–
η	Fin efficiency	–
γ	Heat capacity ratio	–
μ_t	Eddy viscosity	m^2/s
Ω_D	Diffusion collision integral	–
ρ(E)	Energy density	J/m^3
ρ(V)	Volumetric density	kg/m^3
σ_i	Characteristic length of species i	m
$\mathscr{P}$	Perimeter	m

Roman Symbols

$\dot{m}$	Mass flow rate	kg/s
$\mathcal{D}_{\text{ij}}$	Binary diffusion coefficient	m^2/s
$\vec{d}_{\text{i}}$	Diffusion vector for mechanical effects	m^2/s
$\vec{J}$	Diffusive mass flux vector	$kg \cdot m^2/s$
$\vec{V}_{\text{i}}$	Diffusion vector of species i	m^2/s
A	Cross-sectional area	m^2
bTDC	Before top-dead centre	circ
C_p	Specific heat capacity	$J/Kg \cdot K$
D	Diameter	m
D_i	Mass diffusion coefficient for species i	m^2/s
D_T	Thermal diffusion coefficient for species i	$m^2/s \cdot K$
e	Kinetic energy flux	W
E_a	Activation energy	J
f	Fin pitch	m
g	Gravitational acceleration	m/s^2
H	Height	m

h	Heat transfer coefficient	$W/m^2 \cdot K$
H_e	Net heat combustion	W
k	Turbulent kinetic energy	J/kg
$k_{aluminium}$	Thermal conductivity coefficient aluminium	$W/m \cdot K$
k_B	Boltzmann constant	$m^2 \cdot kg/s^2 \cdot K$
K_e	Kinetic energy	J
k_i	Arrhenius reaction rate	–
K_{safety}	Safety factor	–
L	Length	m
l_d	Domain length scale	m
l_v	Volumetric length scale	m
M_w	Molecular weight	kg/mol
P	Power	W
p	Pressure	Pa
Q	Volumetric mass flow rate	m^3/s
Q_r	Radiation heat transfer	W
R	Radius	m
$R_{specific}$	Specific gas constant	$J/Kg \cdot K$
S	Surface area	m^2
Sc_t	Effective turbulent Schmidt number	–
T	Temperature	K
t	Thickness	m
TL	Thermal load	W
u	Velocity	m/s
V	Volume	m^3
W	Width	m
X	Mole fraction	%
Y_i	Mass fraction for species i	%

Chapter 1

Introduction

Continuous advancements and innovation were linked to aviation mere decades ago. Contemporary developments are subtle and its benefits are limited in terms of fuel consumption efficiency. Khandelwal et al. (2013, pp.45) states "leading experts predict the industry to grow in the order of 5 % each year in the coming decades, even more so in the cargo transportation sector." Consequently, concerns are rising and the carbon emissions released by aircraft into the atmosphere must be reduced.

A collaborative research group, comprising of Deltion College, Dutch Electric Aviation Centre and the TU Delft acquired a Cessna 337F Skymaster with the intent to develop a flying test bed for sustainable aviation. One of the internal combustion engines will be modified into a retrofit hydrogen internal combustion engine. Chapter 2 presents the research aim and value of the project, along with recent developments in the hydrogen economy.

Chapter 3 summarises a preceding literature review, including a trade-off between various alternative sustainable fuels which may replace aviation gasoline in the near future. It is anticipated hydrogen combustion offers the most opportunities to accelerate the path towards sustainable aviation. Furthermore, it discusses the complications of modifying an engine into a retrofit hydrogen internal combustion engine.

A four cylinder spark-ignition engine (Lycoming IO-360-A1B6) will serve as test engine. The aim of this MSc. thesis is to design and analyse a test cell for the development of a hydrogen internal combustion engine. Chapter 4 presents a preliminary design of the test cell, which is optimised in the subsequent chapters.

Hydrogen is a volatile element which can leak, subsequently it may accumulate in the test cell and entail a detonation. Hydrogen safety experts request a CFD simulation of the test cell container to minimise the risk of a detonation. Chapter 5 discusses the case studies of the CFD analysis. It concludes the analysis requires two separate CFD models, one to model the diffusion of hydrogen and the other to model the heat balance in the test cell. Chapter 6 and Chapter 7 present empirical models and experimental values from literature to provide for an initial guess of the heat balance and diffusion of hydrogen in the test cell. Literature provides sufficient data for an initial test cell design while the function of the CFD analysis is to optimise the ventilation system set-up. Chapter 8 describes the CFD set-up and presents a few preliminary models based on data gathered in literature. Chapter 9 concludes the report with a proposal for the optimal ventilation set-up. In addition, it provides additional safety considerations to further reduce the risk of a detonation due to a hydrogen leak in the test cell.

Chapter 2

Research Aim Flying Test Bed

The research value and research objective of the flying test bed for sustainable aviation are presented in this chapter. In addition, a research question is posed at the end of the chapter. The aim of this dissertation is to solve this question and to provide useful recommendations to further aid in the challenging journey of developing a flying test bed for sustainable aviation.

2.1 Research value hydrogen engine

A plethora of alternative fuels have the potential to replace fossil fuels in the near future, with each fuel having its benefits and drawbacks. Hydrogen is an abundant element but is expensive to produce, electricity entails low carbon emissions[1] but is characterised by a lower energy density. Despite all the promising research papers demonstrating the potential of sustainable fuels, its application in aviation is limited. The lack of infrastructure and high development costs currently restrict companies to pursue shifting from conventional fossil fuels to alternative fuels.

Table 2.1 displays a trade-off between various alternative fuels. The trade-off clarifies why the collaborative group aims to developed a retrofit hydrogen internal combustion engine. The trade-off originates from a proceeding literature review where alcohols, liquid natural gas (LNG), hydrogen, methane, liquefied petroleum gas (LPG), aviation biofuel and electricity are weighed against each other (Frijters, 2020).

Hydrogen is the fuel of choice to pursue the project with as it scores the highest. Hydrogen has a wide field of application, e.g. chemical and automotive sector. The production costs are expected to decrease in the coming years as newer and cheaper production methods arise and the production volume increases (Canan and Ibrahim, 2019).

Hydrogen propulsion is gaining momentum as awareness of the climate impact of aviation is increasing. A multitude of hydrogen ventures are appearing, all hoping to discover a major breakthrough.

[1]The carbon offset of electricity largely depends on the production method. For example, electricity can be produced through renewable energy sources such as wind energy but as well through coal power plants (which is the dominant production method).

Table 2.1: Trade-off alternative fuels for aviation, with a maximum score of 100 Najjar (2013); Verhelst et al. (2009).

Fuel	ρ(E)[1]	ρ(V)[2]	GHG[3]	Cost	RON	Stock	Total
Weight	5	4	4	3	3	1	
Hydrogen	5	1	5	1	5	5	72
Methanol	2	3	3	4	4	4	62
Ethanol	3	3	3	4	4	4	67
LNG	3	4	3	4	4	3	70
Methane	3	3	3	4	4	3	66
LPG	3	3	3	5	4	4	70
Biofuel	3	4	5	2	3	(×)[4]	66[4]
Electricity	1	1	5	5	5[5]	5	64

[1]Energy density
[2]Volumetric density
[3]Greenhouse gas emissions offset
[4]Aviation biofuel is unfeasible due to limited supply.
[5]Electricity does not have a research octane number, a score of 5 is given as it is in reality infinite.

Profit margins in aviation are relatively low whilst the economical risk to pursue switching from aviation gasoline to hydrogen is high (Smitkova et al., 2011). Therefore, large companies such as Boeing and Airbus or research institutes such as DLR (Deutsches Zentrum für Luft- und Raumfahrt) create joint venture agreements to tackle the challenge together.

Two large undertakings are 'Clean Sky' and Fuel Cells & Hydrogen 2 Joint Undertakings (CleanSky, 2020). Both study the economic and climate impact of hydrogen propulsion and various other sustainable fuels. Clean Sky aims to assess all aspects of sustainable fuels in aviation, of which hydrogen is only a small part. Regarding hydrogen, both undertakings analyse which propulsion system is most suitable for each aircraft class (e.g. short-range, mid-range, long-range et cetera) on an economical basis and analyse the climate impact of each propulsion system by 2050. Therefore the joint ventures focus primarily on fuel cell-powered propulsion and hydrogen combustion through turbines.

Furthermore, some smaller ventures such as ZeroAvia manage to be successful as well. The company is founded in 2017 and strives for zero-emission flight. Smaller ventures usually focus on a niche market as they do not have the same resources as larger ventures. However, the company is gaining traction and recently (December 2020) managed to secure $21.4 million through investors. The company hopes to achieve commercial flight through hydrogen fuel-cell powered flight[2].

[2]`https://www.zeroavia.com/` [Retrieved 21.08.2020]

Fuel-cell propulsion and hydrogen combustion in gas turbines entail the highest potential and future profit, therefore most research revolves around the former two propulsion systems rather than piston aircraft engines. Research on which strategy is most effective to transition from conventional fuels to alternative sustainable fuels is limited.

Therefore, the Dutch Electric Aviation Centre (DEAC), Deltion College and TU Delft set up a collaboration group with the intent to review sustainable alternative fuels and explore the possibilities of modifying an aviation gasoline internal combustion engine. The modified engine will be mounted onto the Cessna 337F Skymaster (depicted in Figure 2.1[3]), and shall serve as a flying test bed for sustainable aviation.

Figure 2.1: The Cessna 337F Skymaster which shall become a flying test bed for sustainable aviation.

The development of dual-fuel system is not discarded yet since the differences in Table 2.1 are small [4]. Nonetheless, the primary goal remains to modify the engine into a hydrogen internal combustion engine.

The purpose of designing a retrofit hydrogen powered internal combustion engine is for it to serve as a stepping stone towards a more sustainable aviation. Hydrogen combustion is not considered to be the solution itself since it is still paired with emissions such as

[3] `https://duurzaam-vliegen.nl/project-3/`[Retrieved 21.08.2020]

[4] It is possible that during the development of the project, problems arise which were unforeseen. If such an event occurs, the trade-off might have to be reconsidered and an alternative fuel might replace hydrogen or can be added to the system. In addition, multiple alternative sustainable fuels may be tested.

water vapour and nitrogen oxides. In addition, it contributes to the release of carbon emissions into the atmosphere, depending on the production method (Haglind and Singh, 2006).

A retrofit hydrogen internal combustion engine includes an additional benefit besides the reduced carbon emissions and potential economical benefit in comparison to an aviation gasoline internal combustion engine. Fuel cells use hydrogen as energy carrier as well, which are proving to be energy efficient whilst carbon emissions are minimal. Fuel cells achieve efficiencies of up to 60 %, internal combustion engines attain an efficiency of 30 % (White et al., 2006). However, fuel cells only generate electricity reliably with nearly pure hydrogen. Currently, it is extremely expensive to produce hydrogen with a low concentration of impurities.

The engine is to serve as a momentum tool, set an example for engine manufacturers and airlines, such that they are willing to make the same step and accelerate the transition from conventional fossil fuels to alternative sustainable fuels such as hydrogen.

The benefits of a hydrogen internal combustion engine are limited whilst fuel cells have a far greater potential. However, it is a financial risk for airlines and manufactures to switch from aviation gasoline or kerosene engines to fuel cells with hydrogen as energy carrier. Contemporary aircraft would require an entire overhaul as the propulsion system is vastly different. Retrofit hydrogen internal combustion engines are a convenient transitional propulsion system. Therefore, the collaborative group has decided to modify a hydrogen internal combustion engine despite fuel cells being considered as the superior technology of the future.

To shortly recap, the aim of the collaborative group is to,

- research whether a hydrogen retrofit model of the internal combustion engine has economical benefits and whether there is a market in aviation for retrofit internal combustion engines operating on alternative fuels;
- further research the combustion process of hydrogen and emission characteristics.

A retrofit hydrogen internal combustion engine has the following benefits,

- no carbon[5] is released into the atmosphere;
- directly transitioning to fuel cell propulsion is expensive, the retrofit internal combustion engine is an effective transitional propulsion system;
- a retrofit hydrogen internal combustion engine is to serve as a momentum tool to accelerate the path towards a hydrogen economy.

[5]Except for a small amount with is generated by lubricating oil reacting with hydrogen in the crankcase

2.2 Research objective

The collaborative research group has acquired a Cessna 337F Skymaster with the intent to transform one of the internal combustion engines. The aircraft is equipped with two aviation gasoline infernal combustion engines, one of which will be replaced by the retrofit hydrogen internal combustion engine.

Accordingly, the objective of the research project is defined as follows,

> *"Develop a hydrogen propulsion system by means of modifying one of the current internal combustion engines and designing a new fuel storage system, being part of a collaborative research project between the TU Delft, DEAC and Deltion college, to convert a Cessna 337F Skymaster into a flying test bed for sustainable aviation."*

Building an effective test cell environment is an essential step prior to experimenting with the internal combustion engine. A second step is to map the consequences of switching from aviation gasoline to hydrogen to study the differences of the combustion process. Thereby a combustion model requires to be set up. The former is the objective of this MSc. thesis while the latter challenge will be tackled by another graduate student.

2.3 Work breakdown structure project

Figure 2.2 depicts the top-level work breakdown structure of a flying test bed for sustainable aviation. The project consists of two large branches, the experiment branch and test cell environment branch, which are further divided into separate groups.

2.3.1 Experiment phase

Experimenting entails researching the most optimal engine configuration and researching the combustion properties of a hydrogen internal combustion engine.

Modifying the internal combustion engine

A hydrogen internal combustion engine has to be developed prior to performing tests with the flying test bed as mentioned previously in Chapter 3. Modifications include changing the fuel mixture mechanism, the injection mechanism and the ignition mechanism (Frijters, 2020). In addition, a fuel storage system requires to be developed to be able to store hydrogen in the aircraft. These modifications will be performed on the ancillary engines. In parallel, researchers will analyse the combustion properties of hydrogen. One of the aims of the research branch is to identify the inefficiencies and further optimise the modifications.

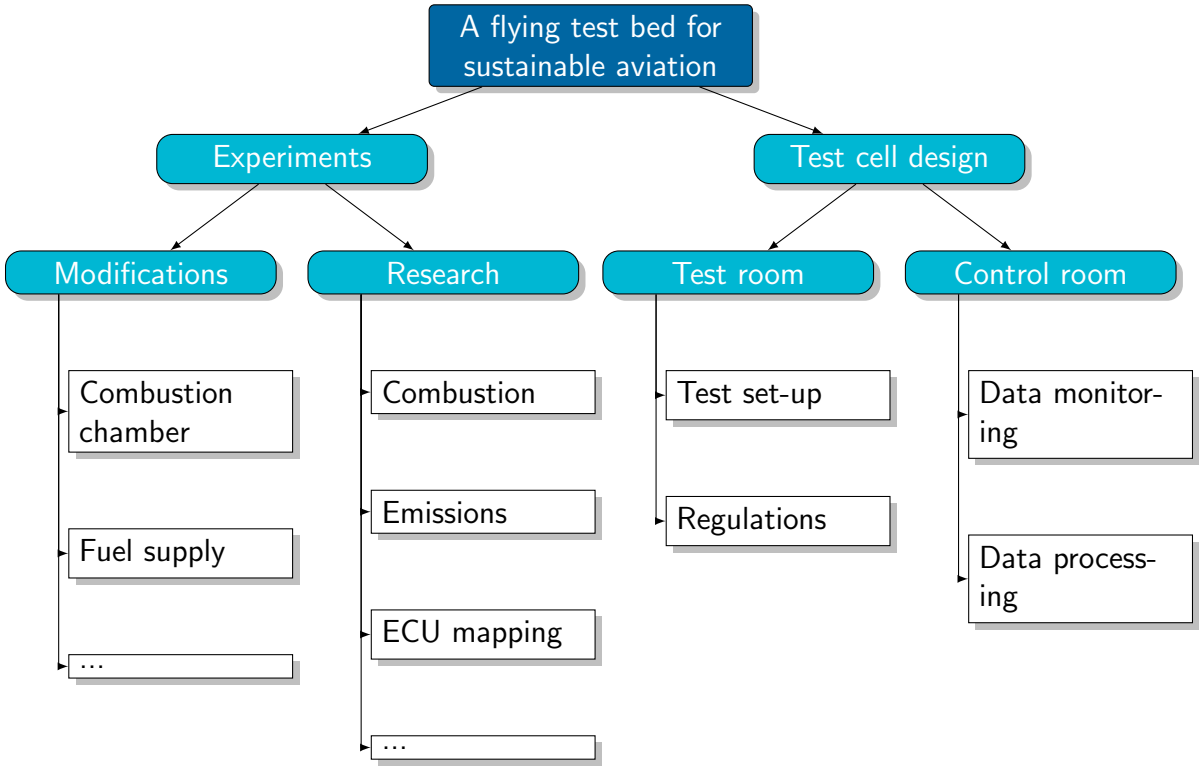

Figure 2.2: Top-level work breakdown structure of a flying test bed for sustainable aviation.

Researching test cell design & hydrogen combustion

The aim is to examine the combustion process of hydrogen, analyse the exhaust gases and map the performance of the engine. Both ground tests and flight tests will be performed, with the purpose to answer the research objective question stated in Chapter 3. The anticipated outcome is for the results of the testing phase to show that an aircraft powered by a retrofit hydrogen internal combustion engine can operate along contemporary aircraft in aviation, without imposing a decline in performance, safety and increasing costs.

2.3.2 Test cell design

The test cell environment includes two 20-feet containers, one houses the test cell room and another the control room. The test set-up is situated in the test cell container whilst the control room houses the data monitoring equipment and control panel. The control room and test cell room are situated in a separate container for safety considerations. The reasoning is further elaborated upon in Chapter 4.

Test room design

The test room branch refers to the test set-up, hence the hardware necessary to perform successful experiments, and the surrounding testing room itself. The test cell has to comply to a myriad of regulations to establish a safe testing environment. For example, the test cell may not be a nuisance to its environment. Furthermore, a heat, ventilation & air conditioning (HVAC) system has to be developed to maintain a reasonable temperature within the test cell and to provide for consistent test conditions in the test cell.

Control room design

The control room refers to the data monitoring, data processing and control panel. Data will be analysed in the test room at a safe distance from the test cell. In addition, the engine will be actively controlled in the control room by setting the throttle position and fuel flow.

2.3.3 Summary of the project plan

To summarise the project plan,

- the test cell environment comprises of two separate 20-feet containers, one houses the test cell and the other the control room;
- experimenting with hydrogen is heavily regulated, the test cell must comply to noise regulations, hydrogen leak procedures et cetera;
- the objective of this MSc. thesis is to design a suitable test cell environment for the development of a retrofit hydrogen internal combustion engine.

2.4 Dissertation research question

The purpose of this report is to develop a test cell design in which the risk of a detonation due to a hydrogen leak is minimal. Therefore, this report does not further discuss the experimental branch in depth, aside a preceding literature review. The findings of the literature are summarised in Chapter 3. The reader is recommended to consult the literature review report as well (Frijters, 2020) as it provides a deeper understanding of the challenges concerning the project.

The dissertation's research question is as follows,

> *"Which test cell design in a 20-feet container minimises the risk of experimenting with hydrogen combustion for the development of a hydrogen internal combustion engine?"*

The research question is further divided into sub-questions,

- Which equipment is required to convert an aviation gasoline internal combustion engine into a hydrogen internal combustion engine?
- How much cooling requires the engine in the test cell?
- What is the energy balance in the test cell environment?
- What are the consequences of a hydrogen leak in the test cell?

The literature review is summarised in the following chapter. Chapter 3 describes the characteristics of hydrogen combustion and the key challenges of the project.

Chapter 3

Path to Hydrogen Combustion

This chapter briefly discusses the subject of hydrogen combustion. Furthermore, it elaborates upon the key challenges of developing a hydrogen economy and designing a retrofit hydrogen internal combustion engine.

3.1 Key challenges hydrogen economy

Despite the first hydrogen engine concept being proposed by Swiss engineer, Francois Isaac de Rivaz in the early 19^{th} century (Das, 1990), the technology is still not in wide use today. Some major challenges have to be tackled prior to shifting to a hydrogen economy. The major issues relate to infrastructure, production, storage and public perception.

The first relates to the fact that hydrogen is an energy carrier and not an energy source. It means the element is not a natural resource, which entails high production costs. The main production method of hydrogen is steam methane reforming (96%). Clean alternative production methods such as water splitting are currently far too expensive to compete with steam reforming of CH_4 (Smitkova et al., 2011).

Furthermore, a hydrogen economy also requires its own infrastructure, which is currently still in its infancy. Either already existing pipelines would need to be repurposed, such as pipes transporting natural gas or a new infrastructure has to be built. The former is time- and cost-efficient but this option is not applicable at every location. Consequently, transforming the infrastructure will take time.

The third is perhaps the most well-known issue related to hydrogen. Although hydrogen has a high energy density, it does not have a favourable volume density. Hydrogen in gaseous (uncompressed) state occupies a volume 9000 times as large as that of aviation gasoline for the same mass (Nojoumi et al., 2009).

At last, the Hindenburg catastrophe in 1937 is the main cause of the the last key challenge. Although many people survived this accident, it still lives in the human memory because it was one of the first aviation accidents recorded on camera. Hydrogen is a volatile element and is characterised by a low minimum activation energy. Consequently, hydrogen is susceptible to ignition when it comes into contact with a high temperature surface. Hydrogen is not necessarily more dangerous to experiment with however. Unlike as with a gasoline leak, where fuel resides in the environment and remains a risk until it is removed, hydrogen diffuses upwards and escapes into the environment.

It is not a small step to transition from fossil fuels to hydrogen. Hydrogen requires time to become a fully green and cost-competitive product. Contemporary key challenges are slowly being resolved. In the latest years, research into hydrogen as the zero-emission fuel of the future has been receiving increasing traction. The production of green hydrogen is rapidly increasing and the public perception is slowly changing as hydrogen is becoming more common due to an increasing use in the automotive industry. Therefore developing a retrofit hydrogen internal combustion engine (H_2ICE) by modifying an internal combustion engine, with the purpose of fabricating a cost-competitive and green alternative product, is an ambitious but realisable objective.

3.2 Hydrogen combustion fundamentals

Hydrogen is an inexhaustible and green energy carrier. This section elaborates upon the characteristics, combustion process and hazards of hydrogen.

3.2.1 Hydrogen combustion reaction mechanism

Equation 3.1 shows the combustion reaction of hydrogen in an internal combustion engine,

$$\begin{gathered} \phi \mathrm{H_2} + \frac{1}{2}\mathrm{O_2} + \frac{1}{2}\left(\frac{79}{21}\right)\mathrm{N_2} \Rightarrow \\ \mathrm{wH_2} + (\phi - \mathrm{w})\mathrm{H_2O} + \mathrm{yN_2} + \mathrm{zNO}_x + (1 - \phi - \mathrm{z})\left(\frac{1}{2}\right)\mathrm{O_2} + \text{Byproducts.} \end{gathered} \tag{3.1}$$

The exhaust gases comprise of nitrogen oxides, water vapour, nitrogen, oxygen, unburned hydrogen gas and a small amount of various byproducts such as carbon dioxide (hydrogen might leak through the liner into the crankcase and react with oil). Ergo, nitrogen oxides and water vapour are the only pollutants emitted with hydrogen combustion. While the negative impact of nitrogen oxides is relatively well known, the effect of water vapour is not. Water vapour is a greenhouse gas as a consequence of the formation of contrails, which traps heat in the Earth's atmosphere (Brand et al., July 2003). However, its effect is difficult to document as water vapour has a relatively short dwell time (six to twelve months). In addition, its effect is contingent upon the altitude and the particle size of water vapour.

Nonetheless, initially the effect of substituting aviation gasoline by hydrogen has to be researched. It is apparent that switching fuel affects the optimal injection timing, fuel mixture strategy, spark timing et cetera. Subsequently, the characteristics of hydrogen combustion have to be well understood.

3.2.2 Hydrogen combustion characteristics

Table 3.1 displays the characteristics of hydrogen combustion in comparison with conventional fossil fuels. Hydrogen features a high energy density, low volume density, high RON (research octane number) and high explosion range. A high explosion range has its benefits and drawbacks. An advantage is that an engine has the ability to operate lean with hydrogen, thereby operating at relatively low temperatures and emitting less pollutants into the atmosphere. On the other hand, there is a higher risk of deflagration and detonation in confined rooms if not accounting for potential hydrogen leakages. In addition, the probability of premature ignition increases if hydrogen leaks into the combustion chamber prior to spark ignition.

Furthermore, hydrogen entails a rapid and explosive combustion process due to its high flame velocity, low quenching distance and short ignition delay. The following section will briefly elaborate upon the significance of these characteristics.

Table 3.1: Fuel properties of hydrogen and conventional fuels (Najjar, 2013; Verhelst et al., 2009).

Fuel	**LHV**[1] **(MJ/kg)**	**RON**	**LEL**[2] **(Vol. %)**	**Ad.**[3] **Flame temp. (K)**	**MIE**[4] **(mJ)**	$\mathbf{T}_{ig}^{5}$ **(K)**
Gasoline	44.5	90	1.3-7.1	2,411	0.29	633
Diesel	42.5	-[6]	0.6-5.5	2,600	0.16	478
Avgas	43.5	98	0.6-5	2,366	0.2	493
Hydrogen	119.9	$\geq$ 130	4-75.0	2,527	0.017	733

[1]Lower heating value (MJ/kg).
[2]Explosion range in gaseous state (volume percentage) .
[3]Adiabatic flame temperature (K).
[4]Minimum ignition energy (mJ).
[5]Auto ignition temperature (K).
[6]Diesel does not have a research octane number.

3.3 Complications of testing with hydrogen

The item list below describes only a few phenomenon to illustrate the complications that come with hydrogen combustion as the focus of this MSc. thesis is on designing the test cell. The preceding literature study can be consulted (Frijters, 2020) for a more thorough analysis.

The main complications of designing and testing a retrofit hydrogen internal combustion engine are regarding;

- Abnormal combustion phenomena
- Leakages
- Volumetric efficiency
- Engine cooling
- Fuel mixture mechanism
- Injection mechanism
- Ignition mechanism

The remainder of this section includes a short summary of each complication mentioned above.

3.3.1 Abnormal combustion phenomena

Abnormal combustion phenomena (backfire, pre-ignition and engine knock) limit the operating envelope of an engine, therefore it is important to document these phenomena. Engine knock should in theory not be an issue during testing as hydrogen has a research octane number of 130 (Lino Guzzella, 2010). However, hydrogen is a unique fuel as it is the lightest element and is very volatile. Hydrogen easily leaks through a conventional fuel injector and therefore can invoke pre-ignition. In addition, a hydrogen-air mixture easily ignites when it comes into contact with a hotspot[1], as the explosion range of hydrogen is very wide and the minimum activation energy is low. Furthermore, hydrogen is very susceptible to backfire[2] due to a combination of a low ignition delay and high flame velocity.

3.3.2 Volumetric efficiency with hydrogen combustion

A second difference relates to the volumetric efficiency. The volume ratio of air to fuel defines the volumetric efficiency inside the combustion chamber. The volumetric efficiency of gaseous hydrogen is lower than aviation gasoline as its volumetric density is lower. In a stoichiometric aviation gasoline-air mixture, aviation gasoline occupies approximately 2 % of the combustion chamber volume whilst air occupies the remaining 98 %. Hydrogen occupies 30 % in a stoichiometric hydrogen-air mixture, meaning air occupies only 70 % of the combustion chamber volume (Das, 1990). Not accounting for this phenomenon in the engine design yields a decrease in engine power of 30 up to 60 % depending on the load condition (White et al., 2006).

[1] Hottest parts inside the combustion chamber.
[2] Depending on the mixture formation mechanism.

3.3.3 Effect of hydrogen combustion on engine cooling

Aircraft internal combustion engines reach high temperatures due to the high flame temperatures inside the combustion chamber. Cooling prevents the engine from overheating and provides the means for the engine to operate at higher compression ratios, and thus a higher efficiency.

Adiabatic flame temperatures of conventional fuels and hydrogen are presented in Table 3.1. Hydrogen has an adiabatic flame temperature of 2,527 K while gasoline has an adiabatic flame temperature of 2,411 K (Verhelst et al., 2009) for a stoichiometric mixture. The cylinder walls should in theory attain higher temperatures with hydrogen combustion.

In addition, the flame quenching distance of hydrogen is lower than that of aviation gasoline. Ergo, an additional amount of heat is transferred to the combustion walls through convection as hydrogen flames can continue to burn in closer proximity to the wall (Verhelst et al., 2009).

However, the engine is built to operate within a specified temperature range, running too cold or too hot will accelerate the wear of the engine. Combustion with hydrogen allows for a leaner mixture than with aviation gasoline for the same power output at cruise performance (Verhelst et al., 2009). Therefore, the engine should operate at leaner conditions once it operates with hydrogen. Subsequently, the temperature in the combustion chamber will naturally decrease and therefore the engine requires less cooling with hydrogen combustion. Engine cooling will be critical to monitor to ensure the prevention of engine wear during experiments.

Aircraft internal combustion engines are primarily cooled through air, the cold atmospheric air cools the engine during cruise. Fans have to push cold air over the engine cylinders in a test cell. In addition, ventilation fans must dispose of the excess hot air. Results of experiments might widely vary despite constant input values without precise control of the temperature conditions. In addition, high temperatures within the test cell are dangerous, especially with hydrogen as it has a low minimum activation energy. Poor ventilation possibly entails a detonation or deflagration in case of a hydrogen leak Wallner T. (2009). Hence, hydrogen safety experts from Inerc BV Hydrogen Safety[3] suggest to set up a computational fluid dynamics (CFD) model to analyse the energy balance and flows within the test cell. Setting up a CFD model is one of the requirements to obtain a permit to be allowed to experiment with hydrogen (Wallner T., 2009). An energy balance is useful to predict the engine temperature and average temperature in the test cell. A model will predict the flows and the diffusion of hydrogen in the test cell in case of a leak. The purpose of the CFD model is to ensure safety and the prevention of deflagration and detonation by means of determining the most optimal set-up of the ventilation system and test set-up.

[3] `https://inerc.nl/` [Retrieved 10.03.2020]

3.3.4 Initial engine modifications

As some of the complications of converting an aviation gasoline internal combustion engine into a hydrogen-powered internal combustion engine are described above, it becomes apparent a multitude of design changes are required.

Modifications will be performed on ancillary engines prior to modifying one of the engines of the Cessna 337F Skymaster. The Lycoming IO-360-1AB6 engine, a four-cylinder spark-ignition engine with a port fuel injection mechanism, will serve as test engine. Table 3.2 summarises the specifications of the Lycoming engine, Figure 3.1 displays the Lycoming engine[4].

Table 3.2: Specifications of the Lycoming IO-360-A1B6 at maximum power rating.

Specification	**Value**	**Units**
Rated power	149.13	kW
Rated speed	2,700	rpm
Bore	130.18	mm
Stroke	111.13	mm
Displacement	5.92	L
Compression ratio	8.70	-
Firing order	1-3-2-4	-
Spark occurs	25	° bTDC

Figure 3.1: The Lycoming IO-360-A1B6 will serve as ancillary engine and will be modified into a hydrogen internal combustion engine.

[4] `https://www.lycoming.com/node/16868`[Retrieved 5.04.2020]

In addition, a six-cylinder spark-ignition engine mounted with a carburettor is currently being repaired such that it can serve as test engine as well.

The literature study (Frijters, 2020) describes the following modifications to convert an aviation gasoline engine into a hydrogen engine.

A necessary modification is the replacement of the fuel mixture mechanism. A carburettor is not the most suitable mixture formation mechanism with hydrogen combustion as the volumetric efficiency is low. The low density of hydrogen entails less room for air to enter the combustion chamber. Consequently the maximum power output decreases, therefore an injection mechanism will be utilised. A large part of the mixture forms inside the combustion chamber with port fuel injection and direct injection, which partially mitigates the volume efficiency losses. Both mechanisms will be experimented with in attempt to increase the power density and efficiency of the hydrogen propulsion system.

Evidently, the optimal injection timing and pressure will have to be researched for optimal combustion. In addition, a hydrogen leak is imminent in a conventional injection mechanism. Hydrogen tends to leak through very small gaps as the element is volatile and light (Sopena et al., 2010). Hydrogen leaks into the combustion chamber prior to ignition if the current injection mechanism is not replaced, potentially inciting premature ignition. Pre-ignition is an unwanted abnormal combustion phenomena in internal combustion engines which has to be avoided. Therefore, a fuel injection mechanism specifically built to operate with hydrogen has to replace the current mechanism.

Yet, hydrogen is so light and volatile that even with a suitable injection mechanism, it might still leak due to engine vibrations. Therefore the injectors must be firmly fixed to the manifold by means of a support (Sopena et al., 2010).

The last predetermined planned modification is regarding the ignition mechanism. It is possible a glow plug or weaker spark is sufficient to ignite the flame since the minimum activation energy of hydrogen is lower than aviation gasoline.

Furthermore, no platinum is allowed in the mechanism as it acts as a catalyst. Platinum provokes an unwanted reaction between hydrogen and air, which results in pre-ignition.

Subsequent modifications are not planned yet. Further research and testing will indicate which design changes must be included.

3.4 Hazards of testing with hydrogen

The hazards associated with experimenting with hydrogen must be documented and minimised prior to implementation of the design changes.

Hydrogen is often stored as a liquid, a gas or as a liquid-gas mixture. Preserving hydrogen in gaseous state under high pressure is most efficient for smaller aircraft such as the Cessna 337F Skymaster. Storing hydrogen in liquid state requires heavier vessels. Liquid storage is often the preferred storage method for larger aircraft as the weight of

the tanks becomes less of an issue (Airbus Deutschland, 2003).

Experimenting with hydrogen entails hazards regardless of the storage method. Hydrogen has the stigma of being extremely volatile and dangerous to experiment with since the Hindenburg disaster in 1937. The crash is assumed to be caused by an electric spark reacting with leaked hydrogen. When the Hindenburg attempted to ground the craft, the airship was cruising through an electric charged atmosphere. Upon the anchor touching the ground, a difference in electric potential caused an electric discharge and thus a spark. The spark ignited the hydrogen-air mixture, causing the airship to crash. Hydrogen should be as safe to operate with as aviation gasoline with the appropriate safety measures (Najjar, 2013). It is lighter than air and therefore naturally escapes into the atmosphere. Aviation gasoline remains near the leakage area as it is heavier than air. Nonetheless, precautions have to be taken to ensure safety near the testing environment. Many guidelines have been set up regarding the use of hydrogen by the European Commission since the Hindenburg disaster in 1937 (Dagdougui et al., 2018).

The institutions who harmonise the rules such as the International Standardisation Organisation (ISO) define furthermore guidelines which will not all be described in this report. Safety precautions include (Najjar, 2013; Dagdougui et al., 2018),

- Fire extinguishing system
- Sensors
- Visual monitoring
- Ventilation
- Sealing off heat sources
- Protective gear
- Cleaning
- Human error mitigation
- Over pressurisation
- Fuel storage

Two examples of how risk in the test cell is kept at a minimum are described below. Safety in the test cell is further elaborated upon in Chapter 4.

3.4.1 Function of sensors in test cell

Hydrogen is invisible to the naked eye and is odourless. Therefore, sensors have to be installed at strategic positions in the test cell. One of the aims of the CFD model is to analyse the diffusion of hydrogen in case of a leak as previously mentioned. Sensors measure the hydrogen volume concentration in a local region of the test cell.

3.4.2 Hazard of heat sources in test cell

Various heat sources are present in the test cell room such as lighting, ventilation fans, a dynamometer et cetera. Hydrogen may come into contact with a warm surface when it is roaming through the test cell room due to a leak in the fuel pipe or fuel tank. The heat sources and ventilation fans have to be strategically positioned in the test cell to minimise the risk of ignition as hydrogen has a low minimum activation energy.

Chapter 4

Preliminary Design Test Cell Environment

The test cell environment must be developed and illustrated prior to assessing the energy balance, engine cooling and diffusion of hydrogen. This chapter displays the schematics of the test cell set-up and test cell environment.

4.1 Schematic of test set-up

The aim is to design a test cell for the development of a hydrogen internal combustion engine by means of optimising the fuel injection, spark-ignition mechanism and modifying the combustion chamber. A safe test cell environment needs to be constructed prior to experimenting.

The first phase is the construction of the test set-up. The aim is to answer the first research question: 'Which equipment is required to convert an aviation gasoline internal combustion engine into a hydrogen internal combustion engine?'. This includes determining all the individual components necessary to be able to perform experiments. In addition, a preliminary model of the test cell will be developed to visualise the construction.

Further research sub-questions such as determining the flows, energy balance and diffusion of hydrogen inside the test cell environment are contingent upon the first phase and are elaborated upon in the following chapters. Note building the test set-up and test cell environment is planned for a later stage as the set-up will likely require iterations as it is in turn contingent upon the hydrogen diffusion and energy balance analysis in the test cell. For instance, additional safety measures might be required to keep the detonation and deflagration risk minimal. Ergo, the schematics presented in this chapter are not finalised versions. The schematics are included as a means to provide the reader with an initial glimpse of the test cell set-up.

The proposition is to build a test cell environment with two separate 20-feet containers. The 20-feet containers are selected as they are easily transported from one location in the Netherlands to another. Experimenting in a small container entails implications but the test cell must be portable to be able to test at either the TU Delft, DEAC or Deltion

College.

One container houses the test set-up, a second container houses the control room. The control room and test cell room must be housed in two separate containers according to the safety guidelines set by the European Union (Dagdougui et al., 2018). Operatives may not be in close proximity of set-ups conducting tests with hydrogen as detonations are lethal. The walls of the containers are not capable of containing the released energy. The container may be annihilated, building a wall within a test container to separate the test cell room and control room does not provide sufficient protection.

A schematic of the test set-up is illustrated below in Figure 4.1.

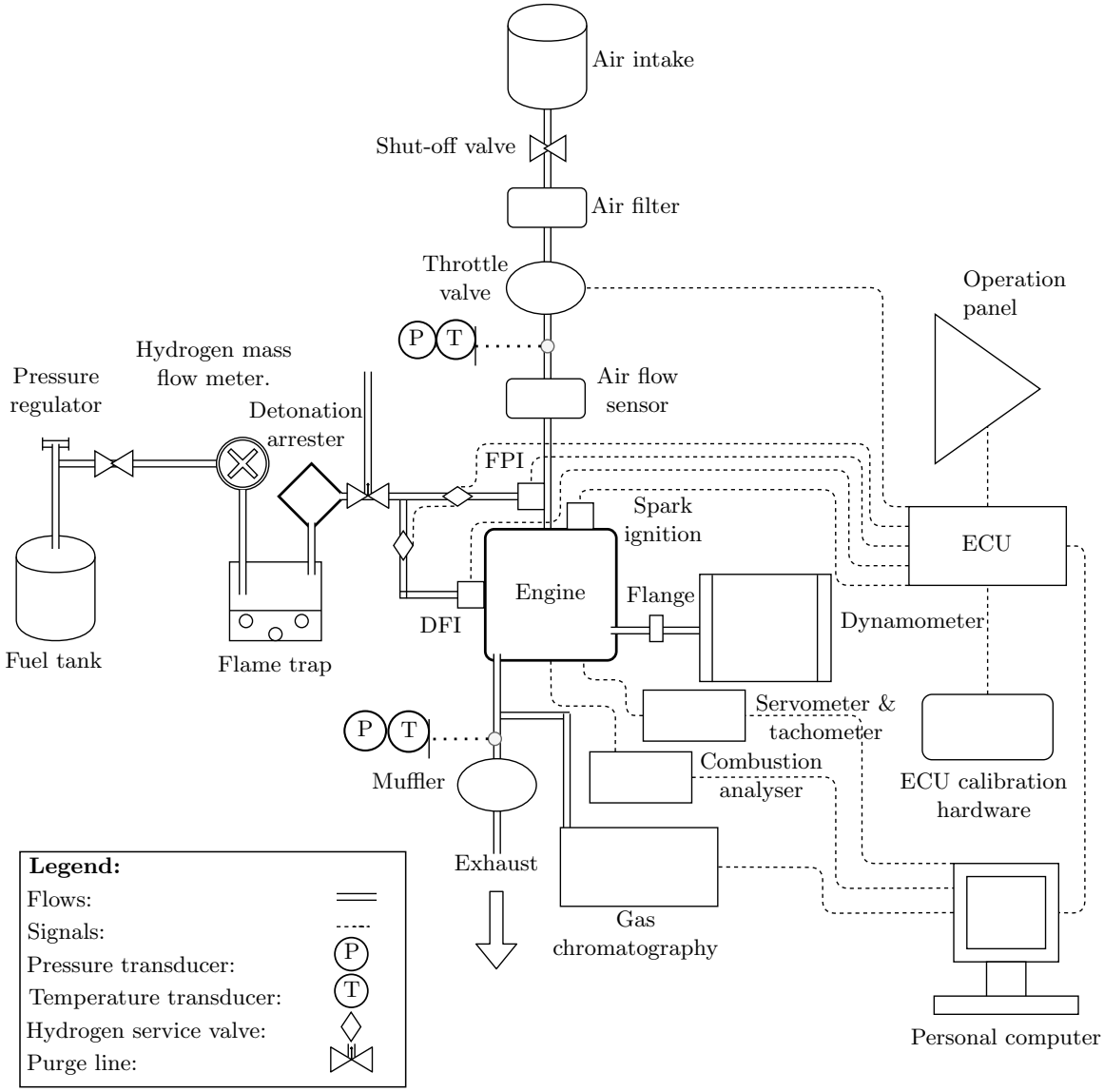

Figure 4.1: Schematic of the preliminary design of the test set-up. Minor alterations are expected at a further stage of the project.

Information is gathered by visiting test cell set-ups in ROC Amsterdam and through literature (Wallner T., 2009; Verhelst et al., 2009). The following sections present a preliminary schematic of the test cell and control room.

The figure is divided into four parts since Figure 4.1 contains much information. Figure 4.2, Figure 4.3, Figure 4.4 and Figure 4.5 each depict a part of the test cell set-up. In the bottom left of each figure a legend is displayed to aid with reading the figure.

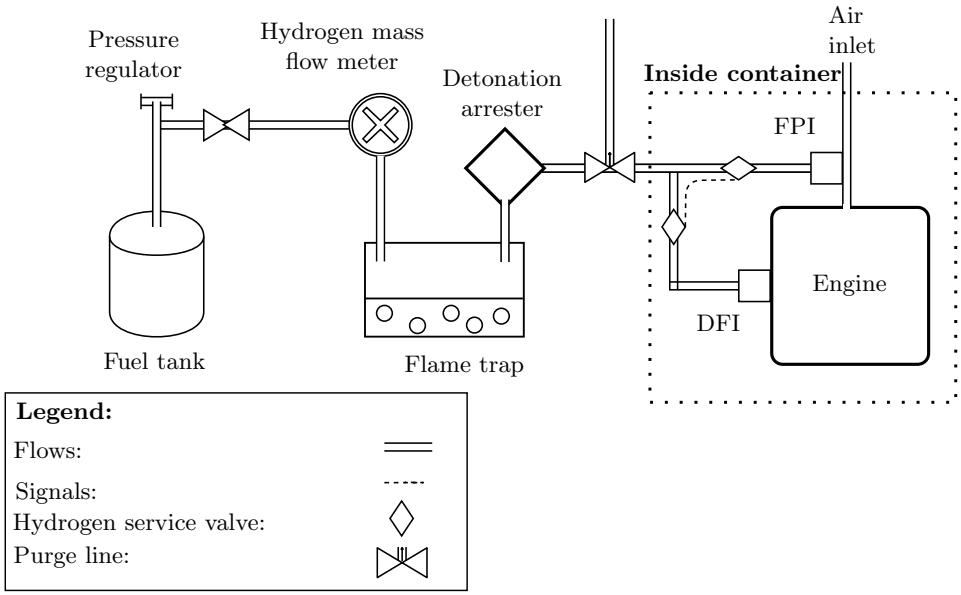

Figure 4.2: Schematic of the preliminary design of the test set-up. To clarify the test set-up, the figure is divided into four parts. This illustration depicts part one.

A legend is depicted in the bottom left of the figure. Furthermore, it can be noticed the illustration is divided into two parts. Dashed lines separate elements inside the container and elements outside the container. Some elements should not be installed in the container to reduce the thermal load and to enhance safety. The hydrogen fuel tank may not be stored inside the test cell container regarding safety concerns (Najjar, 2013). A hydrogen leak inside an enclosed environment may lead to a deflagration or detonation.

On the far left of Figure 4.1 and Figure 4.2 a fuel tank is illustrated. Hydrogen is stored in gaseous state in a high pressure fuel tank. The hydrogen tank includes a pressure relief device to reduce the probability of a detonation, the device enables the possibility to vent hydrogen inside the tank in case of a fire (Durbin and Malardier-Jugroot, 2013).

A flexible fuel line connects the hydrogen tank with the internal combustion engine. The gas flows through various components prior to reaching the engine as visualised in Figure 4.2.

The first element is a pressure regulator, it ensures safe passage of hydrogen gas to

the internal combustion engine by reducing the pressure prior to hydrogen propagating through the fuel pipe. A port fuel mechanism injects hydrogen with a pressure of 20 bar, therefore the regulator reduces the pressure to 20 bar. Subsequently, a shut-off valve which is directly connected to the operation panel enables the possibility to shut-off the hydrogen supply to the engine in case of a malfunction. A manometer measures the pressure after the gas propagates through the pressure regulator, once the gas passes the manometer, it propagates through a mass flow meter as well to monitor the flow. Afterwards, a flame and detonation arrestor prevent gas propagating from the internal combustion engine or fuel injectors back into the hydrogen fuel tank. Note that many of these and the following components will be installed outside the container to reduce the risk of a hydrogen leak in the test cell and to reduce the thermal load.

In the following passage the flow is split up between two different channels, one channel leads towards a port fuel injector while the other leads towards a direct fuel injector. It is planned to test both injectors to compare the efficiency of the mechanisms as previously mentioned in Chapter 3 and (Frijters, 2020). The port fuel mechanism will initially inject the fuel. The direct fuel injector will consequently be part of future modifications as the engine momentarily only includes a port fuel injector. Ultimately, a hydrogen service valve regulates the mass flow and pressure prior to hydrogen flowing through the injectors as the PFI and DFI require different injection pressures.

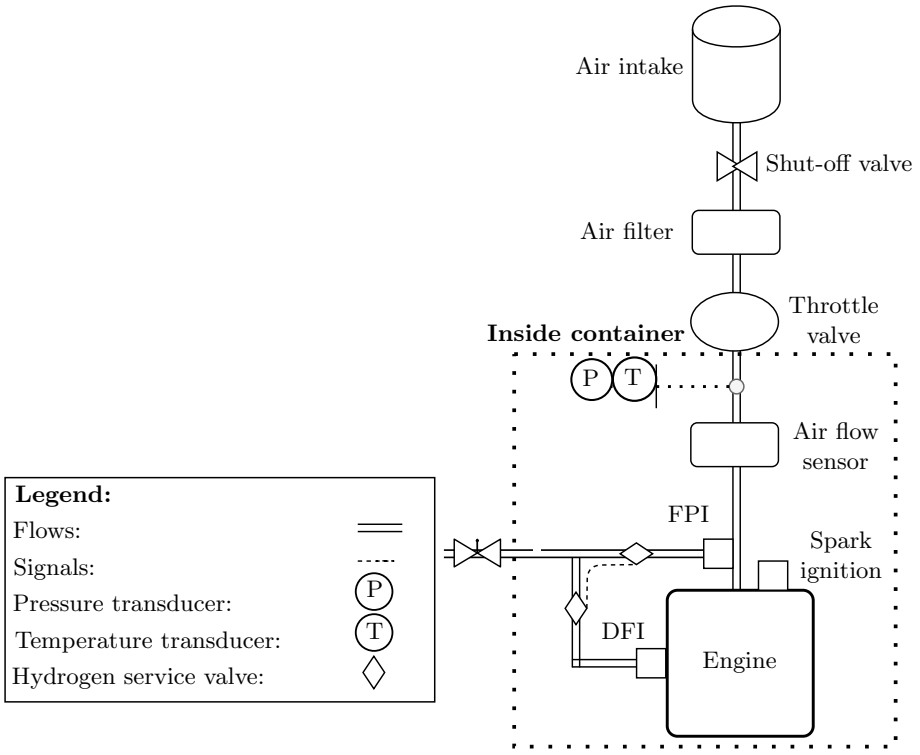

Figure 4.3: Schematic of the preliminary design of the test set-up. To clarify the test set-up, the figure is divided into four parts. This illustration depicts part two.

Figure 4.3 displays the air intake system of the test set-up. Dashed lines separate once more the parts situated in the test cell room and the parts situated outside the room. Air supply for the combustion chamber will be drawn inside from the environment. Air may not be drawn in from within the test cell container as in case of a hydrogen leak in the test cell, hydrogen may propagate through the air inlet, possibly entailing a detonation.

The operation panel is connected to a shut-off valve which can close the air supply immediately. The air supply propagates through an air filter and a throttle valve. A thermocouple and manometer measure the temperature and pressure respectively after the throttle valve. Subsequently, an air flow sensor measures the volume air flow and air propagates to the engine's combustion chamber.

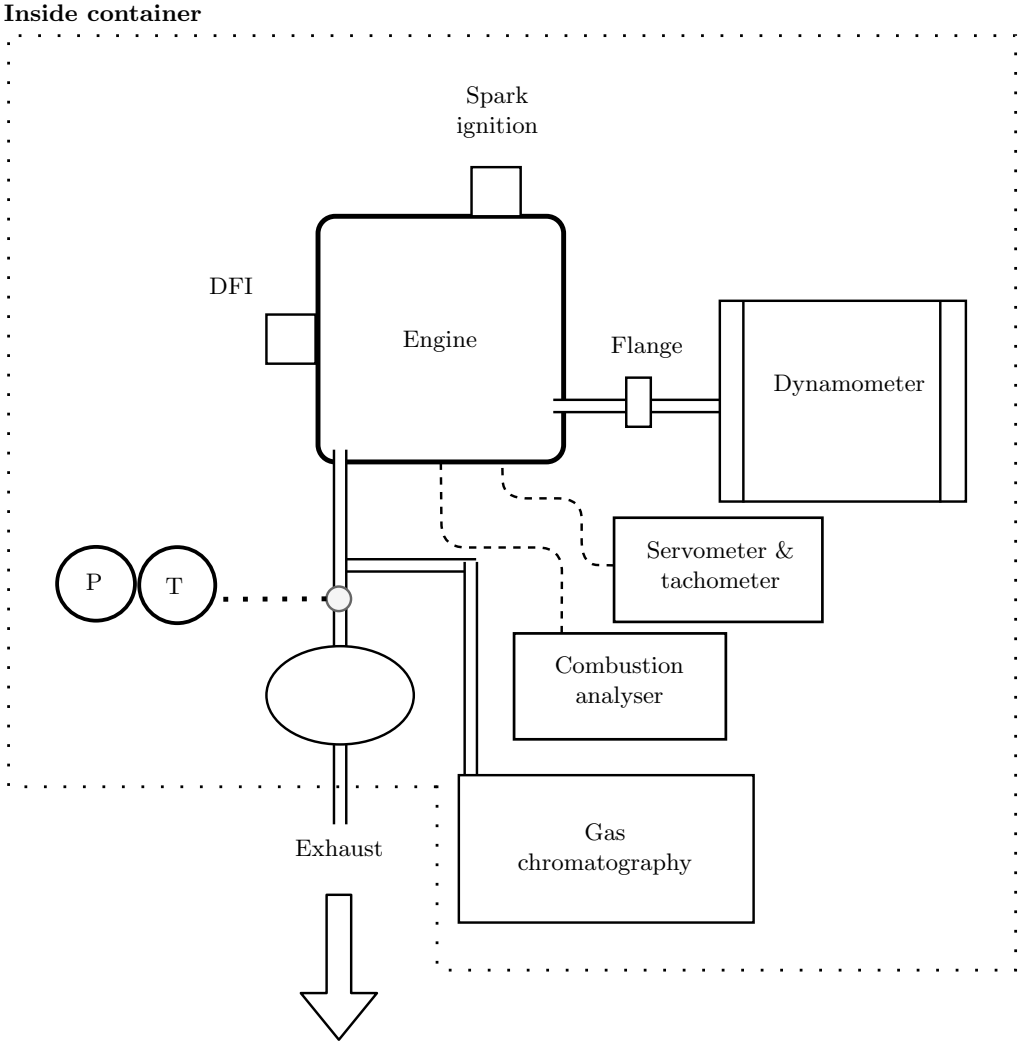

Figure 4.4: Schematic of the preliminary design of the test set-up. To clarify the test set-up, the figure is divided into four parts. This illustration depicts part three.

Figure 4.4 depicts the post-combustion process. All the parts are situated in the test cell room except for the outlet of the exhaust pipe. The engine is connected through an interconnecting shaft and a flange to a dynamometer. The injection mechanism and spark ignition device will require modifications such that it operates with hydrogen as mentioned in Chapter 3. A tachometer and combustion analyser will measure the engine's speed, power, torque and temperature inside the cylinder. The gases flow from the exhaust manifold to the ceiling by passing through a long pipe connected to the ceiling after combustion. It is ensured hot exhaust gases do not get into the proximity of bystanders by connecting the exhaust pipe to the ceiling. Consequently hot exhaust gases are disposed of into the environment through a duct mounted on the ceiling of the container. The last component is the gas chromatography, which measures the concentration of each element of the exhaust gases in the exhaust pipe.

Figure 4.5 depicts the control panel and the connection between the test set-up and the control room. The illustration includes three separate parts, namely elements inside the test container, elements inside the control room and elements outside either room. The electronic control unit (ECU) is connected to the throttle valve and the injectors. The operational panel controls the throttle and fuel flow settings. Output data such as the temperature and pressure measurements are transmitted towards a personal computer in the control room.

The test cell room requires constant monitoring of the atmospheric conditions. Room temperature, humidity and atmospheric pressure influence the outcome of the test experiments, therefore a weather station inside the test cell room will audit the atmospheric conditions. In addition, a fire alarm, a dry fire extinguisher and sprinklers provide for fire safety inside the container (Khandelwal et al., 2013).

A last and crucial component is soundproofing, the test cell will require a permit to operate which can only be acquired if the cell does not exceed the noise limit of the local regulations. A couple of measures can reduce the noise generated by the test cell. These include soundproofing material attached to the walls, long ducts and silencers (Dagdougui et al., 2018).

4.2 Test cell room safety precautions

A 20-feet container houses the test set-up. The experiment is not set up in open-air for the following reasons;

- **Noise:** The cylinders of the engine require cooling. As most aircraft piston engines, the Lycoming engine is cooled internally through oil and externally through air flowing over fins on the outer surface of the cylinders. The atmospheric air enters the engine cabin and cools the cylinder through a hole in the cowling during cruise. Forced-draught fans have to simulate this process in the test cell. A

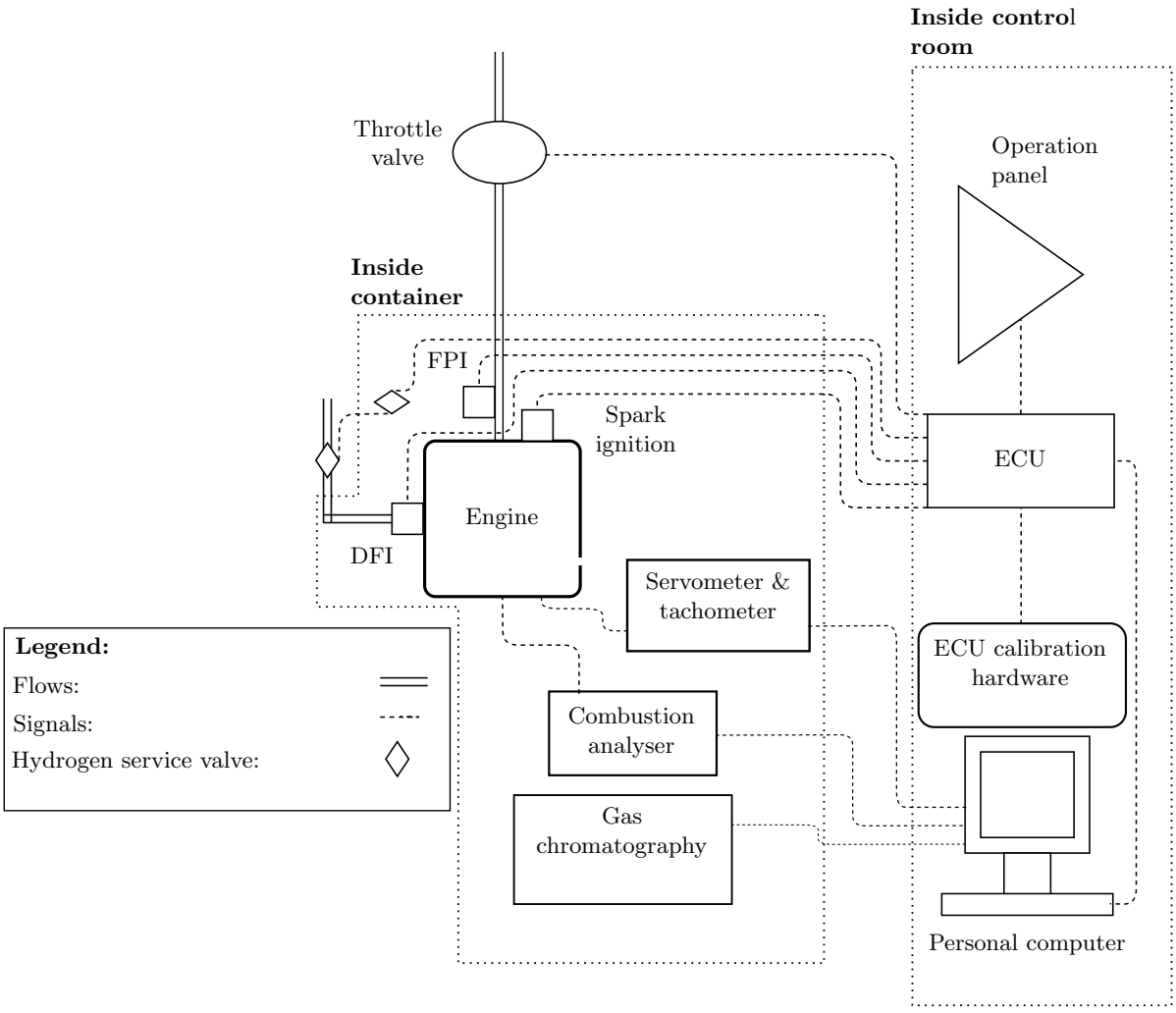

Figure 4.5: Schematic of the preliminary design of the test set-up. To clarify the test set-up, the figure is divided into four parts. This illustration depicts part four.

drawback is the noise the fans produce. Noise can be attenuated through efficient duct design and attenuators by constructing a test cell environment.

- **Safety:** Hydrogen flames are invisible to the naked-eye. Operatives or bystanders could be harmed if they are not careful. A container provides for a controlled environment and isolation[1].

- **Transport:** The test cell environment is designed such that there is opportunity to

[1]In turn, hydrogen accumulation becomes an issue. When not managed well, a container may cause more catastrophe than open-air testing. However with adequate preventive measures, performing tests inside a container is safer.

test at multiple locations across the Netherlands. A 20-feet container can easily be transported by lorries. The logistics would become more difficult if the experiment is set up in open-air.

- **Contamination:** Testing in an isolated environment ensures the consistency of experiments (besides varying humidity and ambient air temperature). Heavy winds could influence the cooling process of the cylinders if experiments are performed in open-air. This is undesirable as the cylinders are most efficient at a specified temperature. The cooling fan must deliver less power if heavy winds cool down the cylinders. It becomes quite difficult however to control the temperature as the sensor readings might become inaccurate due to presence of multiple air flows. Furthermore, the set-up cannot be protected from poor weather conditions, rain, snow, hail, sand and other debris such as leaves. This may either cause damage to the test set-up or cause for unanticipated inconsistencies during testing.

The container design is not inherently safe, various additional precautions are presented in Chapter 9. The following safety topics are discussed in this section;

- Fire safety
- Detonation prevention methods
- Visual monitoring
- Noise dampening
- ventilation & cooling

4.2.1 Fire safety in container

Hydrogen may leak into the container and consequently a hydrogen flame might ignite within the test cell if a small gap or crack appears in the test set-up. One or more sensors must be placed in the test cell to detect the concentration of hydrogen in the event of a leak. Hydrogen flames cannot be extinguished in the same manner as an aviation gasoline flame. The source cannot be directly extinguished as unburned hydrogen has a low minimum activation energy. Extinguishing the fire without shutting-off the hydrogen supply means unburned hydrogen is released into the test cell container and it accumulates, which might entail a detonation. Therefore the first step is to immediately shut-off the hydrogen source prior to extinguishing the fire. An automated system fills the container with heptafluoropropane once the hydrogen supply has been shut-off. Furthermore flame detectors must be mounted on the walls of the container as hydrogen flames are invisible.

4.2.2 Blast wall in container

A hydrogen leak within the test cell may entail a detonation. To enhance safety, one wall of the container requires to be weaker than the others. The impact of a detonation is therefore controlled as debris does not fly in any random direction, but in the direction of the weaker wall. This can be the ceiling or either one of the four side walls of the container. Windows will not be put in the container as it weakens the walls, cameras will provide for visualisation during test experiments.

4.2.3 Visual monitoring of test set-up

Cameras must be installed in the test cell room to provide for continuous visualisation of the test experiment. As the equipment is mounted within a harsh environment, the cameras should be at least ATEX-3 protected[2] (Wallner T., 2009). Furthermore, sensors will be mounted within the test cell to monitor the temperature of the test cell, humidity, hydrogen concentration et cetera. The temperature of the test cell should be maintained at least below the operating temperature threshold of the installed equipment.

4.2.4 Noise dampening

Noise is produced predominantly by the ventilation fans and internal combustion engine in the test cell. Most noise escapes the test cell through the large gaps caused by the ventilation fans itself. Attenuating noise through efficient duct design will be elaborated upon in Chapter 6. Withal, noise can be dampened by attaching foam to the surfaces of the walls. Further analysis is required however whether it is an effective method as noise propagating through the ducts may be predominant. Foams on the inner surface of the container wall may as well affect the flow field.

Noise analysis is not part of this MSc. Thesis besides a simple noise generation analysis of the fans. Noise generation within the test cell must be researched in a succeeding phase of the project.

4.2.5 Ventilation & engine cooling

The purpose of ventilation system is to maintain the environment of an enclosed room at an adequate temperature and to dispose of undesirable particles. Furthermore, one of the ventilation fans will function simultaneously as cooling unit of the engine as well.

Engine cooling

Adequate engine cooling and ventilation are essential as mentioned in Chapter 2. Table 4.1 shows the performance characteristics of the Lycoming engine, provided by the

[2]ATEX-3 protection means the component is rated as gas tight and is able to cope with water projected from a nozzle

Lycoming Manual (2005).

Table 4.1: Engine performance characteristics of the Lycoming engine IO-360-A1B6 (Lycoming Manual, 2005).

Engine rating	**Rpm**	**Power (kW)**	**Fuel consumption (g/s)**	**Max. temp cylinder head (K)**
Normal rated	2,700	149.14	-[1]	533
Performance cruise (75%)	2,450	111.85	9.6	533
Economy cruise (65%)	2,350	96.94	7.41	533

[1]No data provided by (Lycoming Manual, 2005).

The temperature may not rise above a threshold set by the manufacturer, the material deteriorates and the engine becomes less efficient or is demolished. The maximum allowed cylinder head temperature is 533 K as provided by Lycoming Manual (2005). In addition, a distinction must be made between the maximum temperature and maximum continuous temperature. The maximum continuous temperature is the temperature which may not be exceeded during constant cruise performance (477 K (Lycoming Manual, 2005)). The maximum temperature is a temperature threshold which the engine cannot endure for an extended period, which for the Lycoming engine is 533 K.

Atmospheric air cools the engine during cruise. Through the International Standard Atmosphere (ISA) calculation, the true incoming air speed and temperature may be estimated. The design cruise speed of the Cessna 337F Skymaster is approximately 232 km/h and the cruise altitude is 10.000 feet (3.000 m) (Lycoming Manual, 2005). Converting the incoming air to true airspeed (TAS) yields an incoming airspeed of 47.55 m/s. However, air is decelerated through a diverging duct[3]. The cylinder head temperature may not decrease below the minimum operating temperature of 338 K as well (Lycoming Manual, 2005).

Engine baffles redirect the flow inside the engine cowling to provide equal cooling for each cylinder. The cylinders in the second row are not in the direct air stream if the engine is cooled from the front and will therefore receive less cooling without redirection of the air flow. Engine cabins without baffles solve this issue by increasing the fin area of the cylinders which receive less cooling. In the Cessna 337F Skymaster, the fins have an equal amount of fin area as air is redirected within the engine cabin by baffles. Baffles redirect cold air flow such that it flows from the top of the engine cylinders to the bottom. Subsequently, the warm air leaves the engine cabin through a hole in the back. In addition, the outlet of the engine cabin is of varying size. In a cold atmosphere, the diameter is reduced to a smaller size as otherwise the engine may

[3]The ducts apply the principle of the Venturi effect. The air enters through a small hole with diverging walls, causing the incoming air flow to decelerate.

receive too much cooling. The outlet diameter is widened to increase cooling in warm atmospheric conditions.

Figure 4.6 illustrates the air cooling mechanism of the cylinders in an engine cabin. In the middle of the figure, an engine is depicted with two cylinders (which are depicted by the two circles). Cold atmospheric air enters the engine cabin through an inlet. Baffles direct the cold incoming air over the fins of the cylinders. The air warms up due to convective heat transfer, which is depicted by the arrows turning orange. Warm air (red arrows) consequently leaves the engine cabin through an outlet at the rear of the engine cabin.

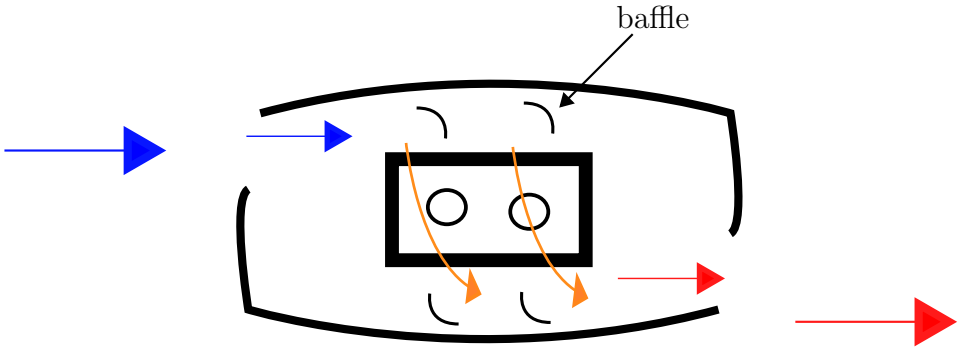

Figure 4.6: Engine baffles direct the flow over the cylinders. Cold atmospheric air enters the engine cabin through the front, subsequently the baffles direct the flow over the engine and the incoming air warm ups. Consequently hot air, depicted by the red arrows, leaves the engine cabin through the rear.

According to tests performed by Deltion College, the cylinder head temperature for maximum efficiency is approximately 453 K. A cooling fan will function as an air flow source to provide for equal cooling among the cylinders. Air flow will be directed from top to bottom of the cylinder. If the ventilation fan would be set in front of the engine and flow would not be redirected, the rear cylinders receive less cooling as they are in the wake of the cylinders in front. One solution would be to increase the air flow to provide sufficient cooling of the rear cylinders, however subsequently the cylinders in front would receive too much cooling, reducing the efficiency of the front cylinders. To mimic the aircraft cooling mechanism, air is induced over the top of the fins by mounting the cooling fan on the ceiling.

Cooling from above is hazardous as in the event of a leak near the engine, hydrogen is pushed downwards. Wallner T. (2009) recommends to mount an outlet duct above each element operating with hydrogen as it has the natural tendency to rise, thereby disposing of hydrogen immediately. However, this is not a valid strategy when the engine is cooled from above.

In theory, the engine may also be cooled from below, but fins are less efficient as they are designed to receive cooling from the top of the cylinder. Figure 4.7 illustrates a

schematic of the internal combustion engine. The schematic is obtained from the Lycoming operation manual (Lycoming Manual, 2005).

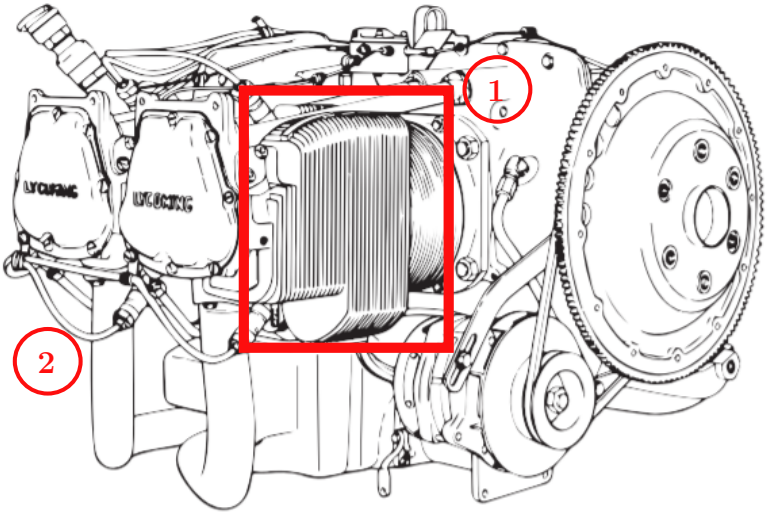

Figure 4.7: Fin geometry of the internal combustion engine. Fins are optimised to be cooled from above. Cooling from below may induce issues as the fin geometry is not symmetrical along the upper and bottom part of the cylinder (Lycoming Manual, 2005).

Area 1 (the area within red rectangular) designates the fin area. One may notice the fins are not symmetrical across the horizontal axis. Fins on the cylinder barrel extend further down than up. Fins on the top of the cylinder encounter a direct and cooler air flow than fins on the bottom plate. Therefore, fins on the bottom plate must extend further down to enhance cooling. If cooled from below, large temperature gradients may occur as the bottom of the cylinder receives too much cooling and the top of the cylinder too little. In addition, the large exhaust pipes (near circle 2) impede some of the incoming cooling air flow if cooled from below.

Withal, designing a ducting system beneath the engine is difficult as the engine will be mounted on a motor stand and various elements of the test set-up are near the engine such as the dynamometer and exhaust pipe.

An alternative option is to pull the air over the internal combustion engine as depicted in Figure 4.8. A fan pulls air upwards through the fume hood over the engine. Air will be primarily pulled in from the sides, subsequently the bottom part of the cylinder will not be cooled sufficiently as less mass flows over the fins. A temperature gradient develops across the surface area of the cylinder which may damage the engine. In addition, air upstream of a fan is less turbulent than downstream, entailing a lower heat transfer coefficient. Therefore cooling from beneath the internal combustion engine is not feasible.

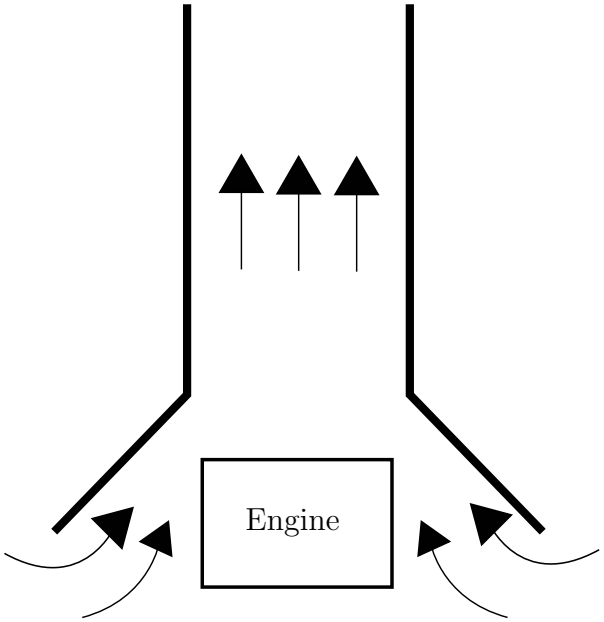

Figure 4.8: An engine will not be cooled sufficiently by pulling the air upwards. Air will be primarily drawn in from the sides, the bottom part of the cylinders will not be cooled well and large temperature gradients across the surface area of the cylinder appear.

Figure 4.9 and Figure 4.10 depict the effect of pulling air instead of pushing it over an object. The black rectangle may represent any object (e.g. an engine). A fan is called a forced-draught fan when it is in front of the object whilst it is an induced-draught fan when it is behind the object. Forced-draught fans entail higher heat coefficients due to the increased turbulence over the object in comparison to an induced-draught fan.

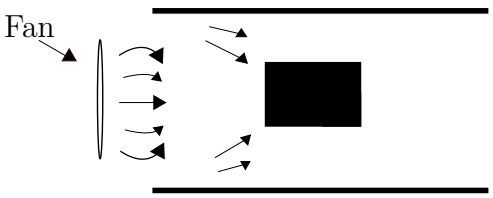

Figure 4.9: A ventilation fan pushes air over the engine entailing high turbulence and therefore a high heat transfer coefficient. The fan is called a forced-draught fan.

Figure 4.10: A ventilation fan pulls air over the engine entailing low turbulence and therefore a low heat transfer coefficient. The fan is called an induced-draught fan

Furthermore, it must be ensured the cylinders only receive cooling by the ventilation fan mounted on the roof. If another air flow interacts with the cylinders, it may become difficult to maintain a constant cylinder head temperature. Hence, the internal combustion engine must be isolated from the remaining air flows in the test cell. A possible solution

is to stretch a fume hood over the geometry of the internal combustion engine.

Ventilation

No data is yet available in literature regarding safe test cell design of hydrogen air-cooled internal combustion engines. Assessing all possible precautions to ensure a safe test cell design will be vital to obtain a permit to experiment with hydrogen.

Experimenting with hydrogen combustion is dangerous since hydrogen must be injected at high pressures, with port fuel injection hydrogen is injected with pressures up to approximately 20 bar. A deflagration or detonation may occur in the container when hydrogen leaks through the fuel pipe or through any other component of the test set-up. In addition, the air flows in the test cell are strong since a fan cools the cylinders. Other test cells often do not include strong air flows as a water jacket cools the engine. This adds an additional layer of complexity to the test set-up. Furthermore, the incoming air potentially pushes hydrogen down as the engine must be cooled from above. The natural tendency of hydrogen is to rise vertically upwards due to the buoyancy effect and therefore it might remain in the container for an extended period.

The ventilation system must ensure efficient disposal of hydrogen and excess heat. Hydrogen safety experts of Inerc BV Hydrogen Safety[4] suggest setting up a CFD model to predict the diffusion of hydrogen and such to optimise the ventilation system. A textbook method offers a good approximation of how much ventilation is required to dispose of hydrogen and excess heat but it does not visualise whether hydrogen and heat accumulate in the test cell. Furthermore, standard guidelines for the optimal ventilation system are not directly applicable to this test cell due to the uniqueness of the test set-up. The standard guidelines do offer an adequate initial guess of the optimal placement however. A CFD simulation is required to predict the flow field in the container and to optimise the placement of the ventilation system to minimise the risk of a detonation. A few other preventive measures may be included such as tilting the container ceiling or container itself to aid in the outflow of hydrogen into the environment if the ventilation system is not sufficient.

It is possible the organisation argues experimenting with a hydrogen air-cooled internal combustion engine within a 20-feet container is inherently unsafe regardless of the precautions. The CFD analysis will provide with an indication of the diffusion of hydrogen in the test cell and whether a safe design is feasible.

The test cell must, amongst others, comply to the following two regulations for hydrogen safety (Wallner T., 2009).

- The volume concentration of hydrogen may not exceed on average 25 % of the LEL-limit in the test cell (except for near the leak).

[4] `https://inerc.nl/`[Retrieved 09.03.2021]

- Hydrogen may not flow over any ignition sources or electrical components.

Note various other regulations are defined but these are presumed to be the most difficult to comply to. A different test cell environment must be built if the CFD simulations show the preceding principles are not met[5].

The 25 % of the LEL-limt implies the hydrogen volume concentration may not exceed 1 % on average in the test cell. Hydrogen is flammable at approximately a volume concentration of 4 %. Wallner T. (2009) sets a safety factor of 4 to ensure hydrogen will not ignite. In addition, all the components in the test cell must be ATEX-3 protected.

Furthermore, the internal combustion engine, dynamometer, lights et cetera, generate heat due to the large amount of power they require to operate. High varying thermal loads are inevitable in enclosed environments. Equation 4.1 should be applied to approximate the required air changes per hour in the test cell environment to maintain an adequate temperature within the test cell (Martyr and Plint, 2012),

$$\text{Ventilation mass flow rate} = \frac{\sum \text{Thermal load}}{C_p \cdot \Delta T \cdot \rho_0} \left[\frac{\text{kg}}{\text{s}}\right]. \tag{4.1}$$

C_p is the heat capacity ratio in J/kg·K, ΔT the change in temperature in the test cell and ρ_0 the density in the test cell.

The thermal loads of the engine, dynamometer, lights & services, forced-draught fans and exhaust pipe are obtained through statistics provided by Martyr and Plint (2012) and are summarised in Table 4.2. The heat loss represents convection of the container walls to the environment.

Table 4.2: Energy balance in the test cell environment (Martyr and Plint, 2012).

Heat source	**Thermal load (kW)**
Engine	135
Dynamometer	10
Lights & services	20
forced-draught fan	15
Exhaust pipe	30
Losses	-2.6
Total	222.4

For example, an engine is estimated to release 135 kW of heat through radiation and

[5]For example, one can attempt to construct a test cell in a building. Large rooms impose less constraints on the ventilation load.

convection, Martyr and Plint (2012) report it to be 0.9 kW/kW of the engine power [6]. Note, the thermal load due to radiation is negligible compared to heat released by convective heat transfer. The thermal load due to radiation equals (Mills and Coimbra, 2015),

$$Q_{\mathrm{r}} = 5.77\varepsilon_{\mathrm{engine}} \left[\left(\frac{t_{\mathrm{s}} + 273}{100} \right)^4 - \left(\frac{t_{\mathrm{w}} + 273}{100} \right)^4 \right]. \tag{4.2}$$

With $\epsilon_{\mathrm{engine}}$ the emissivity of the engine, T_s the engine surface temperature and T_w the container wall temperature. The thermal load due to radiation equals 1.1 kW with the assumption the engine temperature equals 393 K and the engine surface area equals 1.5 m^2. The assumptions of the engine temperature and engine surface area are clarified in Table 6.3. The average cylinder barrel temperature is found to be 393 K in literature (Martyr and Plint, 2012), while the cylinder surface area including the fin area is calculated to be 1.5 m^2.

An internal combustion engine is approximately 30 % efficient, the remaining energy is conveyed to the exhaust ($\pm$ 30 %) or is transformed into heat ($\pm$ 40 %). Martyr and Plint (2012) appoints it as the 30-30-40 rule, a similar rule exists for water-cooled engines, which is called the 30-30-30-10 rule. Water captures most of the heat released in water-cooled engines, $\pm$ 30 % energy is released through cooling water and 10 % through convection and radiation. Therefore water-cooled engines are often tested in smaller rooms than air-cooled engines. Air-cooled engines are often put in 'hangar-type' buildings to cope with the high thermal load caused by convection and to some extent radiation (Martyr and Plint, 2012).

The required ventilation air mass flow rate can be determined for a user-specified temperature difference, Martyr and Plint (2012) suggest to design for a maximum temperature rise of 10 K. With an outside temperature of 25 K, the density equals 1.185 $\mathrm{kg/m}^3$ and the standard specific heat is approximately 1.01 $\mathrm{J/kg \cdot K}$. To obtain a temperature difference of 10 K, the required volume air flow according to Equation 4.1 equals 17.42 m^3/s. The test cell environment is an enclosed environment of 38.49 m^3, meaning 1650 air changes per hour are required to maintain a temperature difference of 10 K. Public rooms or garages require approximately 20 air changes per hour (Martyr and Plint, 2012). This is a consequence of using a small container while testing an air-cooled internal combustion engine. The heat release due to convection is immense, hence powerful ventilation fans are required.

An air flow rate of 17 m^3/s is rapidly observed to be unfeasible, fans larger than 1.5 m diameter are required with noise levels above 100 dB[7]. A reason why the thermal

[6] The maximum power output of the Lycoming engine is $\approx$ 150 kW (Lycoming Manual, 2005)

[7] `https://induvac.com/nl/`[Retrieved 09.11.2020]

load of the engine is immense is due to the cylinders being entirely cooled due to air. Air-cooled engines may be cooled up to 80 % by oil, the Lycoming engine currently is not mounted with an oil cooler. An oil cooler will be required to reduce the thermal load in the test cell. The thermal load of the internal combustion engine reduces from 135 kW to approximately 27 kW in the test cell[8]. Recalculating the total thermal load in Table 4.2 yields a ventilation volumetric flow rate of approximately $7\,m^3/s$ for a temperature change of 10 K. For the test cell a ventilation rate of $7\,m^3/s$ entails 663 required air changes per hour, which is feasible.

Nonetheless, the circulation of air will be complex, it must be ensured no heat or undesirable particles accumulate in the test cell due to poor circulation. Deflagration or detonation may occur in case of a hydrogen leak if hydrogen accumulates in a local region of the test cell. The CFD model will determine the optimal locations of the ventilation fans and cooling fan.

To note, researchers suggest the ventilation system should provide for a temperature difference of 10 K for acceptable working conditions (Martyr and Plint, 2012). However, operatives will not be in the test cell during the tests of the retrofit hydrogen internal combustion engines as the control room is situated in a separate container. Thus the minimum ventilation load is rather imposed by the maximum operating temperature of components, the discharge of undesirable particles in the cell and the release of dangerous gases or liquids in the event of a leak. Nonetheless, it is planned to test various other internal combustion engines which will operate with a different fuel once the project is finished. In addition, the container itself will heat up as it is situated in direct sun light during warm summer days. Many ventilation fans have an operating temperature limit of 323 K[6]. Hence, it may be necessary to maintain a maximum temperature difference of 10 K. Therefore one must aim for a ventilation system which supplies a volumetric flow rate of $7\,m^3/s$.

In addition, various internal combustion engines will be tested in the test cell environment as well. Ranging from small air-cooled piston engines to larger piston engines and possibly gas turbines. These engines might require a higher amount of air cooling as well and it would be favourable if the test cell environment is compatible with as many models as possible.

4.2.6 Test cell room preliminary schematic

In Figure 4.11 shows a preliminary schematic of the test cell room. The aim is to optimise the cooling and ventilation system such that the engine receives sufficient cooling air flow while no heat or hydrogen accumulates within the room. The location of each element in Figure 4.11 is not definitive. The figure is a means to visualise the test cell and to clarify the objective of the MSc. Thesis.

[8]It is assumed the oil cooler will be remotely installed outside the test cell container. Ergo, the oil cooler does not release heat into the test cell.

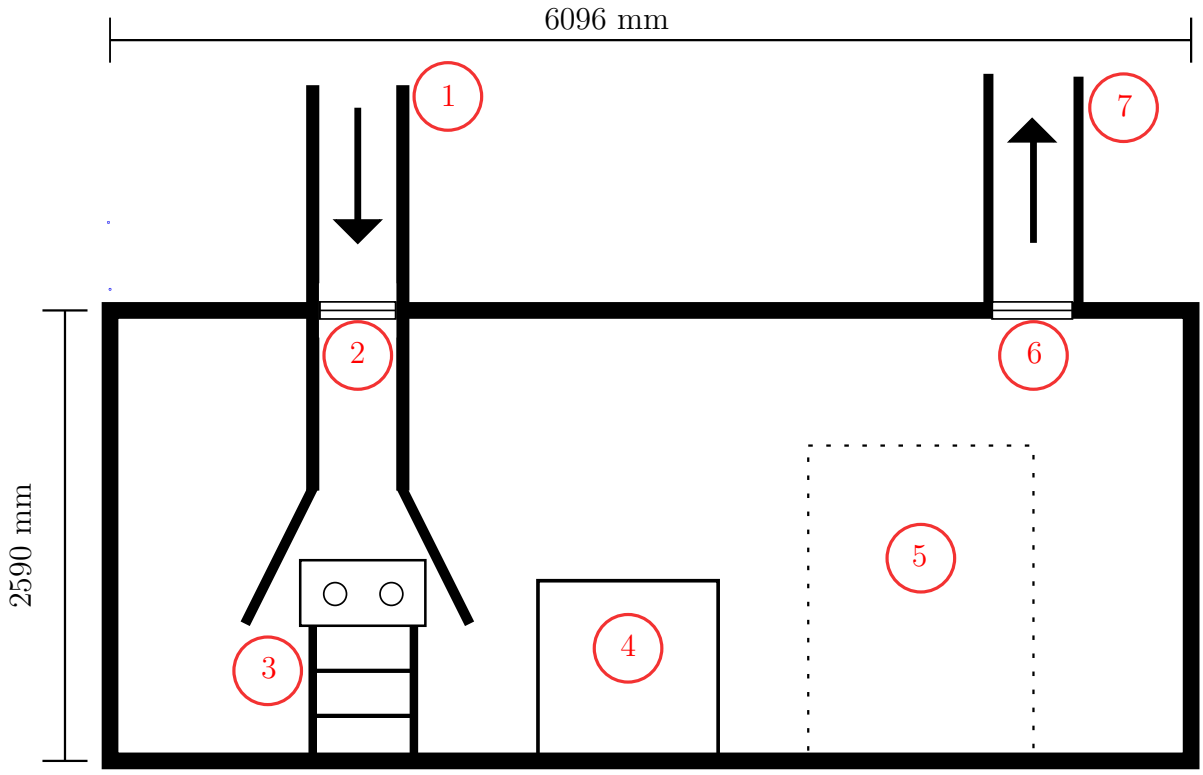

Figure 4.11: Side-view schematic of the test cell room. (1) is an inlet duct, (2) an inlet fan, (3) the engine, (4) the dynamometer, (5) depicts the remainder of the test set-up with an arbitrarily set size of the rectangle, (6) is the outlet fan and (7) the outlet duct.

Figure 4.11 depicts a side-view of the container which stores the test cell. The schematic of the test cell room features seven different elements, the inlet duct (1), the cooling fan (2), the engine paddock (3), the dynamometer (4), the remaining components of the test set-up (5), the outlet ventilation fan (6) and outlet duct (7).

Air enters through the inlet duct (1), drawn in by the ventilation fan (2) which is subsequently directed to the internal combustion engine. A drawback of having the inlet and outlet through the ceiling is that ingress rain or snowfall can interfere with the test cell, therefore a suitable duct system must be designed.

A fume hood isolates the engine from the remaining air flows in the test cell to ensure the internal combustion engine is solely cooled by the ventilation fan. The internal combustion engine is mounted on an engine paddock (3). The engine itself is depicted by the rectangle and two circles. The two circles resemble two cylinders (the Lycoming engine is a four cylinder engine, two cylinders are on each side.)

Furthermore, part (4) represents the dynamometer, which is depicted separately from the remainder of the test cell set-up (5) as it is a large element and expected to

influence the flow field. The dashed lines designate the remainder of the test set-up which only includes smaller elements. Presumably, the smaller elements of the test set-up do not have a large influence on the flow field. The size of rectangle (5) is chosen arbitrarily and will most likely not occupy as much space as indicated in the figure. The remaining components comprise of electrical wires, the combustion analyser, a gas chromatography, a small control unit and a HVAC-unit. In addition, some components may be added during a later stage of the project.

The test set-up includes an electronic box which connects the engine to the control panel, PC and ECU. Note, the position of the weather station, fire alarm, generator, dry fire extinguisher and monitoring system are not depicted in the schematic. The installation of those systems is not a part of the MSc. Thesis. The remainder of the test set-up is situated in the back of the room below the outlet fan (6) and outlet duct (7). The depicted ventilation system will be optimised through literature research and computational fluid dynamics. In addition, the CFD analysis will provide an indication of the most optimal locations for sensors which are able to measure the hydrogen volume concentration in the test cell.

4.2.7 Summary safety precautions

This section contains much information. Therefore Section 4.2 summarises the main points of the chapter in the following list.

- The air propagating through the air inlet of the engine must be supplied from outside the test cell container. Hydrogen may propagate through the air inlet in the event of a hydrogen leak in the test cell container, potentially causing a detonation.

- A fan must cool the engine from above since fins are not optimised to be cooled from below. Consequently, when hydrogen leaks near the engine it may be pushed downwards by the incoming cooling air flow. Therefore a permit to be allowed to experiment with hydrogen will be difficult to obtain.

- A CFD simulation must be performed to model the dispersion of heat and diffusion of hydrogen.

- The CAD model of the CFD analysis must be simplified as otherwise the computational time is too high. The CAD model should include the elements which affect the flow field and heat balance the most.

- Air-cooled engines are often experimented with in hangar-type buildings due to the high convective heat release. Consequently, the thermal load and required ventilation mass flow rate are high in the test cell.

- The estimated required ventilation rate equals $7\,m^3/s$.
- Powerful fans are required which make much noise as the ventilation load is relatively high. Noise analysis is not part of this MSc. thesis and must be further researched.

4.3 Control room preliminary schematic

The function of the control room is to house the monitoring and spare equipment, including ear protectors, spare cameras, tool boxes, computers and a control panel.

Operatives will be able to control the experiment from within the control room by managing the ECU and throttle. The control room will be connected to the test cell room through power cables while cameras will provide for visualisation of the test cell room during testing. Figure 4.12 is an illustration of the floor plan of the control room.

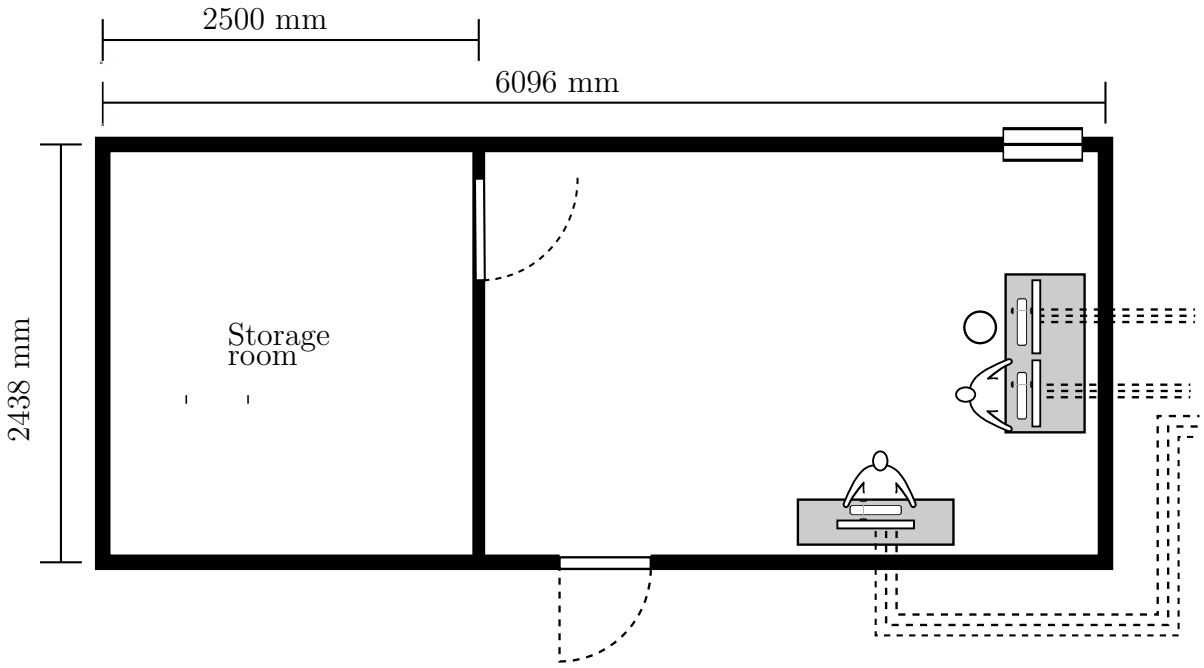

Figure 4.12: Top-view schematic of the control room. The room on the left is a storage room and the room on the right includes the monitoring equipment and control panel.

The dotted lines on the right-hand side of the figure resemble power cables which connect the personal computers and control panel with the test cell.

One can notice the hydrogen tanks are neither stored in the control room or test cell room. The same rational applies to the control room as to why hydrogen tanks cannot

be stored inside the container. They can neither be stored in the test cell container nor in the control room as it conflicts with safety regulations. A hydrogen leak may lead to a disastrous event and therefore they may not be stored within an enclosed environment. In addition, the tanks may not be stored within 5 meters from any building. The hydrogen tanks will be stored safely outside, enclosed by a fence (Hysafe, 2009).

Chapter 5

Introduction CFD Model

The CFD model simulates the cooling of the engine, the diffusion of heat and diffusion of hydrogen through modelling the flow field within the test cell.

Computational fluid dynamics is a trade-off between time and detail. The objective of the set-up is to minimise the computational cost whilst not affecting the results. Computational cost can be minimised by simplifying the model and coarsening the mesh. Subsequently, elements which are crucial to or affect the energy balance, hydrogen diffusion and flow field are further elaborated upon in the coming chapters while the remaining elements are discarded from the CFD model. Doing so will yield a flow field with slight differences from reality, but in areas which are considered to be not essential. Hence, the results obtained through the CFD simulation are plausible while time consumption is minimal.

5.1 Purpose of CFD simulations

The necessity of a CFD simulation is explained in Section 4.2.5. The CFD simulation is a means to optimise the position of each element to obtain a safe and energy efficient test cell.

Forced convection, and to some extent radiation, entail an excess amount of heat within the test cell. Hence, the energy balance has to be determined as the engine requires sufficient cooling. A ventilation system purges the excess heat to avoid the temperature in the test cell exceeding the operation limits of components. High temperatures are a hazard for two reasons. The first is the increasing risk of detonation and deflagration. Hot surfaces within the room may be sufficient to ignite a hydrogen flame due to the relatively low minimum activation energy of hydrogen. Besides the increasing risk of ignition, high temperatures might damage sensitive material present in the test room such as sensors. In addition, varying temperatures might cause issues with the consistency of experiments. However, this phenomena will be difficult to avert as temperatures will naturally differ due to changing seasons (summer, autumn, winter and spring). Nevertheless, the error caused by varying inlet conditions can be estimated.

A second aim of the CFD model is to analyse the consequences of a potential hydrogen leak and how to purge the test cell room most effectively. Some elements inside the test cell affect the flow field and diffusion of hydrogen. For example, the dynamometer is a large component and is situated near the engine, it will likely interfere with the flow field. In contrast, some elements in the test cell do not contribute to the

energy balance or affect the composition of the flows within the test cell and should be discarded from the CFD model to reduce computational time.

5.2 CFD case studies

Through empirical relations the required air cooling velocity is estimated. The required air velocity could also be estimated through the CFD model by including a combustion model and audit whether the engine is sufficiently cooled. However the cooling mechanism of an internal combustion engine includes an oil cooler and cooling fins, these components are difficult to implement and would yield a high computational cost. Furthermore, the size of the mesh is limited by a student license which allows a grid of maximum 512,000 cells. The required cooling air velocity is thus estimated through empirical models. The maximum allowed grid size of 512,000 cells does not further limit or affect the CFD model and set-up.

Nonetheless, the error induced by not including the fins and oil cooler may be estimated. Consequently the computed cooling air velocity can be compared to the results from the empirical model. One can set up a combustion model in Fluent, design the cylinder and cylinder head and subsequently compute the expected error by not including the cooling fins and oil cooler to observe whether the air flow provides for sufficient cooling. Fluent assumes that when hydrogen mixes with air, the mixture ignites when a combustion model is enabled. A hydrogen leak thus cannot be modelled when the combustion model is enabled, therefore two separate models are set up. The models have the same CAD model but differ in a few settings. The differences in set-up are further elaborated upon in Appendix A. The models will be respectively referred to as the energy balance model and the hydrogen diffusion model.

Note, elements may still be designated as a constant heat source in the hydrogen diffusion model. The dispersion of heat can thus be modelled through the hydrogen diffusion model. Heat sources such as the cylinders, dynamometer and lamps are designated as a constant heat source generator. The heat generation by a dynamometer and lights are simple to estimate. The heat generation of an internal combustion engine is complex however, a combustion cycle comprises of four strokes and does not generate heat at a constant rate. Therefore, as aforementioned, a separate energy balance model is developed to analyse whether the fan provides sufficient cooling for the engine cylinders.

In addition, the heat balance is not modelled through the energy balance model for each model as consequently a separate simulation must be run for the hydrogen leak and dispersion of heat. The heat balance and diffusion of hydrogen are modelled in the same simulation to save time.

The total temperature rise cannot be accurately modelled in the CFD model due to the complexity of the cooling mechanism and the limitation of a student license in ANSYS (Analysis System) Fluent. The dispersion of heat is modelled with underestimated

temperatures as the cooling fins and oil cooler are not included. The error must be estimated as the absolute temperature will be underestimated. One may compute the buoyancy velocity of warm air to observe how much it increases or decreases by varying temperature. If proven the buoyancy velocity of warm air does not change much due to a small rise in temperature, the model remains an effective tool to observe whether in local regions warm air accumulates.

5.2.1 Hydrogen diffusion model

The hydrogen diffusion model is the principal model. A hydrogen leak will be simulated along with the heat balance and consequently the diffusion of hydrogen and temperature profile are analysed. The dispersion of heat will be simulated by designating each heat source as a constant heat generator as aforementioned. Note the absolute temperature rise is incorrect as the convective heat transfer of the engine is underestimated.

The ventilation system must be designed such that the temperature limit in the test cell is not exceeded and hydrogen is disposed of as effectively as possible. The CAD model will include a hydrogen leak model which conveys hydrogen into the test cell.

5.2.2 Energy balance model

The energy balance model is a secondary model which has the purpose of comparing the cooling air velocity obtained in CFD to the one obtained through the empirical model.

A combustion model cannot be implemented in the hydrogen diffusion model as Fluent assumes a hydrogen-air mixture would instantaneously ignite. The cylinders are designated a constant heat source in the hydrogen diffusion model, while in the energy balance model, combustion occurs within the cylinders. One may presume the air cooling velocity may also be verified through the hydrogen diffusion model. However, since the engine has four strokes, the precise error of designating the heat generation in the cylinders as a constant heat source cannot be estimated. Therefore a second model, which includes a combustion model is developed. The results of the energy balance model are not utilised for the optimisation of the ventilation system. It is solely a means to verify the cooling air velocity which is computed through the empirical model.

Chapter 6

Empirical Model Energy Balance

Air-cooled engines are generally tested in hangar-type buildings to cope with the high thermal load. The temperature rise in the test cell may entail issues as components include a maximum operating temperature.

In this chapter, the heat released by the internal combustion engine during experiments is estimated along with the cooling air velocity. Furthermore a duct system and ventilation fans are selected, which are able to effectively dispose of the excess heat.

6.1 Assessment engine air cooling

The engine requires sufficient cooling, the inside wall temperature in a combustion chamber may rise up to a temperature of 873 K (Gibson, 1919). High wall temperatures may cause engine knock or detonation within the combustion chamber which is detrimental for the efficiency of the engine (Sagar and Agarwal, 2018). Furthermore, materials expand on prolonged contact with the high flame temperatures. Gibson (1919) mentions that an expansion in one direction of 1/250 of the cylinder thickness may be enough to permanently damage the engine. Cooling prevents distortion and expansion of the engine, although the engine may not operate too cold either. Higher temperatures entail a higher efficiency as the flame ignites more rapidly, delaying the optimum spark ignition timing and increasing the overall maximum pressure in the combustion chamber (Verhelst et al., 2009).

6.1.1 Engine cooling empirical approach

The required air flow velocity to cool the engine cylinders is estimated through an empirical model. The method yields an initial guess rather than an accurate measure due to the following assumptions.

- The cylinder itself is considered to be a smooth surface, hence no cavities in the geometry are accounted for. The model will overestimate the required air velocity as the actual surface area of the engine is larger due to protrusions in the geometry. The fin area will be accounted for however, this rather refers to additional material on the outer surface of the cylinder such as bearings.

- The fin area is approximated by assuming an average length in the longitudinal and lateral direction. Fins vary in length along the cylinder and the surface area is difficult to compute. In addition, the spacing between two adjoining cylinders is

limited as internal combustion engines are designed to be as compact as possible. Fins in longitudinal direction are limited in length due to the adjoining cylinders. Fins extend further down and up in lateral direction as there is sufficient space. The fin area is approximated as rectangular plates, the method to estimate the fin surface area is illustrated in Figure 6.1.

- The air flow velocity and air temperature are assumed to be constant along the fins. The flow velocity decreases slightly due to friction and does not strike each side of the cylinder with the same velocity. Particularly the bottom plate of the cylinder receives less direct air. Martyr and Plint (2012) observe the heat loss of the bottom horizontal plate to be approximately half of the upper horizontal plate. In addition, the temperature of the incoming air velocity increases along the surface area as heat is conveyed from the engine outer surface to the incoming air stream. Subsequently the temperature difference between the engine and air velocity decreases entailing a decrease in heat transfer coefficient along the engine surface area. Furthermore, the surface temperature is assumed to be identical across the surface. An average heat transfer coefficient will be computed through an empirical model to minimise the error. It will either entail a slight overestimation or underestimation.

- Heat is conveyed to the engine block through conduction, which is not accounted for in this method, entailing an overestimation of the required cooling air velocity.

- Humidity effects are not accounted for yielding a slight overestimation or underestimation.

The following approach is utilised to estimate the required air velocity,

Step 1: Estimate the heat transfer coefficient

Step 2: Estimate the total thermal load (Equation 4.1)

Step 3: Select the ambient temperature

Step 4: Determine the total surface area (including the fin area)

Step 5: Calculate the fin efficiency

Step 6: Estimate the average surface temperature of the piston engine

Step 7: Calculate the cooling air velocity

In Table 6.1 summarises the required parameters to obtain an initial guess of the cooling air velocity.

Table 6.1: Variables test cell environment to compute the required air velocity.

Parameter	**Value**	**Parameter**	**Value**
$T_{environment}$	298 K	$D_{exhaust}$	0.08 m
$T_{cylinder\ head}$	453 K	$h_{wall\ test\ cell}$	25 $W/m^2 \cdot K$
P_{engine}	149.14 kW	$T_{test\ cell}$	308 K
p_0	101,325 Pa	$T_{cell\ wall}$	303 K
$R_{specific}$	287 $J/kg \cdot K$	L_{engine}	0.78 m
C_p	1,001 $J/kg \cdot K$	W_{engine}	0.87 m
T_{engine}	453 K	H_{engine}	0.491 m
ϵ_{engine}	0.9	$W_{test\ cell}$	2.44 m
$T_{exhaust}$	873 K	$H_{test\ cell}$	2.59 m
$L_{exhaust}$	1.2 m	$L_{test\ cell}$	6.10 m

The heat transfer equation is as following,

$$Q = h \cdot A \cdot (T_s - T_a) \tag{6.1}$$

The ambient temperature (T_a), surface temperature (T_s), heat transfer coefficient (h) and the respective surface areas (A) must be solved for. In literature, several empirical equations are suggested to estimate the heat transfer coefficient.

The first empirical equation is suggested by Schey and Biermann (2020). The equation is deduced from a wind tunnel experiment with non-turbulent air flow. Varying air mass flow rates are directed over a cylinder with a bore diameter of 114.3 mm and a fin pitch of 7.5 mm. The cylinders were heated by an electrical heating unit. The researches observe an optimal cooling air flow velocity of 21.9 m/s.

The second relation is proposed by Gibson (1919), various experiments with aircraft engines were performed with air velocities between 8.9 m/s and 26.8 m/s. The bore diameter varied from 31.75 mm to 95.25 mm, with power ratings ranging from 80 kW to 150 kW. Gibson (1919) performed experiments with copper fins. It was observed there is only a slight difference in dissipation coefficients by comparing a few of the results with aluminium alloy fins. Gibson (1919) explicitly mentions that the empirical relation can be used as well for fins with aluminium alloys. Fin lengths vary from 16 mm to 41 mm with pitches ranging from 4 mm to 19 mm.

The third equation is suggested by Magarajan et al. (2012) and is deduced from experimenting with motorcycle engines. Fins of motorcycle engines usually have a larger pitch (10 - 20 mm) and therefore might be slightly less accurate. All three empirical methods are deduced from tests with induced-draught fans. In the test cell forced-draught fans will be utilised to cool the cylinders, which entail more turbulence and thus a higher heat transfer coefficient. This induces an error which will be further

treated in Section 6.1.2.

The three empirical equations to estimate the heat transfer coefficient are as follows,

$$\mathrm{h}_1 = (2.47 - \left(\frac{2.55}{f^{0.4}}\right) \cdot u^{0.9} + 0.0872 \cdot f + 4.31, \tag{6.2}$$

$$\mathrm{h}_2 = u^{0.71} \cdot 2.11 \cdot f^{0.44} \cdot L_{\mathrm{fin}}^{-0.14}, \tag{6.3}$$

$$\mathrm{h}_3 = 241.7 \cdot \left(0.0247 - 0.00148 \cdot \frac{L_{\mathrm{fin}}^{0.8}}{f^{0.4}}\right) \cdot u^{0.73} \tag{6.4}$$

With f the fin pitch, h the heat transfer coefficient and u the velocity. The empirical equation of h_2 is selected as the empirical relation of Gibson (1919) is deduced from testing with aircraft engines. Nonetheless, the result is compared to the alternative heat transfer coefficients as the paper is slightly outdated and the fins on the Lycoming engine are more efficient. As mentioned in the paper, the minimum fin pitch that is tested with is 4 mm, smaller fin pitches were not possible at the time. The production of the IO-360 series began in 1955 (Lycoming Manual, 2005), meaning smaller pitches were possible and thus the fins are more efficient. The actual error is difficult to determine as the smaller pitches raise the possibility to decrease the fin length and thus the surface area and mass. It does not necessarily imply the required cooling velocity is reduced.

It can be noted that the heat transfer coefficient depends on the incoming cooling air velocity. Hence, the velocity must thus be solved for through an iterative process. Table 6.3 summarises the results which one may find at the end of this section.

Subsequently, the ambient temperature and surface temperature of the engine are estimated. By preference, the test cell can be operated continuously, regardless of the weather conditions. A warm summer day constraints the test cell the most. An ambient temperature of 303 K is chosen to model for the worst case, which represents a warm summer day.

The empirical model approximates the heat release of one singular cylinder. Hence, the average surface temperature equals the average temperature of the engine cylinder. To estimate the surface temperature of the cylinder the following two cooling mechanisms must be accounted for.

The first cooling mechanism are the fins attached to the outer surface of the cylinder. A varying fin area along the outer surface of the cylinder entails disproportionate cooling, and therefore a temperature gradient. In addition, some of the heat conveys to the engine block causing the temperature at the base of the cylinder to decrease.

Note, the base of the cylinder (piston and crankcase) is cooled by oil. Oil is essentially the primary cooling mechanism of the cylinder, accounting for approximately 80 % of the total cooling (Martyr and Plint, 2012).

Both mechanisms induce a temperature gradient along the cylinder barrel which cannot be accounted for and thus induces an unknown error. Ultimately, a temperature of 393 K is chosen as literature suggest the cylinder head temperature has to be maintained at ± 453 K. A temperature of 393 K is decided upon as Gibson (1919) reports this to be the mean value of the cylinder barrel with a cylinder head temperature of 453 K during the wind tunnel experiments.

Step four includes estimating the surface area of the cylinder. The following table summarises the dimensions of one cylinder (Lycoming Manual, 2005).

Table 6.2: Engine data Lycoming IO-360-A1B6 (Lycoming Manual, 2005).

Parameter	**Dimension**	**Parameter**	**Dimension**
Bore	135 mm	n_{fins}	37
Stroke	111 mm	$L_{fin\ longitudinal}$	14.4 mm
Wall thickness	44 mm	$L_{fin\ lateral}$	35 mm
Fin thickness	22 mm	$k_{aluminium\,alloy}$	151 $W/m^2 \cdot K$
Fin pitch	3.5 mm	$L_{cylinder}$	327 mm

The area of the cylinder without fins is approximated as,

$$S_{cylinder} = (2 \cdot (R_{cylinder} + 2 \cdot t_{wall\,thickness})) \cdot \pi \cdot L_{cylinder} \tag{6.5}$$

The fin surface area must be estimated following the computation of the cylinder surface area. The fin data presented in Table 6.2 are average fin lengths in lateral and longitudinal direction (fin lengths vary along the length of the cylinder).

Figure 6.1 shows a simplified schematic of the fin geometry. In the left figure the dimensions of the cooling fin and cylinder are displayed while in the figure on right it is presented how the surface area of the fins is approximated. Starting with the left figure, the inner circle represents the combustion chamber, with length A resembling the bore diameter and length B being the wall thickness of the cylinder. Furthermore, length C equals the lateral fin length and D the longitudinal fin length. The right figure illustrates how the fin surface area is approximated. The fin is separated into two rectangles, one in lateral direction and one in longitudinal direction. The blue or upper rectangle is the cooling fin in lateral direction and the rectangle below or the blue rectangle is the cooling fin in longitudinal direction. Note two blue rectangles and two red rectangles can be made on one side of a fin.

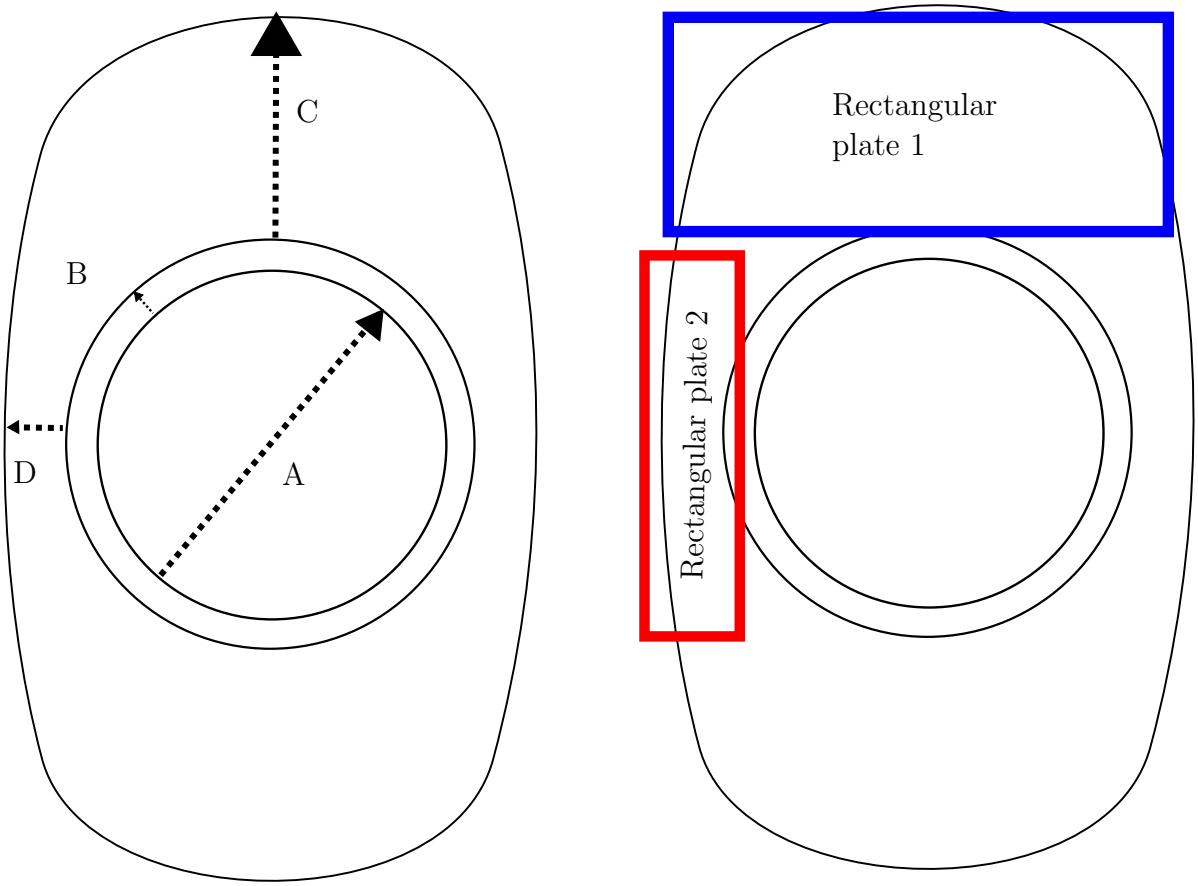

Figure 6.1: Simplified schematic of the fins circumventing the cylinder, note the dimensions are not scaled to proportion of the cylinders of the Lycoming engine.

The area of the rectangle in lateral direction may be approximated as,

$$A_{\text{fin, lateral}} = (D_{\text{bore}} + 2 \cdot H_{\text{fin longitudinal}} + 2 \cdot t_{\text{wall}}) \cdot H_{\text{fin, lateral}} \cdot 2 \cdot 2 \cdot 37. \tag{6.6}$$

The rectangle in longitudinal direction equals,

$$A_{\text{fin, longitudinal}} = (D_{\text{bore}} + 2 \cdot t_{\text{wall}}) \cdot H_{\text{fin, longitudinal}} \cdot 2 \cdot 2 \cdot 37. \tag{6.7}$$

Note the area of each plate is multiplied by two twice. Once as the fin surface area has two rectangles in lateral direction and two in longitudinal direction as shown in Figure 6.1. It is furthermore multiplied by two once more as each fin plate has a front and a back side. Subsequently, the sum is multiplied by 37 as the cylinder encompasses approximately 37 fins.

The area of the side walls are neglected as the thickness of each fin is only a fraction of the fin width and height.

The temperature at the tip of the fin is lower than the temperature at the base of the fin, the heat transfer coefficient decreases with increasing fin length and hence the efficiency decreases. Often the larger and thicker the fin, the lower the efficiency. The efficiency has to be estimated separately for the lateral and longitudinal direction. To estimate the fin efficiency, the fin parameters must be determined. The perimeter of one fin in lateral direction equals,

$$\mathscr{P}_{\text{lateral}} = ((\text{D}_{\text{bore}} + 2 \cdot \text{H}_{\text{fin longitudinal}} + 2 \cdot \text{t}_{\text{wall}}) + t_{\text{cylinder wall}}) \cdot 2, \tag{6.8}$$

and in longitudinal direction,

$$\mathscr{P}_{\text{longitudinal}} = ((\text{D}_{\text{bore}} + 2 \cdot \text{t}_{\text{wall}}) + t_{\text{cylinder wall}}) \cdot 2. \tag{6.9}$$

To proceed, the base surface area of the fin must be determined. The following steps are computed separately for the fins in lateral direction and fins in longitudinal direction.

$$\text{A}_c = \mathscr{P} \cdot t_{\text{fin}} \tag{6.10}$$

The fin parameter β can then be solved for,

$$\beta = \sqrt{\frac{h \cdot \mathscr{P}}{k_{\text{aluminium}} \cdot A_c}}. \tag{6.11}$$

Multiplying β by the respective fin lengths yields the second fin parameter,

$$\chi = \beta \cdot L_{\text{fin}}. \tag{6.12}$$

Ultimately, the fin efficiency can be determined through Equation 6.13,

$$\eta_{\text{fin}} = \frac{1}{\chi} \left(\frac{e^{2 \cdot \chi} - 1}{e^{2 \cdot \chi} + 1} \right). \tag{6.13}$$

As aforementioned in Chapter 4, Martyr and Plint (2012) observe that the heat released due to convection approximates 0.9 kW/kW for an air-cooled internal combustion engine without oil cooling. An oil cooler disposes of approximately 80 % of the heat within a cylinder. The thermal load of one cylinder equals,

$$Q_{\text{cylinder}} = \frac{P_{\text{engine}} \cdot 0.9 \cdot 0.2}{4}. \tag{6.14}$$

The equation is divided by four as the Lycoming engine includes four cylinders. With a maximum engine power rating of 149.14 kW, the heat release of one cylinder equals 6,750 W. The heat release of one cylinder is set equal to the sum of the Q_{lateral}, $Q_{\text{longitudinal,upper}}$ and $Q_{\text{longitudinal,bottom}}$, with Q_{lateral} equal to,

$$Q_{\text{lateral}} = h_{\text{lateral}} \cdot (A_{\text{base}} + A_{\text{fin lateral}} \cdot \eta_{\text{fin lateral}}) \cdot (T_{\text{surface}} - T_{\text{ambient}}), \tag{6.15}$$

and $Q_{\text{longitudinal,upper}}$ equal to,

$$Q_{\text{longitudinal,upper}} = h_{\text{longitudinal}} \cdot (A_{\text{base}} + A_{\text{fin longitudinal}} \cdot \eta_{\text{fin longitudinal}}) \cdot (T_{\text{surface}} - T_{\text{ambient}}). \tag{6.16}$$

As the bottom part of the cylinder is not in direct contact with the incoming cooling air velocity, the convective heat transfer is approximately half of the upper part of the cylinder (Martyr and Plint, 2012),

$$Q_{\text{longitudinal,bottom}} = \frac{Q_{\text{longitudinal,upper}}}{2}. \tag{6.17}$$

The sum must then be divided by the thermal load and iterated until the fraction equals one.

$$\frac{Q_{\text{lateral}} + Q_{\text{longitudinal,upper}} + Q_{\text{longitudinal,bottom}}}{Q_{\text{one cylinder}}} = 1 \tag{6.18}$$

Solving the steps above yields the results summarised in Table 6.3.

Table 6.3: Summary of fin parameters in lateral and longitudinal direction for one cylinder.

Parameters lateral	**Value**	**Parameters longitudinal**	**Value**
$A_{\text{one cylinder}}$	0.9 m^2	$A_{\text{one cylinder}}$	0.32 m^2
$A_{\text{base cylinder}}$	0.084 m^2	$A_{\text{base cylinder}}$	0.084 m^2
$\mathscr{P}$	0.35 m	$\mathscr{P}$	0.29 m
A_c	7.65E-4 m^2	A_c	6.33E-4 m^2
β	13.23	β	14
χ	0.46	χ	0.21
η_{fin}	93.5 %	η_{fin}	98.5 %
h	58.13 $W/m^2 \cdot K$	h	65.45 $W/m^2 \cdot K$
Q	4,761.73 W	Q_{upper}	1,324.44 W
		Q_{bottom}	662.22 W
General data			
Parameter	**Value**	**Parameter**	**Value**
T_{ambient}	303 K	T_{surface}	393 K
Thermal load one cylinder	6,750 W	$u_{\text{cooling air}}$	27.5 m/s

For a velocity of 27.5 m/s, the other two empirical relations yield heat transfer coefficients of 62.46 $W/m^2 \cdot K$ (h_1) and 64.26 $W/m^2 \cdot K$ (h_3) respectively.

6.1.2 Engine air cooling experiments in literature

Modelling the cooling of the engine in detail in the CFD model is not feasible. Estimating the required cooling velocity is a means to approximate the flow field in the test cell to consequently analyse the dispersion of heat and diffusion of hydrogen. Simulating the cooling system is difficult through CFD as fins have to be included, an accurate combustion model, a 3D-model of the engine requires to be designed and oil cooling has to be accounted for. A simplified model of the engine will be put into the CFD model such that it can be observed where heat and hydrogen accumulate in the test cell environment. The velocity of the cooling air has to be known however as it influences the flow field inside the container. The air velocity estimated through empirical models is compared to tests performed in literature.

Gibson (1919); Reddy Kummitha and Reddy (2017); Schey and Biermann (2020) have published plenty of data of required air cooling velocities with respect to the fin dimensions, engine power rating and cylinder bore diameter. In literature, air cooling velocities

of 0 to 60 m/s are reported for various engines. Gibson (1919) presents Table 6.4 for air-cooled aircraft engines.

Table 6.4: Relation between the cooling air velocity and bore diameter of a cylinder.

$\mathbf{D_{bore}}$ **(mm)**	$\mathbf{u_{air\,cooling}}$ **(m/s)**
50.8	13.41
76.2	17.88
101.6	22.35
152.4	31.29
203.2	40.23

The Lycoming engine includes cylinders with a bore diameter of 111.35 mm. Interpolating yields an air cooling velocity of 24.12 m/s, slightly lower than the value obtained through the empirical model. However, the test is performed with an ambient temperature of 295 K, unlike the empirical method which applies an ambient temperature of 303 K. The empirical model yields an air velocity of 24.25 m/s with an ambient temperature of 295 K. A difference is expected as the fin dimensions differ. In addition, the base area of the cylinder and the side walls of the fin surface area (where the cylinder connects with the engine block) are not accounted for in the empirical model. The actual surface area is therefore underestimated and hence the velocity is overestimated.

Two factors are still neglected of the obtained air velocities above, which must be accounted for.

The tests are performed with an ambient air temperature of 295 K and at maximum power settings for a prolonged period of time. The fan supplies sufficient cold air when the temperature of the cylinder head can be maintained at a temperature of approximately 453 K. However, in practise this is not necessary as engines often do not operate at maximum power output for extended periods. During testing the engine is not required to run for hours at wide open throttle. Nevertheless, operating at maximum power should still be a possibility for non-continuous operation. The maximum cylinder-head temperature allowed for shortened time periods is 533 K. Martyr and Plint (2012) observe, through testing, an inverse proportional relationship between the permissible temperatures and velocity. By dividing the maximum permissible non-continuous cylinder-head temperature with the maximum continuous cylinder-head temperature and subsequently raise the velocity to the power of 1/0.4, the required air cooling velocity is obtained. The ratio for the Lycoming engine is 533 K/453 K = 1.18, thus the velocity must be multiplied by $1/1.18^2.5 = 1/1.51$. Reducing the velocities in Table 6.4 by the factor 1.51 yields an updated relation between the air cooling velocity and bore diameter of the cylinder. Table 6.5 presents the updated values of the relation between the two parameters.

Table 6.5: Actual required air cooling velocity with respect to the bore diameter at lower power settings.

$\mathbf{D_{bore}}$ **(mm)**	$\mathbf{u_{air\,cooling}}$ **(m/s)**
50.8	9.48
76.2	11.18
101.6	14.75

The required cooling velocity of the Lycoming internal combustion engine is reduced to 15.97 m/s. The fin dimensions of the tested engines differ from the Lycoming engine, an error in the range of 10 % to 20 % is plausible (Gibson, 1919). The error range is deduced from observing the variance of results from experiments with different engines.

Furthermore, Gibson (1919) induced an air flow in the wind tunnel by generating a pressure differential through installing induced-draught fans at the rear of the tunnel. Induced-draught fans invoke little turbulence in comparison to forced-draught fans. Forced-draught fan will cool the Lycoming engine in the test cell, entailing a higher convective heat transfer coefficient due to the increase in turbulence. Most tests performed in wind tunnels require minimum turbulence and therefore are equipped with induced-draught fans. Hence, the air velocity should further be divided by a factor to obtain a more accurate guess. Howbeit, one requires to solve the turbulence cascade for which no empirical equation is defined. 15.97 m/s is defined as the absolute upper limit whilst it is expected the required air cooling air velocity is lower.

Note that the cooling load depends on the mass flow rate as well. If the engine is cooled with a high incoming air velocity but a low mass flow rate, the engine will not be sufficiently cooled. Since the heat transfer is deduced from tests performed in wind tunnels, the duct or fan mounted above the engine should be of considerable size relative to the cylinder. However since the cylinders are relatively small and sizeable ventilation fans are already required due to the high required cooling air velocities, it is presumed the fans provide sufficient air mass to cool the engine.

The test cell is developed to be portable to raise the possibility of testing in either the neighbourhood of Deltion College or the TU Delft. A drawback however is, besides requiring intensive ventilation, the noise regulations the test cell has to comply to in various environments. Fans produce high noise levels which are a nuisance to the environment in the neighbourhood of the test location. The noise limits differ depending on the environment (industry, living space,...). It is apparent the lower the noise the fans produce, the simpler it will be the find suitable test locations. Most areas in the Netherlands impose a non-continuous noise limit of 65 - 75 dB. The maximum continuous noise limit is approximately 50 dB (Van Den Berg, 2007). A second constraint is the contents of the test cell. Possible test locations will be limited regardless of noise as

hydrogen is dangerous to experiment with. ATEX (ATEX = atmospheres explosible) is a French organisation which categorises the potential hazard of a test set-up. The higher the potential danger ATEX considers to test cell to be to its environment, the more limited the possible test locations will be.

6.2 Ventilation fan selection

Various classes of fans exist such as the centrifugal fan and axial fan. Axial fans are compact and thus convey more air mass flow for the same size. A drawback is that they do not cope well with high resistances to airflow (e.g. pressure losses induced by ducts). Centrifugal fans are more efficient and are able to operate at higher pressures (Martyr and Plint, 2012). Ducts will be designed for the test cell to reduce noise and to shield the test cell from poor weather conditions. Axial fans are selected to provide the high required air velocity and mass flow. The ducts may not be too long as otherwise the flow resistance is too large and the axial fans stall. The design of the ducts will be elaborated upon in Section 6.3.

One of the axial ventilation fans must function as cooling fan as well as it is cost-effective, efficient and entails less air recirculation. High air circulation may be an issue when heat or hydrogen is captured inside a flow field and cannot be disposed of to the environment. Furthermore, high air circulation entails turbulence and enhances the mixing of hydrogen with air.

Table 6.6 lists two of the axial fans offered by Induvac [1],

Table 6.6: Axial fans offered by Induvac.

Ventilator	**Type**	**Power (kW)**	**Rpm**	**Capacity (m^3/h)**	**Total pressure (mmH_2O)**	**Noise dB(A)**
U/EI-EIL 564	80B4	0.75	1,380	8,500-12,000	14-24	73.0
U/EI-EIL 715	100L4A	2.2	1,425	13,000-21,000	17-40	77.0

Induvac offers a wide range of axial fans, the above two are selected due to their compatibility with the requirements of the test cell container. Due to budget constraints (the collaborative group is offered a budget by the government, the group does not receive the grant if a specified minimum amount is not spent each year), ventilation fans have to be selected prior to testing. The fan model of the U/EI-EIL 564 and U/EI-EIL 715 is depicted in Figure 6.2, the base model of the two axial fans are the same. The U/EI-EIL 564 has an inner diameter of 560 mm while the U/EI-EIL 715 has an inner diameter of 710 mm. The inner diameter refers to the diameter of the model without casing.

[1] `https://induvac.com/nl/` [Retrieved 10.11.2020]

Figure 6.2: The base model of the U/EI-EIL 564 and U/EI-EIL 715.

The intention is to set up a ventilation system of four fans consisting of two different models for the following reasons. Axial fans produce noise in the range of 60 dB up to 100 dB. With noise related to the axial velocity squared induced by the fans, selecting four fans instead of two fans reduces the noise generated by the ventilation system. In addition, four ventilation fans add a higher degree of freedom in directing the air flow. Two fans must be installed on the roof, one for cooling the engine[2] and one for the disposal of hydrogen in the event of a leak. Two fans near the floor of the test cell are necessary as well. The Lycoming engine must initially operate with aviation gasoline for calibration. In addition, the test cell may be used for various other internal combustion engines operating on different fuels such as liquid natural gas. When a leak occurs with a liquid in the fuel pipe, it remains on the floor. Subsequently fumes evaporate which needs to be purged through fans near the floor of the test cell. An inlet ventilation fan near the floor furthermore directs heat and fumes towards the ambient air.

Fans mounted on the roof will entail higher duct losses as a rain cap is required to avoid the ingress of rain. The fans on the roof thus must be of higher capacity than the fans installed on the side walls. In addition, noise of the fans mounted on the ceiling propagates vertically upwards while the fans mounted on the side walls are a nuisance for the environment as noise subsequently propagates through the environment in horizontal direction. Hence, smaller ventilation fans on the side walls are a benefit in terms of noise.

Selecting the most suitable fan is a trade-off between noise generation and perfor-

[2]As aforementioned in Chapter 6, fins are optimised for cooling from above. Cooling from below is in theory an option as well but the engine is mounted on a motor stand. Therefore cooling from beneath the engine is excluded despite it being favourable for the disposal of heat and hydrogen.

mance. The U/EI-EIL 564 is selected to be mounted on the side walls as a result of its relative low noise level. With a surface area of 0.246 m^2 and capacity of 2.3 - 3.333 m^3/s, the axial air velocity is in the range of 9.3 - 13.38 m/s, depending on the pressure losses. Note the U/EI-EIL 564 does not cope well with large pressure losses and is likely to stall if mounted on the ceiling due to the pressure losses induced by the rain cap and duct. The U/EI-EIL 715 is larger and may be mounted on the roof. The capacity ranges between 3.6 m^3/s and 5.8 m^3/s with an axial velocity in the range of 8.87 m/s to 14.32 m/s.

The performance characteristics of the fans are presented in Table 6.7.

Table 6.7: Total pressure in relation to fan capacity for the U/EI-EIL 564 and U/EI-EIL 715 axial fans.

	Capacity (m^3/h)												
	8,500	9,000	9,500	10,000	11,000	12,000	13,000	14,000	15,000	16,500	18,000	19,500	21,000
Fan type	**Total pressure (mmH_2O)**												
U/EI-EIL 564	24	23	22	21	17	14							
U/EI-EIL 715							40	38	36	32	28	23	17

The units of total pressure of fans are often presented in mmH_2O (=9.806 65 Pa). The higher the total pressure loss, the higher the resistance to the flow and the lower the capacity. For instance, a ducting system with long straight sections, with multiple corners and a grid mounted on the inlet or outlet entails a large resistance to the incoming flow and hence yields high static and total pressure losses. Pressure losses are caused by friction along the boundary layer, energy is lost and thus the static and total pressure decrease across the duct. Each axial fan has a maximum resistance it is able to operate with, the fan stalls if the flow resistance is higher than 24 mmH_2O for the U/EI-EIL 564.

The total pressure in Table 6.7 is defined as the total pressure difference across the fan. High total pressures are paired with lower fan capacity. A low fan capacities entails that the total pressure at the inlet of the fan is reduced by the ducts and corners inflicting friction and thus yielding a higher total pressure differential across the fan boundary since the total pressure in front of the fan is reduced. However, the efficiency decreases due to the energy losses and thus the capacity decreases. Ducts may not be larger than they should be as it decreases the efficiency of the fan. The function of ducts is to protect the test cell environment from poor weather conditions and to reduce the noise produced by the fans. Researchers have demonstrated that noise can be reduced up to 6 dB with ducts of 2.6 m long (Martyr and Plint, 2012). The design of the ducts is further elaborated upon in Section 6.3.

The estimated required air cooling velocity is 15.97 m/s, while the U/EI-EIL 715 can offer a maximum inlet velocity of 14.03 m/s without ducts. However, the obtained value of 15.97 m/s is for an induced-draught fan for ambient air temperatures of 295 K and continuous economy cruise power settings. The engine may be tested at lower throttle settings and equivalence ratios, entailing lower cylinder temperatures. Withal the air flow will be guided through converging augmented ducts, meaning the flow is redirected through four converging channels to control the temperature and provide for equal cooling of the cylinders [3]. The axial velocity of the incoming cooling air must increase according to the Venturi effect with converging ducts. Hence the flow is directed through augmented ducts over the cylinders and subsequently warm air enters the test cell environment. Furthermore, it must be ensured that only the air entering through the ventilation fan mounted on the ceiling cools the engine. The optimal cylinder temperature becomes difficult to maintain and in all probability will wind up running too cold if the incoming air of the three remaining ventilation fans influence the cooling of the engine. Consequently, in some leakages hydrogen is pushed downwards and is not immediately disposed of to the environment.

The noise limit of the test cell is yet to be determined as it has to be set by a regulator of the city the tests are planned in. In the event the test cell is below the noise limit, a second cooling fan can be acquired to test the engine at higher power settings must the U/EI-EIL 715 not offer enough cooling power. High pressure axial fans of the same radii as the U/EI-EIL 715 (and the U/EI-EIL 564) are available on the market such as the ones offered by Sodeca which are shown in Table 6.8[4],

Table 6.8: Two high pressure axial fans offered by Sodeca.

Model	**Speed (Rpm)**	**Installed power (kW)**	**Maximum airflow (m^3/h)**	**Mass (kg)**	**Noise level (dB(A))[1]**
HTP-56-2T-10	2,920	7.5	25,500	147	89.0
HTP-71-4T-7.5	1,450	5.5	31,700	141	90.0

[1] The provider mentions the noise level is measured at an equivalent distance of twice the fan's span plus the diameter of the impeller, at a minimum of 1.5 m.

6.3 Ventilation system duct design

Ducts provide protection to bad weather conditions and are to function as silencers. As aforementioned, ducts induce static and total pressure losses as energy is lost due to

[3] This structure will not be included in the CAD model as it is too complex to include. Instead a fume hood will be designed which yields a similar effect on the flow field.

[4] `https://www.sodeca.com/` [Retrieved 15.01.2021]

friction along the boundary layer. Shortened ducts do not provide sufficient protection from poor weather conditions and do not reduce the noise, while long ducts decrease the efficiency of the axial fans. Furthermore, grids and corners induce higher losses than straight sections. Figure 6.3 depicts empirical loss factors which incur in ducts (Martyr and Plint, 2012).

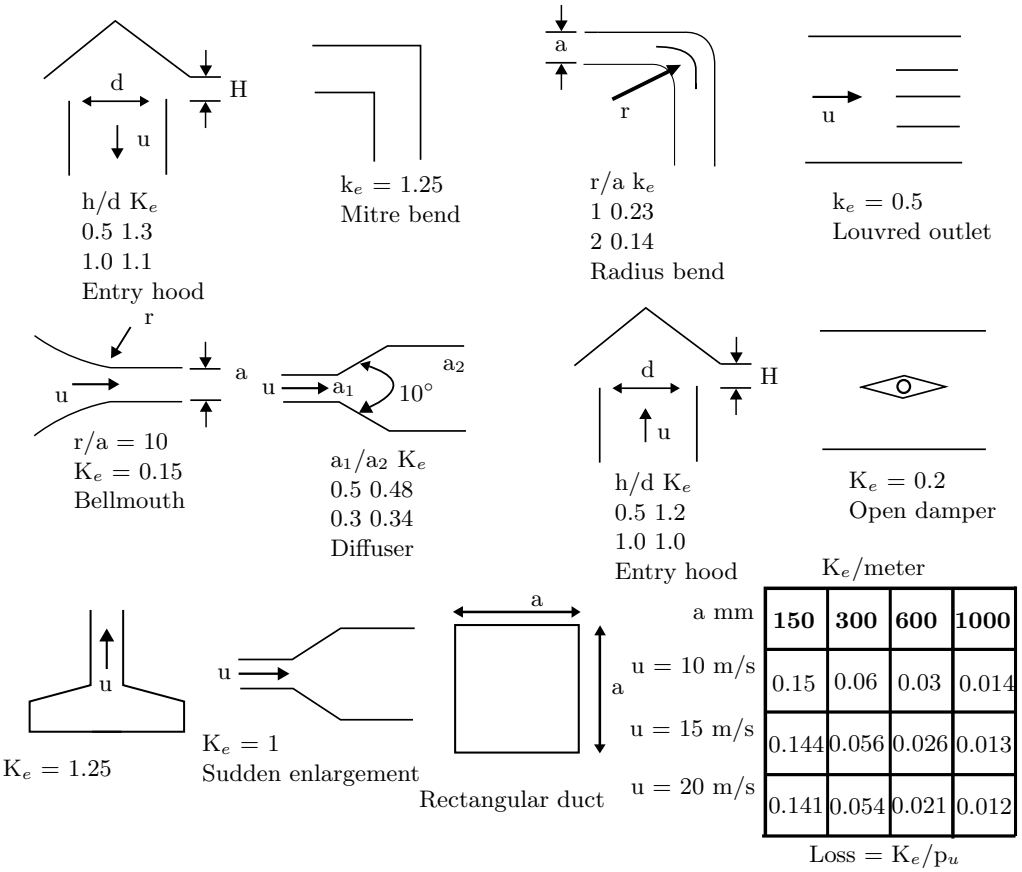

Figure 6.3: Empirical loss factors in ducts suggested by Martyr and Plint (2012).

K_e depicted in Figure 6.3 for each duct section is the loss factor. The lost factor must be multiplied with the dynamic pressure to obtain the pressure loss due to the specific section. In the right bottom corner a table is shown, the table displays the pressure losses per meter in a straight rectangular duct for a certain duct diameter in millimetre. For example, if the duct diameter is 150 mm and the velocity inside the duct is 10 m/s, the pressure losses induced by the straight rectangular section is $0.15 \cdot L_{duct}$.

A preliminary design of the ducts is illustrated in Figure 6.4. A definite detailed design of the ducts must be constructed at a further stage of the project. Preliminary calculations are performed to estimate the losses incurred by the ducts in this section. The capacity loss of the fans is estimated and therefore the mass flow rate through the channels and

air cooling velocity can be determined.

The direction of the air flow through the two ventilation fans mounted on the side of the walls is chosen arbitrarily. Note that four fans instead of two are depicted as in Figure 4.11. In Section 6.2 the choice is made to opt for four ducts. The ventilation set-up must still be optimised and the Figure 6.4 does not illustrate the final optimised design. The figure is depicted as a means to visualise the duct system and to comprehend the induced losses.

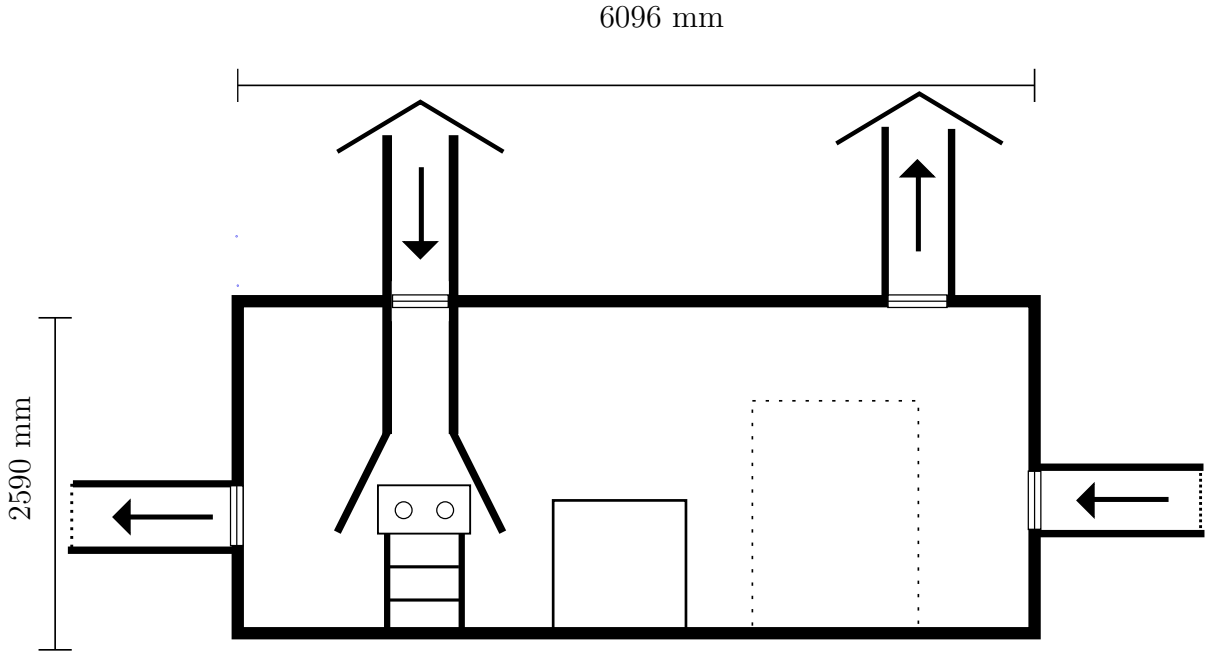

Figure 6.4: Preliminary illustration of the duct system of the test cell. The direction of the air flow of the two fans mounted on the side of the walls is set arbitrarily.

6.3.1 Inlet and outlet debris protection

External termination protects the test environment from ingress rain, snow, sand, dust particles, leaves et cetera. Motorised louvres can be mounted on the outer ends of the ducts in case of extremely poor weather conditions. A rain cap in the Netherlands should be sufficient to protect the components in the container. In Figure 6.4, rain caps may be noticed at the top of the roof ducts. The ducts near the side of the walls have dotted lines which resemble a louvre or a grid to prevent debris such as leaves to enter the test cell.

6.3.2 Duct silencers to reduce noise

Noise propagates to the outside environment through small gaps, ill-fitted doors and ventilation ducts, which are the largest pathways to the environment. Fan noise varies by the square of the head pressure (change in static pressure across the fan) in isolation, meaning doubling the flow resistance yields a fourfold increase in noise (or 6 dB). Noise should increase due to the addition of ducts as ducts entail in theory flow resistance. However, a few solutions exist to attenuate the noise propagating through ducts, yielding a net decrease in sound power level.

Sounds attenuation is efficient for longer ducts, the standard length in industry is 2.4 m (Heinsohn, 1991). For the initial guess of the pressures losses incurred by the duct, assuming a duct length of 2.4 m is adequate. Noise is reduced by implementing duct silencers or attenuators along the length of the duct. This method often entails roughening the surface of the ducts or perforating the duct surface. Wool encased ducts in perforated galvanised steel sheets attenuate noise, especially at frequencies of approximately 500 Hz and above (Martyr and Plint, 2012). With high speed axial fans frequencies will be high, and thus it becomes a powerful tool to reduce noise. A drawback is however the increased energy loss along the length of the ducts. The longer the duct, the greater the sound attenuation but the greater the loss in energy as well. Furthermore, directing noise vertically through roof mounted-stacks is a classical method to reduce nuisance.

The pressure losses in ducts relate to head velocity, surface roughness, size et cetera. Martyr and Plint (2012) observe losses are between 1 - 10 Pa/m for straight sections, with the larger number relating to smaller ducts[5]. Selecting the most optimal design is a compromise between noise, velocity and power loss. Doubling the air velocity by reducing the size of the duct by a factor two, increases the pressure losses by a factor four. The actual pressure losses will even be higher as a smaller duct size inclines higher friction losses. The sound level increases by approximately 18 dB with pressure losses increasing by roughly a factor of four. Therefore, air velocities should not be exceeding the maximum required air velocity as noise levels increase rapidly.

Heinsohn (1991) mentions attenuators are most efficient with an incoming air velocity of 12 m/s. This may be an extremely effective tool to reduce noise with an inlet air cooling velocity of maximum 15.97 m/s. Furthermore, head velocities should not exceed 20 m/s due to the high sound level and structural strength of the material. Velocities over 20 m/s are possible within ducts but only in ones that are specifically designed to deal with high velocities and higher pressure losses. Nonetheless, as the required cooling does not require to be that high, this should not raise any concerns. One has to note the noise levels in Table 6.6 and Table 6.8 are for the fans in isolation. Despite the attenuators and possibly directing the fan vertically upwards, converging channels

[5]In smaller ducts relatively more air is contact with the surface and therefore friction losses are higher

entail a higher dynamic pressure and therefore increased head pressure. Noise values may exceed the values presented in the two aforementioned tables despite the efforts to minimise it. Europe (Control of Noise at Work regulations 2005[6]) has set the regulations regarding maximum exposure level to noise for employers. The regulations are displayed in Table 6.9.

Table 6.9: Maximum exposure limits in Europe (Martyr and Plint, 2012).

	Daily or weekly exposure (dB)	**Peak pressure exposure (dB)**
Lower exposure action value	80	135
Upper exposure action value	85	137
Absolute exposure action value	87	140

The exposure limits can be interpreted as following, once the test cell exceeds the lower exposure action value, hear protection and training has to be provided to the operatives. If the upper exposure action value of 85 dB is exceeded, measures have to be taken to reduce noise and hearing protection is obligatory. The absolute exposure limit is the sound level to which no operative may be exposed to with hearing protection. Inside the test cell noise levels will exceed the above mentioned noise limits, therefore wearing hearing equipment is obligated if the test cell is entered[7]. Note, it does not mean the test cell may be put anywhere as long as it complies to the exposure limits presented in Table 6.9. Testing with hydrogen combustion at the location must be permitted as well.

6.4 Duct system energy losses

The losses inflicted by the ducts must be estimated. Note that in Figure 6.3, a loss factor of 0.5 is defined for a louvred outlet. For the louvred inlet no example is given as loss factors widely vary depending on the angle and amount of louvre blades. Pressure losses induced by most louvred inlets are too high for an axial fan to cope with, therefore it may be a better option to mount a grid on the inlet duct to intercept leaves or other debris. Louvred inlets are generally utilised in urban environments as they reduce noise up to 15 dB across a duct of 0.6 m (Gibson, 1919). The trade-off of increasing pressure loss to noise reduction is often made in inhabited spaces to reduce noise below 50 dB. However near a test cell environment, noise limits are less restrictive.

The grid pressure loss depends on the density of the structure. For ease of calculation, an inlet pressure loss factor K_e of 0.5 is assumed such that it matches the outlet loss factor. No data is found on loss factors induced by grids. It may be possible if

[6] `https://www.hse.gov.uk/NOISE/regulations.html` [Retrieved 28.03.2021]

[7] In context of noise, in all probability the test cell may not be entered at all in context of safety.

the loss factor is higher, or the duct design is altered and pressure losses increase, a different set of ventilation fans must be selected. Nonetheless, the ventilation mass flow rate should remain in the region of the current mass flow in the test cell. Therefore it will not affect the results of the CFD analysis. Table 6.10 displays the pressure losses in the duct which are estimated through Figure 6.3 and Figure 6.4.

Table 6.10: Estimated pressure losses induced by the preliminary duct system design of the test cell.

Duct section	**Type**	**Velocity (m/s)**	**Velocity press. (Pa)**	**Fitting loss factor (Ke)**	**Press. drop (Ke/m)**	**Length (m)**	**Press. loss (Pa)**
Inlet forced draught-fan, mounted on side wall							
Circular duct	U/EI-EIL 564	11.84	85.84		0.02	2	3.43
Inlet grid	U/EI-EIL 564	11.84	85.84	0.5			42.93
Inlet forced draught-fan, mounted on ceiling							
Entry hood	U/EI-EIL 715	12.05	88.93	1.1			97.8
Circular duct	U/EI-EIL 715	12.05	88.93		0.02	3.2	5.69
Diffuser	U/EI-EIL 715	12.05	88.93	0.48			42.68
Outlet induced draught-fan, mounted on side wall							
Circular duct	U/EI-EIL 564	11.84	85.84		0.02	2	3.43
Louvred outlet	U/EI-EIL 564	11.84	85.84	0.5			42.68
Outlet induced draught-fan, mounted on ceiling							
Circular duct	U/EI-EIL 715	13.1	105.7		0.02	2	4.23
Discharge hood	U/EI-EIL 715	13.1	105.7	1.0			105.7

Note that the calculation must be iterated a few times. The duct induces a pressure loss, inducing a decrease in velocity, which in turn entails a decrease in dynamic pressure and hence the pressure loss decreases. The duct losses are estimated with rectangular

ducts instead of circular ducts since the pressure loss coefficient of a circular duct is not defined in (Martyr and Plint, 2012). Circular ducts induce less pressure losses for the same surface area. Circular ducts suit the test cell better than rectangular ducts as noise pollution is less and pieces fit together well. Rectangular ducts occupy less space as they may be shorter, however for the test cell environment that should not be a factor.

The pressure losses in the duct must be summed up along with the initial losses (efficiency losses) provided by the manufacturer. The accumulative pressure losses of the four ventilation fans are summarised in Table 6.11.

Table 6.11: Fan total pressure losses induced by the duct and fan itself.

	Manufacturer pressure losses (Pa)	**Duct pressure losses (Pa)**	**Accumulative pressure losses (Pa)**
U/EI-EIL 564 inlet fan (side wall)	140	46.36	186.36
U/EI-EIL 564 outlet fan (side wall)	140	46.36	186.36
UU/EI-EIL 715 inlet fan (ceiling)	170	146.17	316.17
U/EI-EIL 715 outlet fan (ceiling)	170	109.93	279.93

Table 6.12 depicts the performance of each fan with duct losses included. Note the larger fans are mounted on the ceiling as they are able to cope with larger pressure losses.

Table 6.12: Ventilation fan performance including duct losses.

Fan type	**Velocity (m/s)**	**Volume flow (m^3/s)**
U/EI-EIL 564 inlet	11.84	2.92
U/EI-EIL 564 outlet	11.84	2.92
U/EI-EIL 715 inlet	12.05	4.58
U/EI-EIL 715 outlet	13.15	5

The ventilation fans will communicate with each other through frequency regulators to maintain the pressure in the test cell environment approximately 1 bar. The capacity of

both U/EI-EIL 715 are set at $4.58\,m^3/s$. Hence, the ventilation load in the test cell is $\approx 7.5\,m^3/s$.

The velocity of the cooling air will be $12.05\,m/s$ if the U/EI-EIL 715 is to function as cooling fan with duct losses included[8]. Consequently, the noise produced will approximately be 76 dB. Presuming the velocity must not be further increased to cool the engine sufficiently, the limits imposed by the Control of Noise at Work Regulations of 2005 are attainable (Dagdougui et al., 2018). Attenuators or duct silencers might not be necessary and thus duct losses are not expected to increase much further than documented in this section. Nonetheless, literature suggest attenuators can reduce noise up to 10 - 15 dB/m for ducts with a diameter of 500 mm if an issue arises.

The maximum ambient temperature is allowed to be 312 K during maximum throttle settings, as the ventilation fans have a maximum operating temperature of 323 K. The ventilation system should provide for enough cooling of the test cell unless a heat wave is present since the average temperature in the Netherlands is between 278 K and 288 K. The absolute maximum allowed ambient temperature for test experiments is 300 K if no oil cooler were mounted on the engine with the current ventilation set-up, hence testing days would be limited[9] .

The maximum operating temperature of sensors are generally approximately 343 K (Hübert et al., 2014). Furthermore, it has to be noted that the flash point of jet-A and kerosene is ≈ 311 K. Sufficient flammable vapour is present to induce an ignition once the temperature in the test cell exceeds 311 K during experiments with jet fuel or kerosene. Test cells are designed such that the lower temperature threshold of 311 K is not exceeded. The engine will operate with aviation gasoline to test the performance and to audit whether the internal combustion engine has degraded during early testing. The temperature inside the test cell must thus be monitored well.

6.5 Combustion chamber heat generation

A second aim of the CFD analysis is to indicate whether the engine cylinder head temperature is maintained at the desired temperature and whether the estimated air cooling velocity is correct. The energy balance model is a means to verify the estimated average temperature rise and cooling air velocity obtained through the empirical methods.

The cylinder head temperature must be maintained at a temperature of 453 K during cruise economy performance. Furthermore, the maximum cylinder head temperature is 533 K and maximum continuous cylinder head temperature is 477 K (Lycoming Manual, 2005). These temperatures may be reached during peak power settings. Figure 6.5

[8]Without the inclusion of converging ducts.

[9]In reality the limit would even be lower since the convective heat transfer of the sun on the wall of the container would be higher than assumed in this method.

shows the equivalence ratio with respect to percent of best power[10], specific fuel consumption, cylinder head temperature and exhaust gas temperature. The range of the economy and maximum power cruise settings is represented as well at the bottom of the graph. Best economy cruise is approximately attained at an equivalence ratio of 0.9 and max power cruise at 1.1 (Lycoming Manual, 2005).

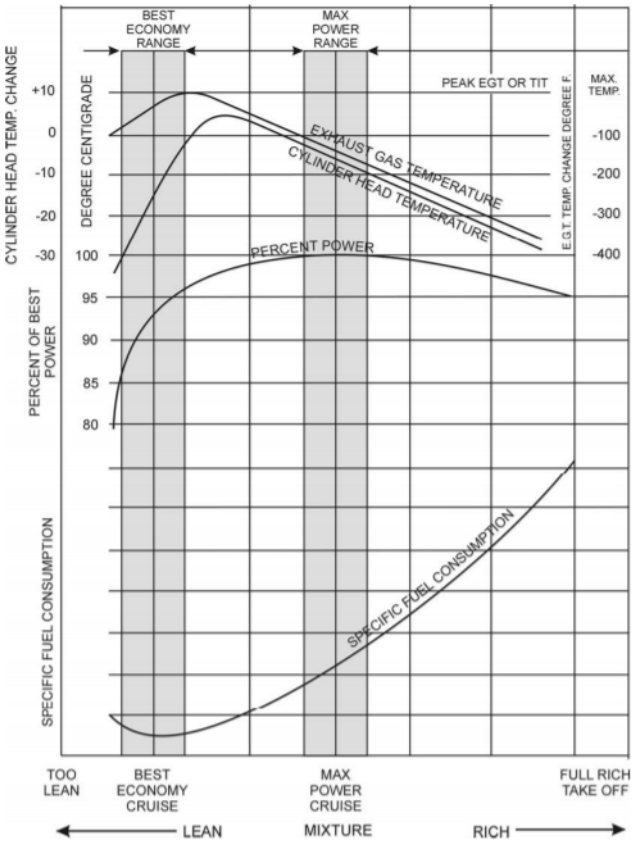

Figure 6.5: Equivalence ratio in relation to percent of best power, cylinder head temperature, specific fuel consumption and exhaust gas temperature (Lycoming Manual, 2005).

In practice, estimating the required engine cooling is not performed in CFD. Through textbook methods and literature research, the flow velocity and volumetric flow rate are estimated. In Section 6.1 the required ventilation volumetric flow rate and air velocity are determined through an empirical method. With an ambient temperature of 295 K, the required cooling air velocity equals 15.97 m/s. The cooling air offers according to the empirical model sufficient cooling such that the cylinder head is maintained at a

[10] At high altitudes air is thinner and therefore the maximum power decreases (mass flow of incoming air decreases). Best power refers to the maximum power achievable at the respective altitude, not the normal rated power of 149.14 kW.

temperature of 533 K at maximum throttle, or at 453 K at economy cruise settings (75 % power). However, the results must be verified since the empirical model is based on experiments with older engines and thus with less efficient fins.

The engine performance is simulated by developing a combustion model in ANSYS. Four combustion chambers are designed with each having a fuel and air inlet. The power settings can be varied by setting the inlet air and fuel. The temperatures within the combustion chamber are accurately simulated due to a built-in combustion model in Fluent. In the remainder of this section, the known errors are discussed.

6.5.1 Exclusion cooling fins in CFD

The cooling fins are not modelled as otherwise the computational cost would be too expensive. The surface area of the cylinder is therefore substantially lower. The additional surface area cooling fins form is, as estimated in Section 6.1, 1.2 m^2. One could add the surface fin area to the cylinder uniformly in radial direction in the CAD model as illustrated in Figure 6.6.

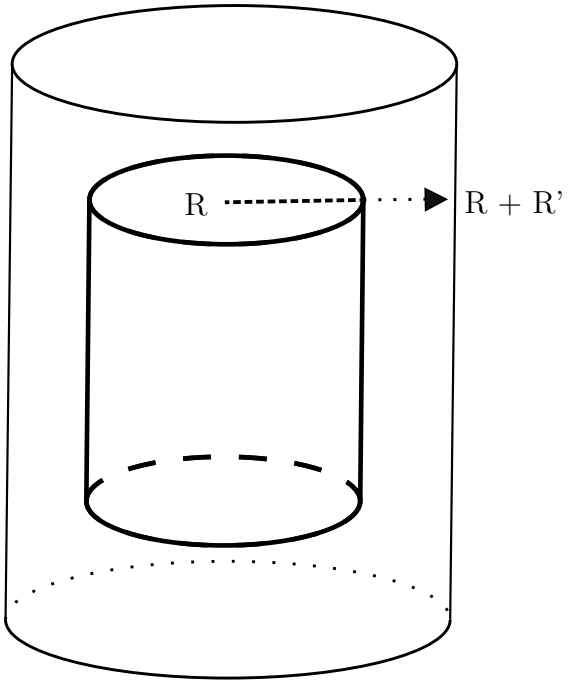

Figure 6.6: The cylinder without fins has a radius of R, and with fins R + R'.

A drawback of the method is however the added mass and size of the cylinder. The total surface area of one engine cylinder is the the surface area of the cylinder itself ($(\text{Circumference}_{\text{cylinder}} + 2 \cdot T_{\text{cylinder wall}}) \cdot L_{\text{cylinder}}$) plus the surface area of the fins. If the length of the cylinder is 0.327 m (Lycoming Manual, 2005), the radius of the cylinder requires to be 0.3 m. Ergo, the radius is increased by a factor six which affects

the downstream flow. Therefore the fin area is not added to the cylinder area in the CFD model.

6.5.2 Exclusion oil cooling in CFD

Oil captivates approximately 80 % of the heat released by an internal combustion engine. Including oil cooling in the CFD model is complex and therefore not included in the model. The walls in the combustion chamber attain approximately temperatures of 873 K (Martyr and Plint, 2012). Since the conduction of aluminium alloy is $151\,\mathrm{W/m^2 \cdot K}$, and the thickness of the cylinder wall is 4.4 mm, the temperature of the outer surface of the cylinder barrel may be assumed to heat up to 873 K as well if no oil cooling is applied. If the steady state temperature of the cylinder is 393 K, the cooling system decreases the temperature of the cylinder barrel by 480 K. One could simply assume since the oil cooling system provides for 80 % of the cooling, the temperature of the cylinder should increase by $480 \cdot 0.8 = 384$K. A large error would be obtained with this assumption however since the heat transfer due to convection increases with increasing surface temperature. Reddy Kummitha and Reddy (2017) developed models of various cylinders with detailed fins in ANSYS without including oil cooling. The cylinder barrels attain a temperature of 623 K without oil cooling and with an air cooling velocity of 10 m/s. The cooling air thus decreases the cylinder barrel temperature by 250 K.

6.5.3 Engine geometry approximation in CFD

A small error is induced as the contour of the engine is assumed to have a smooth surface in the model. The Lycoming engine has cavities in its contour and its not one solid block. The internal combustion engine has furthermore a larger temperature gradient as heat conducts through thin walls instead of going through a solid block as in the model. The temperature gradient yields a varying heat transfer coefficient while in the model a constant coefficient is predicted.

In addition, since the the engine is modelled as a solid, the weight and thus conduction are overestimated.

6.5.4 Error estimation cylinder temperature in CFD

In Section 6.1 the area of the fins, ventilation load and thermal load are determined. Since the area of the cylinder without fins is 15 % of the area with cylinders, it is assumed it provides for 15 % of the cooling. The temperature in the model is therefore expected to decrease by $250 \cdot 0.15 = 37.5$K. The actual temperature decrease will be slightly higher as part of the heat is conveyed to the engine block. Withal, the heat transfer of the engine without fins may be slightly higher as well. An area with fins has a lower heat transfer coefficient than one without fins. The temperature at the tip of the fins is lower

than at the base of the cylinder barrel, entailing a reduced heat transfer coefficient.

To note, a decrease of 37.5 K is a factor ten lower than the actual temperature decrease of the cylinder barrel.

6.6 Error estimation energy balance in CFD

The average temperature increase in the test cell will be substantially lower than estimated through the empirical model as the internal combustion engine entails about 30 % of the heat load in the model. The total thermal load in the test cell is 69.4 kW. In Section 4.2.5 the estimated total thermal load is estimated to be 202.2 kW, however the draught-fans and services are not included as heat sources in the model. Combined they release about 35 kW, which has to be subtracted from the total thermal load of 202.2 kW. In addition, the oil cooler captivates a large part of the heat released by the engine, which has to be subtracted from the total thermal load as well. Consequently the average temperature rise in the ANSYS model may be estimated through Equation 4.1,

$$\Delta T_{\text{test cell}} = \frac{(\text{TL}_{\text{total}} - \text{TL}_{\text{services}} - \text{TL}_{\text{draught fan}) \cdot 0.84}}{Q_{\text{ventilation}}}, \tag{6.19}$$

yields a temperature rise of 3.45 K in the simulated model. In Section 7.1.2 the buoyancy velocities will be computed, including the buoyancy velocity of warm air. It will be determined whether underestimating the convective heat transfer in the test cell influences the dispersion of heat in an enclosed environment.

Chapter 7

Hydrogen Leakages in Enclosed Environments

Hydrogen has the natural tendency to rise due to its buoyant force. The density of hydrogen (0.0898 kg/m^3) is 14 times lower than that of air (1.225 kg/m^3). Analysing the behaviour of hydrogen in an enclosed environment aids in developing the most suitable ventilation system to enhance safety.

7.1 Hydrogen diffusion in test cell room

Hydrogen and warm air rise to the ceiling of the test cell environment in still wind. However, in local regions high air velocities may disrupt the natural tendencies. Hydrogen and heat may accumulate if high velocities dominate the local flow field. Regions of high air velocity must be covered well in the 3D model. Especially regions of high air velocity striking into an object such as near the cylinder. The high incoming air velocity over the internal combustion engine may cause local air circulation in the wake of the piston engine. The wake will be different than in practice as the contour of the components will be simplified. Nonetheless, the error can be estimated by changing the geometry of the engine cylinders into for example a smooth cylinder.

7.1.1 Ignition catalysts hydrogen

The buoyant force of hydrogen is an additional safety feature of the element as it does not linger when it leaks. However, in enclosed environments such as the test cell container hydrogen may accumulate beneath the roof or be captured in local flow fields. The buoyant force of hydrogen equals,

$$F_{\text{buoyancy}} = \Delta\rho \cdot g \cdot = 11.13N \tag{7.1}$$

The density of air and hydrogen equal 1.225 kg/m^3 and 0.090 kg/m^3 respectively. Both the diffusion and rising velocity influence the behaviour of hydrogen in ambient air. The rising velocity of hydrogen, driven by the buoyant force cannot be determined directly. The velocity depends on the shape, size, turbulence, density, friction forces and drag. Furthermore, the diffusion velocity depends on the diffusion coefficient which varies by T^y, with y in the range of 1.72 - 1.8 (Hysafe, 2011). Predicting the flow pattern of hydrogen in an enclosed room is challenging as research is limited.

Hydrogen mixes rapidly with air, almost four times faster than air with air. Zones with high concentration of hydrogen are thus additionally dangerous as the rapid mixing is a safety concern. Therefore, zones which are possibly poorly ventilated or regions near the leak require to be assessed well. It is expected these zones are mostly near the ceiling of the test cell or in the neighbourhood of the internal combustion engine. Components of the test cell set-up should be concealed and gaps at the bottom of an element which may capture hydrogen must be sealed-off. For example, if the camera has a small cavity at the bottom of its contour, it should be sealed-off.

Hydrogen will be pushed downwards since air is pushed downwards near the cylinders. Once it flows into the direction of the edges of the confined space, it escapes the high velocity flow field and begins to rise. If hydrogen particles cement in cavities in the bottom contour of an object, it may accumulate and entail a detonation.

The explosion limit ranges from 4 to 75 % and the detonation limit ranges from 13 to 59 % at room temperature. Ultimately, safety standards suggest the concentration of hydrogen may not exceed 25 % of the lower explosion limit. The volume concentration in the test cell thus may not exceed 1 % hydrogen volume concentration on average in the test cell (Hysafe, 2009).

Ignition due to autoignition is quite unlikely as the autoignition temperature of hydrogen is 733 K. Ignition due to autoignition should not be entirely discarded as catalytic surfaces may lower the limit and ignite a flammable mixture (Verhelst et al., 2009).

Hydrogen is most likely ignited by electrical charged particles due to a low minimum activation energy (Hysafe, 2009). Hydrogen reacts with both metal and non-metal particles. The minimum activation energy of hydrogen is 0.0017 mJ, which is only a fraction of the energy required to ignite a carbon-based fuel. Equation 7.2 (Arrhenius equation) relates the reaction rate to the temperature, with E_a the activation energy, R the universal gas constant and T the absolute temperature,

$$k_i = A_i T^{b_i} e^{(E_a/RT)}. \tag{7.2}$$

The Arrhenius equation predicts the reaction rate to double with each temperature increase of 10 K. A weak spark is sufficient to ignite a flame, with the probability increasing with rising temperatures.

The physics of electric discharge with hydrogen is complex and may be an entire research in itself. For example dust may enter the test cell environment, which is likely to happen since the container is in all probability situated in a remote field. Dust may either get positively or negatively charged due to friction with the ducts or more importantly due to friction with the rapidly spinning forced-draught fans. Especially during winter, when the ambient air is dry and the humidification is low, the concentration of charged particles is high. The risk of deflagration and detonation might be larger in winter than during summer due to the increase in charged particles. The relation between the lower explosion limit and temperature can be determined through the following equation

(Biennal Report, 2005),

$$c_{LEL} = c_{LEL}(300K) - \frac{3.14}{\Delta H_c}(T - 300) = 4.0 - 0.013(T - 300)[\text{vol\%}]. \quad (7.3)$$

With temperature in K and H_c the net heat of combustion in W. The lower explosion limit equals 4.1 % for an ambient temperature of 293 K. For an ambient temperature of 273 K the lower explosion limit equals 4.3 %. The difference in lower explosion limit is relatively low. The risk of detonation and deflagration due to a charged particle is presumed to be larger in winter than during summer[1].

Biennal Report (2005) states as well that hydrogen may detonate as a cause of its positive Joule-Thomson coefficient. The temperature of hydrogen gas increases upon expansion instead of decreasing. During one instance of testing it may have caused a hydrogen-air cloud mixture to ignite. However, this happens rarely as a temperature increase of 6 K is measured when hydrogen leaks from a 20 bar source into ambient air. Nonetheless, researchers report instances where hydrogen detonates when no possible cause could be identified, exposing the difficulty of experimenting with hydrogen (Biennal Report, 2005).

7.1.2 Hydrogen & air flows in the test cell

The buoyant velocity of hydrogen is in the range of 1.2 to 9 m/s, depending on the temperature, density, turbulence, friction force and drag (Biennal Report, 2005). Hydrogen forms a cloud mixture with air once it leaks into the test cell. Note that the diffusion coefficient of hydrogen with air is high. Consequently, hydrogen spreads itself across the container. Therefore, hydrogen must be disposed of as soon as possible once it enters the test cell.

With an incoming air velocity of $\approx$ 16 m/s, the velocity flow field will strongly influence the flow of hydrogen in the test cell in case of leakage. Furthermore, the buoyant velocity of warm air is in the range of 0.1 - 0.2 m/s and will thus rise slower than hydrogen[2] (Blomqvist, 2009).

The buoyant velocities are further compared to the average room velocity. The average velocity is difficult to estimate due to the multi-dimensional nature of the flow. Hagstrom and Siren (2000) proposes the following relation to estimate the average room velocity in an enclosed environment. The empirical relation (Equation 7.4) is derived for a steady-state solution.

[1] Not taking into account the change in minimum activation energy due to temperature change.

[2] Experiments were performed in a test room with a temperature of approximately 293 K, the hot air comprised of a temperature of $\approx$ 298 K.

$$u_r = \left(\frac{1}{0.664} \frac{e_{\text{input}} + e_{\text{sources}}}{V_r} \right)^{1/2} \left(\frac{V_r}{A_s} \right)^{2/3} \tag{7.4}$$

The method stems from the conservation of kinetic energy,

$$\frac{dE_r}{dt} = e_{\text{input}} - e_{\text{output}} + e_{\text{sources}} - e_{\text{sinks}} \,. \tag{7.5}$$

Addition of kinetic energy into the cell environment by a source is considered to be instantaneous. In Equation 7.4, u_r stands for the average velocity, e_{input} and e_{sources} represent the kinetic energy flux in [W] within the test cell such as jet airs or heat generation sources, V_r equals the total volume of the test cell environment and A_s the total surface area of the test cell environment.

As can be noted, the sinks and outputs are assumed to be zero in Equation 7.4. No sinks are present in the test cell environment while the influence of the exhaust draught-fans are negligible. The exhaust fans dispose air, however the momentum is created upstream of the flow inside the room. Therefore the exhaust fans yield a negative kinetic energy, meaning the average velocities increase further. However, the influence of the exhaust fans are local and proven to be small (Hagstrom and Siren, 2000). The kinetic energy of the inlet ventilation fans equal,

$$e = \frac{1}{2}\rho u^3 A = \frac{1}{2}\rho u^2 Q = \frac{1}{2}\rho \frac{Q^3}{A^2} \tag{7.6}$$

With e the kinetic energy flux, Q the volume flow rate in m^3/s and A the area of the fan. The kinetic energy flux for both inlet fans must be computed.

Convection prompts transport of air as well. For heat generation sources such as the internal combustion engine, exhaust pipes and dynamometer, the following equation is utilised,

$$e_h = 5.3 \cdot 10^{-5} \cdot \rho \cdot \text{TL} \cdot (\Delta H + H_o) \,. \tag{7.7}$$

With TL the thermal load or convective heat released into the confined room, e_h the kinetic energy flux of the convective heat released, H the height between the heat source and the ceiling of the enclosed environment and H_o the height between the virtual origin of the plume[3] and the height of the heat source.

Furthermore, friction forces are accounted for with flow being assumed being fully turbulent across the walls of the container. The complete method is derived in the paper of Hagstrom and Siren (2000) if a deeper understanding of the method is desired.

[3]The plume is the concentrated heated area of air above the heat source. With the naked eye the plume is often not seen. A concentrated plume of smoke can be observed above the object when an object ignites. The author refers to this as the plume of the heat source.

In Table 7.1 the parameters are shown, for H_o a value of twice the diameter is chosen as proposed by (Hagstrom and Siren, 2000). K_e is the symbol for total kinetic energy, ergo the sum of the energy sources in the enclosed room.

Table 7.1: Kinetic energy balance method to estimate the average velocity in the test cell container (Hagstrom and Siren, 2000).

Parameter	**U/EI-EIL 564**	**U/EI-EIL 715**	**IO-360-A1B6**
	Fan calculations		
Q (m^3/s)	2.8	4.5	
A_{fan} (m^2)	0.25	0.4	
ρ (kg/m^3)	1.225	1.225	
	Heat source calculation		
TL (W)			135,000
ΔH (m)			2
H_0 (m)			0.92
	General		
H_{cell} (m)	2.59	2.59	2.59
L_{cell} (m)	6.10	6.10	6.096
W_{cell} (m)	2.44	2.44	2.438
V_{cell} (m^3)	38.5	38.5	38.5
S_{cell} (m^2)	73.93	73.93	73.93
e (W)	221.64	336.69	25.59
u (m/s)	1.87	2.3	0.28
	Total average velocity room		
Total average u (m/s)	3.04		

Only the internal combustion engine is included as heat source in the analysis. The internal combustion engine releases most of the heat of the energy sources while only raising the total average velocity in the test cell by 0.5 %. Therefore the dynamometer and exhaust heat pipe are not included. The average velocity in the test cell is dictated by the ventilation fans. The buoyant force or velocity of hydrogen is higher than hot air, hence hydrogen molecules will rise more rapidly to the ceiling of the test cell than warm air.

Nonetheless, there is a large deviation between the downstream regions of the ventilation fans and the remaining of the test cell. In addition, the average computed air velocity in this section is the average non-directional velocity. The average current in the test cell will thus include velocities much lower than 3.04 m/s.

Therefore, while warm air will be easier to direct and control than hydrogen through the ventilation fans due to a lower average velocity, both warm air and hydrogen may accumulate near the ceiling.

7.2 Hydrogen leak analysis in test cell

The concentration of hydrogen may not exceed on average 25 % of its lower explosion limit in the test cell. Hence, the volume concentration may not be higher than 1 % (Hysafe, 2009). Hydrogen leaks are simulated in various locations in the test cell. A leak may occur due to a rupture in the fuel pipe or through a gap in the internal combustion engine.

The ventilation system must be able to control hydrogen leaks of varying strengths. Weak leakages refer to small ruptures or gaps where hydrogen is released into the test cell environment at low velocities. Strong leakages refer to the diffusion of hydrogen at higher velocities and high mass flows. Weak leakages are dangerous in environments with low air circulation as hydrogen molecules remain grouped and linger for a prolonged period in the enclosed environment.

The ventilation load in the test cell is relatively high, therefore weak leaks[4] are presumed to be less dangerous than strong leaks. With strong leaks, hydrogen escapes at velocities much higher than the average velocity within the test cell. Hence strong leaks at various locations are simulated as the diffusion is difficult to control. If the ventilation system is able to control strong hydrogen leaks, it is presumed weak leakages are of no concern either. To note, detonation may occur instantaneously when very large pipe ruptures or wide gaps appear and yield high volume concentrations of hydrogen which exceed the lower explosion limit of hydrogen in the test cell. No system of ventilation fans can prevent a catastrophe in this event. The risk of detonation in the test cell cannot be reduced to zero. The purpose of the CFD analysis is to minimise the possibility of a detonation.

Hydrogen will be supplied through a high-pressure fuel tank. The storage tank is installed outside as storing the tank inside the test cell is dangerous and illegal. A fuel pipe connects the hydrogen fuel tank with the internal combustion engine.

The dimensions of the fuel pipe are extracted from available equipment at the Deltion college, while the pressure within the pipe is obtained through published test experiments (Green and Glasson, 1992; Yip et al., 2019). Table 7.2 shows the inner diameter of the fuel pipe, the fuel pipe pressure and the cross sectional area of the fuel pipe.

The density of hydrogen in the fuel pipe can be deduced from the equation of state,

[4] In case a weak leakage does not cause an instantaneous detonation.

Table 7.2: Fuel pipe dimensions, supplying hydrogen from the hydrogen fuel tank to the internal combustion engine.

Parameter	**Value**
D_{pipe}	6 mm
p_{pipe}	1 - 20 bar
A_{pipe}	28.27 mm^2

$$p = \rho \cdot R_{\text{specific}} \cdot T. \tag{7.8}$$

With R the specific gas constant of hydrogen equal to 4124.2 J/kgK. The temperature is assumed to be constant within the fuel pipe at 287K. Hence, the density of hydrogen within the pipe ranges from 0.0898 kg/m^3 to 1.796 kg/m^3. Figure 7.1 (Walter, 2001) shows the accuracy of the equation of state,

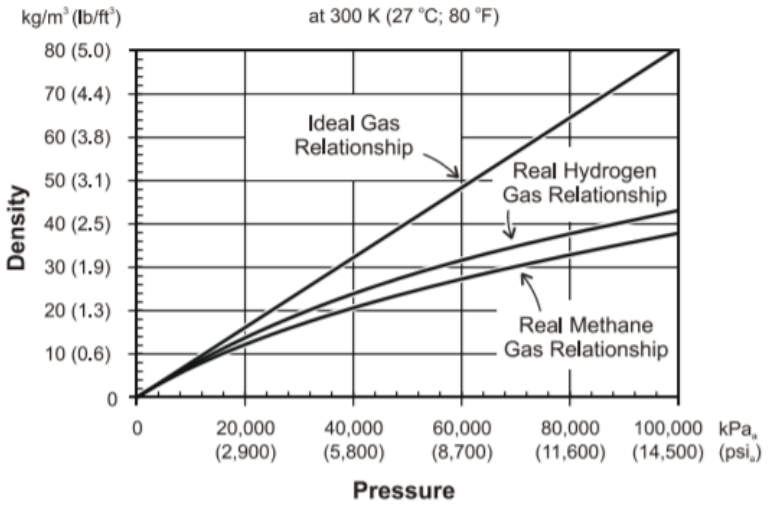

Figure 7.1: Density in relation to pressure for hydrogen and methane (Walter, 2001).

It can be noted assuming a linear relation between pressure and density is valid at lower pressures. The required pressure of the pipe relates to the injection pressure[5]. The initial plan is to experiment with a port fuel injector, which requires an injection pressure of approximately 20 bar. Direct injection may be attempted during an advanced stage. Direct injection should be combined with liquid hydrogen, which is currently not the preferred storage method in the Cessna 337F Skymaster. To simulate leakages for the worst case scenario, it will be assumed the pipe pressure is 20 bar.

[5]Unless a system is mounted on the engine to compresses the gas again. However, such a system is rather inefficient since the gas is already pressurised in the fuel tank.

The gap diameter in the fuel pipe is difficult to predict when the pipe ruptures. Various experiments are performed in literature. Most researchers, as Taira et al. (2015), experiment with gaps in the range of 0.01 - 10 mm. Although gaps of 10 mm have a low probability of occurring, most leak gaps are in the range of 0.01 mm and 1 mm. Leakage gaps of 10 mm will be simulated as well to design for the worst case conditions.

The highest probability of a leak is not due to a rupture in the fuel pipe but due to loose connectors. If connectors are not mounted well, hydrogen leaks through a small gap into the test cell environment. Connectors are primarily in the neighbourhood of the internal combustion engine, therefore CFD experiments with leakages near the internal combustion engine are performed.

Small gaps in the fuel pipe or injector may be seen as a converging-diverging duct. As the cross sectional area of the gap is relatively small to the cross sectional area of the flow, the leakage flow is likely to be choked. The fuel pipe transports hydrogen with pressures up to 20 bar, hence the momentum jets of leakages are strong. It can be calculated whether the flow through the leakage gap is choked or not and hence, whether the flow is sonic or even supersonic through Equation 7.9,

$$\frac{p_S}{p} \geq \left(\frac{2}{\gamma+1}\right)^{\gamma/(\gamma-1)}. \tag{7.9}$$

The heat capacity ratio of hydrogen equals 1.41, which is similar to the heat capacity ratio of air (Walter, 2001). The flow is choked at a pressure ratio of 1.89 across the boundaries according to Equation 7.10.

$$\frac{p_{\text{test cell}}}{p_{\text{pipe}}} \geq \left(\frac{2}{\gamma+1}\right)^{\gamma/(\gamma-1)} = \frac{1}{1.89} \tag{7.10}$$

The pressure ratio between the fuel pipe and the test cell environment is in the range of 1 - 20. Ergo, the flow of the hydrogen leakage through the gap will be sonic.

Experiments have shown the actual pressure ratio where the flow becomes choked is 4.1 instead of 1.89. In Table 7.3 the experimental relation between pressure and jet velocity of a hydrogen leak which has been observed by researchers is summarised (Molkov and Brennan, 2011).

Table 7.3: Flow condition of hydrogen leak with various pressure ratios.

Pressure ratio	**Flow state**
p_{pipe} / $p_{\text{test cell}}$ = 1 - 4.1	Subsonic
p_{pipe} / $p_{\text{test cell}}$ = 4.1 - 41.2	Sonic under-expanded jets
p_{pipe} / $p_{\text{test cell}}$ = 41.2 >	Supersonic under-expanded jets

The same experiment concludes the flow becomes supersonic at a pressure ratio of 41.2. The error ensues from the ideal gas law assumption (Equation 7.9). It should not affect

the analysis since the pressure in the fuel pipe is 20 bar. Yet, during the sensitivity leakages of varying strength will be simulated.

Nonetheless, the jet momentum of the leakage will be a sonic under-expanded jet with a pressure ratio of 20. The flow of the leakage is choked and the velocity equals the speed of sound of hydrogen in the throat of the gap. The speed of sound of hydrogen equals 1270 m/s at atmospheric conditions (Hysafe, 2011). An example of a leak through a fuel pipe rupture is illustrated in Figure 7.2.

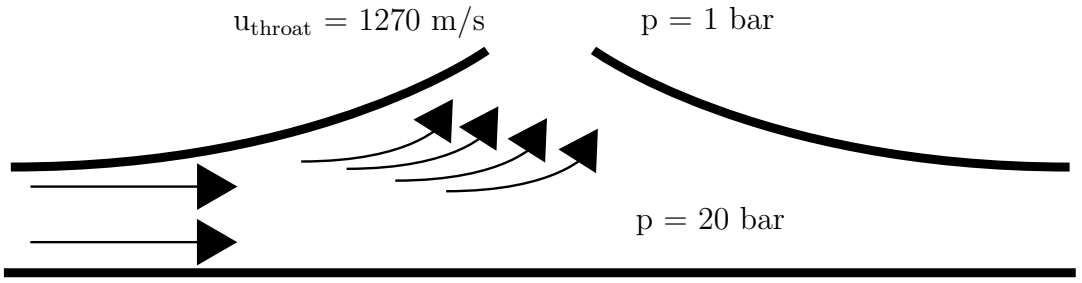

Figure 7.2: Pressure difference between the fuel pipe and the container during the experiment. The hydrogen flow in the throat of the leak is sonic.

The mass flow through the gap depends on the area of the pipe, pipe pressure and temperature while it is disconnected from the downstream conditions when the flow is choked. The mass flow of a hydrogen leakage can be estimated through Equation 7.11 (Anderson, 2011),

$$\dot{m} = \frac{p_{\text{pipe}} \cdot A_{\text{throat}}}{\sqrt{T_{\text{pipe}}}} \sqrt{\frac{\gamma}{R} \left(\frac{2}{\gamma + 1} \right)^{(\gamma+1)/(\gamma+1)}} \tag{7.11}$$

The density in the throat can be approximated through Equation 7.12,

$$\rho_{\text{throat}} = \left(\frac{2}{\gamma + 1}^{\left(\frac{1}{\gamma-1}\right)} \right) \cdot \rho_{\text{pipe}}. \tag{7.12}$$

The according temperature in the throat can be estimated as,

$$T_{\text{throat}} = \left(\frac{2}{\gamma + 1} \right) \cdot T_{\text{pipe}}. \tag{7.13}$$

Subsequently the following flow conditions of the leak are summarised in Table 7.4,

Table 7.4: Hydrogen flow properties in the fuel pipe and throat of the leakage gap.

Variables	D_{gap} = 0.1 mm	D_{gap} = 1 mm	D_{gap} = 10 mm
p_{pipe} (bar)	20	20	20
T_{pipe} (K)	287	287	287
$R_{hydrogen}$ (J/kg K)	4,124.2	4,124.2	4,124.2
ρ_{pipe} (kg/m^3)	1.712	1.712	1.712
$p_{test\ cell}$ (bar)	1	1	1
A_{gap} (mm^2)	0.0079	0.79	78.54
T_{gap} (K)	238.17	238.17	238.17
ρ_{gap} (kg/m^3)	1.09	1.09	1.09
u_{gap} (m/s)	1,270	1,270	1,270
$\dot{m}_{gap}$ (g/s)	0.01	1.004	100.42

The under-expanded jet will cause a shockwave in the container which may be heard. Yüceil et al. (2000) have experimented with small leaks and observed a Mach number of 2.28 at a pressure ratio of 7.75 at a height of 8 times the diameter, after which Mach disks appear and the velocity quickly reduced. In addition, a Mach number of 2.85 at a pressure ratio of 15.57 is observed. Note that the pressure ratio defined in Yüceil et al. (2000) is between the chamber and the nozzle, thus between the throat and the container. The maximum Mach number is thus expected to be between 2.28 and 2.85 at a short distance from the gap. Yu et al. (2013) and Schefer et al. (2006) performed similar experiments and obtained identical trends regarding the Mach disks as well. Most notable, Schefer et al. (2006) analysed the Mach disks for hydrogen leakages with nozzle gaps between 1 to 2 mm. It will therefore be interesting to simulate a leak in Fluent and observe whether the Mach number attains a value between 2.2 to 2.8 at ≈ 8 diameters above the nozzle.

Furthermore, it is interesting to note that the length of the hydrogen plume with a pressure ratio of 20 is in the range of 1 to 2 m according to Hysafe (2009). The length of the plume is hence an additional method to validate the hydrogen plume in Fluent.

7.3 Risk assessment of hydrogen leakages

In the following section the risk of each potential leak within the test cell is documented. Subsequently precautions are suggested to mitigate either the likelihood or severity of a leak to enhance the safety in the test cell.

The hydrogen supply through the fuel pipe will be automatically closed-off by a shut-off valve upon detecting a leak during experiments. This process may take less

than 1 second (Wallner T., 2009). Additional measures must be taken to dispose of the remaining hydrogen if it remains in the test cell. It will be simulated whether the volume concentration of hydrogen remains below 1 %.

If through the CFD simulation it is concluded that all hydrogen is disposed of with the ventilation system, and hydrogen concentration remains below 1 %, it does not entail hydrogen deflagration and detonation are not possible. A wide array of possible leaks may occur during testing, which not all can be modelled for as the computational cost would be immense. In the event that a leak with a gap diameter of 50 mm appears or a connector detaches, the hydrogen volume concentration will exceed the allowed limit. No ventilation system is able to cope with such hydrogen leakages. Despite the probability of such an event is close to zero, it should be kept in mind the risk of deflagration or detonation can never be completely eliminated.

7.3.1 Crankcase vent leakage

Hydrogen leaks from the combustion chamber through the liner into the crankcase (Frijters, 2020). Consequently hydrogen accumulates in the crankcase and the pressure rises. Therefore the crankcase must be vented to the environment through an outlet pipe. The pipe is mounted on the bottom of the Lycoming engine and if loosely connected hydrogen leaks into the test cell container. The mass flow of hydrogen leaking into the test cell is difficult to estimate as it depends on the amount of hydrogen flowing through the liner. Initial tests by Deltion college proved that leakages through the outlet pipe are quite likely compared to other potential leak sources.

It must be noted leakages through the crankcase are composed of a hydrogen-oil mixture. Such a cloud mixture may descend to the floor instead of rise towards the ceiling. The cloud mixture might be better disposed of through the bottom of the test cell container than the top.

7.3.2 Fuel injector leakage

The fuel injector is mounted on top of the cylinder head. Hydrogen may leak into the test cell due to the high volatility of hydrogen. Gaps in the fuel injector are small but the mass flow rate may still be relatively high due to an injection pressure of 20 bar.

7.3.3 Fuel pipe rupture

Fuel pipes are rated to handle pressures up to 200 bar (Taira et al., 2015). Ruptures are improbable but can be devastating as the pressure ratio between the fuel pipe and test cell is high. In addition, the gap diameter is difficult to predict in the event of a rupture.

7.3.4 Wall crack

Hydrogen combustion may exert more force on the cylinders walls than aviation gasoline combustion (Wang et al., 2019). Hydrogen may leak through small cracks of which the mass flow rate varies by the diameter of the gap.

7.3.5 Intake manifold leakage

If fuel is injected through an intake manifold or carburettor[6], a loose connection may entail hydrogen leaking into the test cell from the top of cylinder. The hydrogen mass flow rate into the test cell will in this scenario be relatively high.

7.3.6 Exhaust manifold leakage

Some of the unburnt hydrogen particles may leak through a loose connection near the exhaust manifold. The concentration of hydrogen will be low, hence the severity of such an event is low.

7.3.7 Inlet valve leakage

The valves are situated near the top of the cylinder. Hydrogen may leak through the valve, the severity is presumed not to be large since the gap is small and the pressure is low.

7.3.8 Risk map hydrogen leakages excluding safety considerations

The following letters depict each scenario,

- A $\longrightarrow$ crankcase leakage
- B $\longrightarrow$ fuel injector leakage
- C $\longrightarrow$ fuel pipe rupture
- D $\longrightarrow$ wall crack
- E $\longrightarrow$ intake manifold leakage
- F $\longrightarrow$ exhaust manifold leakage
- G $\longrightarrow$ leakage through valve

[6]In Chapter 3 it is mentioned both are not suitable for hydrogen combustion, for initial tests however fuel may be mixed with the two former mechanisms to calibrate the engine.

The severity and likelihood of each scenario are determined through literature (Wallner T., 2009; Wang et al., 2019; Chen and Mao, 2017; Yip et al., 2019) and through information provided by Deltion college.

Table 7.5: Risk map hydrogen leakages in the test cell container without precautions. On the y-axis the likelihood of an event is depicted and on the x-axis the severity of an event. One should further reduce the risks in the test cell.

Likelihood \ Severity	1	2	3	4	5
1				D	
2		G			C
3					B
4	F	A			E
5					

7.3.9 Risk map of hydrogen leakages with safety considerations

The risk of experimenting with hydrogen in a confined environment is greatly reduced by incorporating precautions. The following precautions mitigate to a certain extent the risk.

- A double pipe wall encasing the fuel pipe reduces the risk of a leak through the fuel pipe to nearly zero.
- All the electric components in the test cell must be sealed gas tight and must be ATEX-3 protected equipment.
- Instead of testing initially with four cylinders, testing with one cylinder reduces the incoming mass flow rate and the severity of a leak.
- Intake manifold leakages are more severe if one experiments with a carburettor or intake manifold injection. With port and direct fuel injection hydrogen does not flow through the intake manifold and a leak will only occur if hydrogen flows back into the manifold from the combustion chamber. Subsequently the severity and probability of a hydrogen leaking through the valve decreases.
- Sensors should be strategically placed to measure the power, outlet temperature, and mass flow rate through the pipes and injectors. If discrepancies are noticed it might indicate a leak is present. For example one should place sensors in the outlet ducts to measure the concentration of hydrogen in the test cell. If hydrogen is detected, the hydrogen supply is immediately shut-off by a valve and the severity of a leak decreases.

One may note in Table 7.6 the risk in the test cell is greatly reduced but not reduced to zero by incorporating the risk mitigation techniques. Risk mitigation is further discussed in Chapter 9 and the risk map in Table 7.6 will be iterated once more.

Table 7.6: Risk map of hydrogen leakages in the test cell container with precautions.

Likelihood \ Severity	1	2	3	4	5
1	G,F		D		C
2	E	A			
3		B			
4					
5					

7.4 Intermediate summary hydrogen leakage assessment

The following list includes the most important aspects of this chapter.

- Hydrogen has a buoyancy velocity in the range of 1.2 to 9.1 m/s and warm air approximately 0.3 m/s. The non-directional average velocity equals 3.04 m/s and therefore it is expected, while warm air is less difficult to control, both warm air and hydrogen will accumulate near the ceiling.
- Charged particles entail the highest risk of causing a detonation.
- The hydrogen volume concentration should be kept below 1 % on average in the test cell.
- The leakage mass flow rate of hydrogen is difficult to predict, the risk of a detonation can never be reduced to zero, it can only be minimised.
- The flow through the leakage gap will be choked. The velocity through the gap will equal $M = 1$ or $u = 1270$ m/s for a pressure ratio of 20 between the leak source and the test cell.
- Leaks through the fuel injector and the outlet pipe of the crankcase ventilation are most likely.

The following step is to set-up the CFD model which is elaborated upon in Appendix A. Consequently the flow field in the test cell is simulated and the results are analysed.

Chapter 8

Ventilation System Initial Model Propositions

The verification, validation and initial models are presented in this chapter. In addition, a sensitivity analysis is performed to measure the effect of the simplifications included in the CFD model. The results are subsequently presented to hydrogen safety experts to obtain feedback. The final design of the ventilation system is a combination of the initial models and the feedback provided by the hydrogen safety experts. The final optimised model is presented in Chapter 9.

8.1 CAD model set-up

The first step in developing an effective ventilation system is to summarise the findings from the previous chapters and simulate models which comply to these findings. Consequently, the three most effective models are compared to each other in detail. Intermediate conclusions are made with the trends observed in the initial models. One of the three models is subsequently optimised and selected as the design to be presented to the hydrogen safety experts.

One can develop a detailed model of the test cell environment to capture the flow, diffusion of hydrogen and heat balance in detail. However, the flow is not required to be modelled in such detail. The geometry of the CAD model must first be simplified to the extent that the computational time is minimised while still satisfactory conclusions can be obtained.

8.1.1 CAD model geometry approximation

Elements such as the engine and dynamometer will be modelled as simple blocks as they are expected to be essential elements with regard to the energy balance and air current. Modelling the actual engine block is difficult as it entails a high computational cost. This should not raise too much of a concern for the energy balance. However, it may affect the flow field as for example a block with sharp corners may yield an entirely different flow field than a block with round corners. Note, objects which are not expected to influence the flow field and energy balance are discarded as mentioned in Chapter 5. The components which are included in the model are the container itself, the engine

(including the cylinder and combustion chamber), dynamometer, lamps, ducts, fans and exhaust pipe. The selection is based upon analysing preceding CFD model set-ups of Hysafe (2009) and comparing the size and heat generation of elements inside the test cell.

The behaviour of warm air and hydrogen are analysed in Chapter 7. Both warm air and hydrogen are expected to rise to the ceiling, while near high velocity flow fields warm air and hydrogen may be captured and linger for an extended period in a local region. It remains uncertain whether the particles may accumulate in the wake of the engine and near the ceiling. The 3D model requires to be set up such that in both regions the flow field is predicted well. A careful note must be taken by not including all the geometries and contours in detail as they have downstream influence.

An infinite amount of models should be simulated to capture all the possible scenario's since experiments will be performed in various circumstances. A sensitivity analysis will be performed to observe the consequences of varying boundary conditions and variations in contours of the geometries to be time-efficient.

8.1.2 Base design CAD model in DesigModeler

The base model of the 3D CAD model is shown in Figure 8.1. The outer block resembles the walls of the container. Two ducts are mounted on the roof and two ducts are mounted on the side walls.

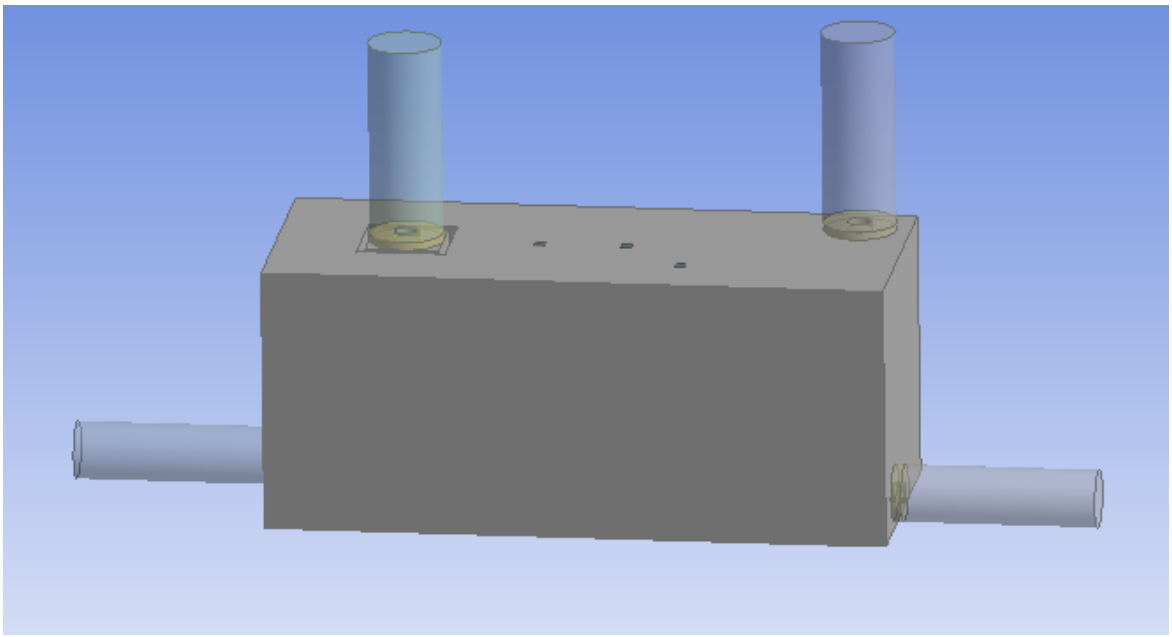

Figure 8.1: Outer surface of the CAD model of the container in DesignModeler.

The interior of the CAD model is illustrated in Figure 8.2. Note that the base-model is not the optimised model, the position of the ventilation ducts and direction of the air flow induced by the fans might still be altered. Only the straight duct sections are included in the model. The pressure losses induced by the rain caps, outlet louvres and inlet grid are included in the model while the geometry of the objects are excluded from the model for simplicity.

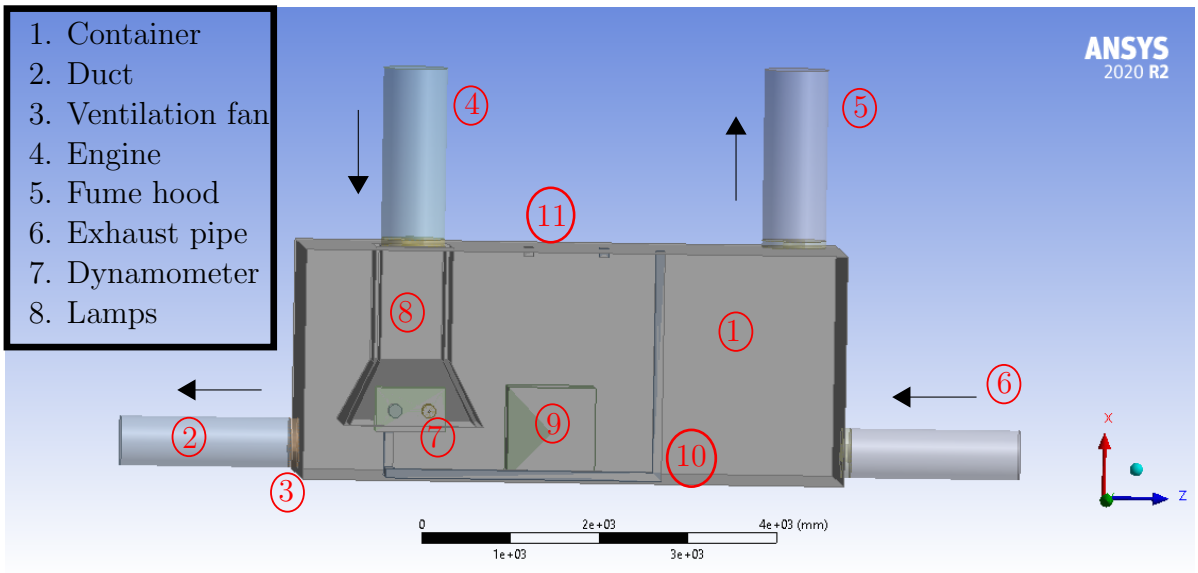

Figure 8.2: Interior of the CAD model of the container in DesignModeler.

Eight numbers may be distinguished in Figure 8.2. Number 1 represents the fluid zone of the test cell. Number 2 is an outlet duct, the outlet duct is attached with a fan (number 3) where the duct and container connect. The outlet fan (number 3) is mounted in the proximity of the engine with the purpose to instantaneously dispose of warm air released by the engine. In addition, a second function of the fan is to direct hydrogen immediately toward the environment if a leak is present near the engine. Note that duct 4,5 and 6 all include ventilation fans which are mounted at the intersection between the duct and the container as with duct 2.

The fan mounted on the the walls on right-hand side of the container (number 6) directs the flow to outlet duct number 2 and is thus an inlet. This fan is assigned to redirect the flow to duct 2 if some hydrogen or warm air is directed to the rear of the container. Researchers have recommended the method (Hysafe, 2009), although often in test cells where hydrogen is stored at lower pressures. It may be possible the momentum jet and buoyancy forces of warm air and hydrogen are too strong and consequently both warm air and hydrogen rise to the ceiling of the container regardless. The set-up of the fans in the container should be changed in that circumstance.

Number 7 designates the Lycoming engine, comprising of an engine block attached with four cylinders. Most CFD analysis in literature model the engine as a simple unit block to reduce the computational cost (e.g. Wallner T., 2009). Air-cooled retrofit hydrogen internal combustion engines are not experimented with yet, or no data is yet available in literature. Most simulations include a model of a water-cooled engine or a fuel cell. The air velocities in a water-cooled engine test cell are much lower. In addition, one must consider the air velocities are highest near the engine for an air-cooled engine. Therefore the geometry of the engine is modelled with more accuracy.

A 3D model of the internal combustion engine is illustrated in Figure 8.3. Smaller cylinders inside the larger cylinders may be observed if one looks closely. These inner cylinders resemble the combustion chambers, while the outer cylinders represent the cylinder head, and cylinder barrels. Cold air propagates through the fume hood (number 8) through duct 4 and consequently flows over engine cylinders into the test cell. Numbers 9 and 10 represent the exhaust pipe and dynamometer respectively (both are designated as heat sources). Finally, number 11 represents two small lamps mounted on the ceiling, which are included due to a small contribution to the energy balance and to observe the effect on the flow field of parts mounted on the ceiling.

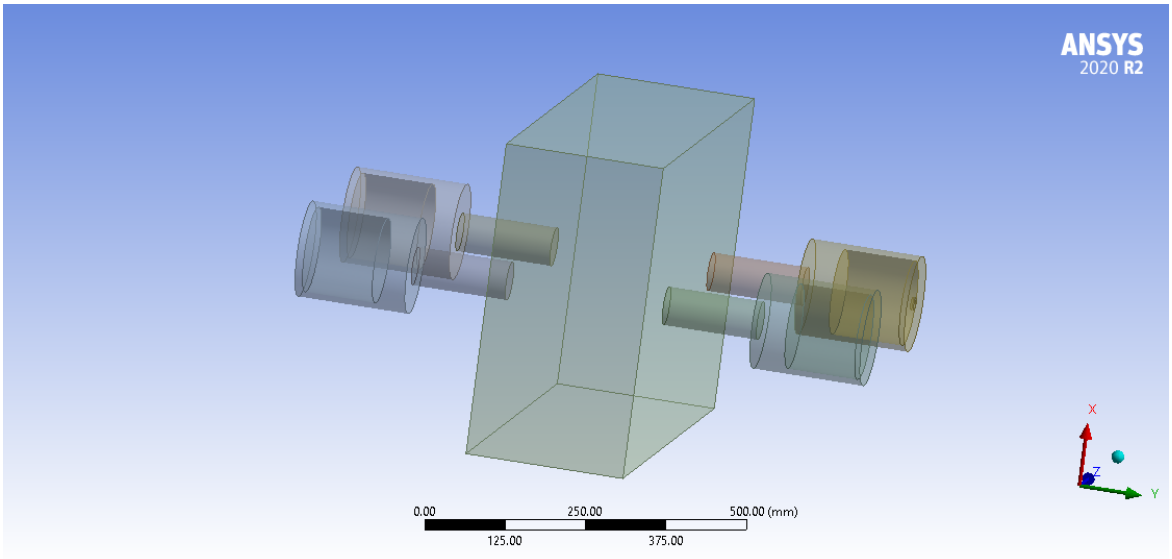

Figure 8.3: Engine CAD model in close-up view in DesignModeler.

The cooling fan includes a fume hood in the CAD model which encapsulates the engine. The test cell will include augmented ducts instead of a fume hood. The augmented ducts guide the flow through converging channels over the top of each engine cylinder, hence the duct will separate into four channels. Augmented ducts are preferred over one large fume hood since the engine block itself is not required to be cooled by air. The design of the converging ducts is not included in the model as it is too complex. A possible design of the augmented ducts is illustrated in Figure 8.4.

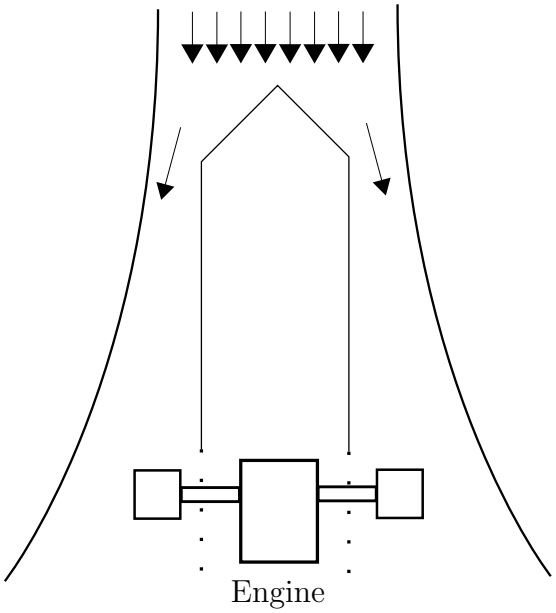

Figure 8.4: Possible design of the augmented ducts, The design is not included in the CAD model as it is too complex.

The ducts extend over the cylinders to isolate the air flow. The remaining flows in test cell may not influence the cooling of the cylinders. The fume hood represents a simplified geometry of the augmented ducts which directs the flow towards the engine in one large channel.

Elaborating further upon Figure 8.2, outlet fan number 2 must ensure hydrogen and warm air do not accumulate beneath the engine by redirecting the flow in the local region in combination with inlet fan 6. Particulates may accumulate beneath the engine due to the strong vertically downwards directed air flow induced by fan 4 mounted on the ceiling.

The risk of this set-up stems from hydrogen escaping the air flow imposed by fan 2. Hydrogen and warm air must leave the test cell container through outlet 5 if they are not disposed of by outlet fan 3. The fan in the rear is pushing hydrogen towards the front which may entail poor outflow towards duct 5. The opposing flow may lead to hydrogen and warm air accumulating near the ceiling of the container. The CFD simulation must provide with a definitive answer. The set-up of the ventilation system is further discussed in Section 8.2.

Note that a leakage is unpredictable, a rupture may appear in the fuel pipe, a connection may come loose or hydrogen may leak from the fuel injector through the spindle into the test cell container (Hysafe, 2009). The size of the gap, the momentum jet and location of the leak are difficult to predict and the risk of detonation due to a hydrogen leak can only be minimised but not reduced to zero.

The base models must comply to the following criteria set by Hysafe (2009).

- The momentum of a hydrogen leak is high due to the large pressure differential between the fuel pipe and test cell container. Subsequently, the momentum jet rapidly weakens as hydrogen is a light element, the velocity of hydrogen eventually decreases to the buoyancy velocity (1.2 - 9.1 m/s) and rises to the ceiling of the test cell container. The air velocity induced by the fans influence the diffusion of hydrogen but cannot entirely control the flow direction of hydrogen.

- Natural ventilation is preferred over forced ventilation for small hydrogen leaks. Forced ventilation enhances the disposal of hydrogen but entails turbulence. Turbulence promotes the mixing of air with hydrogen. The shock waves will be stronger and thus more energy is released in the event of a detonation due to the turbulence. In addition, fans with more rotations per minute increase the velocity, which in turn may increase the concentration of charged particles entering the test cell. The following relation is suggested by leading hydrogen experts,

$$Q_{\text{Ventilation}} = \frac{100}{\text{LEL}} \cdot Q_{\text{Leak}} \cdot K_{\text{Safety}}. \tag{8.1}$$

  The lower explosion limit of hydrogen (LEL) equals 4 % and K_{Safety} is a safety factor which researchers suggest to be four. The required ventilation rate imposed by Equation 8.1 cannot be met through natural ventilation as hydrogen leakages may entail relatively high mass flow rates. Note that larger air mass flow rates are always preferred for very large leaks (gap diameter $\geq$ 1 mm (Hysafe, 2009)) since turbulence becomes less relevant. The ventilation rate should equal the ventilation rate imposed by Equation 8.1 for small leaks while for larger leaks it is the minimum required ventilation rate.

- Solving Equation 8.1 with a fuel pressure pipe of 20 bar and gap diameter of 1 mm yields a leakage flow rate of 1 g/s and thus a required ventilation rate[1] of 1.12 m^3/s. The required ventilation volumetric flow rate increases to 111.36 m^3/s for a fuel pipe pressure of 20 Pa and leakage gap of 10 mm. Note, with the appropriate risk mitigation methods a leakage gap of 10 mm should not occur.

- One of the outlet fans should be mounted near the floor of the wall, the test cell may be used in the future for various other fuels such as liquid natural gas or liquid hydrogen. Furthermore, tests will initially be performed with aviation gasoline to calibrate the engine. A ventilation fan near the floor must purge the fumes of liquid fuel as in the event of a leak it drops down to the floor and eventually evaporates.

[1] The hydrogen concentration is assumed to be homogeneous in the test cell in Equation 8.1.

- Inlet and outlet ducts may not be set in proximity of each other as warm air, particulates and hydrogen may not re-enter the container once it leaves the test cell.

- Fans on the side of the walls must be at least a few centimetres above the ground as they may not pull in sand, water, snow or any other unwanted particles.

8.1.3 CFD boundary & cell zone conditions input

The inputs for all the boundary conditions of the CFD model are included in the following tables. The inputs of the fan pressure jumps are summarised in Table 8.1 below.

Table 8.1: Ventilation fan performance including duct losses. Only the pressure jump is an input in ANSYS Fluent.

	Velocity (m/s)	**Vol. flow rate (m^3/s)**	**Pressure jump (Pa)**
U/EI-EIL 564 inlet	11.84	2.92	85.86
U/EI-EIL 564 outlet	11.84	2.92	85.86
U/EI-EIL 715 inlet	12.05	4.58	88.93
U/EI-EIL 715 outlet	12.05	4.58	88.93

Note that both U/EI-EIL 715 operate at the same capacity, even though the duct losses are slightly higher for the inlet duct. The U/EI-EIL 715 are designated with the same pressure jump for simplicity. Hence, the disposal fan operates slightly below maximum capacity.

The boundary conditions are summarised in Table 8.2.

Table 8.2: Boundary conditions for the model in Fluent.

Boundary conditions	
Inlet duct	$p_0 = 0$ Pa
Outlet duct	$p_s = 0$ Pa
External walls	h = 25 W/m^2K
Hydrogen leakage[1]	0.095 - 100 g/s
Combustion fuel inlet[2]	4.96 g/s
Combustion air inlet[2]	203 g/s

[1] The hydrogen leakage is only applicable in the hydrogen diffusion model.
[2] The combustion fuel and air inlet are only included in the energy balance model.

Note that the hydrogen leakage inlet boundary condition is only included in the hydrogen diffusion model while the combustion fuel inlet and combustion air inlet are only defined in the energy balance model.

The inputs for the heat generation sources are summarised in Table 8.3.

.

Table 8.3: Heat source generation inputs in ANSYS Fluent

Heat source	**Volumetric heat generation W/m^3**
Dynamometer	500
Lamps	100,000
Exhaust pipe	30,000
Combustion chamber[1]	2,341,096

[1] The combustion chambers are set as heat generation sources in the hydrogen diffusion model. In the energy balance model the combustion chambers are designated as a constant heat generation source but rather includes a combustion model to simulate heat.

The heat generation for a few sources seem very high but note that the volumetric heat generation must defined in ANSYS Fluent. The volume of a lamp in the CAD model is very small and therefore it entails a high volumetric heat generation. The combustion chambers are appointed a constant heat generation source in the hydrogen diffusion model while in the energy balance model a combustion process is simulated. Fluent assumes the leaked hydrogen ignites when it comes into contact with air if combustion is enabled for the diffusion model and therefore the diffusion of hydrogen cannot be simulated. Therefore the cylinders are designated as a constant heat source instead.

8.1.4 Hydrogen leak model in ANSYS Fluent

The optimisation is initially performed with a leakage gap of 10 mm and fuel pipe pressure of 20 bar, despite gaps in the range of 0.1 - 1 mm being most common (Hysafe, 2009). In the sensitivity analysis, smaller gaps will be tested to observe the consequences.

The ventilation rate is based on leakages of pure hydrogen. The benefit of hydrogen combustion in comparison to hydrogen fuel cells is that hydrogen is not required to be pure. The main production method of hydrogen for hydrogen combustion is by steam methane reforming and entails a purity of $\approx$ 96 % - 99 % (Rosen and Koohi-Fayegh, 2016). The remaining elements in the mixture comprise of carbon elements which may have a small effect on the leakage. The mass fraction percentages of the carbon elements are very low however and presumed to be negligible.

The strength of the hydrogen leak determined in Chapter 6 for a gap with a diameter of 10 mm is restated in Table 8.4.

Table 8.4: Mass flow and velocity inlet condition input values for ANSYS and error in comparison to physical leakage for $D_{gap} = 10\,mm$.

Parameter	**Value**
$\mathbf{p_{pipe}/p_{test\ cell}}$	20
$\dot{\boldsymbol{m}}_{\text{leakage}}$	100 g/s
$\mathbf{u_{throat}}$	1.270 m/s

The inlet will be defined as a pressure ratio inlet with a total pressure of 12 bar and dynamic pressure of ≈ 8.7 bar. The above two pressure ratios are the values of the flow state in the throat. Consequently, ANSYS Fluent computes the density through Equation 8.2,

$$\rho = \frac{p_{\text{tot}}}{R \cdot T}. \tag{8.2}$$

The density thus equals $1.08\,kg/m^3$, the velocity is subsequently computed through the defined dynamic pressure,

$$u = \sqrt{\frac{2 \cdot p_{\text{dynamic}}}{\rho}} \tag{8.3}$$

Finally, the mass flow rate through the leak is computed through the conservation of mass which equals 2.69 g/s.

$$\dot{m} = \rho \cdot A \cdot u \tag{8.4}$$

The flow parameters will be compared to the results in ANSYS Fluent as part of the verification of the mesh.

An identical leakage is simulated for all three models. A side view of the simulated leak is presented in Figure 8.5. Note that Figure 8.2 shows the front view of the container. Figure 8.5 displays a 2D contour with hydrogen mass fraction as colour scheme. Hydrogen propagates through a gap in one of the cylinders into the test cell container. The cylinder which includes the leak is designated by point 7 in Figure 8.2. The colour red entails a high concentration of hydrogen while blue entails a volume concentration of zero.

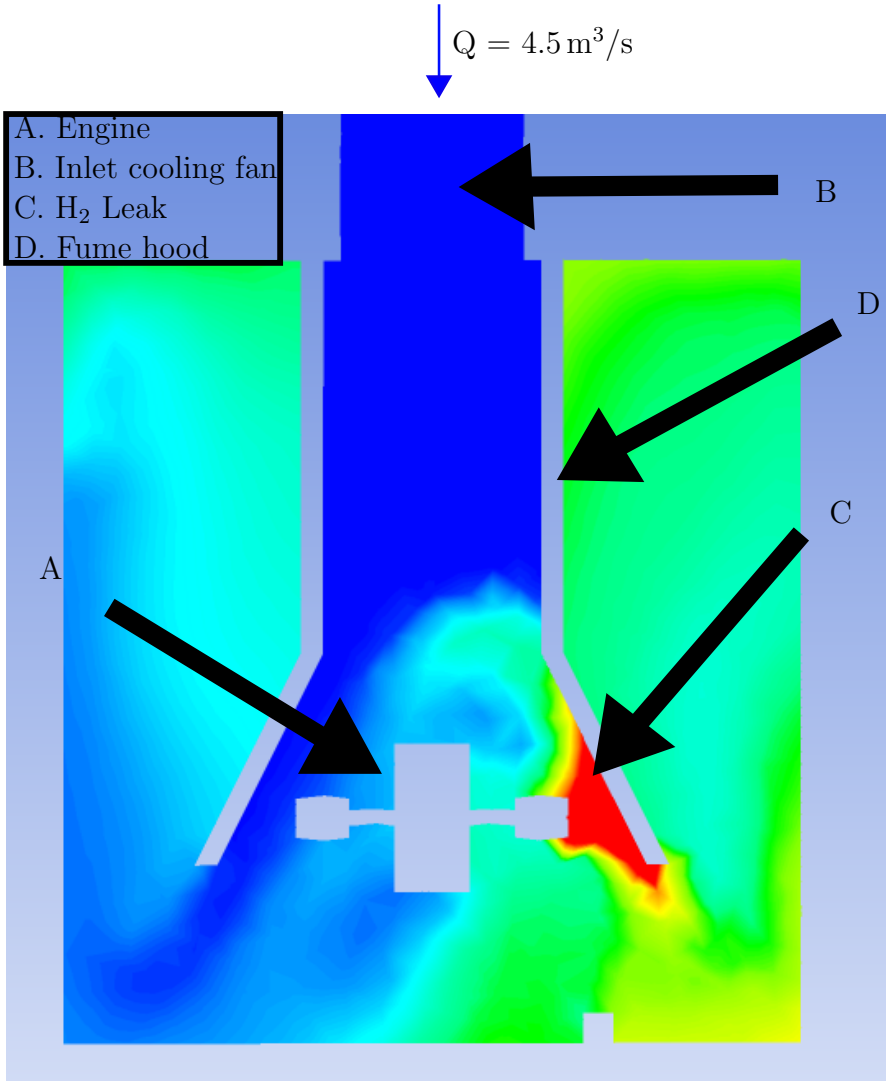

Figure 8.5: Wide-angle view of the hydrogen leakage in the test cell. Leakage ($\dot{m}$ = 0.1 kg/s) through a large gap (D = 10 mm) near the cylinder of the internal combustion engine.

Cold air enters the test cell through the ventilation fan mounted on the ceiling, it supplies a cooling air volumetric flow rate of 4.5 m^3/s. (A) is the internal combustion engine, (B) the inlet duct through which cold air is pushed through, (C) indicates the leak and (D) is the contour of the fume hood. All four fans are operating with their respective pressure jumps of 85.86 Pa and 88.93 Pa. The depicted cylinder is one of the rear cylinders of the engine in the test cell (point 7 in Figure 8.2).

A close-up image of the leakage is illustrated in Figure 8.6. (A) is the leakage gap of hydrogen modelled as a pressure inlet, (B) is the cylinder and (C) is the contour of the fume hood.

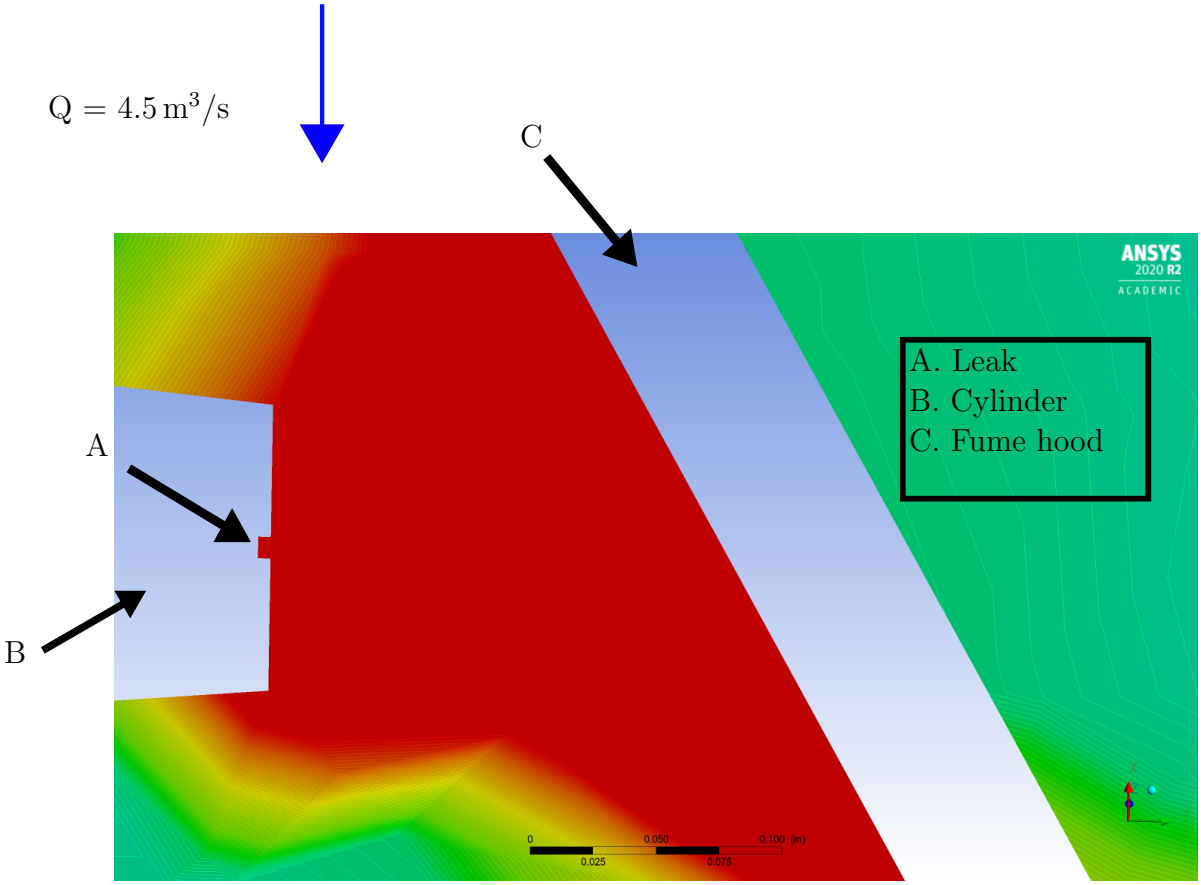

Figure 8.6: Leakage ($\dot{m} = 0.1\,\mathrm{kg/s}$) through a large gap (D = 10 mm) near the cylinder of the internal combustion engine. (A) is the leakage gap of hydrogen modelled as a pressure inlet, (B) is the engine cylinder and (C) is the contour of the fume hood.

A few more notes must be described prior to setting up the first models.

- The fuel pipe will be shut-off once the leakage has been detected during the experiment. The models below depict a result for a continuous hydrogen leak, thus a steady-state solution. A steady-state solution is sufficient for determining the most effective model and to observe whether hydrogen accumulates in local regions. However, the hydrogen volume concentrations provided by the models might be inflated as one will observe, it depends on how much time it requires for the sensors to detect the leak. The hydrogen leak will be interrupted in the subsequent section by changing the boundary condition of the hydrogen leakage from a pressure inlet to a wall.

- A leakage gap of 10 mm is very high and unlikely to occur during the experiment. Nonetheless, it is possible thus it may be considered as the absolute worst case

scenario. Hydrogen volume percentages will likely exceed the limit in such an event (as one will notice in the figures). The ventilation volumetric flow rate which is required to cope with such leakages is unfeasible (according to Equation 8.1 the ventilation rate should equal 111 m^3/s).

- One must multiply the depicted mass fraction by ≈ 14 to convert from mass fraction to volume concentration[2]. In ANSYS Fluent, there is only the option to plot the contour of the mass fraction, plotting the volume concentration is not possible.
- The ducting which encapsulates the internal combustion engine may not be straight but should be angled. The fume hood is a separate enclosed space in the test cell, the volume concentration of hydrogen will be high near the internal combustion engine if a wall is close near a potential leak source. Figure 8.7 and Figure 8.8 illustrate the effect of having an angled duct instead of a straight duct.

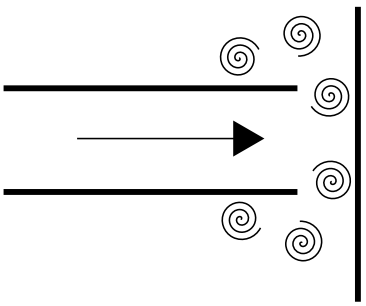

Figure 8.7: Hydrogen dispersion, impact on straight duct.

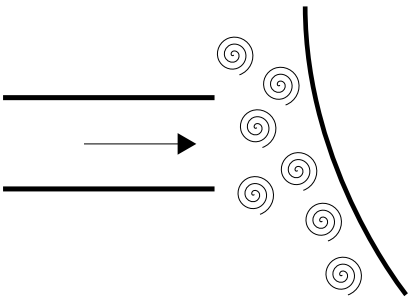

Figure 8.8: Hydrogen dispersion, impact on an angled duct.

8.2 Ventilation system CFD models

The three most effective ventilation systems are displayed in this section. The following model propositions are presented to hydrogen safety experts. The model will then be iterated once more according to the recommendations of the safety experts to obtain a final optimised ventilation system.

8.2.1 Ventilation system proposal 1

Figure 8.9 depicts the first model with a velocity contour as colour scheme. Air enters the test cell through duct 1 mounted on the ceiling. Inlet duct 2 directs air from the rear of the container to the front with the intention to dispose of warm air and potentially hydrogen through outlet duct 4 in the front. Furthermore, duct 3 is a second outlet.

[2]The ratio of air density to hydrogen density is ≈ 14.

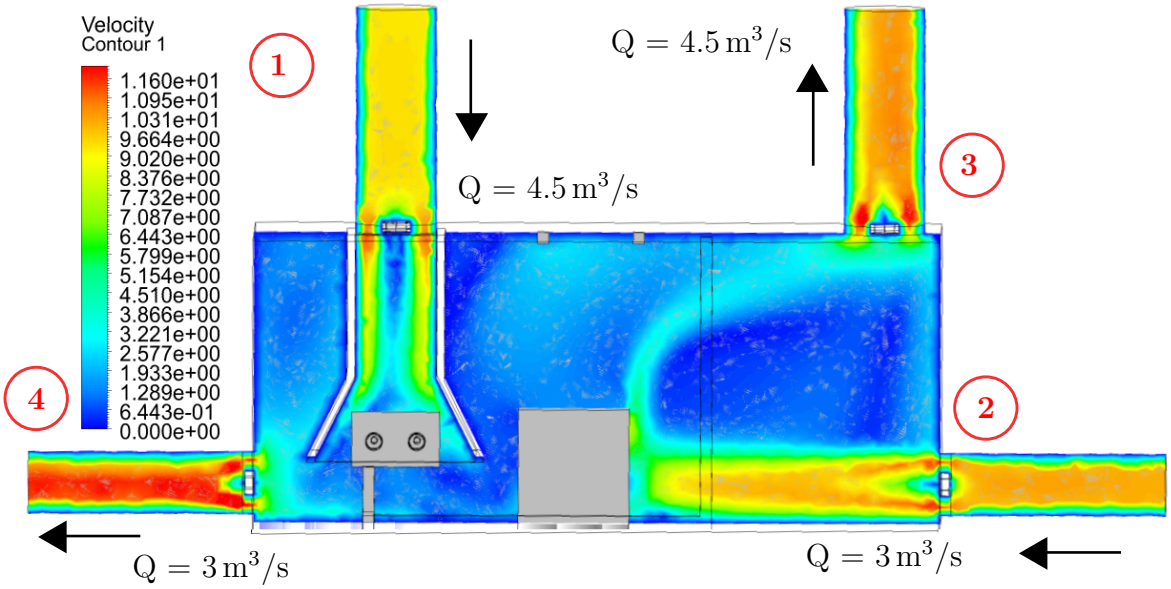

Figure 8.9: Velocity contour of model 1. Duct 1 and duct 2 push air into the test cell while duct 3 and 4 are outlets.

Figure 8.10 depicts the hydrogen mass fraction profile of model 1 through a colour scheme.

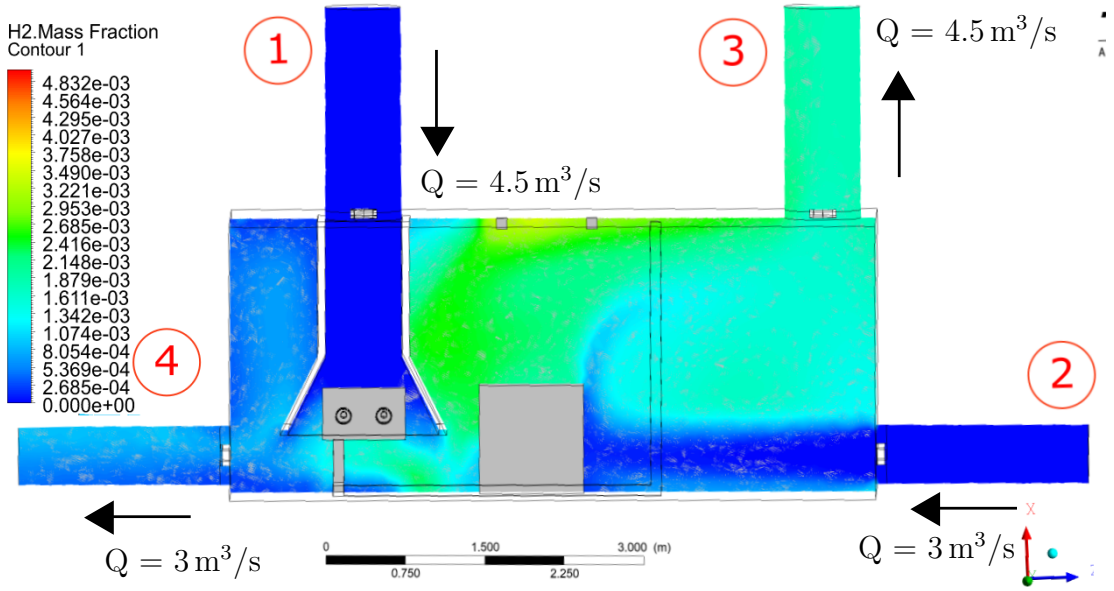

Figure 8.10: Hydrogen mass fraction contour of model 1. Duct 1 and duct 2 push air into the test cell while duct 3 and 4 are outlets.

ANSYS Fluent does not include a hydrogen volume concentration colour scheme. The observed values must be multiplied by a factor 14 to convert from hydrogen mass fraction to hydrogen volume fraction. Note that the results presented in this section are steady-state solutions. The leak is continuously conveying hydrogen into the test cell. The hydrogen supply through the fuel pipe will be shut-off immediately in practise. The observed values are thus possibly inflated. Transient tendencies are not captured in this section as it is only a means to compare models and to audit which set-up is most suitable.

Most hydrogen is disposed of through duct 3 mounted on the ceiling. A forced-draught fan does not influence the upstream flow enough to capture the dissipated heat and hydrogen entering the test cell through the leak. The momentum jet of hydrogen is too strong and therefore it rises to the ceiling and eventually is disposed of through the outlet duct mounted on the ceiling. Outlet duct 4 is not effective in disposing hydrogen. In addition, part of the hydrogen molecules flowing towards duct 3 are pushed back to the front of the test cell by the fan in duct 2. Note that volume concentrations of up to 4.9 % may be observed in the test cell.

The temperature profile in the test cell may be observed in Figure 8.11. The temperature contour ranges from 300 K (colour blue) to 305 K (colour red).

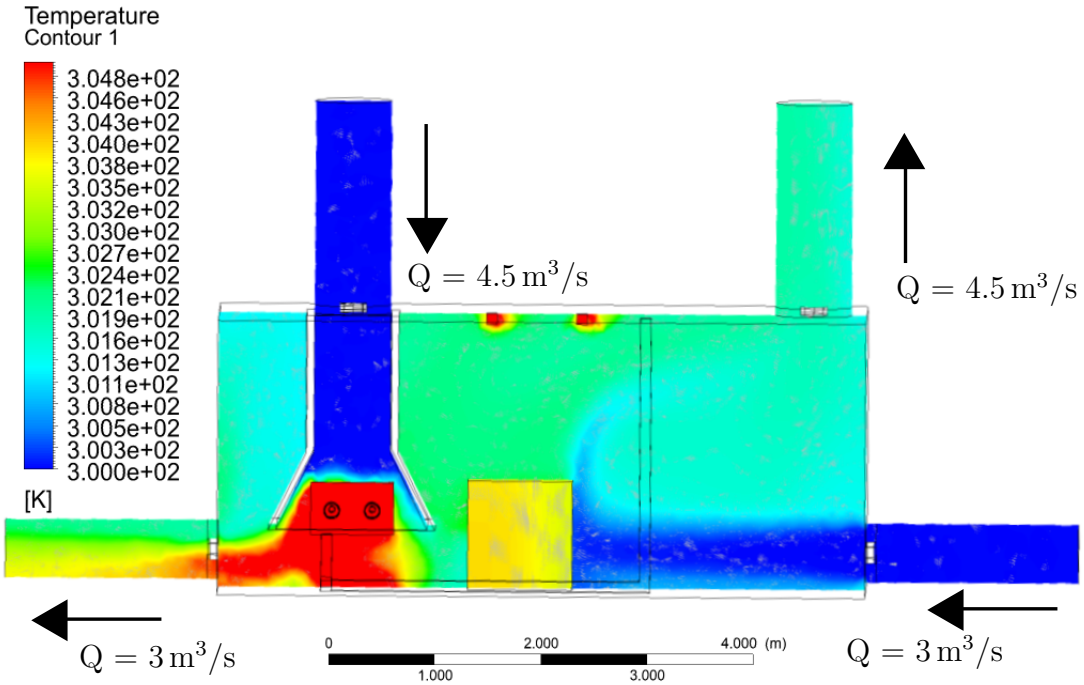

Figure 8.11: Temperature profile of model 1. A combustion process occurs in the cylinders in this model to be able to verify the expected temperature rise in the test cell.

The temperature in the test cell is expected to rise by 10 K. The temperature rise in the test cell is underestimated by this model due to not including the fin geometry and heat release of services. The temperature rise in the CFD model is estimated to be 3.45 K in Section 6.5.4[3]. The average temperature rise in the test cell is in the range of 3 to 4 K as the ambient temperature is set at 300K in the simulation. Hence, the empirical model approximates the temperature rise in the test cell well.

8.2.2 Ventilation system proposal 2

Model 2 is depicted in Figure 8.12. The boundary and cell zone conditions are set identical to the settings of model 1.

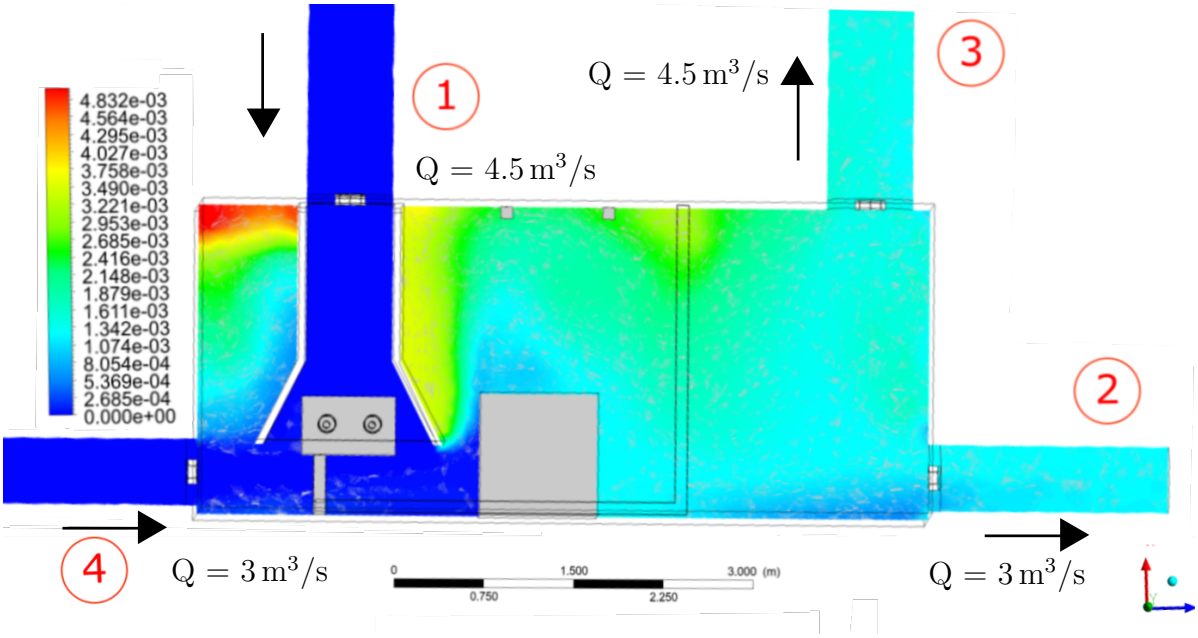

Figure 8.12: Hydrogen mass fraction contour of model 2 with a leakage gap diameter of 10 mm and source pressure of 20 bar.

Duct 1 and duct 4 are inlets for model 2, while duct 2 and duct 3 are outlets. The flow through duct 2 and duct 4 have been reversed in comparison to model 1. Model 2 includes a few benefits and a few drawbacks compared to model 1.

The accumulation of hydrogen near the top left of the figure may be noticed. The circulation is poor near the upper left corner of the container with both outlet fans mounted at the rear of the container. The buoyant forces of hydrogen are presumed to be stronger than the flow field. An angled roof could be a solution to direct the

[3]The temperature contours are obtained through the energy balance model to verify the temperature rise in the test cell.

flow towards the ceiling fan. This may be dangerous however, for example assume the roof is angled by a wooden structure. The angled roof may contain gaps near the wall since the contour of the container wall is rippled. Cavities may appear in the roof contour due to poor fitting. Consequently, hydrogen may accumulate in those cavities. Alternatively the entire container may be tilted to direct hydrogen towards the rear of the container. Tilting the container is inconvenient however and a more suitable solution will be provided in Section 8.2.5.

In contrast to model 1, this ventilation set-up averts the accumulation of heat and hydrogen beneath the engine. Furthermore, the diffusion of hydrogen is controlled well as hydrogen flows smoothly from the front of the container to the rear. The average volume concentration of hydrogen in model 2 is therefore lower than in model 1 (which may be observed through the colour scheme). One drawback however is the accumulation near the roof near the top left corner of the container.

Furthermore, the average temperature in model 2 is slightly higher than in model 1. Duct 4 immediately disposes some of the warm air released by the engine. Warm air must propagate through the entire container prior to being disposed of in model 2. Therefore is the average temperature slightly higher in the test cell, which may be deduced from the temperature profile depicted in Figure 8.13.

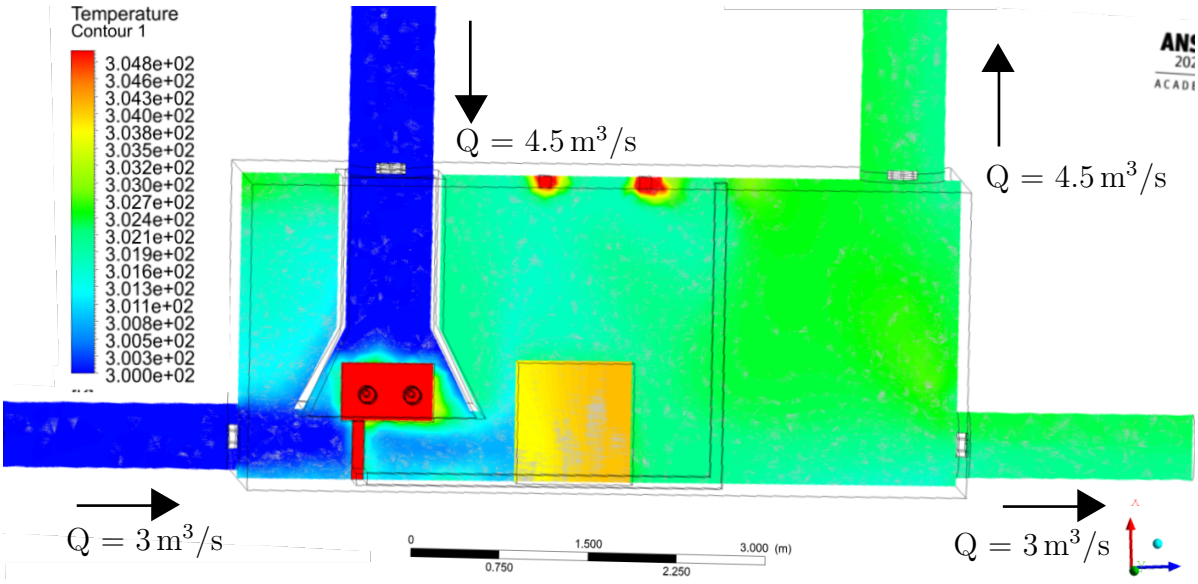

Figure 8.13: Temperature profile of model 2. The temperature ranges from 300 K (blue colour) to 305 K (red colour).

8.2.3 Ventilation system proposal 3

Model 3 is identical to model 2 except for the placement of the fans at the rear. The contour and wire frame of duct 2 and 4 may be seen in the figure but the flow in the respective channels is not visible. The fans in ducts 2 and 3 are not positioned on the same plane. The outlet fan mounted on the roof is behind the depicted 2D contour and the outlet fan mounted on the side wall is mounted in front. The inlets remain duct 1 and 4 and the outlets remain duct 2 and 3.

The hydrogen mass fraction profile of model 3 is depicted in Figure 8.14. Note that the hydrogen mass fraction scale is slightly different. In model 3 it ranges from 0 to 0.01 while for the previous two models it ranges from 0 to 0.005.

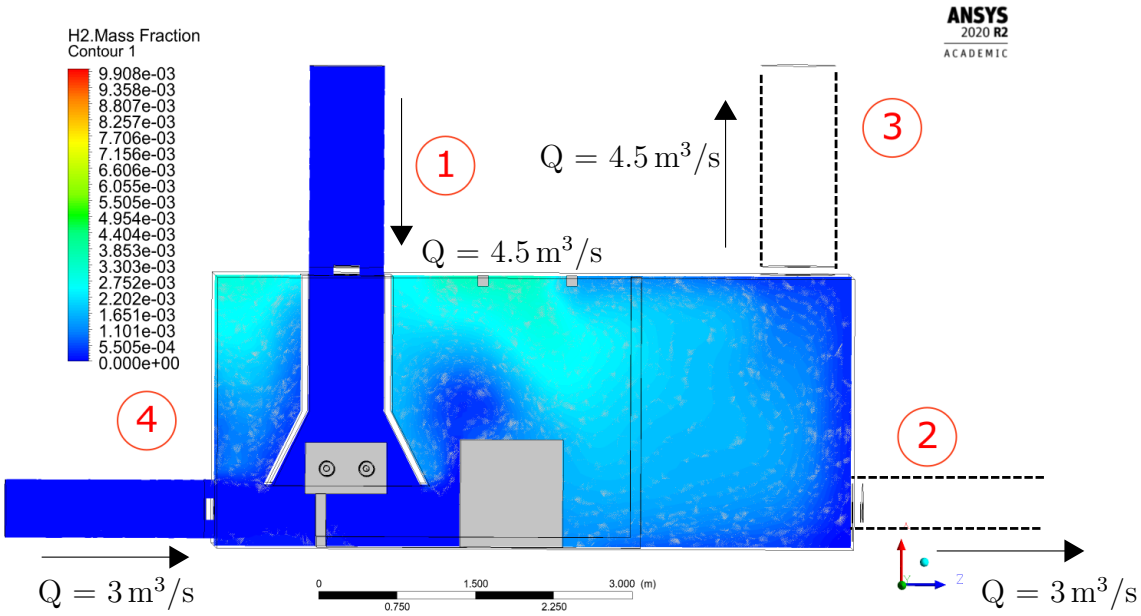

Figure 8.14: Hydrogen diffusion in model 3 with a leakage gap diameter of 10 mm and fuel pipe pressure of 20 bar.

The benefit of model 3 with respect to model 2 is the larger air circulation in the rear of the container as the outlet ducts are distanced from each other. The outlet fans interact with each other upstream in model 2, yielding an overall lower outlet mass flow rate.

Table 8.5 shows the difference in total outlet mass flow between model 2 and 3.

Table 8.5: Outlet volumetric flow rate for model 2 and model 3.

	Model 2	**Model 3**
Q	7.1 m^3/s	7.35 m^3/s

Furthermore, warm air and hydrogen are less likely to accumulate in the corners at the rear of the container in model 3. The temperature dispersion for model 3 is nearly identical to the temperature profile in Figure 8.13.

8.2.4 Intermediate conclusions CFD models

the following observations are made by testing various ventilation set-ups;

- Cross ventilation is most effective regarding the disposal of hydrogen and warm air. Flow is directed from one side to the other with fans mounted on the two opposing walls of the test cell. Therefore turbulence and mixing decrease while the disposal of hydrogen and heat increase.

- Installing the inlet and outlet ventilation fans on opposing sides furthermore enforces the flow to move in one direction. A pressure differential is generated within the test cell, a natural flow from the front of the test cell to the back emerges which guides hydrogen and warm air to the environment primarily through the outlet duct mounted on the roof.

- Hydrogen may accumulate near objects mounted on the ceiling. Near lamps for instance slightly higher hydrogen volume concentrations are noticed than elsewhere in the room. Flow circulation is low at the ceiling as the inlet ducts only dictate the flow near the floor of the container. Elements mounted on the ceiling may impede the outflow of hydrogen.

- Heat and hydrogen accumulate beneath the engine as the cooling fan pushes air downwards, an inlet ventilation fan must actively push the flow towards the rear of the container. It is not effective to pull the flow into an outlet duct mounted near the internal combustion engine as fans do not have much influence upstream.

- The supply of hydrogen through the fuel pipe should be shut down automatically by a shut-off valve once a leak is detected. The total hydrogen mass entering the test cell may be overestimated since a steady-state simulation is performed. A few methods will be applied to capture the transient tendencies of hydrogen. The boundary condition of the hydrogen leak will be changed into a wall once the solution has converged in the following section. Consequently, the flow field will be captured at multiple succeeding pseudo time steps to observe the diffusion of hydrogen. The time frame between each pseudo time step remains unknown however since the simulation remains a steady-state solution.

8.2.5 Roof vents to prevent hydrogen accumulation

Roof vents are an effective tool to dispose of hydrogen when it accumulates in a local region in the container. Especially model 2 and 3 can greatly benefit from roof vents to dispose of hydrogen accumulating near the upper left side of the container.

The roof vents in Figure 8.15 are proposed [4]. The roof vents are powered by a small engine.

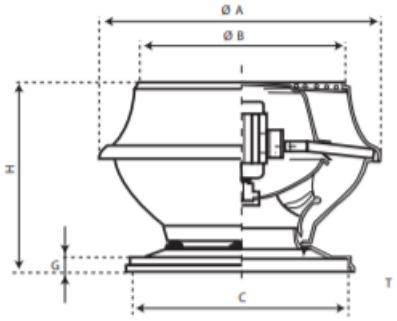

Figure 8.15: Roof vents will be mounted on the ceiling to prevent the accumulation of hydrogen in poorly ventilated areas.

The characteristics of the proposed roof vent are displayed in Table 8.6.

Table 8.6: Characteristics of the proposed roof ventilation vents

Parameter	**Value**
R_{vent}	125 mm
$\dot{m}_{vent}$	$0.25\,m^3/s$
u_{vent}	2 m/s

8.3 First iteration ventilation system design

A first iteration of the ventilation system is developed by incorporating the intermediate conclusions of Section 8.2.4, the model is illustrated in Figure 8.16.

The model is identical to model 3 besides two roof vents near the roof. The roof vents are indicated by two arrows as the contours of the vents are difficult to notice. Hydrogen accumulated in the top left of the test cell in model 3. The roof ventilators ensure the accumulation of hydrogen is bypassed. Model 3 with roof ventilators is established as the most effective design to dispose of heat and hydrogen.

It can be noted that the maximum hydrogen volume concentration in Figure 8.16 equals 7 %. Hydrogen leaks for an infinite amount of time and therefore the values

[4] https://www.nedair.nl/service/

are slightly inflated as. Nonetheless, 7 % considerably exceeds the allowed limit and a solution must be found.

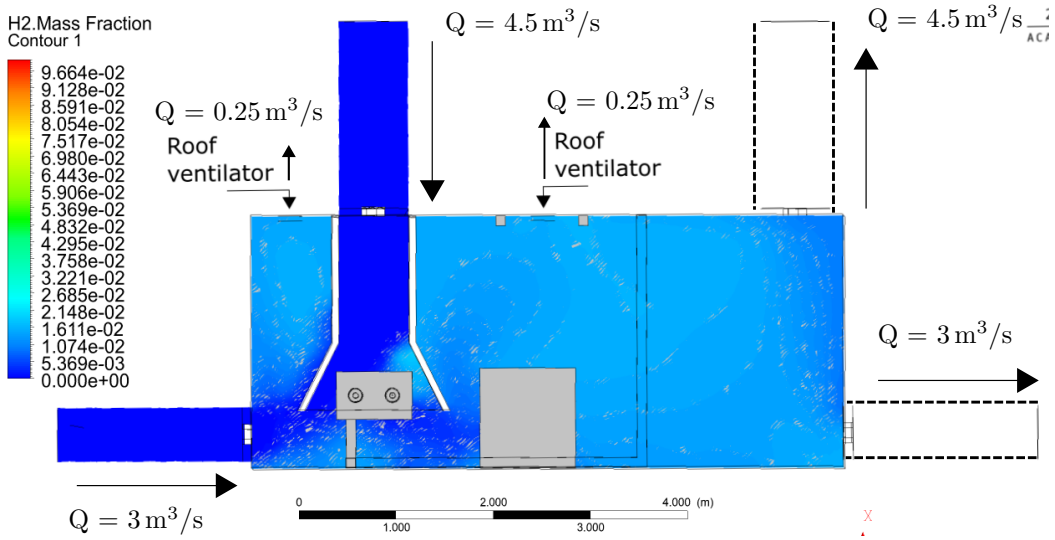

Figure 8.16: First iteration ventilation system for the test cell. The hydrogen mass fraction contour is depicted in the figure.

However, first the transient tendencies are captured to further analyse the model. The state in Figure 8.17 is obtained after one iteration with the hydrogen supply shut-off.

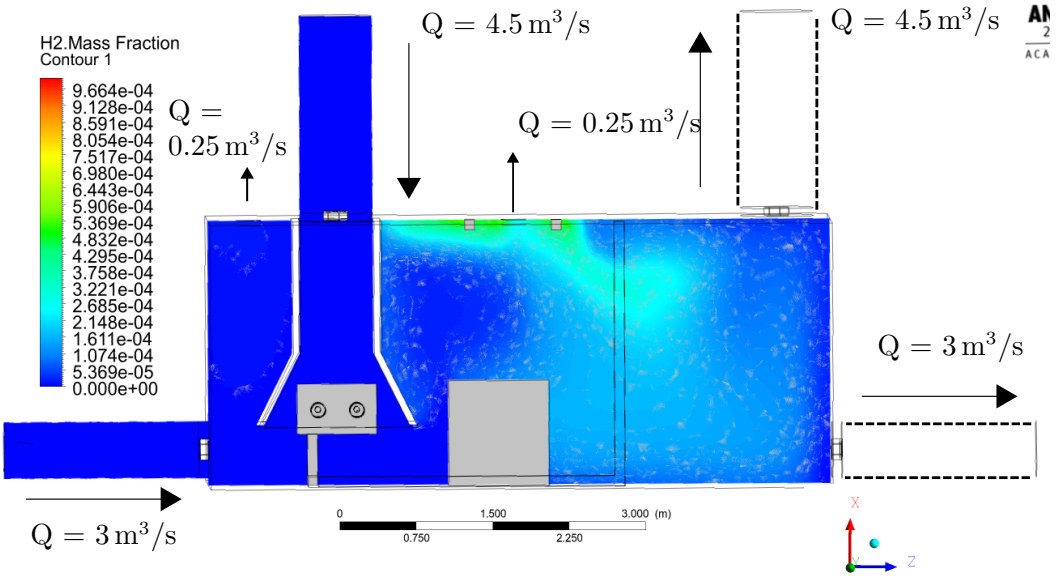

Figure 8.17: Hydrogen diffusion one iteration after the fuel supply has been shut-off. The model depicted is the first iteration of the ventilation system design.

The inlet boundary condition of the leakage is set to a wall to observe the transient tendencies of the diffusion of hydrogen ANSYS Fluent. The diffusion of hydrogen in the test cell is analysed by setting the time scale factor to 1E-7.

Some hydrogen remains in the test cell but it does not accumulate in any local region. The model includes an initial leak of 0.1 kg/s, the maximum hydrogen volume concentration is reduced to 0.14 % after one pseudo time-step.

Furthermore, Figure 8.18 depicts the hydrogen mass fraction contour in the test cell after three pseudo time steps. Figure 8.18 illustrates no hydrogen accumulates in the test cell and is disposed of well over time.

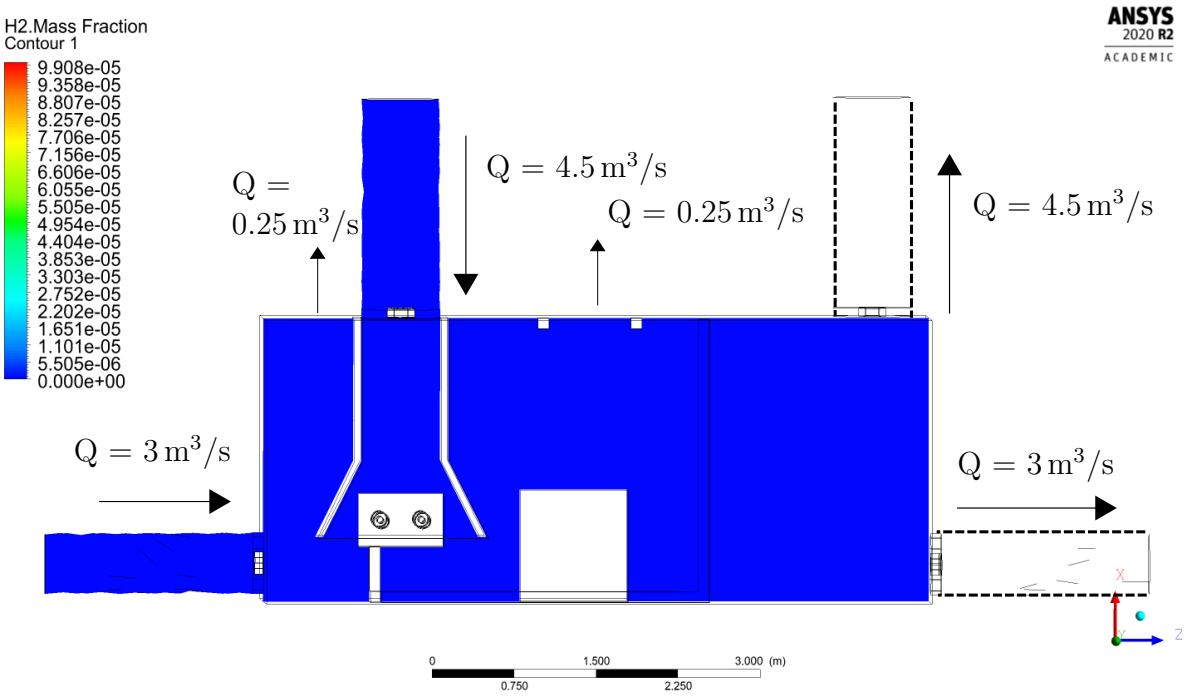

Figure 8.18: Hydrogen diffusion three iterations after shut-off for the first iteration of the ventilation system design.

One may furthermore not neglect the dispersion of the hydrogen-air mixture in the test cell. In the middle right of the test cell hydrogen is present in both Figure 8.17 and Figure 8.18 as enough time elapses for hydrogen to mix with air. Hydrogen should not be present in this region as electrical equipment is situated in the rear of the container. The risk should be further mitigated despite each component being ATEX-3 protected (gas- and dust tight). Hydrogen is observed near the middle of the test cell as well for leaks with smaller diameters and lower leak mass flow rates.

Additional precautions are necessary to reduce the risks depicted in Table 7.6. When hydrogen leaks it must immediately be directed to the environment. Hydrogen

has therefore less time to mix with air and does not descend and flow over electrical equipment in the rear of container. Alternatively, a design can be developed such that hydrogen cannot reach the remainder of the test set-up. The first step to obtain a permit is achieved if one can find a solution for hydrogen propagating over the test set-up.

A possible solution is depicted in Figure 8.19. A gas tight wall prevents hydrogen flowing over the remainder of the test cell. The suggestion will be further discussed in Chapter 9.

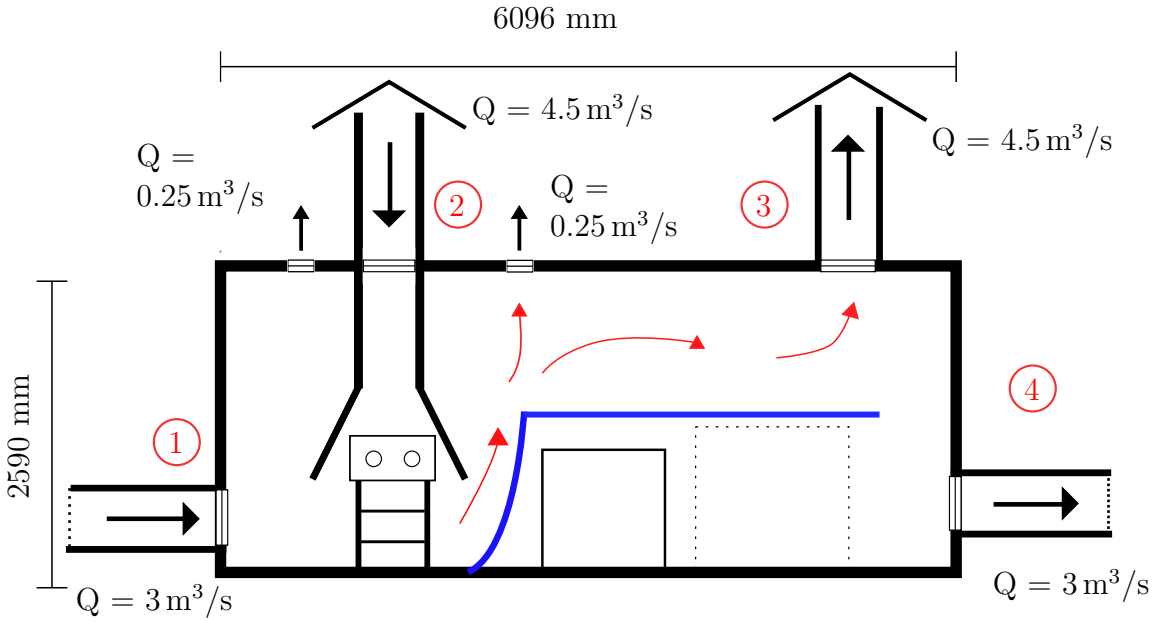

Figure 8.19: A gas tight wall prevents hydrogen flowing over the dynamometer and electrical equipment in the test cell.

8.4 ANSYS Fluent CFD model verification

A converged CFD solution is not a warranty on a physical representation of reality. Errors in the set-up, such as setting incorrect boundary conditions, poor meshing, or an inaccuracy in the geometry of the 3D model yield poor results.

8.4.1 CFD model verification strategy

Fluent provides researchers with a few guidelines and methods to ensure the solution has converged. The following methods are utilised to verify the mesh;

- Grid inspection
- Residuals meet minimum criteria and converge

- Audit mass balance
- Audit flow conditions in test cell
- Refining the mesh

Grid inspection

Grid inspection is a technique to examine the quality of the mesh. The grid must comply to the following criteria defined by ANSYS Fluent. The mesh is considered to be obsolete and should be adjusted if it does not meet one or more criteria described in Table 8.7.

Fluent defines a quality of 0.75 as good. Yet, the mesh quality must be raised to a higher quality if possible.

Table 8.7: The mesh must comply to the following quality factors. The skewness factor and aspect ratio must be minimised while the cell quality must be maximised.

Quality factor	**Limit**
Maximum aspect ratio	$\leq$35
Maximum skewness	$\leq$0.95
Average skewness	$\leq$0.35
Minimum cell quality	$\geq$0.01
Average cell quality	$\geq$0.75

Mesh convergence by monitoring residuals

The second step is to monitor the residuals. A simulation is run when a mesh conforms to the criteria defined in Section 8.4.1. Each simulation must meet the following residual convergence criteria.

- The trend of the residual curve must be linear. Hence, the residual is neither increasing nor decreasing over numerous iterations.
- The continuity equation, velocity equation and species residuals attain a convergence value of 10E-3 or less.
- The energy equation must attain a residual value of 10E-6 or less.

ANSYS Fluent monitors the scaled residuals by standard, ergo the absolute change in value between each iteration. The flow conditions in the test cell continuously vary due to the spinning ventilation fans. The residuals are expected to fluctuate even when the

simulation has converged. One can normalise the residuals in Fluent, subsequently the residuals monitor displays the difference between each iteration in percentages instead of absolute values. The slope of the residuals should flatten when the simulation converges and the normalised setting is selected.

Cell mass balance

The mass balance is checked upon convergence. The mass balance is defined as the difference between mass entering the cell subtracted by mass flowing out of the cell. This value should be zero as by the conservation of mass. Fluent monitors both the maximum negative and maximum positive change in mass between cells, hence a negative and positive value. The negative value refers to more mass leaving the cell than entering, while a positive value refers to less mass leaving than entering the cell. The net imbalance may not be larger than 1 % of the smallest mass flux in the domain[5].

Monitoring flow parameters

The following step is to analyse the flow and energy conditions in the test cell. For instance, the ventilation fans must equal the input values and the engine must attain a physical temperature. The simulation is discarded if impractical values are obtained or values do not accord with the input values.

Mesh refinement

The mesh is refined when it complies to all the previous criteria. Coarse meshes have the benefit of less computing time while fine meshes provide more detail. A balance must be found between the computational cost and detail.

The initial mesh will be coarse, which will be refined by a factor 1.5 until the flow conditions (engine temperature, mass flux) do not differ by more than 1 % compared to the previous mesh. To ensure the small difference is no coincidence, a visual inspection is performed to compare the differences between each mesh. The mesh is considered to be sufficient if none or only small differences are observed. The guideline of ANSYS Fluent mentions that the allowed tolerance during a mesh refinement should be set by the user itself, Fluent does not define a tolerance value as it highly depends on the purpose of the simulation. Most users often apply a difference of 1 % between subsequent meshes for rougher analysis while only very small percentages are allowed for finer analysis. For example, a 1 % difference is considered to be significant for optimising the efficiency of a turbine blade[6].

One must note that the solution which is obtained is a pseudo steady state solution. An average value will be documented of the flow parameters by pausing the simulation at multiple iterations.

[5]The smallest mass flux in the test cell will be the mass flow inlet of hydrogen.

[6]`https://www.afs.enea.it/project/neptunius/`[Retrieved 10.02.2021]

8.4.2 Verification results

The mesh convergence of the pseudo steady state solution is shown in Table 8.8. The maximum average engine temperature is measured by documenting the temperature at multiple pseudo time steps. The temperature is documented once the solution has converged. Hereafter an average temperature is obtained, which partially mitigates the error induced by the transient tendencies of the solution.

Table 8.8: Change in average engine temperature with mesh refinement. The average value is documented by taking the average value at five different pseudo time steps.

	Engine max. average temperature (K)
Mesh 1 = 44,000 cells	757.9
Mesh 2 = 71,480 cells	766.18
Mesh 3 = 116,950 cells	787.9
Mesh 4 = 171,549 cells	747.92
Mesh 5 = 230,973 cells	740.3
Mesh 6 = 305,493 cells	720
Mesh 7 = 359,936 cells	691.4
Mesh 8 = 477,989 cells	695

Larger temperature gradients are observed for the coarser meshes. Finer meshes ($\approx$ 300,000 cells+) have maximum fluctuations of 2 K, while coarser meshes may have fluctuations up to 30 K. A visual inspection is performed on the velocity flow fields. Refining the mesh beyond 300,000 did not yield additional detail by observing the flow field. Only small differences are observed between mesh 6 and 7. Mesh 6 may be considered to be a sufficiently dense grid considering the purpose of the CFD analysis. The test cell includes many simplifications, a very refined mesh does not necessarily provide more information. The objective is to obtain results to subsequently provide the test cell constructor with adequate recommendations. However, the difference in engine cylinder temperature between mesh 6 and mesh 7 equals 4 %, a denser mesh is selected to ensure the quality of the simulation. The difference in percentage between mesh 7 and 8 is 0.4 %, therefore mesh 7 is selected as final grid. In Appendix C the mesh refinement is illustrated through depicting the velocity profile of each grid.

One may observe the ventilation volumetric flow rate is less than 7.5 m^3/s in Table 8.8. Fluent computes the maximum inlet velocity[7] rather than the mean velocity through the fan for a designated pressure jump. The fan velocity is estimated in Section 4.2.5 through Equation 8.5,

[7]The velocity is higher near the edges of a fan than near the middle.

$$\frac{Q_{\text{fan}}}{A_{\text{fan}}} = u_{\text{fan}}, \tag{8.5}$$

which yields the mean fan velocity. Subsequently the volumetric flow rate through the fan is underestimated. The influence of changing the inlet volumetric flow rate will be studied during the sensitivity analysis. Nonetheless, the ventilation fans will not constantly be operating at maximum power and therefore the selected pressure jump is valid as well[8].

The residuals of one of the optimised models are displayed in Figure 8.20. Fluent is only able to show the last 5000 iterations and therefore the residuals between iterations 1 and 5000 are not visible in the figure. The grid complies to the convergence criterion of residuals.

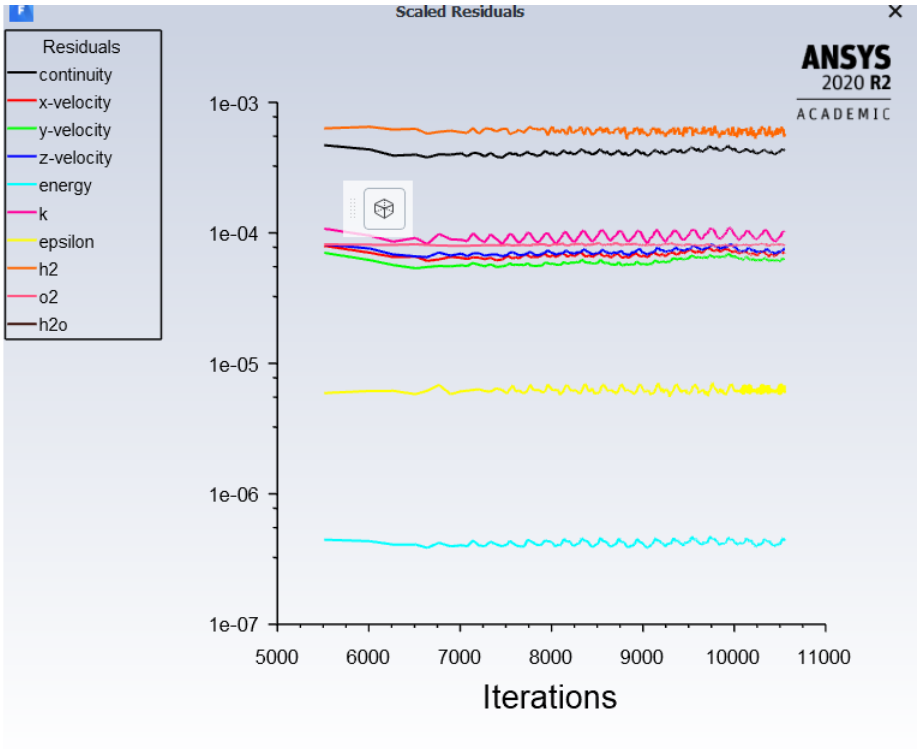

Figure 8.20: Small fluctuations may be noticed in the residuals of the optimised model due to transient tendencies at the steady-state solution for a mesh size of ≈ 350,000 cells.

The absolute values of the scaled residuals in Figure 8.20 are displayed in Table 8.9.

[8]In fact, the ventilation fans will rarely operate at maximum power, simulating the flow field with a slightly lower inlet volumetric flow rate is thus of low consequence

Table 8.9: Residuals for the optimised model with 13,816 iterations (simulation time 10 hours and 36 minutes).

Equation	**Residuals**
Continuity	$4.86 \cdot 10^{-04}$
X-velocity	$7.57 \cdot 10^{-05}$
Y-velocity	$8.99 \cdot 10^{-05}$
Z-velocity	$9.55 \cdot 10^{-05}$
Energy	$5.03 \cdot 10^{-07}$
k	$9.91 \cdot 10^{-05}$
ϵ	$4.62 \cdot 10^{-06}$
Fmean	$5.77 \cdot 10^{-04}$
Fvar	$8.37 \cdot 10^{-05}$

The quality parameters of the final mesh are displayed in Table 8.10. The net imbalance criteria is met with a maximum imbalance of 0.0949 %. The highest value of the maximum positive and negative mass imbalance is divided by the smallest mass flux value in the test cell to obtain the net imbalance percentage. The mesh complies to the remaining criteria as well.

Table 8.10: Mesh quality factors of the final mesh.

Quality factors	**$\approx$ Mesh = 350,000 cells**
Average cell quality	0.84
Minimum cell quality	0.16
Maximum skewness factor	0.94
Maximum aspect ratio	0.14
Maximum net imbalance (kg/s)	3.50E-07
Minimum net imbalance (kg/s)	4.10E-07

The effect of reducing the pseudo time step of the solver can be observed in Figure 8.21 (as explained in Appendix A.2.5).

The scaled residuals between iterations must decrease when the time scale factor is reduced and the solution has converged. Note, the residuals in Figure 8.21 are not for the optimised model but of a coarser mesh. The figure clarifies the applied approach and the convergence method is employed for each simulation.

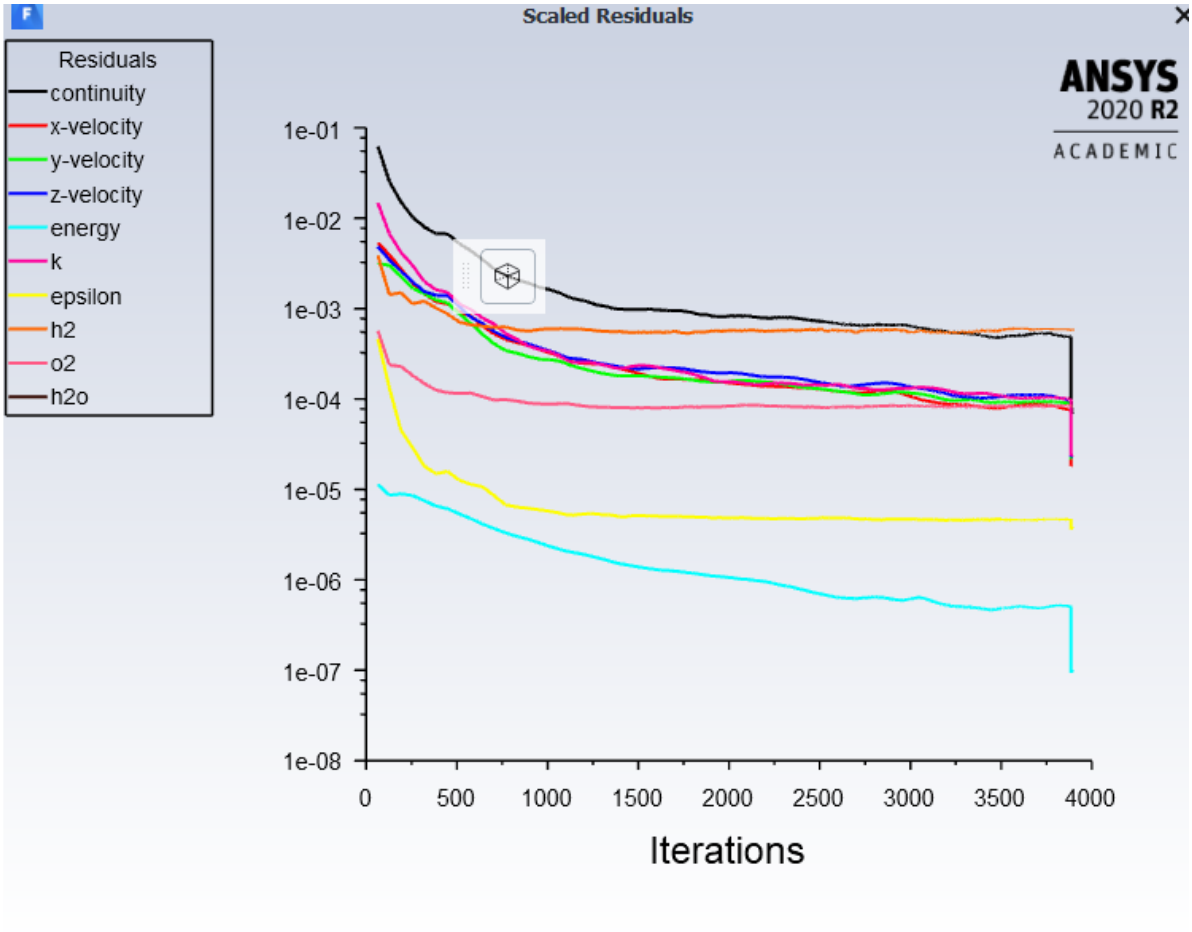

Figure 8.21: Scaled residuals decrease when the time scale factor is reduced.

8.5 Validation CFD model ventilation system

Validation generally succeeds the CFD simulation. Part of the validation assessment precedes the simulations since a few flow parameters are estimated in Chapter 4, Chapter 6 and Chapter 7 through empirical models. The fans are selected and the buoyancy tendencies of warm air and hydrogen are estimated in Chapter 6. The results obtained in Chapter 6 must be compared to the CFD simulations. For example, whether the designated pressure jump of the ventilation fans results in a capacity which aligns with data provided by the manufacturer. In addition, the ducts induce pressure losses which are estimated through empirical models. The calculated losses should be compared to the results obtained through Fluent. First, the energy balance and cooling velocity will be validated.

8.5.1 Validation heat balance and air cooling system

The combustion model is included to validate the required air cooling velocity and temperature rise in the test cell obtained through the empirical method and literature. Validation is necessary as the piston engines in literature and the ones utilised to obtain the empirical model include older engine models.

The cylinder temperature is obtained through the energy balance model in ANSYS Fluent. Figure 8.22 displays the cylinder temperature with stoichiometric aviation gasoline within the combustion chamber. (A) is the combustion chamber, (B) the cylinder barrel, (C) the inlet air flow and (D) the connection to the engine block.

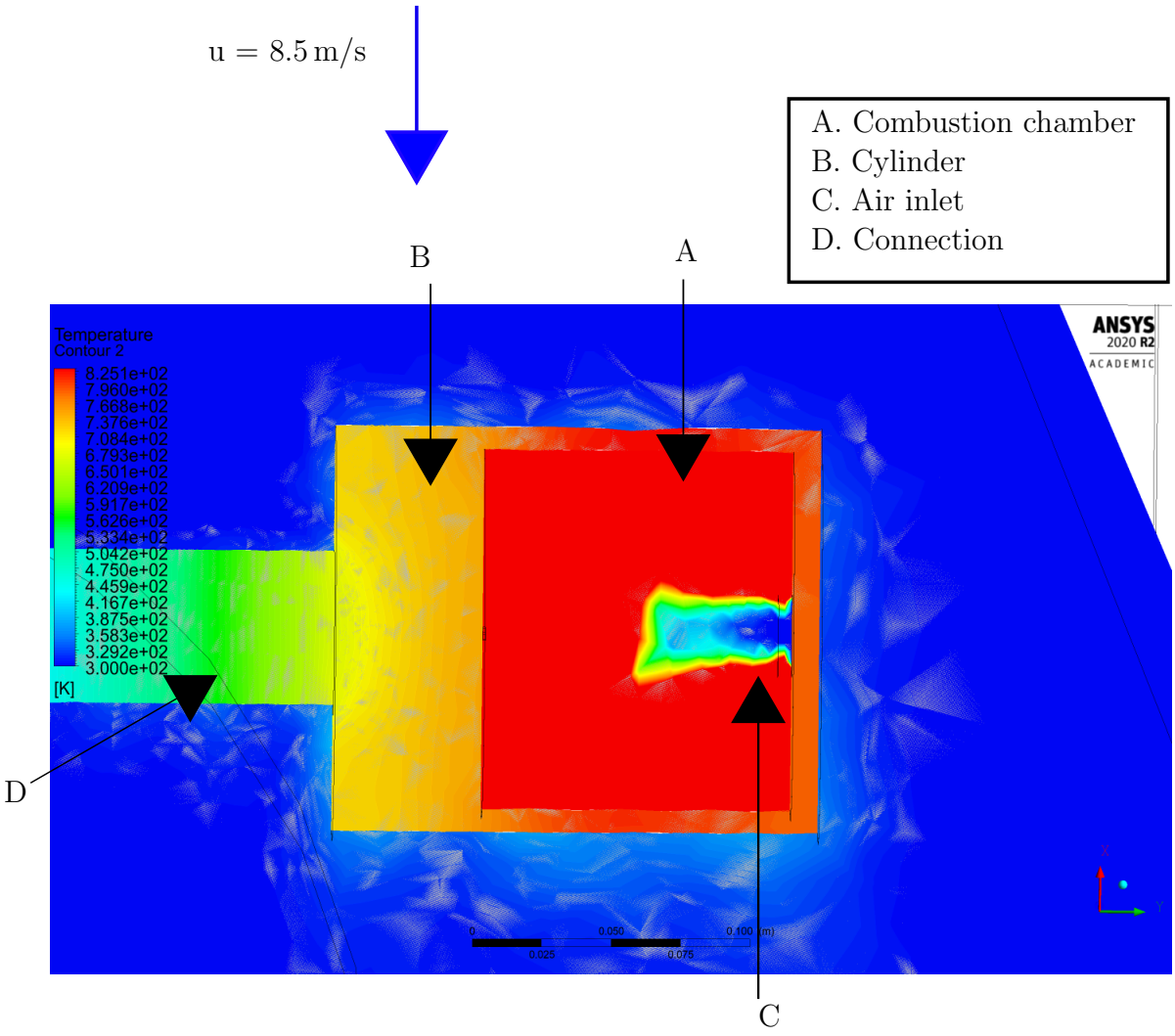

Figure 8.22: Cylinder temperature in the energy balance model, stoichiometric aviation gasoline combustion occurs within the test cell. (A) is the combustion chamber, (B) the cylinder barrel, (C) the inlet air flow and (D) the connection to the engine block.

The aviation gasoline inlet spray is too small to be noticed and is similar to the air flowing into the combustion chamber through the inlet (C in Figure 8.22). The model includes aviation gasoline combustion as data is limited on combustion chamber temperatures with hydrogen combustion. In addition, the equivalence ratio will decrease for a retrofit hydrogen internal combustion engine, it is presumed less cooling air is required to maintain the engine cylinder temperature at 453 K as discussed in Chapter 6. Nonetheless, the cooling fan will include a margin of safety in case more air cooling is required to maintain the engine cylinder temperature with hydrogen combustion. Further research is required to model the combustion chamber temperature with hydrogen. The inlet air and aviation gasoline mass flow for economy cruise power settings are obtained through (Lycoming Manual, 2005).

One may notice grey contours near the cylinder in Figure 8.22. One must visualise the contour of the flow parameter on a grey 2D plane to obtain a visual of the 2D plane displayed in Figure 8.22. The colour scheme is modelled on top of the grey plane. Consequently, the grey contours of the 2D plane overlap with the colour contour. These grey contours of the 2D plane are sometimes visible within the figure and is merely a slight visual imperfection.

The estimated temperature in Section 6.5.4 for the cylinder walls is 835.5 K without oil cooling and cooling fins. The obtained cylinder wall temperature in ANSYS Fluent is 800 K with pressure jumps of 85.86 Pa and 88.93 Pa for the U/EI-EIL 564 and U/EI-EIL 715 respectively.

The pressure jumps entail an air cooling velocity of 8.5 m/s over the cylinders, which is considerably lower than the estimated 15.97 m/s. However, one obtains a cooling velocity of 15.97 m/s with induced draught-fans. ANSYS Fluent predicts a cooling velocity of 8.5 m/s is sufficient with forced draught-fans.

The velocity of the cooling fan may still be adjusted in the test cell container by reducing or increasing the cross sectional area of the duct. The estimated required air cooling velocity is presumed to be an accurate initial guess and thus simulating the hydrogen diffusion model with the estimated pressure jumps of 85.86 Pa and 88.93 Pa for the U/EI-EIL 564 and U/EI-EIL 715 respectively is valid.

8.5.2 Hydrogen & air flow tendencies in the test cell

It may be noted in Figure 8.11 and Figure 8.13 (temperature profiles in model 1 and 2) warm air does not accumulate in local flow fields. The flow of warm air is primarily dictated by the high velocities in the test cell. An average test cell velocity of 3.04 m/s is estimated in Section 7.1.2, which is furthermore observed in Fluent as well. The buoyant velocity of warm air released by the internal combustion engine yields 0.28 m/s. Warm air is thus predicted to be dictated by the high average velocity within the test cell. In contrast, the buoyancy velocity of hydrogen ranges from 1.2 m/s to 9.1 m/s prior to mixing with air. Specifically in model 3 it can be observed hydrogen accumulates in the

top left corner of the test cell whilst warm air is disposed of.

8.5.3 Flow parameters empirical model versus CFD

Experimental values are compared to the obtained values from the CFD model and summarised in Table 8.11.

Table 8.11: Experimental values obtained through literature or empirical methods versus values obtained in ANSYS Fluent.

Variables	**Experimental**	**ANSYS**
$Q_{\text{U/EI-EIL 715}}$ (m^3/s)	4.58	3.77
$u_{\text{U/EI-EIL 715}}$ (m/s)	12.05	12
$Q_{\text{U/EI-EIL 564}}$ (m^3/s)	2.92	2.35
$u_{\text{U/EI-EIL 564}}$ (m/s)	11.84	11.5
$u_{\text{hydrogen leak}}$ (m/s)	1,270	1,300
$T_{\text{Dynamometer}}$ (K)	303 - 323	305
$p_{\text{loss duct}}$ (Pa)	3.6	3.43
$u^1_{\text{Average test cell}}$ (m/s)	3.04	2.5 - 3.5
$T_{\text{Hydrogen flame}}$ (K)	2,318	2,248
$T^2_{\text{Average test cell}}$ (K)	10	2.5-3.5

[1] The average test cell velocity in ANSYS is roughly estimated by observing the flow field in post CFD.
[2] The temperature rise is expected to be underestimated due to the neglect of the cooling fins and services in the model. The expected temperature rise in the test cell is estimated to be 3.45 K.

8.5.4 Anticipated errors cylinder & test cell temperature

A large difference may be noted in temperature rise between the experimental and post CFD results from ANSYS Fluent in Table 8.11. The average temperature rise in the test cell according to the experimental values should be approximately 10 K, while Fluent estimates a temperature rise in the range of 2.5 K to 3.5 K. The error is induced by not including the cooling fins on the cylinders and by not including the heat released by the fans and services. It is estimated in Section 6.5.4 Fluent models a temperature rise of approximately 3.04 K by not including these heat sources, which complies to the observed temperature rise in the test cell.

8.6 CFD model sensitivity analysis

The CFD model includes various simplifications for which the repercussions are not documented well yet such as simplifying the geometry of the engine. In addition, the ambient parameters will vary from day to day. One can further model what occurs during a storm (changing boundary conditions). In essence, an infinite amount of CFD models can be set up to analyse the effect of each component or each event in detail.

The shape of objects and boundary conditions are experimented with to analyse the effect of a varying design and a varying environment in this section.

8.6.1 Varying hydrogen leak flow rate

Two simulations are performed, one includes a mass flow rate of 0.1 kg/s whilst the other entails a mass flow rate of 0.05 kg/s.

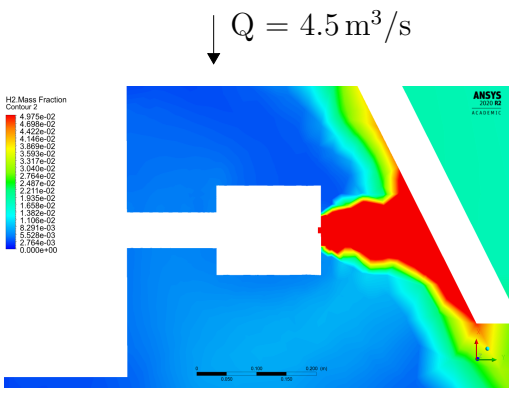

Figure 8.23: Momentum jet of a leak with a mass flow rate of 0.1 kg/s.

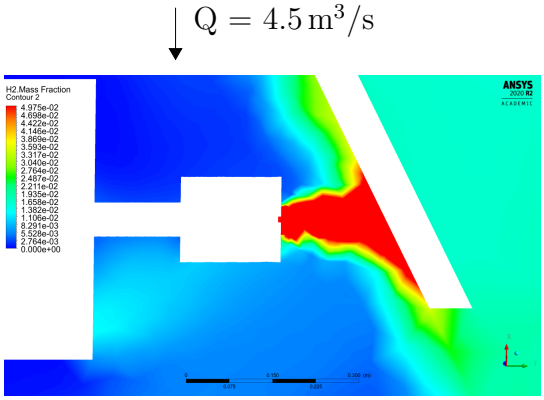

Figure 8.24: Momentum jet of a leak with mass flow rate of 0.05 kg/s.

The simulation with a mass flow of 0.1 kg/s is depicted in Figure 8.23, Figure 8.24 depicts the model with a hydrogen mass flow of 0.05 kg/s.

The colour scheme depicts the hydrogen mass fraction in the figure. One may observe the mass fraction in the left figure is higher than in the right figure, which is expected due to a larger leak. The diffusion of hydrogen in the area is similar however. The highest concentration is observed near the leak after which it is pushed downwards by the cooling air from above. Leaks from varying sizes are therefore expected to behave similarly.

8.6.2 Varying dynamometer geometry

hydrogen and warm air may be captured in the wake of an element. The wake downstream of the element depends on its contour. For example, an object with round corners will yield a different wake than an object with sharp corners. In the following example,

one model includes a dynamometer with a sharp corner (Figure 8.25) and another with a rounded corner (Figure 8.26).

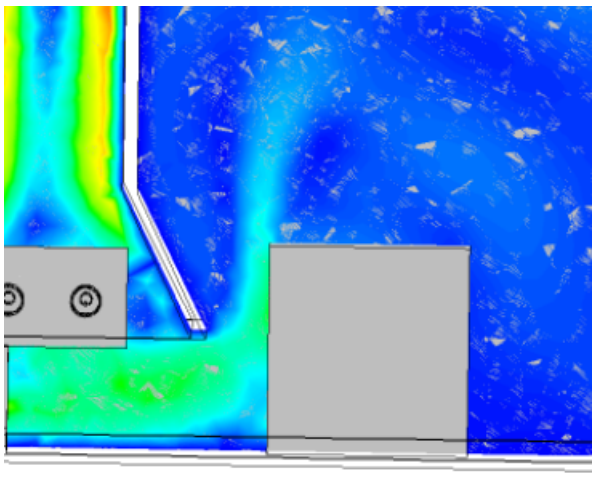

Figure 8.25: Model including a dynamometer with sharp corners.

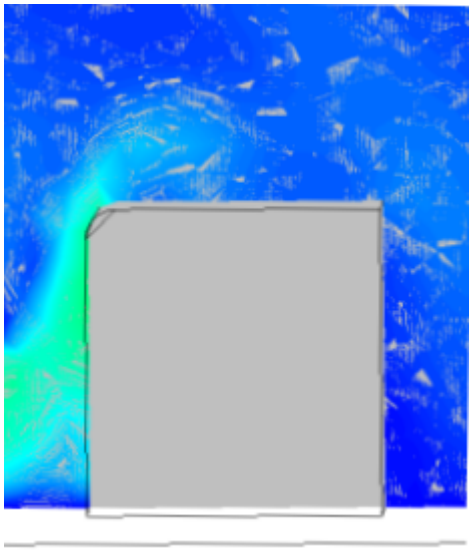

Figure 8.26: Model including a dynamometer with a rounded corner.

A difference in wake may be noticed, the effect on the flow field however is observed to be minimal. In addition, the strength of the wake with the rounded corners is not strong enough to capture hydrogen. An increase in hydrogen volume concentration is not observed in the area.

8.6.3 Varying origin hydrogen leak

A leak in the test cell container is depicted in Figure 8.27. The leak is situated near the container wall in the back and is caused by a fuel pipe rupture. Note that hydrogen leaks into the test cell container through a leak situated behind the engine. Therefore flows in 3 ducts are not visible.

Leakages near the piston engine are presumed to have the highest probability of occurring. Leakages due to a fuel pipe rupture are dangerous as well. The fuel pipe must enter the test cell through a hole in the wall as the tank is stored outside the container.

Air circulation in the local region near the depicted leak in Figure 8.27 is low and may entail slow diffusion of hydrogen. The leakage does not lead to zones of high hydrogen volume concentration in the test cell. Hydrogen diffuses more gradual as the momentum jet is not released in a confined space as is with a leakage near the engine. Yet, hydrogen molecules do come into contact with the entire test set-up. Nonetheless, it must be noted the fuel supply will be shut-off rapidly and less hydrogen will flow over the test set-up.

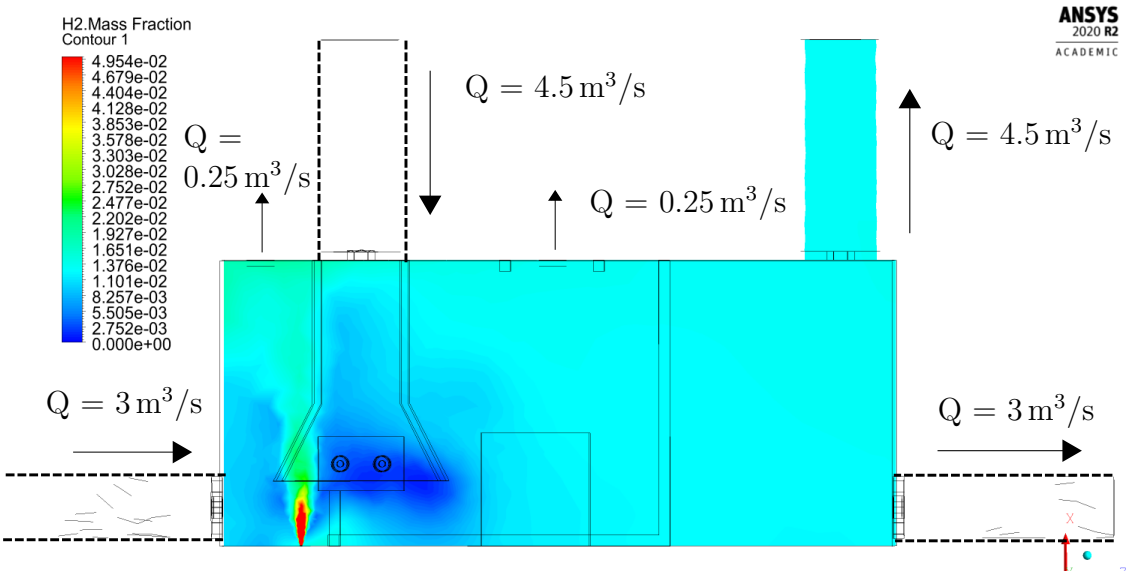

Figure 8.27: Hydrogen leak due to a rupture in the fuel pipe with $\dot{m} = 0.1\,\mathrm{kg/s}$.

Figure 8.27 illustrates the diffusion of hydrogen in the entire test cell. Figure 8.28 zooms in on the leak and depicts the position of the leak and the engine.

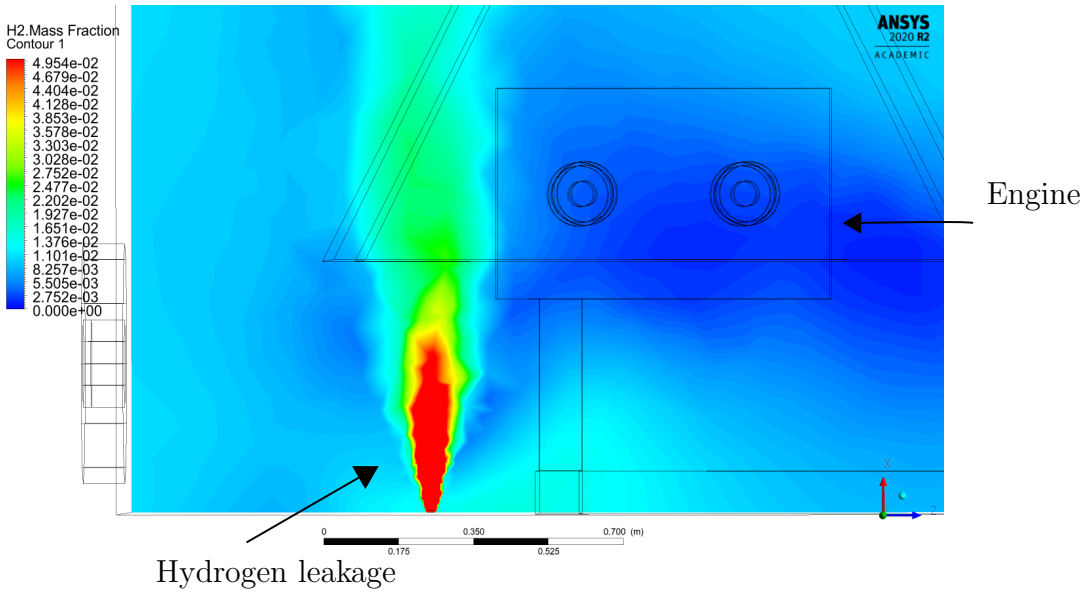

Figure 8.28: Fuel pipe rupture with a leak mass flow rate of $\dot{m} = 0.1\,\mathrm{kg/s}$.

Figure 8.29 depicts a 3D figure of the hydrogen mass fraction in the test cell. 3D figures are not included for the previous models since often the contours are not very clear. The purpose of the model propositions is to compare the diffusion of hydrogen in the test cell, however one may only observe clear differences in 2D figures and not 3D figures.

The contours are opaque and this 3D figure mostly depicts the hydrogen mass fraction near the walls of the container. Nonetheless, it shows when a fuel pipe rupture occurs, hydrogen diffuses across the entire test cell which imposes a large hazard.

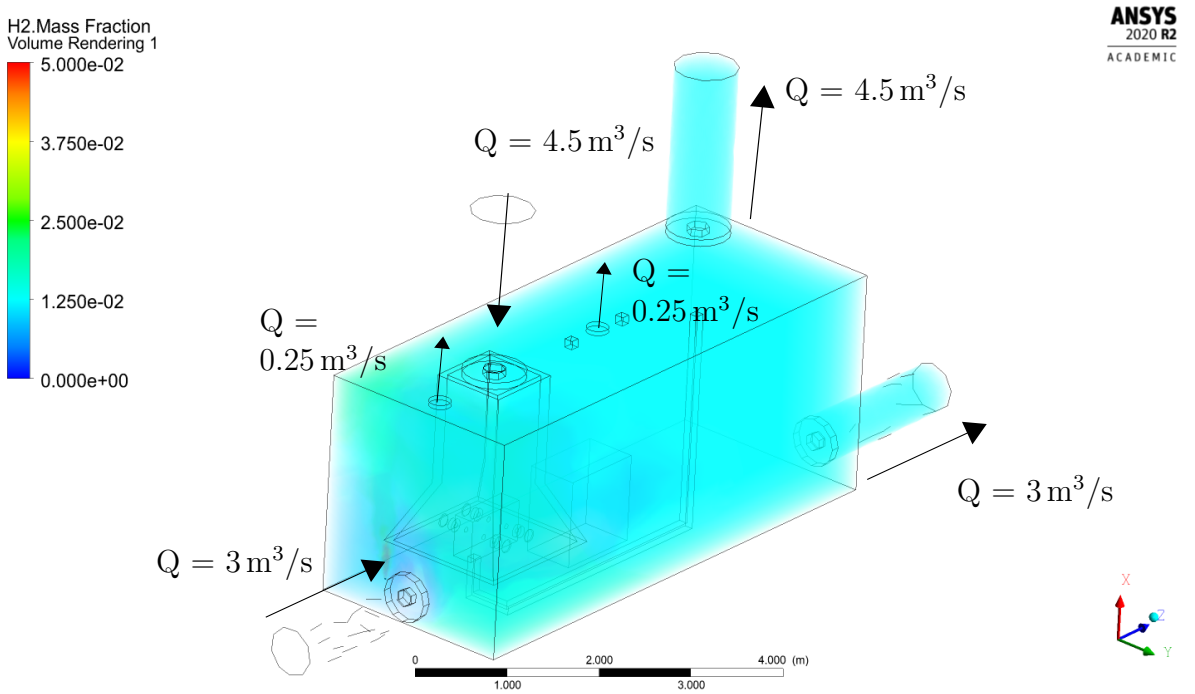

Figure 8.29: Fuel pipe rupture with a leak mass flow rate of $\dot{m} = 0.1\,\mathrm{kg/s}$. The 3D figure depicts the hydrogen mass fraction in the container.

8.7 Summary initial ventilation system designs

A short summary is presented in this section to give a clearer overview of all the findings in this chapter.

- Hydrogen is supplied through a fuel pipe which transports the fuel from the storage tank outside to the internal combustion engine. The pressure inside the fuel pipe is 20 bar.
- The probability of detonation and deflagration can never be reduced to zero. The minimum activation energy of hydrogen is low and therefore in many cases in the past the ignition cause remains unknown. One must implement as much risk mitigations methods to minimise the risk.
- Hydrogen has a high diffusion coefficient and will therefore diffuse rapidly in the

test cell if not disposed of immediately.

- Leakages near the internal combustion engine have the highest probability of occurring. It is most likely to leak through the fuel injector and outlet pipe which vents the crankcase.
- Ventilation fans do not affect the flow much upstream. It is difficult to directly pull hydrogen into an outlet duct towards the environment.
- Hydrogen may flow over the test set-up in the back of the container which includes various ignition sources. The ignition sources should be sealed off and a gas tight wall must compartmentalise the set-up.

Chapter 9

Final Design Test Cell

The three model propositions and intermediate optimised design are presented to hydrogen safety experts. The results of that meeting are discussed in this section along with the final design of the ventilation system and test cell.

9.1 Recommendations hydrogen safety experts

The final design is presented to hydrogen safety experts of Inerc BV Hydrogen Safety[1] who grant permits to experiment with hydrogen.

The suggestions of the experts must be implemented in the CFD model. The experts did not have experience yet with air-cooled hydrogen internal combustion engines. The following conclusions are obtained by combining the outcome of the simulation results presented in the previous chapter and the knowledge of the experts.

To further decrease the risk, the engine must be compartmentalised from the remainder of the test set-up entirely as illustrated in Figure 9.1.

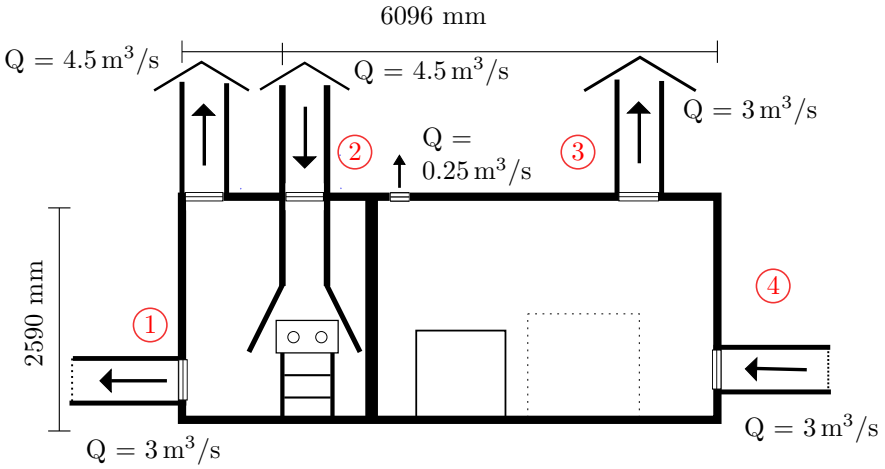

Figure 9.1: The engine is separated from the remainder of the test set-up to minimise the interaction of hydrogen with potential ignition sources.

One should attempt to minimise the interaction between hydrogen and the test set-

[1] `https://inerc.nl/` [Retrieved 22.03.2021]

up. The energy balance and required ventilation volumetric flow rate must be iterated since some heat sources are separated and the total thermal load differs from the initial analysis in Chapter 6. Note that the ventilation system set-up requires a redesign and Figure 9.1 is merely an example.

The engine is situated in a separate room on the left-hand side while the dynamometer and remainder of the test set-up are situated in the room on the right. Note that the remainder of test set-up is depicted by dashed lines as in Chapter 4. Both the size of each compartment and the size of the remainder of the test set-up depicted by the dashed line are set arbitrarily. The remainder of the test set-up comprises of electrical wires, a HVAC-unit, combustion analyser, gas chromatography and other elements which may be included in the future. In addition, the width of the left and right compartment is not determined yet. The test set-up itself is not very large and hence the width of each compartment is not crucial as long as the set-up fits in the room. The effect of a varying width in the engine room will be analysed in the sensitivity analysis to determine whether the diffusion of hydrogen is highly dependant on the size of the room.

A second suggestion is regarding the outlet vent of the crankcase which is mounted on the bottom of the engine. Most hydrogen engine test cell set-ups include water-cooled engines which have the outlet vent of the crankcase mounted on top of the engine. The Lycoming engine has the outlet vent of the crankcase mounted on the bottom of the engine block. Hydrogen may leak due to a loose connection of the crankcase vent pipe with the engine block. One must know the pressure in the crankcase is near 1 bar and the leak comprises of an oil-hydrogen mixture. Such a mixture will likely not rise to the ceiling and must be disposed of through the bottom of the test cell. One air compressor or ventilation fan must direct the leaking cloud mixture directly towards an outlet to mitigate the risk.

Furthermore, the outlets should not include ventilation fans. The combination of confined rooms and high velocities impose a large hazard. The probability of detonation would be highest in the outlet ducts if ventilation fans would be included. The high velocities, wall ducts and ventilation fan entail friction and hence charged particles. In addition, the volume concentration is relatively high in the outlet duct since all hydrogen must be disposed of through the outlets if a leak occurs in the test cell. Note that when the outlet fans are excluded, the pressure rises in the test cell and the performance of the ventilation fans mounted in the inlet ducts reduce.

An additional note is regarding the maximum allowed diameter of the ventilation ducts, which may in theory not be larger than 10.5 cm (F.R. et al., 2005). The highest risk to the test cell environment stems from charged particles which may enter through the ducts near the side of the walls or the cooling fan. Particles may become charged due to high velocities in the duct and due to contact with a ventilation fan upon entering the test cell. Experiments have shown that particles which become charged due to contact with the spinning ventilation fans may invoke a hydrogen flame. In addition, the pressure

rises when hydrogen leaks into the duct. The hydrogen volume concentration may be high in the duct since it is a separate enclosed space and there is less space for hydrogen to diffuse.

The maximum size of the duct in which detonation cannot occur is related to the 7-λ rule. λ is a characteristic length for the detonation cell size and is sensitive to the composition of the hydrogen-air mixture. The detonation cell size can be calculated through a typical track of triple points from intersecting shockwaves (F.R. et al., 2005). The size is difficult to predict and to this date no accurate method exists to predict λ. The 7-λ rule is currently the most widely accepted model but still includes a large confidence interval of 100 %. λ varies by temperature, mixture concentration, pressure et cetera.

The 7-λ rule entails that a detonation cannot occur when the duct diameter is not larger than 7 times λ_{minimum}. The minimum value of λ is 1.5 cm in air for a temperature of 300 K and occurs at a stoichiometric mixture.

A detonation may still occur in smaller ducts due to the inaccuracy of the method, however its is very unlikely and in addition high volume concentrations of hydrogen are not expected inside the duct as shown in the CFD simulations. The hydrogen safety experts suggest to reduce the diameter of the ducts to $\approx$ 10 cm based on the 7-λ rule and good judgement. Therefore the fan must include multiple smaller ducts such that a hydrogen flame cannot transition into a detonation inside the ducts. An example is illustrated in Figure 9.2, the larger duct must converge into multiple smaller ducts.

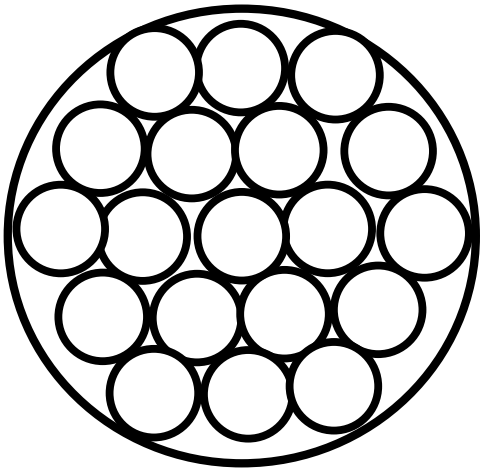

Figure 9.2: The maximum allowed diameter of the ducts is $\approx$ 10.5 cm, therefore the large ducts must converge into multiple smaller ducts as depicted in the figure above. The amount of ducts depicted in the figure above is chosen arbitrarily.

Note that detonations may still develop in the test cell. A hydrogen-air mixture may always detonate in the test cell room outside the ducts. The probability of detonation in a well-designed test cell will be further discussed in Section 9.6.

The risk of charged particles igniting a flame can be further minimised by ensuring

all the elements in the test cell are grounded. Furthermore, all elements should be ATEX-3 protected as well as additional safety precaution.

Another remark is to develop a fail-safe system. A fail-safe system should be constructed for the unfortunate event a ventilation fan does not function and hydrogen leaks through a gap into the test cell. The ventilation system must be able to operate at twice the minimum required ventilation rate imposed by Equation 9.1.

$$Q_{Ventilation} = \frac{100}{LEL} \cdot Q_{Leak} \cdot K_{Safety} \tag{9.1}$$

To ensure the ventilation system is able to operate at at least the minimum required ventilation rate, two fan systems must be powered by two different energy sources. The system may either include two sources operating at a different phase or one of the systems operates on batteries while the other is powered by a generator.

Note that with natural ventilation the required ventilation rate of Equation 8.1 will not be met and thus a mechanical ventilation system is required.

An additional suggestion is that inlet and outlet ducts may be installed in proximity of each other in case the outlet duct extends further up than the inlet duct. Hydrogen cannot re-enter the container through the inlet duct in the event of a hydrogen leak when the outlet duct is longer due to the buoyancy effect. Hydrogen will rise upwards and even when a wind gust directs hydrogen towards the inlet duct it will not re-enter the test cell. An example is illustrated in Figure 9.3 and Figure 9.4.

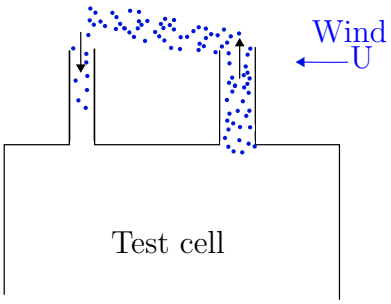

Figure 9.3: hydrogen might flow back into the container when an inlet and outlet duct are of the same height when wind pushes hydrogen towards the inlet.

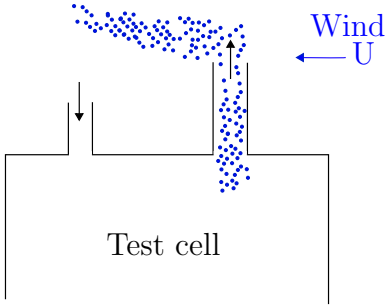

Figure 9.4: Hydrogen does not re-enter the container when the outlet duct extends further upwards than the inlet due to the buoyancy force of hydrogen.

A further remark is to develop a simulation of the detonation and deflagration process in the test cell. This is beyond the scope of the MSc. thesis however and such a model must be realised during a future stage of the project. One has to analyse which material and which thickness is required to minimise the consequences of a detonation.

A last remark is regarding the container walls. A 20-feet container is characterised by ridged walls. Hydrogen rises again along the walls of the container if hydrogen is pushed downwards. The rippled contour of the container walls will induce turbulence and this must be accounted for.

An additional sensitivity analysis, energy balance and diffusion model will be performed to analyse the effect of the remarks on the flow field of the test cell.

9.2 Final design ventilation system

The final design is proposed in this section in combination with an updated energy balance schematic of the compartmentalised room. Schematics are included with a side view, front view and top view of the container with the boundary conditions incorporated.

9.2.1 Iteration test cell energy balance

The energy balance and required ventilation rate do not change much in comparison to the previous model. The total thermal load reduces by $\approx 15\,\mathrm{kW}$ as the dynamometer and some small remaining test set-up elements are not in the same room as the engine. The remaining components which release heat are in the compartmentalised room with the internal combustion engine. Reiterating Equation 9.2 and subtracting the dynamometer and smaller test set-up components from the thermal load equation,

$$\text{Ventilation rate} = \frac{\sum \text{Thermal load}}{C_p \cdot \Delta T \cdot \rho_0}, \tag{9.2}$$

yields a required ventilation volumetric flow rate of $6.13\,\mathrm{m^3/s}$ for the thermal load within the compartmentalised room. The second room requires a ventilation rate of approximately $2.2\,\mathrm{m^3/s}$ due to the inclusion of the fans, lamps, services and dynamometer.

The required ventilation rate for hydrogen disposal may be estimated through Equation 9.3.

$$\mathrm{Q_{Ventilation}} = \frac{100}{\mathrm{LEL}} \cdot \mathrm{Q_{Leak}} \cdot \mathrm{K_{Safety}} \tag{9.3}$$

One must note a ventilation system for hydrogen disposal is based on a risk analysis and good judgement. For example, hydrogen might leak due to a fuel pipe rupture into the test cell. However, such an event is unlikely with the appropriate mitigations according to the hydrogen safety experts. A certified fuel pipe in combination with a double-wall entails a very low probability of hydrogen propagating into the test cell. Therefore the ventilation system is not designed for such an event. Instead, the ventilation system is designed for a scenario with a higher probability of occurring and one with is slightly more difficult to prevent.

A leak through the fuel injector is considered to be the worst case scenario in the test cell container. Schefer et al. (2006) denote hydrogen injectors include an orifice of 1.5 mm. Hydrogen may leak due to the abrasive nature of the fuel through the back-end of the injector orifice. One should note the gap further widens due to abrasion, the industry standard is to assume the gap diameter increases by 10 %. The strongest leak is therefore expected to be a gap of 1.65 mm and a pressure of 20 bar, entailing a leak mass flow rate of 2.69 g/s. The required ventilation rate for the disposal of hydrogen yields approximately $3\,m^3/s$ according to Equation 9.3. The total required ventilation rate is therefore dictated by the thermal load and not the disposal of hydrogen. Note that the ventilation system must be a fail-safe design and therefore two separate ventilation systems of $3\,m^3/s$ are required.

One should further note that the maximum allowed diameter of the ducts is 10.5 cm. Around the fan itself the duct may be larger and it may encapsulate the fan as depicted in Figure 9.5.

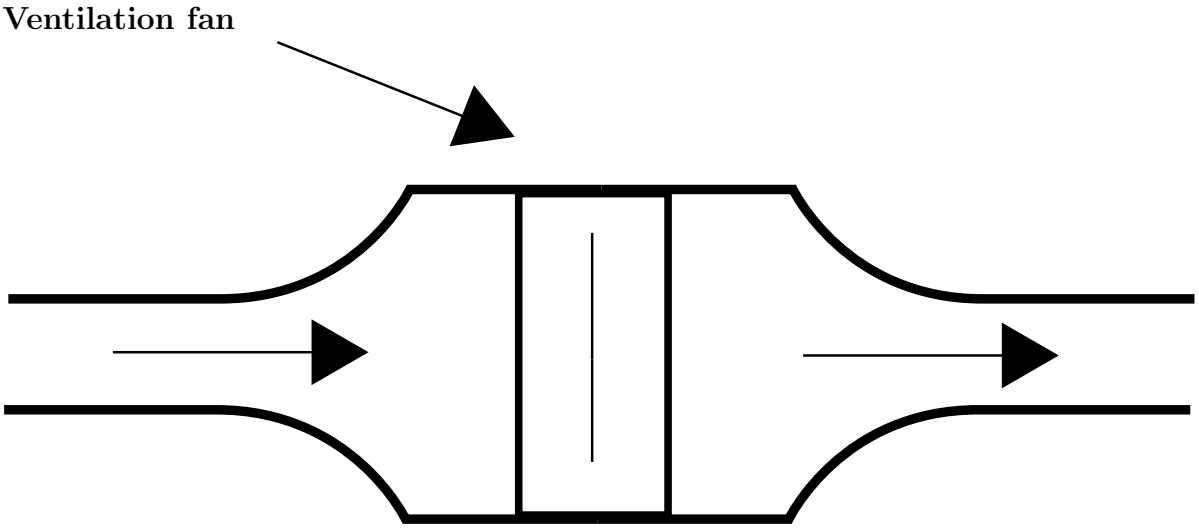

Figure 9.5: The duct must converge to a maximum diameter of ≈ 10.5 cm. Converging ducts induce a loss factor of $K_e = 0.15$.

The duct losses are presented in Figure 6.3 and it designates a pressure loss factor of 0.15 for a converging duct. A loss factor of 0.15 entails a decrease in capacity of less than 1 mmH_2O and is therefore neglected. One should note that a loss factor of 0.15, is the loss factor for one converging duct. The flow must be separated in multiple converging ducts however and the actual loss factor will probably be higher. Nonetheless the loss factor remains negligible if it increases by a factor 2. The converging ducts will not be included in the CAD model as it is too complex and would raise the cell count substantially.

9.2.2 Updated hydrogen leak model in CFD

The characteristics of a fuel injector leakage are displayed in Table 9.1.

Table 9.1: Hydrogen leak propagating through the fuel injector. A gap may appear due to the abrasion of impurities in the hydrogen fuel mixture with the injector wall.

Parameter	Value
Temperature [K]	287
Pressure [bar]	20
Volume [L]	0.2
Orifice diameter [mm]	1.65

When the fuel pipe is shut-off by a valve, the mass flow and pressure within the fuel pipe decrease. The fuel pipe will include multiple shut-off valves to minimise the hydrogen mass within the fuel pipe which can flow into the test cell. The length between the enclosed part of the fuel pipe and the shut-off valve may be assumed to be 5 m (Hysafe, 2009). The hydrogen safety experts mention the standard hydrogen fuel pipe inner diameter is approximately 6 mm. The volume within the fuel pipe past the shut-off valve is therefore 0.14 litre, Figure 9.6 illustrates the purpose of a shut-off valve.

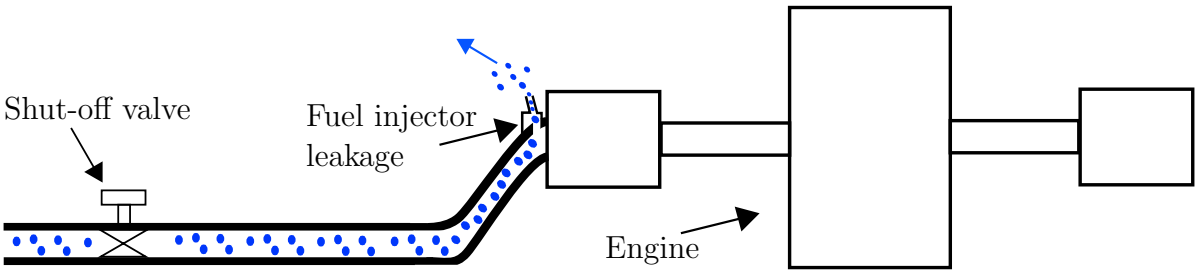

Figure 9.6: A shut-off valve impedes the flow from propagating further through the fuel pipe and eventually the test cell. The hydrogen past the fuel pipe will flow into the test cell with varying velocity and mass flow rate.

The mass flow rate and fuel pipe pressure decrease once the fuel pipe has been shut-off. The time variant mass flow rate through the gap can be estimated through the software tool HyRAM. HyRAM computes the following time variant flow parameters as depicted in Figure 9.7 with Table 9.1 as input parameters.

Hydrogen is released from the fuel pipe within 0.3 s once the fuel supply is shut-off. Wallner T. (2009) furthermore mentions the valve is shut-off within 1 second once the leak is detected. Note that it takes 5 seconds for a leak of 2.69 g/s to fill the container with an average hydrogen volume concentration of 1 % without ventilation. Venetsanos et al. (2011) performed hydrogen leak experiments in a confined room. Hydrogen sensors

detected a hydrogen concentration of 50 % LEL in less than 10 seconds. Current hydrogen sensors send a signal to the control room once a hydrogen volume concentration of 10 % is detected.

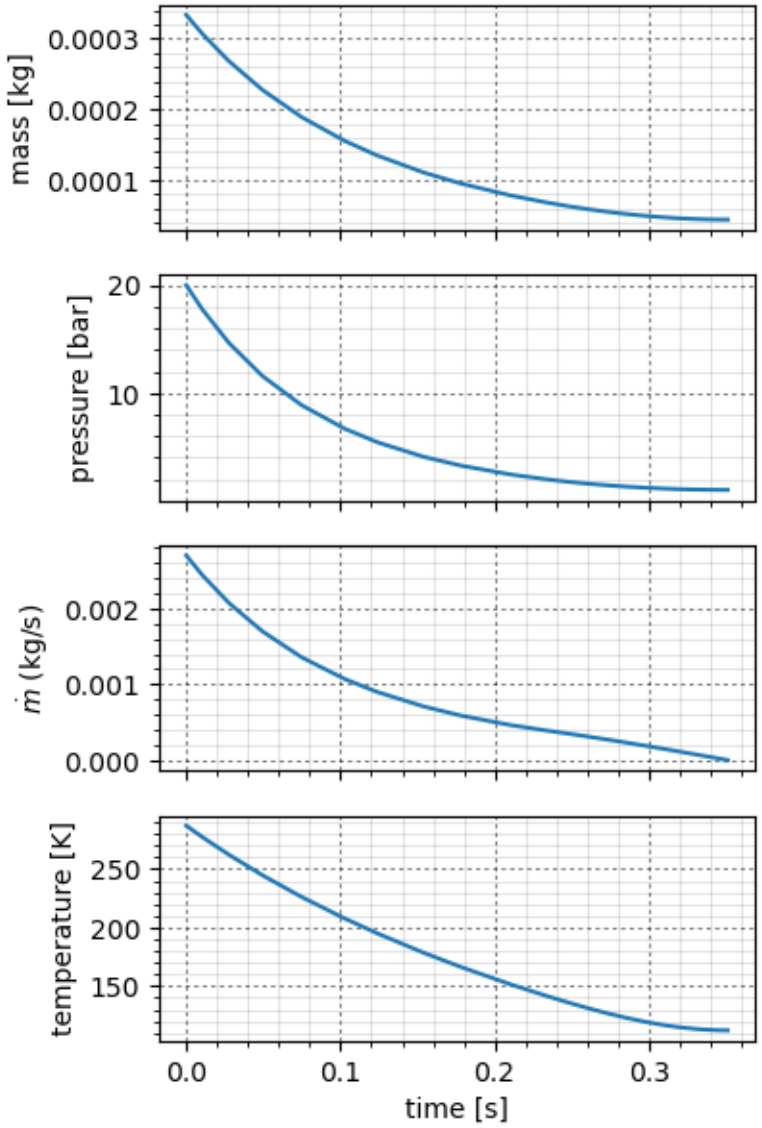

Figure 9.7: Hydrogen mass, pressure, mass flow rate and temperature through the fuel pipe. All hydrogen enters the test cell within approximately 0.33 s once the fuel supply is shut-off.

The precise time between the inception of a leak and a detection remains a knowledge gap. Therefore, the ventilation system must be able to handle situations where hydrogen leaks continuously and the container will be filled according to a steady-state. In addition, the shut-off valve mechanism may malfunction. The hydrogen safety experts

from Inerc mention as well that designing a ventilation system is based on a risk analysis, CFD analysis and good judgement. There does not exist one rule which defines the precise required ventilation rate or set-up.

The leak which is included for the final design is similar to the one modelled in Chapter 8. The diameter is reduced from 10 mm to 1.65 mm as depicted in Figure 9.8

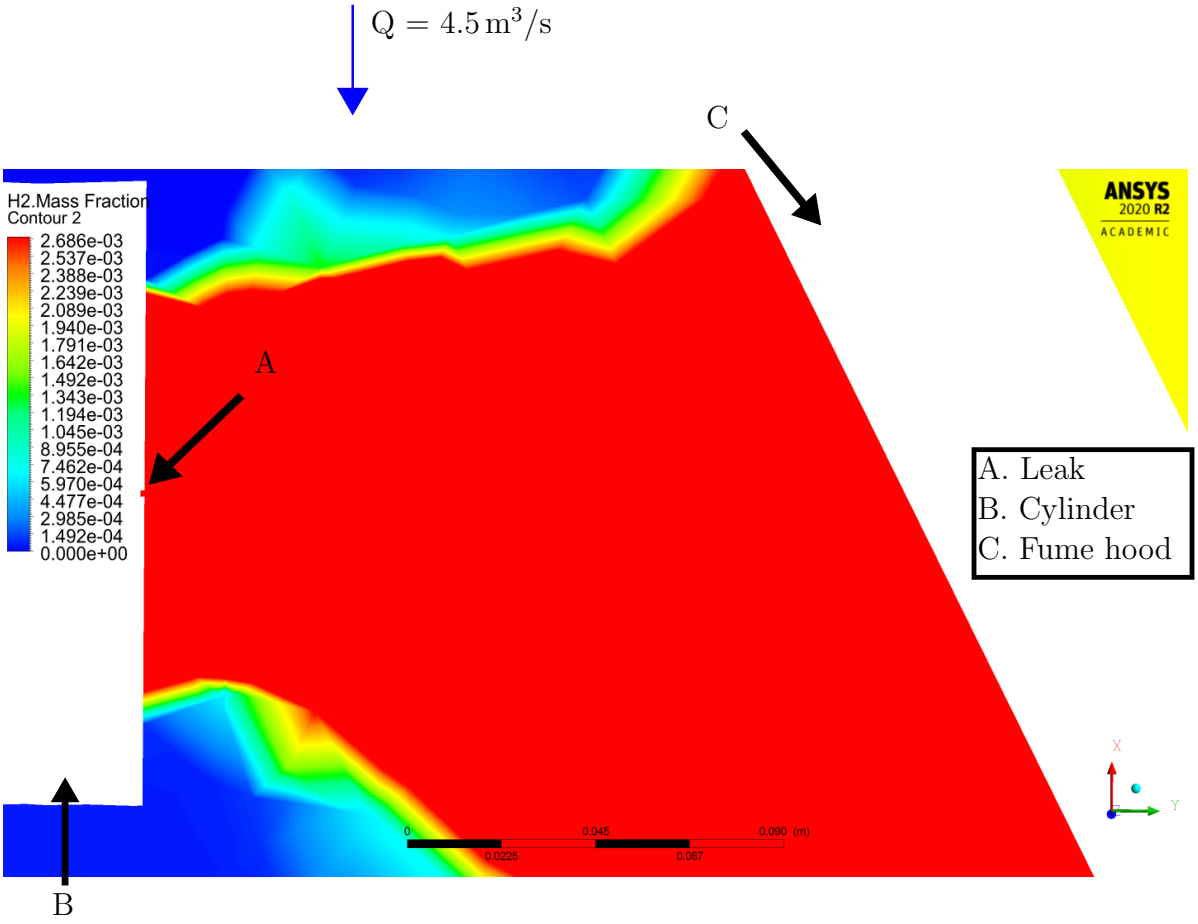

Figure 9.8: Leakage ($\dot{m} = 2.69\,\mathrm{g/s}$) through a small gap (D = 1.65 mm) near the cylinder of the internal combustion engine. (A) is the hydrogen leakage modelled as a pressure inlet, (B) is the engine cylinder and (C) is the contour of the fume hood.

9.2.3 Final design proposal CAD model & schematics

The following step is to design the final ventilation system set-up. The CAD model of the compartmentalised room is depicted in Figure 9.9. Note that the width of the engine room and the room which includes the remainder of the test set-up such as the dynamometer may be altered.

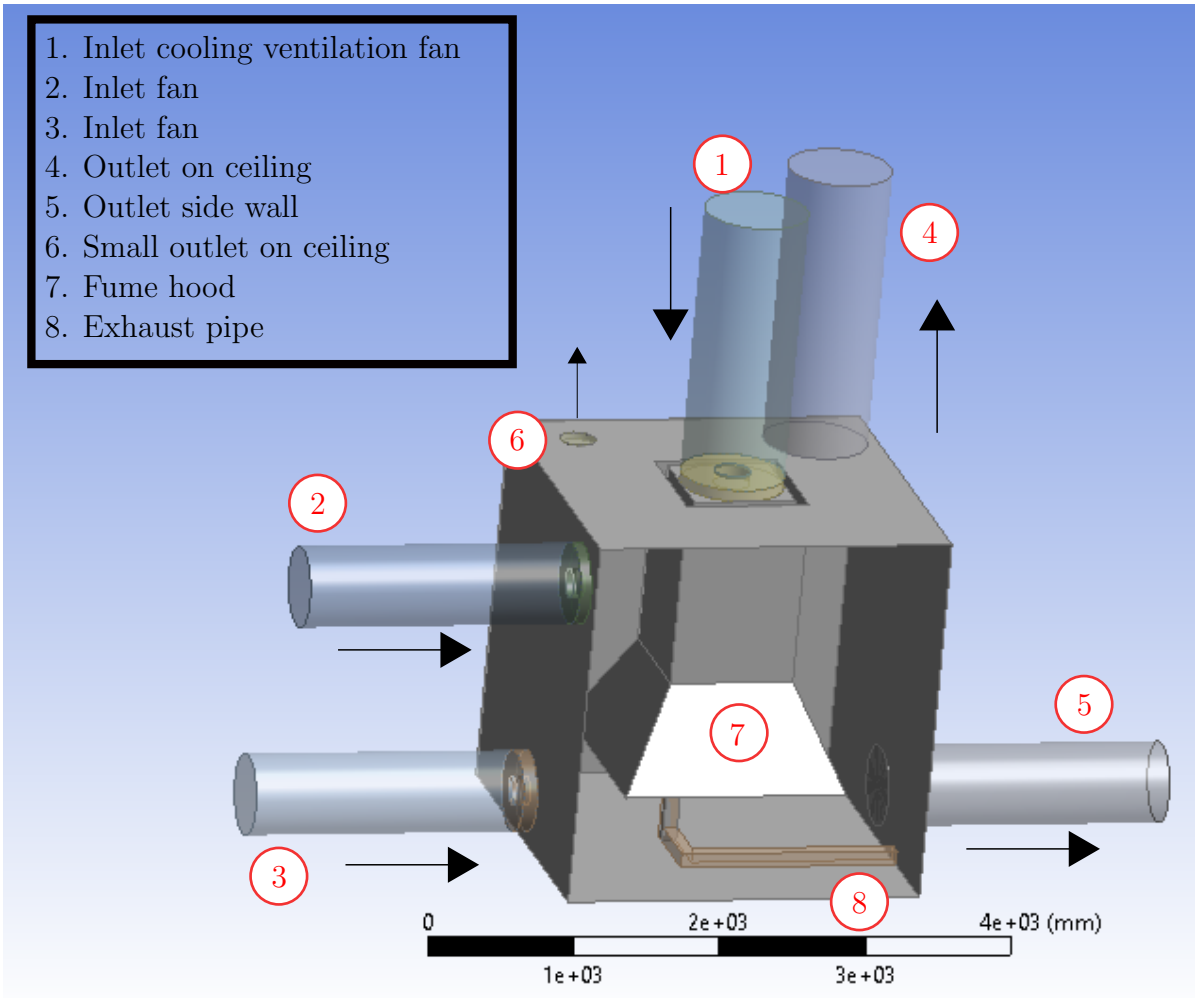

Figure 9.9: Final design of the compartmentalised room in the container. The ventilation system includes 3 inlet fans and 3 outlets.

The inlet fans provide less cooling air due to the exclusion of the exhaust fans. The pressure in the test cell is larger than in the previous experiment, hence fans supply less air for an equal amount of work. The volumetric flow rate through each inlet fan and the volumetric flow rate through each outlet duct will be presented in each schematic and figure in this chapter.

Number 1 is the cooling ventilation fan, 2 and 3 are additional inlet fans. Duct 1 includes an U/EI-EIL 715 fan, duct 2 an U/EI-EIL 454 fan and duct 3 an U/EI-EIL 564 fan. The specifications of the U/EI-EIL 454 are displayed in Table 9.2, the duct losses are incorporated in the given capacity. Note that due to the exclusion of the extraction (outlet) fans the inlet volumetric flow rate decreases as well.

Table 9.2: The U/EI-EIL 454 axial fan offered by Induvac.

Model	**Speed (Rpm)**	**Installed power (kW)**	**Capacity (m^3/h)**	**Mass (kg)**	**Noise level (dB(A))[1]**
U/EI-EIL 454	1,380	0.25	5,000	147	22

[1] The defined capacity includes the losses induced by the duct system.

Number 4 is an outlet duct mounted on the ceiling and 5 is an outlet duct mounted on the side wall. Furthermore number 6 is a smaller outlet duct which is included to prevent the accumulation of hydrogen in the upper right corner. The inclusion of the smaller outlet duct follows an identical though process as for the inclusion of the roof vents in Chapter 8. Note that number 4,5 and 6 are outlet ducts without the inclusion of fans. Ventilation fans may not be included in the outlets of the test cell as suggested by the hydrogen safety experts. Outlets contain a relative high concentration of hydrogen in a small enclosed space. Ventilation fans spin rapidly which can lead to the charging of particles and subsequently the ignition of the hydrogen-air cloud mixture in the duct.

The model will be explained further through the side view, front view and top view schematic, which include the boundary conditions. Figure 9.10 illustrates the side view schematic of the final design.

The inlet and outlet duct mounted near the floor are not visible in the side view schematic as they are mounted in the front and back plane respectively. For each fan it is depicted how much air flows through the duct and how much heat it disposes of or adds to the container. For instance, the ventilation cooling fan supplies a volumetric flow rate of $3\,m^3/s$ and adds 5 kW of heat due to the fan. Outlet duct 1 in turn has an outlet volumetric flow rate of $3.3\,m^3/s$ and disposes of 33 kW heat. The inlet and outlet volumetric flow rates are computed through ANSYS Fluent. Note that most air is disposed of through outlet duct 1 since its diameter is 0.7 m while the outlet duct mounted on the side wall is characterised by a diameter of 0.5 m. The small outlet duct (3) mounted on the roof has a diameter of 0.2 m. Outlet duct 1 is designed with a larger diameter than the other outlet ducts to enhance the disposal of warm air and hydrogen near the ceiling.

The engine is illustrated to be in the middle of the 2.5 m wide compartmentalised room. The size of the compartmentalised room is currently chosen arbitrarily and in the sensitivity analysis the effect of enlarging the engine room is analysed. Number 2 represents the engine cooling fan in Figure 9.10. The inlet duct is shorter in length than the outlet duct as otherwise the inlet fan in duct 2 may pull hydrogen into test cell if hydrogen is disposed of through outlet duct 1 and 3. Note that the inlet volumetric flow rate is reduced to $3\,m^3/s$, due to not including exhaust fans the pressure inside the container rises and the performance of the inlet fans decrease. Therefore a third inlet fan is

included in the model such that compartmentalised room is sufficiently ventilated.

The room on the right of the engine includes the remainder of the test set-up, including the dynamometer. The room includes two ventilation fans but are not visible in the side view schematic since they are mounted in the front and back plane.

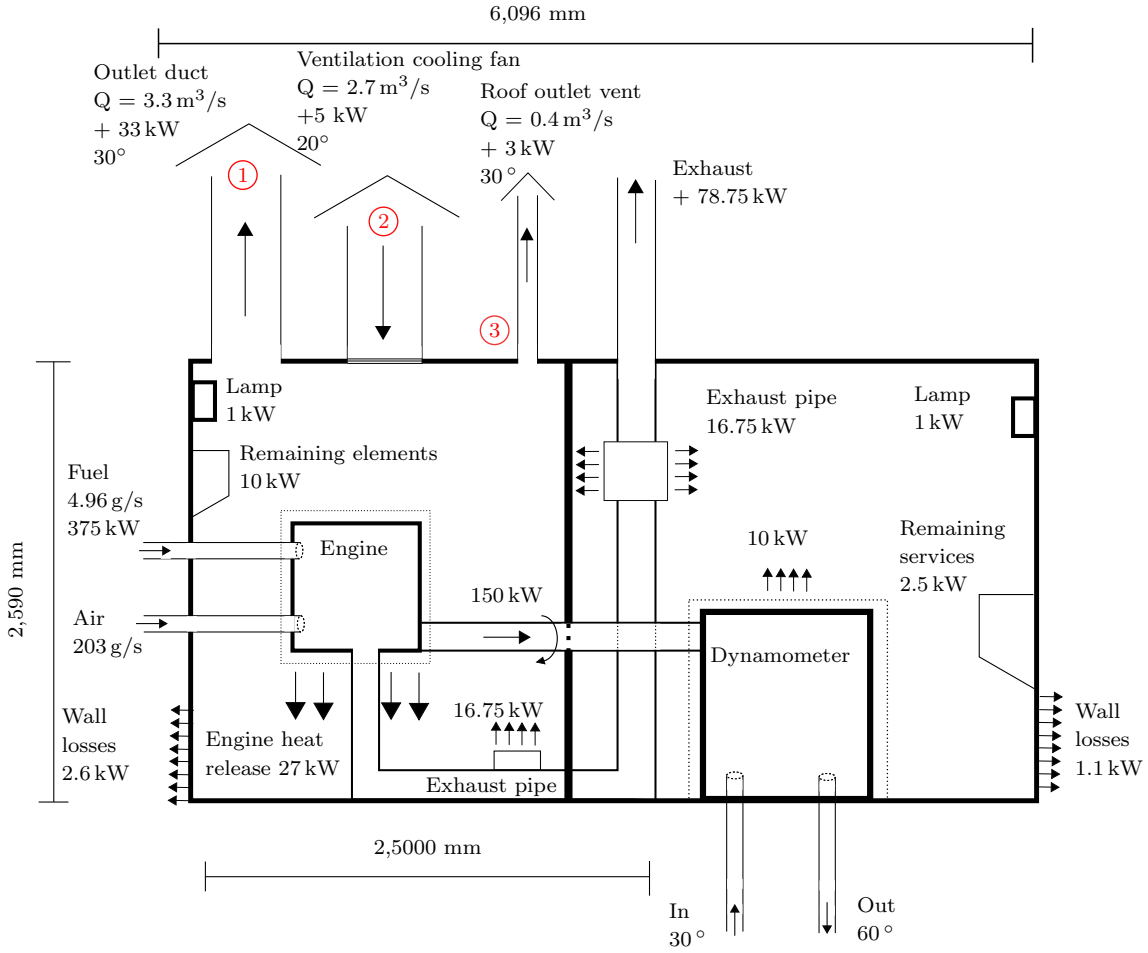

Figure 9.10: Schematic of the side view of the final design including the energy and air flow balance in the container.

Figure 9.11 illustrates the front view of the optimised model.

Inlet 1 serves two purposes, hydrogen propagates into the crankcase from the combustion chamber through the liner and mixes with oil. The pressure in the crankcase therefore increases and must be vented. The vent of the crankcase is mounted on the bottom of the Lycoming engine and might leak. A hydrogen-oil mixture is heavy and does not immediately rise. The most effective method is to immediately push the mixture towards an outlet, which is possible since a leak propagating through the crankcase is weak. The pressure inside the crankcase is only slightly higher than 1 bar (Hysafe, 2009) and the leak is therefore not sonic. The first function of inlet 1 is to push the hydrogen-oil mixture directly into the outlet through duct 4 in the event of a leak. Sec-

ondly, inlet fan 1 is directly beneath the engine and therefore part the heat released by the engine is disposed of as well primarily through duct 4.

One must further note a ventilation fan near the bottom of the container is necessary if one wants to test with aviation gasoline as liquid fuel remains on the container floor instead of rapidly rising to the ceiling in the event of a leak.

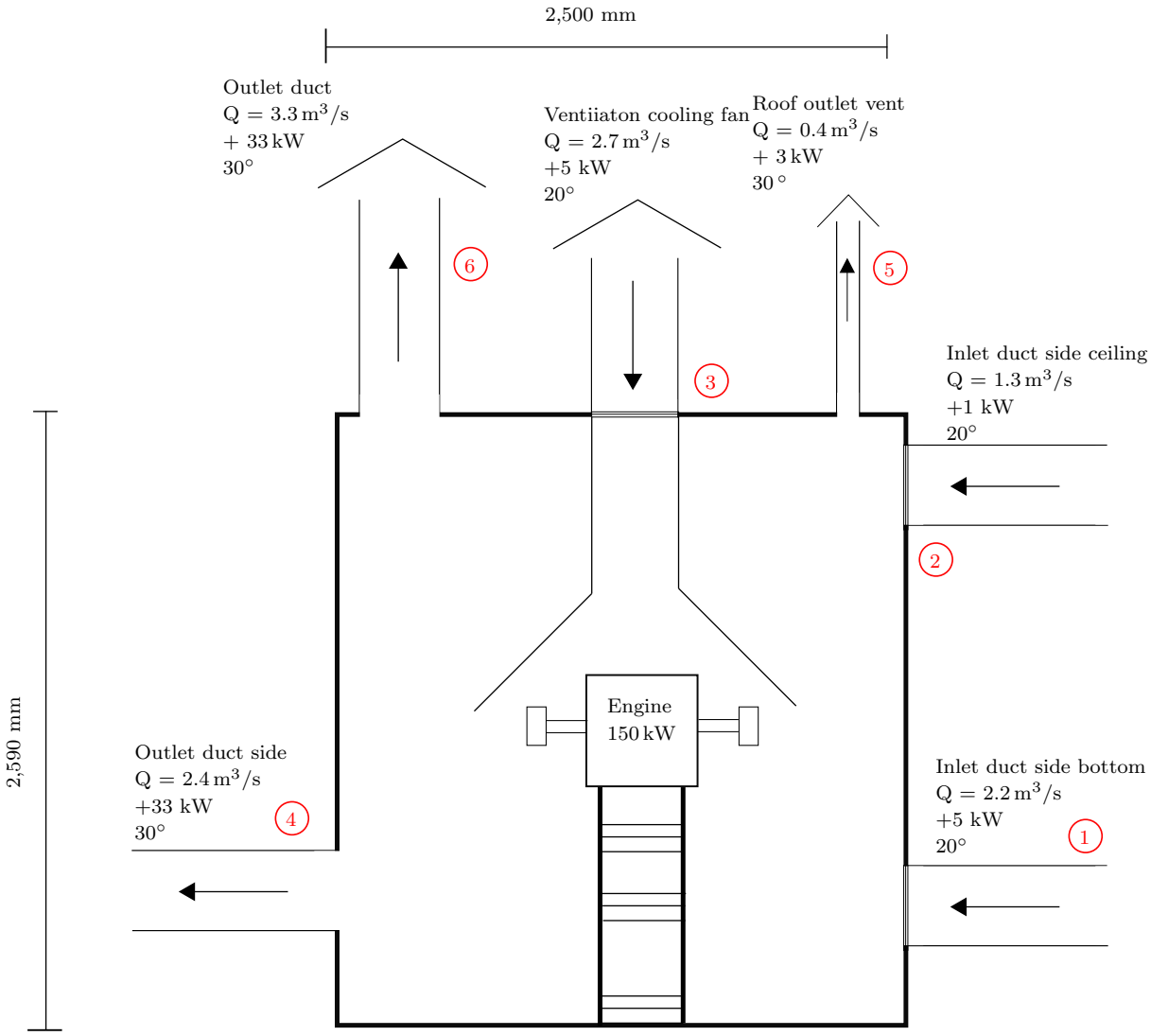

Figure 9.11: Schematic of the front of the final ventilation system design including the energy balance and ventilation volumetric flow rates.

Figure 9.12 depicts the top view of the same model. Fan 1 represents the cooling fan of the engine, including the U/EI-EIL 715 fan while duct 2 resembles the large outlet duct. Duct 3 represents the smaller roof outlet while fan 4 is the U/EI-EIL 564 fan mounted near the floor of the container and 5 the U/EI-EIL 454 mounted near the roof. Duct 6

is the outlet duct mounted on the side wall.

Duct 7 represents the inlet fan in the room on the right and 8 represent the outlet fan. Note that duct 7 cannot be mounted on the adjacent wall on the right as the container still requires a door. Both duct 7 and 8 include a U/EI-EIL 564 since the room requires approximately at least 2.2 m^3/s. Furthermore, duct 8 is mounted on the side walls instead of the roof since the duct losses are less in this instance. Duct 8 may include a fan since no hydrogen is expected to propagate from the engine room to the room on the right.

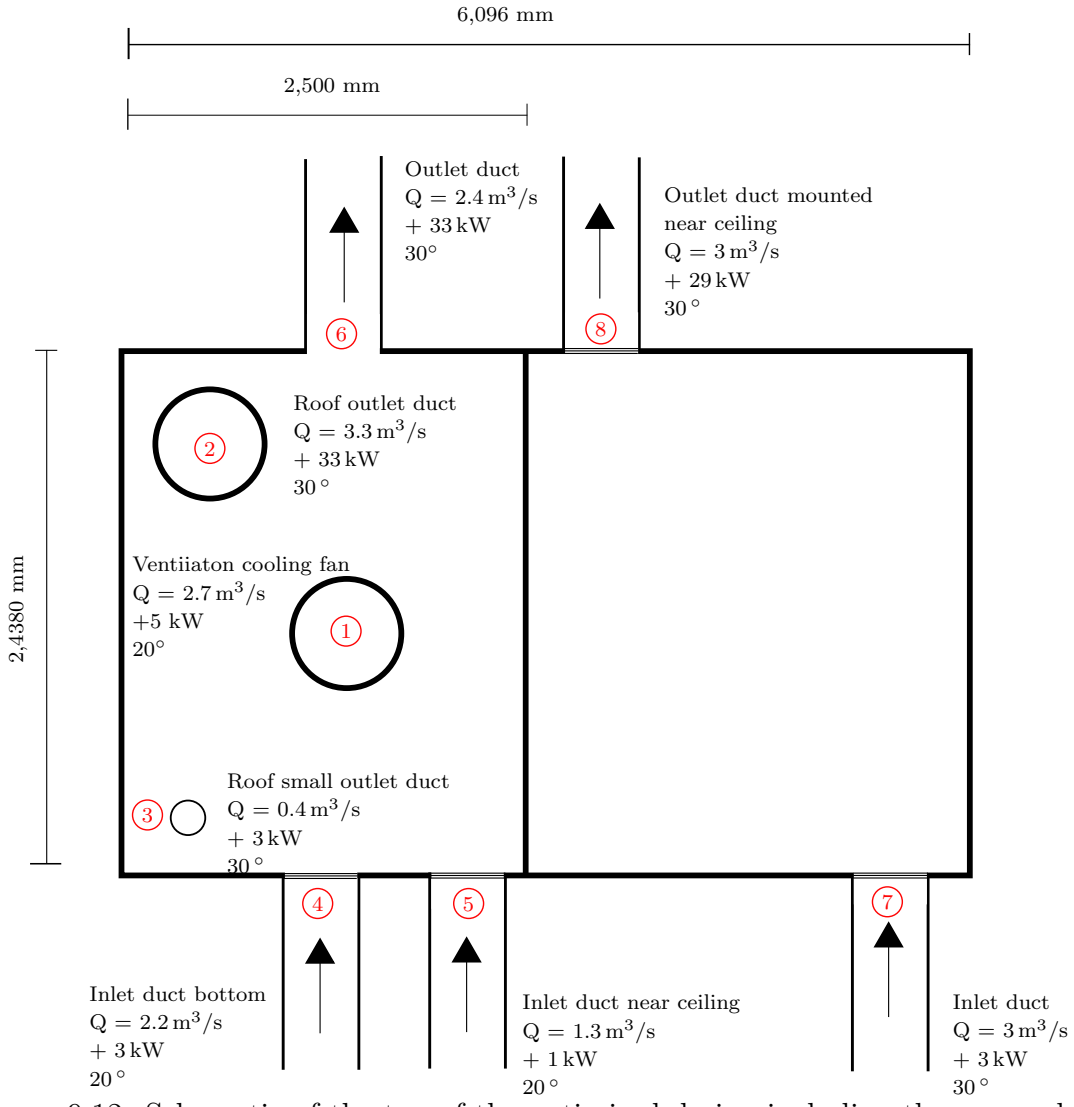

Figure 9.12: Schematic of the top of the optimised design including the energy balance and required ventilation volumetric flow rates.

The following simulations include a fuel injector leakage with a gap of 1.65 mm and injection pressure of 20 bar, hence the mass flow rate of the leak is 2.69 g/s. The velocity

profile is displayed in Figure 9.13.

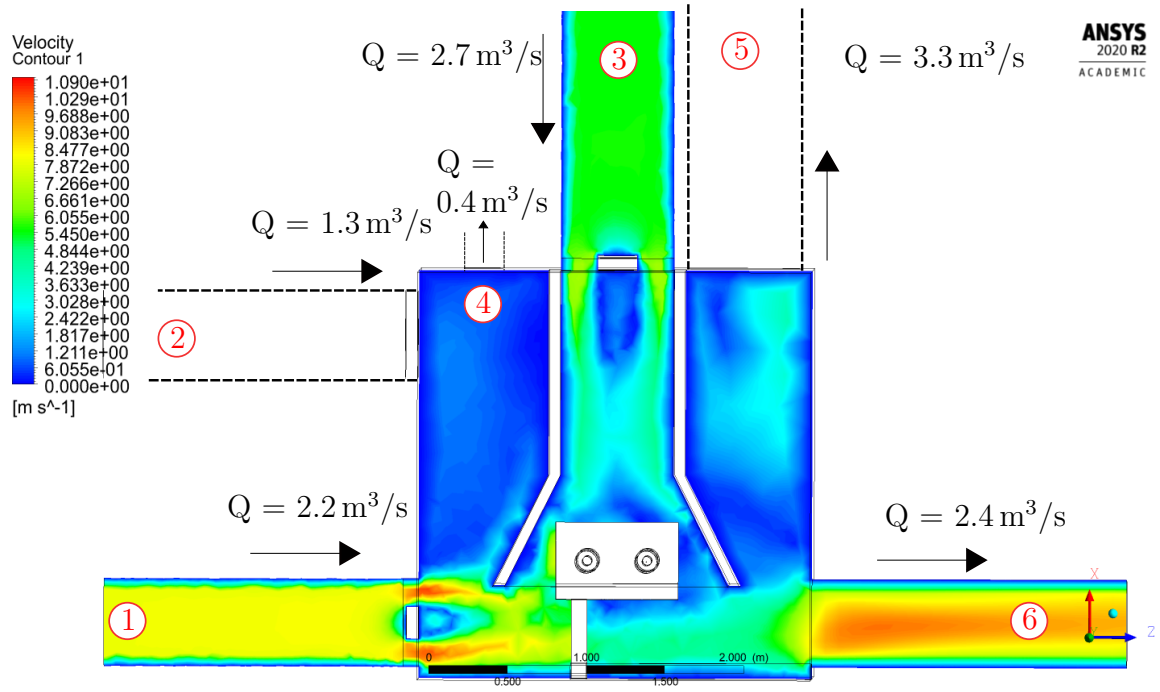

Figure 9.13: Velocity profile in the compartmentalised room for a leak with D_{gap} = 1.65 mm and $\dot{m}$ = 2.69 g/s. The room includes 3 inlet fans and 3 outlets (without fans).

To note, the U/EI-EIL 564 and 454 (fan 1 and 2 in Figure 9.13) must be operating on a different phase or power source than the U/EI-EIL 715 (fan 3 in Figure 9.13) to obtain a fail-safe system. Thus one ventilation system includes the cooling fan as inlet and the other includes the U/EI-EIL 564 inlet fan mounted near the floor of the container and the U/EI-EIL 454 fan mounted on the side wall near the ceiling.

Two ventilation systems may be distinguished from each other. Table 9.3 depicts how the ventilation fans should be coupled to obtain a fail-safe system.

Table 9.3: The ventilation system is divided into two separate systems to enhance safety. Both systems are able to dispose enough hydrogen in the worst case scenario leak.

Ventilation system 1		**Ventilation system 2**	
Inlet	Q (m^3/s)	Inlet	Q (m^3/s)
U/EI-EIL 715	2.7	U/EI-EIL 564	2.2
		U/EI-EIL 454	1.3

The required ventilation rate during the worst case scenario leak is estimated to be 2.69 m^3/s. Therefore each distinctive ventilation system must at least include a ventila-

tion rate of 2.69 m^3/s. Note that due to the exclusion of outlet fans the volumetric flow rate through the fans is reduced.

A cloud mixture will still be pushed to an outlet (although less efficiently) if for instance fan 3 does not function while fan 1 and 2 do. The situation may also be reversed in case fan 1 and 2 do not function anymore and fan 3 does.

Figure 9.14 depicts the diffusion of hydrogen in the compartmentalised room solved by the Maxwell-Stefan equations. The model includes a roughness coefficient to account for the rippled container walls.

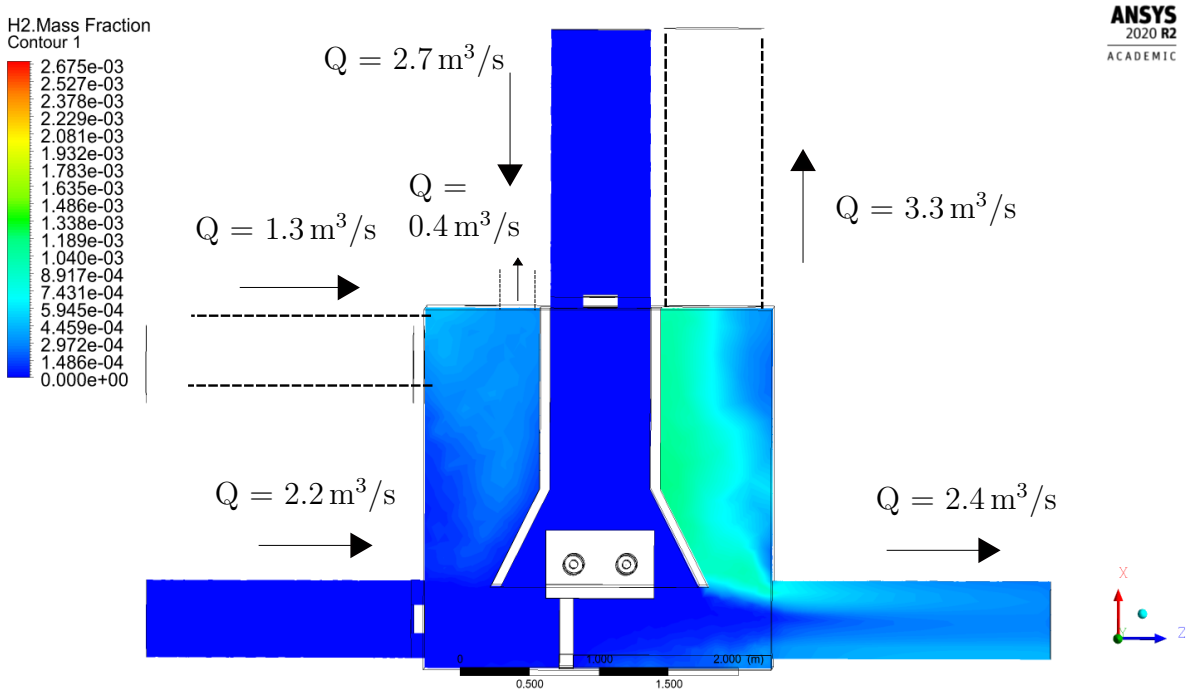

Figure 9.14: Hydrogen diffusion in the compartmentalised room for a leak with D_{gap} = 1.65 mm and $\dot{m}$ = 2.69 g/s. The volume concentration remains below 4 % for a steady-state solution.

The colour scheme displays the mass fraction of hydrogen in the test cell ranging from 0 % to 0.28 %. The colour red entails a volume concentration of 4 % and blue a volume concentration of 0 % if one converts the percentage range from mass fraction to volume concentration. The concentration of hydrogen does not exceed 4 % in the test cell according to the simulation since no red colour may be noticed in the figure[2].

The ventilation system therefore meets the requirement and effectively disposes

[2]The volume concentration does naturally exceed 4 % in the proximity the leak, decreasing the volume concentration below 4 % is expected however and cannot be prevented.

hydrogen gas to the open-air. The test cell must comply to a few more safety guidelines such as handling deflagration and detonation processes well. Initial ideas such as tilting the container to enhance the disposal of hydrogen are not necessary, an efficient ventilation system is sufficient to maintain the hydrogen volume concentration below the explosion limit.

It is possible as well to plot 3D figures in ANSYS Fluent. Figure 9.15 depicts the mass fraction of hydrogen of the final model in 3D.

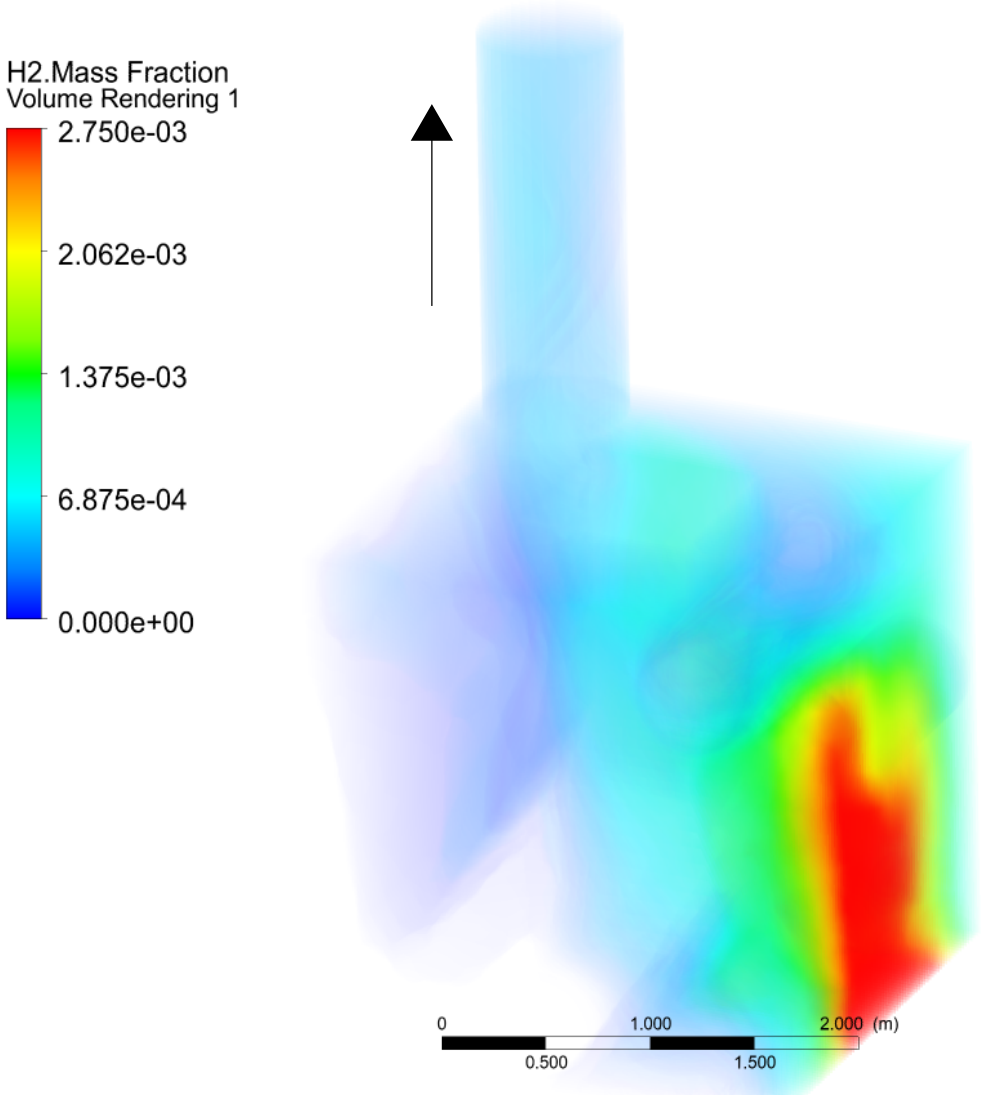

Figure 9.15: 3D figure of the diffusion of hydrogen in the compartmentalised room for a leak with $D_{gap} = 1.65\,mm$ and $\dot{m} = 2.69\,g/s$. The volume concentration remains below 4 % for a steady-state solution.

The volume concentration ranges from 0 % to 4 %. Mostly 2D contours are included in this report since 3D figures are difficult to read. Some regions in the figure are fully transparent as no hydrogen is present. Therefore the inlet ducts are for example not visible in Figure 9.15. Regions with high volume concentrations are opaque which limits the visualisation of the hydrogen mass fraction behind the contour. For example, the diffusion of hydrogen in the rear of the container cannot be observed in the figure due to the high hydrogen volume concentration near the leak (red contour).

The outlets are visible however, one can note the large outlet duct mounted on the roof accompanied by the arrow which designates the flow direction in the duct. The outlet duct mounted near the floor is more difficult to identify. Note that the inlet duct mounted near the floor is in the front of this 3D figure and the outlet duct mounted near the floor is in the back.

Figure 9.15 shows no hydrogen accumulates in the test cell and the overall average hydrogen volume concentration does not exceed 4 % except near the leak as can be observed by the red zone on the right-hand side of the figure.

The temperature profile is displayed in Figure 9.16.

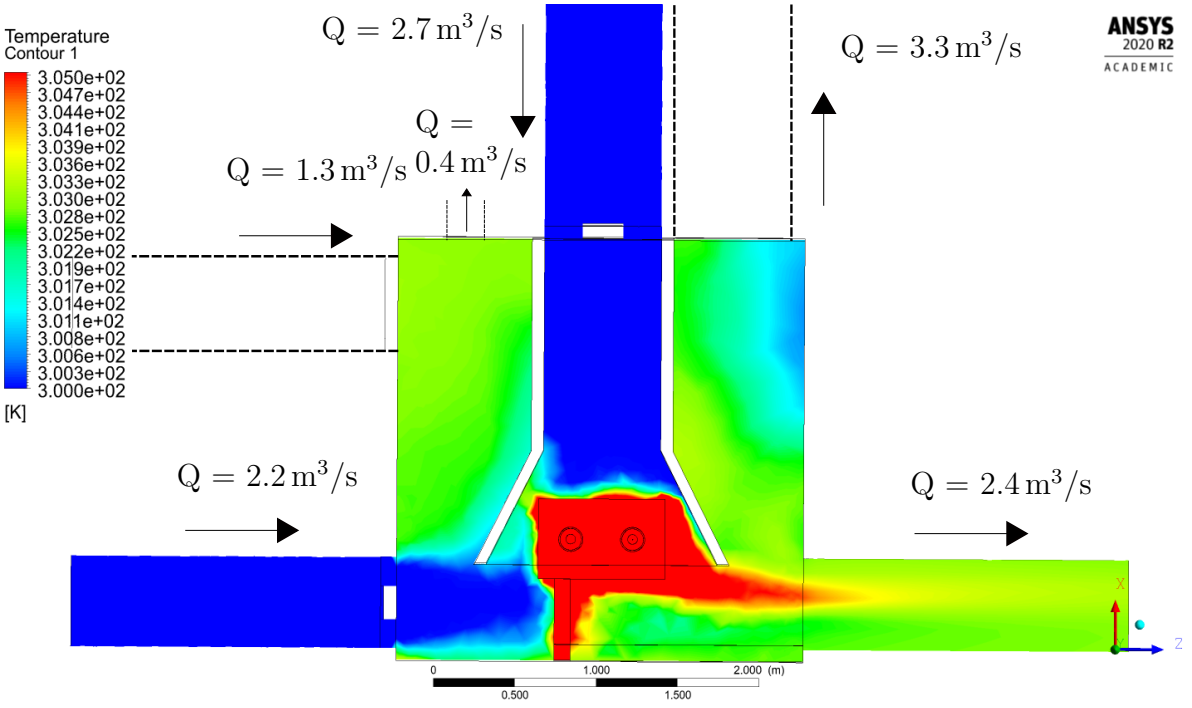

Figure 9.16: Temperature profile in the compartmentalised room for a leak with D_{gap} = 1.65 mm and $\dot{m}$ = 2.69 g/s.

Note from Chapter 6 that when the simulations displays a temperature rise of ≈ 3 K, the actual temperature rise will be 10 K due to neglecting the heat release from the cooling

fins of the engine. The simulation shows a temperature rise of roughly 3 K in the test cell and thus the ventilation system is considered to supply a sufficient amount of fresh air. Note that a large part of the heat released by the engine is directly disposed of due to the inlet fan and outlet mounted near the floor.

9.3 Validation hydrogen plume by HyRAM

HyRAM is a specialised tool to model hydrogen plumes and to perform risk analysis with. The model of the leak which is included in the models above is put in a separate simulation in Fluent in a larger well-ventilated enclosure and compared to the results obtained through HyRAM.

Figure 9.17 depicts the hydrogen plume simulated in HyRAM and Figure 9.18 the hydrogen plume in ANSYS Fluent. A white and blue oval depict respectively the height of the maximum mole fraction contour in the figures.

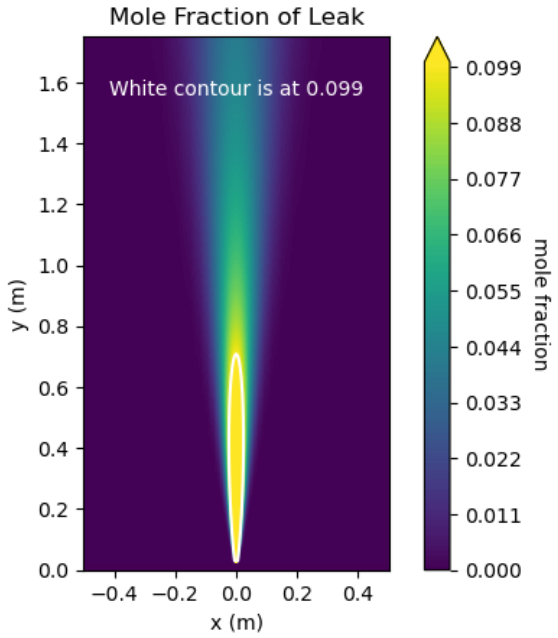

Figure 9.17: Hydrogen leak modelled in HyRAM, the colour scheme presents the mole fraction. The yellow contour shows where the plume attains a mole fraction of at least 0.099. At a height of 0.75 m the concentration decreases.

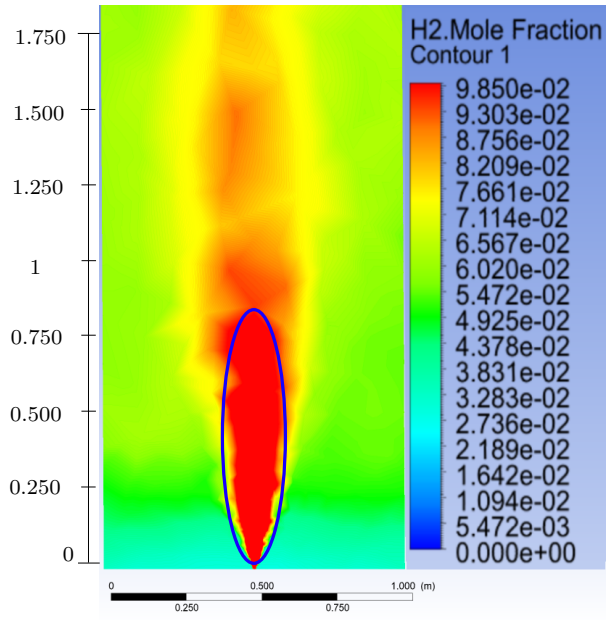

Figure 9.18: Hydrogen leak modelled in Fluent, the colour scheme presents the mole fraction. The red contour shows where the plume attains a mole fraction of at least 0.099, at a height of 0.8 m the concentration decreases.

Yu et al. (2013); Yüceil et al. (2000) and Schefer et al. (2006) observed the hydrogen plume should extend approximately 1 to 2 m upwards if the plume is not interrupted.

In addition, the maximum Mach number should be between 2.28 to 2.85 at a short distance from the nozzle since the leak is a sonic under-expanded jet. Note that the highest velocity is observed slightly past the edge of the nozzle since the throat of the leak is very thin and the flow suddenly expands.

The model is validated for hydrogen plumes in open-air or for large well-ventilated enclosures. In smaller confined rooms, the model does not perform well according to the hydrogen experts from Inerc BV Hydrogen Safety.

In both figures, the mole fractions of hydrogen are plotted. The maximum fraction is resembled by a yellow contour in the left figure and red contour in the right figure. The nozzle of the leak is defined by a diameter of 1.65 mm and pressure of 12.9 bar, which reassembles a source pressure of 20 bar. The hydrogen plume extends with a hydrogen mole fraction of 0.099 up until a height of ≈ 0.75 m in HyRAM and ≈ 0.8 m in Fluent.

Only small differences may be observed between the plumes. The hydrogen plume in Fluent is expected to be larger since the leak is simulated in a large enclosed room instead of in open air. Some hydrogen molecules remain in the room and increase the average hydrogen mole fraction. It can be noticed the hydrogen mole fraction around the plume is approximately 0.04 and not 0 as simulated in HyRAM.

Furthermore, it may be noticed the hydrogen plume is wider in Fluent than in HyRAM (the x-scale for both figures is 1 m). Fluent does not accurately model flows with high Mach numbers if the cells are not well aligned with the shock waves. Aligning the cells with the shock waves is difficult for this model as it includes complex geometries. The grid density and computational time would need to be increase substantially to obtain an accurate representation of the shock waves. In addition, the plume is wider due to modelling the plume in a confined room. It must be further noted that HyRAM itself is not fully accurate according to the hydrogen experts. The experts and HyRAM developers are working on a solution to solve the error but are still uncertain on how to solve the issue.

Figure 9.19 displays the velocity contour of the hydrogen plume modelled in ANSYS Fluent. The length of the plume extends up to approximately 1.75 m (for a velocity of 3 m/s.) The highest velocity the plume attains is $\approx$ Mach 2 a few millimetres above the leak. Experiments in literature attain Mach numbers between 2.28 - 2.85 Mach as discussed in Chapter 7. The shock waves induced by the leak are expected to include a slight error since it is difficult to model supersonic flows in Fluent. The mesh must be very accurate and structured near the leak to model the Mach disks accurately. However a structured grid near the leak is difficult to attain and would entail an overall decrease in mesh quality due to the complex geometries near the leak such as the engine.

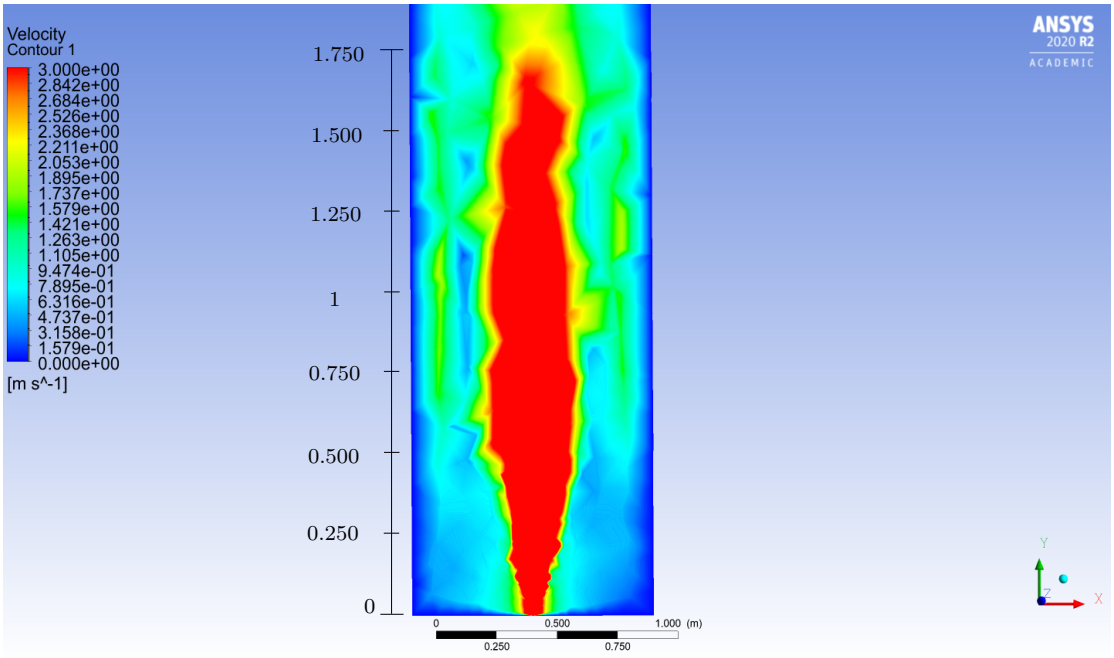

Figure 9.19: Hydrogen leak modelled in Fluent with a nozzle diameter of 1.65 mm and nozzle pressure of 12.9 bar. The colour scheme presents the velocity which ranges from 0 to 3 m/s.

9.4 Sensitivity analysis final design

An additional sensitivity analysis is performed for the final design as it includes a few design changes and the inclusion of the wall roughness coefficient. Note that for each experiment the same set of fans is utilised, however due to a changing flow field the volumetric flow rate provided by each fan might change. The volumetric flow rate through the inlet fans and volumetric flow rate through the outlet ducts is presented in each figure.

9.4.1 Effect of ridged container walls

The hydrogen safety experts have recommended to include a constant wall roughness coefficient to account for the turbulence induced by the ridged container walls. In Figure 9.14 a roughness coefficient is included to account for the ridged container walls while Figure 9.20 comprises of smooth walls. Only very small differences are noticed in the diffusion of hydrogen in the container.

The inclusion of a constant roughness coefficient is merely an approximation of the grooves in the container walls. The accumulation of hydrogen near the ceiling must still be monitored well as the ripples may hinder to a certain extent the outflow of hydrogen into the ambient environment.

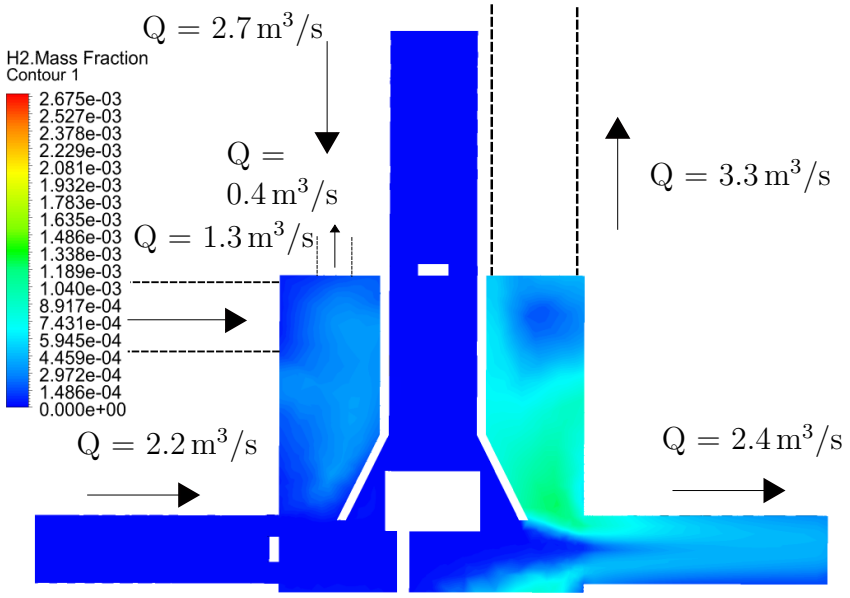

Figure 9.20: Hydrogen diffusion in the compartmentalised room for a leak with D_{gap} = 1.65 mm and $\dot{m}$ = 2.69 g/s. The container walls are modelled as smooth walls (roughness coefficient = 0).

The velocity profile of the container with smooth walls is depicted in Figure 9.21.

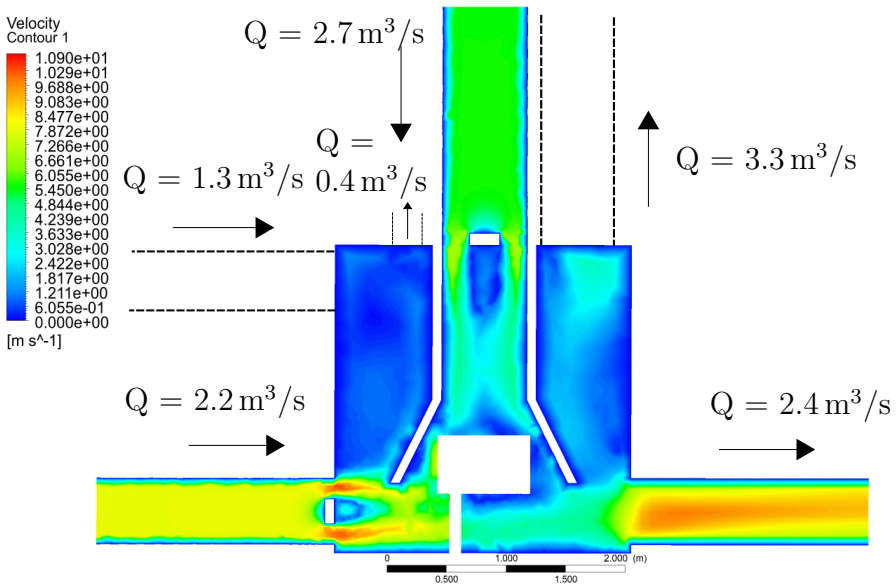

Figure 9.21: Velocity profile in the compartmentalised room for a leak with D_{gap} = 1.65 mm and $\dot{m}$ = 0.002 69 kg/s. The room includes 3 inlet fans and 3 outlets (without fans).

The velocity near the container wall is relatively low and therefore its effect on the diffusion of hydrogen and the velocity profile is negligible. One must look closely to observe differences between and Figure 9.13 and Figure 9.21.

9.4.2 Maxwell-Stefan diffusion versus Fick's law

The diffusion of hydrogen may be solved by two different models in Fluent, by solving the Maxwell-Stefan equations or by applying Fick's law. Both models are explained in Appendix B.

Fick's law is a more general approach and benefits from a lower computational cost while the Maxwell-Stefan equations are more comprehensive but increase the computational cost. The previous simulations in this chapter include the Maxwell-Stefan approach. It is expected that with Fick's law the diffusion of hydrogen slightly increases in the test cell since the mass diffusion coefficients cannot be negative in Fick's law. Thus the model assumes more rapid diffusion of hydrogen with air than the Maxwell-Stefan equations estimate.

The diffusion of hydrogen in the container by applying Fick's law is depicted in Figure 9.22.

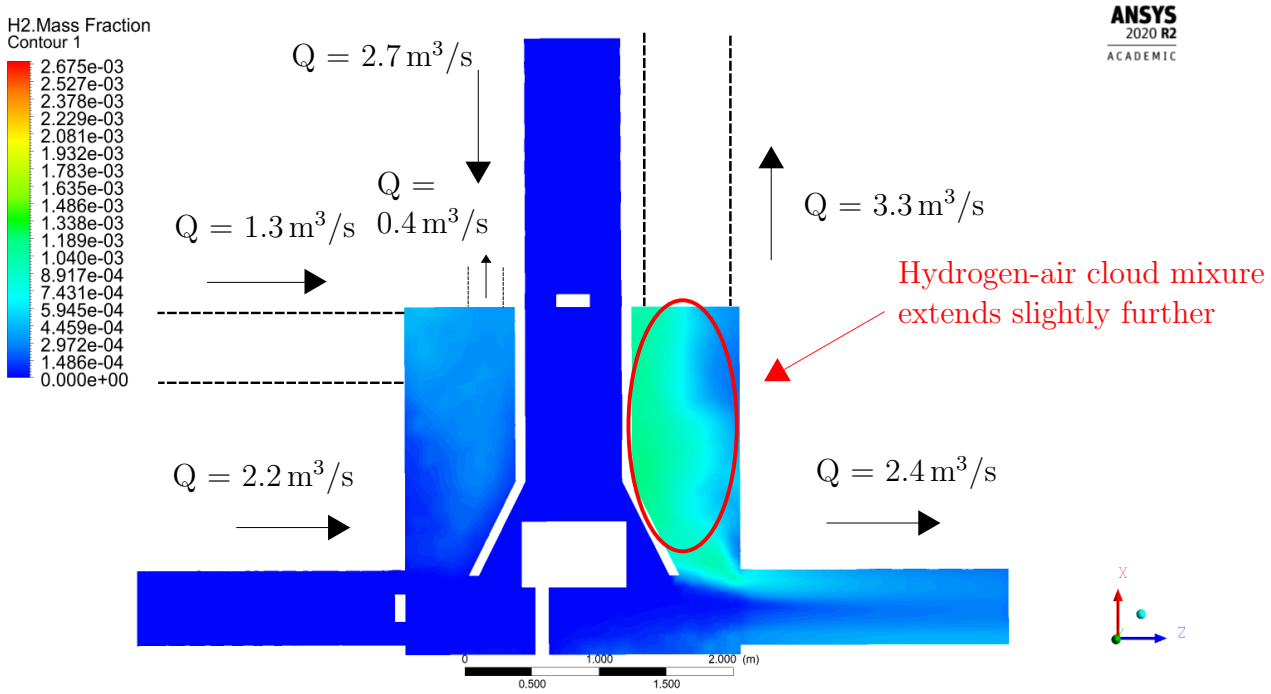

Figure 9.22: Hydrogen diffusion (Fick's law) in the compartmentalised room for a leak with $D_{gap} = 1.65\,mm$ and $\dot{m} = 0.002\,69\,kg/s$. The volume concentration remains below 4 % in a steady-state solution.

Slight differences may be noticed in the diffusion profile. For example, the hydrogen-air cloud mixture in the region where the concentration is highest (indicated by the red oval) is smaller than the one depicted by the Maxwell-Stefan approach. Nonetheless the differences are small and both models can be utilised.

9.4.3 Fail-safe ventilation system

The hydrogen safety experts suggest to design a ventilation system which supplies twice the minimum required volumetric flow rate to dispose of hydrogen to obtain a fail-safe system. The ventilation set-up comprises of two ventilation systems of which each system is able to supply at least $3\,m^3/s$. One of the two systems is turned off to analyse the volume concentration during a power failure which causes one of the systems to shutdown.

Power failure ventilation system 1

The ventilation fan mounted on the roof is one system and the ventilation fans mounted on the side wall are the second. The ventilation fans mounted on the side walls are turned off for the first analysis as depicted in Figure 9.23.

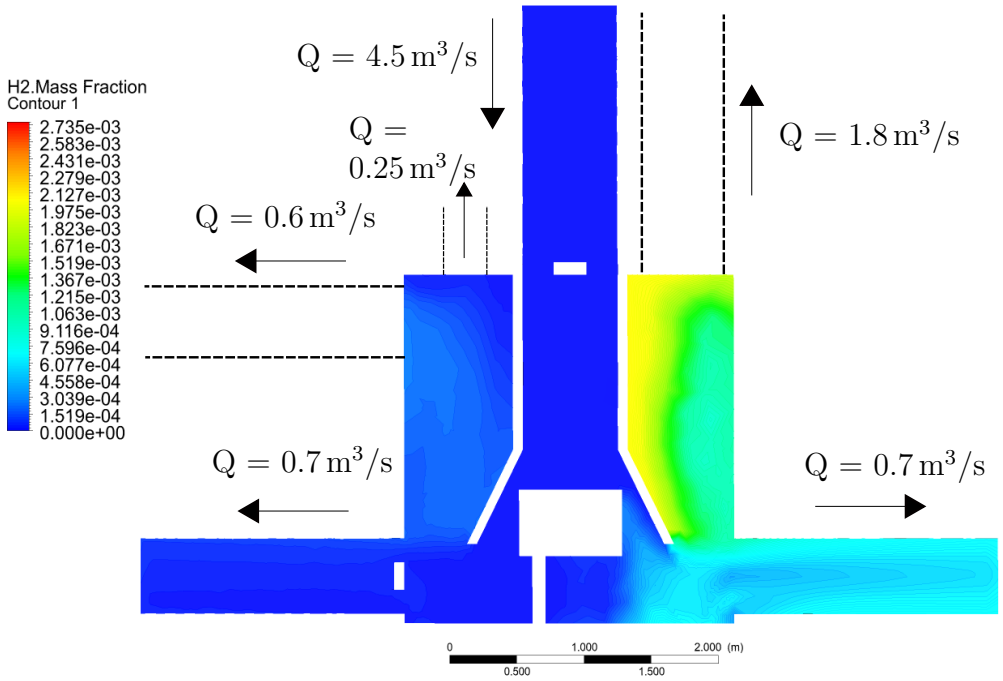

Figure 9.23: Hydrogen diffusion in the compartmentalised room during a power failure of one of the ventilation systems (1). The characteristics of the leakage are $D_{gap} = 1.65\,mm$ and $\dot{m} = 2.69\,g/s$. The volume concentration remains below 4 % for a steady-state solution.

A red contour resembles a volume concentration of 4 % and a blue contour a volume concentration of 0 %. It can be noticed that the maximum volume concentration in the 2D contour is equal to 2 %, about a factor 1.5 to 2 more than when both ventilation systems operate. Note that the leak propagates through the right-hand side of the engine and therefore most hydrogen is disposed of through the ducts on the right rather than the ducts on the left.

Power failure ventilation system 2

The second ventilation system has been turned off, hence the cooling fan mounted on the roof is an outlet duct as displayed in Figure 9.24.

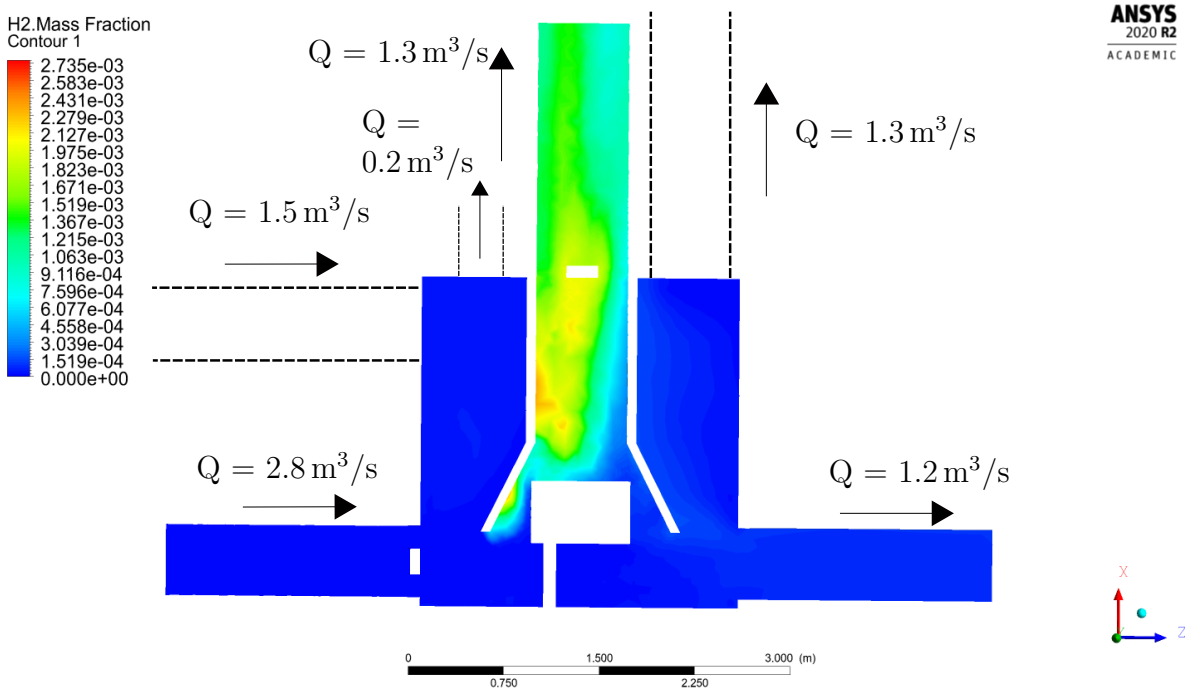

Figure 9.24: Hydrogen diffusion in the compartmentalised room during a power failure of one of the ventilation systems (2). The characteristics of the leakage are $D_{gap} = 1.65\,\text{mm}$ and $\dot{m} = 0.002\,69\,\text{kg/s}$. The volume concentration remains below 4 % in a steady-state solution.

Most hydrogen escapes the test cell through the fume hood into the ambient environment as no air pushes hydrogen down. The volume concentration is relatively high in the fume hood since the duct itself is a small enclosed space. An orange contour may be noticed in the middle of the figure and thus it is potentially dangerous to have a leak during a power failure. Yet, the probability of a leak during a power failure is very unlikely and the hydrogen volume concentration is on average low and does not exceed 4 %.

The ventilation system is a fail-safe design since both individual systems still meet the requirements.

9.4.4 Varying size test cell room

The width of the compartmentalised has been set arbitrarily to this point. The sensitivity of the width of the engine room is analysed below. Figure 9.25 depicts an engine room with a width increased from 2.5 m to 4.5 m.

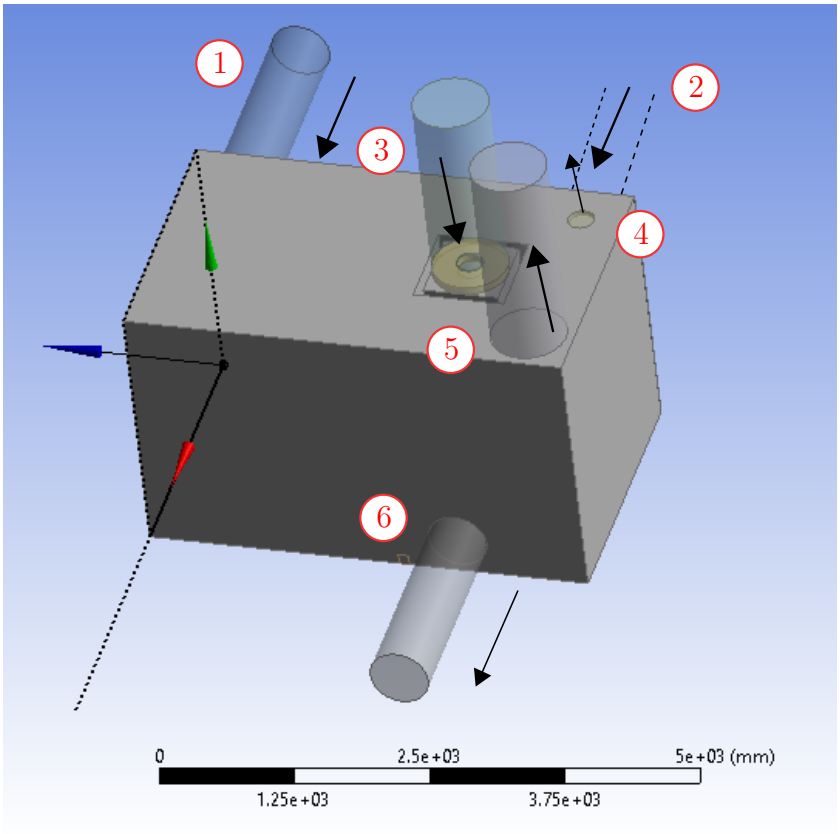

Figure 9.25: The width of the compartmentalised room has been increased from 2.5 m to 4.5 m.

The engine is positioned near the wall in the rear of the container in Figure 9.25 since it must be connected to the dynamometer. Inlet fan 1 is mounted near the front of the container. The fan could also be placed on the adjacent side wall on the left such that it pushes air straight from the front of the container to the rear but note that potentially a door will be placed in the front wall of the container. Inlet fan 2 must direct the air beneath the engine to outlet duct 6 hence duct 2 and 6 are mounted in proximity of the compartmentalisation wall as well. Furthermore, number 3 represents the inlet cooling fan which is mounted directly above the engine, number 4 is the small outlet duct and number 5 the large outlet duct.

Furthermore, the placement of duct 1 in respect with 4 and 5 should be discussed. Duct 2,3 and 6 are set because the engine must be placed close to the wall but duct 1,4 and 6 could switch sides. It might be beneficial to place the large and small outlet ducts on the opposite side in comparison to the current set-up. The inlet duct mounted on the side wall near the ceiling would then switch position as well and move to the rear and be positioned above inlet duct 2. Mounting the outlet ducts near the compartmentalisation wall is potentially dangerous since hydrogen will be directed towards the compartmentalisation wall and might leak into the room of the dynamometer if the gaps in the wall are relatively large. It is still uncertain however how large the gaps in the wall need to be to connect the engine with the remainder of the test set-up.

The advantage of the current set-up is that in most situations hydrogen is disposed of more rapidly since the outlet ducts are mounted near the internal combustion engine. In addition, hydrogen will flow in the direction of the dynamometer room regardless if the leak is direct towards the compartmentalisation wall. In that case hydrogen must be pulled from the area as fast as possible and therefore the large outlet duct should be mounted near the compartmentalisation wall.

Furthermore, with the three outlet ducts mounted on the same side cross-ventilation is included as well. Cross-ventilation is preferred since it entails a gradual pressure gradient in the test cell as discussed in Chapter 8.

Figure 9.26 depicts the hydrogen mass fraction profile or hydrogen volume concentration profile in the range of 0 % to 4 %.

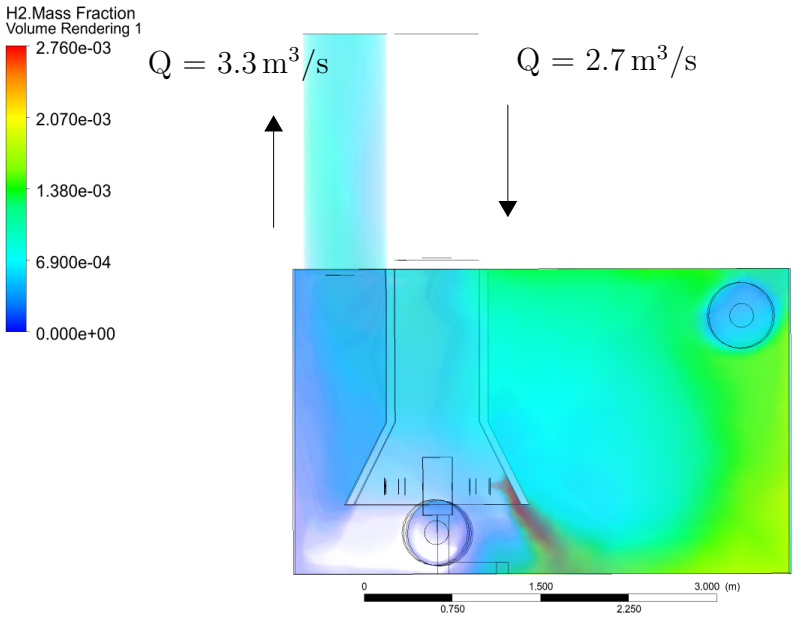

Figure 9.26: The width of the compartmentalised room has been increased from 2.5 m to 4.5 m.

The worst case condition for this ventilation system set-up would be when the leak is directed towards the front of the container, hence the leak is directed towards duct 1 in Figure 9.26. The leak is identical to the one utilised in the previous models.

The volume concentration reaches a maximum of $\approx 1.5\,\%$ near the right-hand side in the container except for near the leak. Hence, during the presumed worst case conditions, the hydrogen volume concentration remains well below the minimum LEL-value of hydrogen.

9.4.5 Varying hydrogen leak flow direction

The direction of the hydrogen leak has not been altered yet, in the following analysis the leak will be projected upwards instead of one which aims to the side. Figure 9.27 shows a leak which is projected vertically upwards directly towards the ventilation fan.

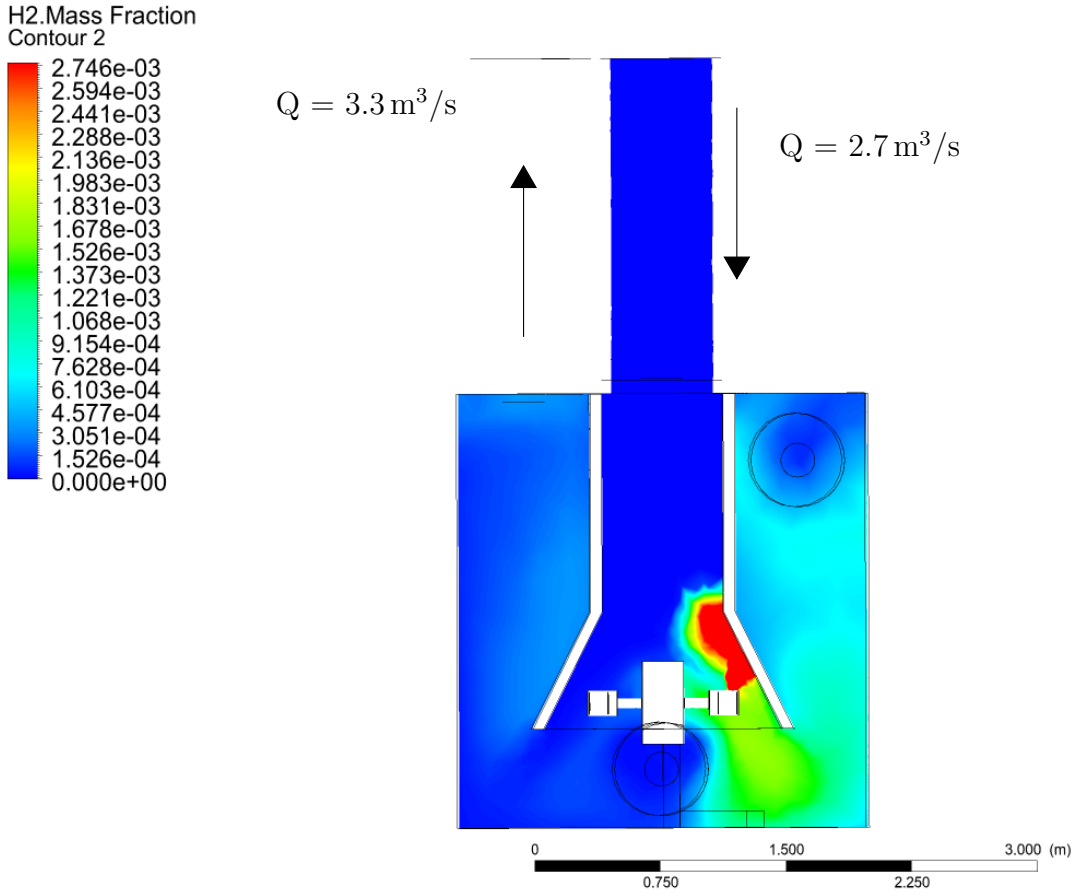

Figure 9.27: A hydrogen leak in the fuel injector with a gap of 1.65 mm and $\dot{m} = 2.69\,\mathrm{g/s}$. The leakage flows vertically upwards in the direction of the ventilation fan mounted above the engine.

The colour scheme depicts a hydrogen volume concentration range of 0 % to 4 % presented by a blue and red colour respectively. The hydrogen plume reaches a height of approximately 0.4 m after which it is pushed down by the cooling fan. The cloud mixture exceeds a hydrogen concentration of 4 % near the leak but remains below the LEL-limit in the remainder of the test cell.

Figure 9.28 shows the hydrogen diffusion profile in the frontal plane of the container. The volume concentration is disposed of well and the average concentration in the test cell remains low.

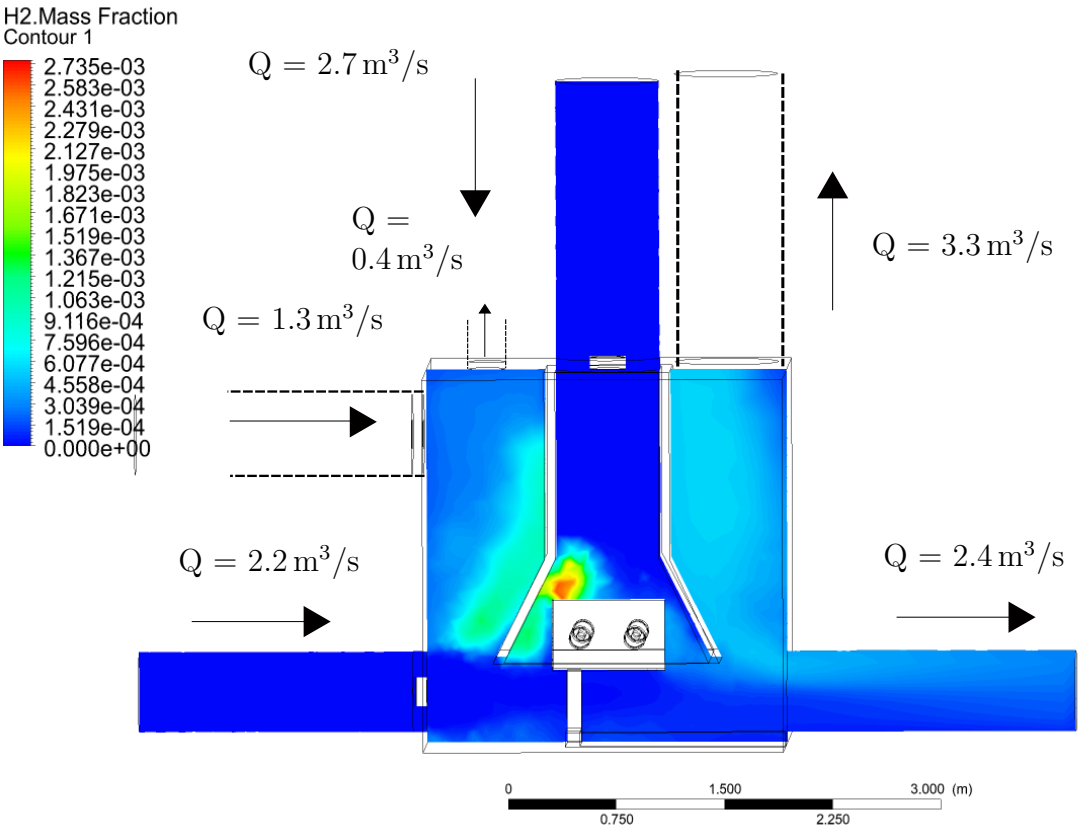

Figure 9.28: A hydrogen leak in the fuel injector with a gap of 1.65 mm and $\dot{m}$ = 2.69 g/s. The leakage flows vertically upwards in the direction of the ventilation fan mounted above the engine.

At last, a 3D-profile of the hydrogen diffusion profile is presented in Figure 9.29. Hydrogen diffuses well and the risk of a detonation or deflagration is low as the lower limit of the LEL is not exceed in the test cell except for near the leakage.

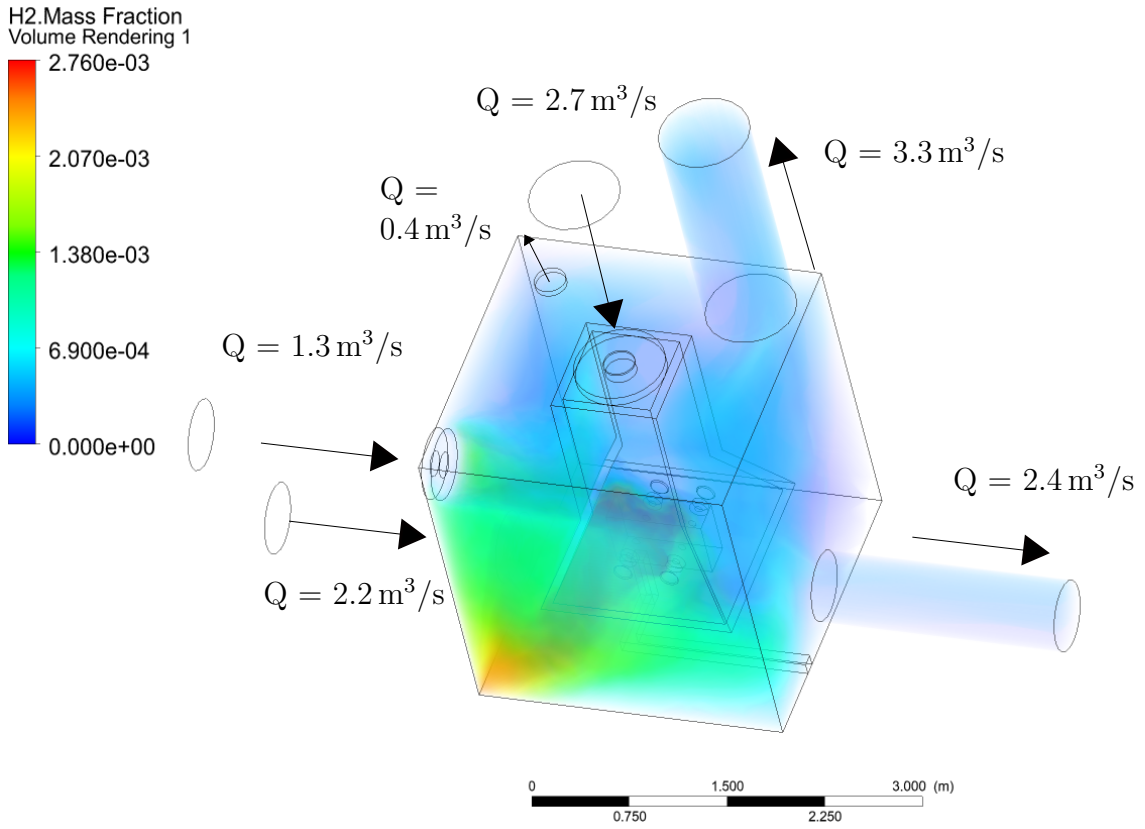

Figure 9.29: 3D-plot of a hydrogen leak in the fuel injector with a gap of 1.65 mm and $\dot{m} = 2.69\,\mathrm{g/s}$. The leakage flows vertically upwards in the direction of the ventilation fan mounted above the engine.

9.5 Additional test cell safety considerations

A few additional safety precautions must be defined, a CFD analysis to design a suitable ventilation system is only part of obtaining a permit.

- The physical flow field will differ from the results displayed in this report as simplifications are made to simulate the model in ANSYS Fluent. For example, the wake formation of the engine may be different than as shown in the CFD results as air will flow through fins. Helium should be conveyed through the fuel pipe prior to testing with hydrogen. Helium has similar characteristics to hydrogen and is an effective tool to validate the CFD results. Helium may be furthermore utilised to check for leaks before experiments are performed. Alternatively a nitrogen-air mixture can be used as well (Hysafe, 2009).

- One should experiment with only one cylinder operating on hydrogen instead of all four during initial tests. Subsequently, testing with a small external cylinder instead of the cylinders of the Lycoming engine is safer. Testing with cylinders of smaller scale should not limit ongoing research, particularly during the initial stage of the experiments.

- The ducting system may need to be adjusted, therefore the pressure losses induced by the ducts may increase. Alternative fans should be selected when the pressure losses exceed the maximum total operative pressure of the U/EI-EIL 564 and/or U/EI-EIL 715.

- Charged particles are most likely to be the cause of ignition in the test cell. Particles upon entering the ducts may become charged due to friction with the surface walls or due to the rapidly spinning ventilation fans. The risk of charged particles should be further documented. Literature should be reviewed on how to prevent or minimise charged particles entering the test cell.

- The internal combustion engine is not maintained at the desired temperature if the engine is not isolated from the air flows present in the test cell. Air flows in the test cell may affect the cooling of the cylinder barrel and cylinder head, inclining less efficient combustion. One must be careful with designing the encapsulation. Hydrogen accumulates near the encapsulation which isolates the engine and initially traps hydrogen in a confined space. The cooling fan pushes it downwards but due to the strong initial momentum jet, hydrogen accumulates in the local region near the engine. The encapsulation must be at a safe distance from the internal combustion engine to minimise the volume concentration of hydrogen in the event of a leak.

- Sensors must be mounted in the fuel pipe to measure the mass flow rate of hydrogen, the strength of the leak may be measured through the sensors when a leak occurs. In addition, sensors must be mounted near the internal combustion engine as leakages near the engine are most likely. Furthermore, sensors should be placed in the outlet ducts. Note that sensors should be mounted on the ceiling since a thermal layer is present beneath the ceiling of the test cell container due to the high thermal load. The warm air causes the sensors to detect hydrogen at a slower rate. In the outlet ducts, no thermal layer is present and thus a hydrogen leak is detected earlier. In addition, elements such as lamps may not be mounted on the ceiling either as they can impede the outflow of hydrogen into the environment. Sensors should be able to detect at least a hydrogen volume concentration of 0.4 % (10 % of the minimum LEL-value). A signal should be send to the control panel when a hydrogen concentration of 0.4 % is detected and the test set-up must be shutdown automatically. Note that the system must be connected to the shut-off valves as well to block the fuel supply.

- The ventilation fan which functions as cooling fan can be mounted on the side wall of the container instead of on the ceiling. Mounting a fan on the side of the wall requires less effort and prevents the risk of hydrogen or plumes re-entering the test cell.

- A large part of the air entering the test cell through the cooling fan is not required to cool the engine. Part of the air may be utilised to cool the engine while the remaining air can be used for circulation near the ceiling. Hence, part of the air can be utilised to cool the engine through the augmented ducts while the remaining air flows through the remaining smaller ducts and is directed towards the ceiling. Only two inlet fans would be required if a large ventilation fan is utilised as the U/EI-EIL 715. For example, $1.5\,m^3/s$ air will be used to cool the engine and $1.5\,m^3/s$ to recirculate the air near the ceiling. A second inlet mounted on the bottom of the container supplies the remaining $3\,m^3/s$. The inlet fan which is currently mounted on the side of the wall depicted in Figure 9.11 is in that case not required. The example is illustrated in Figure 9.30. Both U/EI-EIL 564 may then be utilised in the remaining room which includes the dynamometer.

- A total ventilation rate of $6\,m^3/s$ is required to sufficiently cool the container. The U/EI-EIL 715 supplies a maximum ventilation rate of $4.5\,m^3/s$ and the U/EI-EIL 564 a ventilation rate of $3\,m^3/s$. However, a ventilation system of two U/EI-EIL 564 is not sufficient to cool the test cell since no outlet ducts will be included. The volumetric flow rate through the outlet reduces and the pressure increases in the container by excluding the outlet fans. The ventilation system should thus either include two U/EI-EIL 715 fans or two U/EI-EIL 715 fans and one U/EI-EIL 564 depending on the chosen configuration. As aforementioned, the cooling fan may simultaneously circulate the air near the ceiling as well and therefore two inlet ventilation fans would be sufficient.

- The flash point of kerosene and Jet A-1 is 311 K as mentioned in Section 6.4. Kerosene and jet A-1 evaporate when the temperature of the container exceeds the threshold of 311 K and subsequently flammable vapours appear in the test cell. The temperature in the container may exceed 311 K when the ambient temperature is 301 K. Careful notice must be taken in the summer during testing since the flammable vapours impose a hazard.

- The length of the ducts mounted on the roof should be longer for the outlets than for the inlet duct. Hydrogen tends to rise upwards, thus if a leak occurs in the test cell and hydrogen is disposed of through the outlet duct mounted on the roof, it might re-enter the test cell through the inlet duct. However, hydrogen cannot re-enter the test cell when the outlet duct is slightly longer as hydrogen will rise upwards and escape the test cell environment. Hydrogen might flow in the direction of the inlet duct and re-enter the test cell if the outlet duct is shorter.

Figure 9.3 and Figure 9.4 illustrate the example. Note that the same precaution must be taken for the exhaust pipe.

- No components may be mounted on the ceiling except for the outlet and possibly an inlet duct. Hydrogen forms a layer on the ceiling, if elements are mounted on the ceiling they may act as ignition sources. In addition, objects mounted on the ceiling may impede the outflow of hydrogen or may enhance mixing by adding turbulence to the flow.

- Inert gases such as nitrogen may decrease the concentration of oxygen in an enclosed environment. A system which automatically conveys nitrogen into the test cell in the event of a leak may prevent a detonation.

- A double wall can be used to ensure no hydrogen leaks from the fuel pipe. Hysafe (2009) mentions the probability of a hydrogen leak into the test cell due to a fuel pipe rupture is negligible and must not be taken account for during the design of the optimal ventilation system with appropriate precautions.

- Every element in the container must be grounded such that particles do not become charged in the test cell. Charged particles impose the largest hazard due to the low minimum activation energy of hydrogen. Note that continuity bonding should be utilised to avoid static sparks when designing parts.

- The diameter of ducts in the test cell may not be larger than 10.5 cm according to the 7-λ rule. A hydrogen flame cannot transition into a detonation in such a small area and therefore the large duct should converge into multiple smaller ducts.

- Each sensor, or component in the test cell that is powered by electricity must be ATEX-3 protected. Surfaces that attain high temperatures and include electric wires may invoke an ignition. ATEX-3 protection are components which are gas and dust tight.

- Explosion vents should be mounted on the ceiling of the container. The vents should automatically open when the pressure inside the test cell exceeds a predetermined threshold. The pressure relief ensures a deflagration cannot transition into a detonation.

- To reduce the probability of a detonation in the test cell a simulation of a deflagration and detonation process should be performed.

- A mechanical inspection must be planned prior to testing the engine. Fittings, weldings and gaskets must be checked in accordance with the safety guidelines (e.g. no large impurities or screwing at the incorrect torque) (Hysafe, 2009).

- The fuel pipe must be purged with an inert gas prior to testing to ensure no flammable mixtures may form in the pipe. Hydrogen may not be introduced until the fuel pipe has been purged at least three times and the oxygen content of the residual gas is reduced below a predefined process specification impurity level (Hysafe, 2009).

- Hydrogen can only spontaneously ignite when the storage pressure exceeds 30 bar (Hysafe, 2009). Hence, with the current test set-up an ignition due to the rising temperature of the hydrogen-air cloud mixture upon expansion (negative Joule-Thomson coefficient) is impossible. Port fuel injection may also be performed with higher pressures than 20 bar. One should be careful by increasing the injection pressure as the risk rapidly rises.

- Operatives must purge the fuel pipe after each experiment. Flammable mixtures may form in the fuel pipe or a leak may form as well when the test cell is non-operative.

- Large amounts of energy may be released upon impact of hydrogen with an object due to the high momentum of the leak. The engine encapsulation for example imposes therefore a hazard. Hysafe (2009) states that titanium, cerium, zirconium, hafnium and their alloys should be avoided. Aluminium alloys do not impose a hazard unless the material is rusty or hydrogen impacts on smears of aluminium (form of surface deformation). Impurities in the material must be minimised and the fume hood must be regularly cleaned as otherwise an aluminium fume hood is incendive as well.

- Hydrogen sensors will sound an alarm when the hydrogen volume concentration exceeds 0.4 % or 10 % LEL. It remains a knowledge gap how much time elapses between the rupture and detection of the leak. It will valuable to test the performance of the detectors prior to experimenting with the engine.

- The hydrogen safety experts mention air compressors might be a good alternative solution to cool the engines since they do not induce high levels of turbulence. Turbulence enhances mixing and strengthens a detonation when one occurs.

- A fire extinguishing system is vital to enhance the safety in the test cell. A system must be designed which is linked to the flame and leak detectors.

- Further analysis is required regarding the required thickness of the elements in the test cell such as the fume hood. The material must be thick enough to endure hydrogen leaks and deflagration or potentially detonations.

Figure 9.30 below presents the example defined in the list above. The inlet and outlet

volumetric flow rates are an estimate based on the inlet fans which are included and the size of the outlet ducts. Currently all the mass flowing through the inlet ventilation mounted on the roof is directed towards the engine. However the engine does not require that much mass flow to be cooled. Part of the air can also be utilised to circulate air near the ceiling of the container. For example, $1.5\,m^3/s$ air flows over the engine cylinders and $1.5\,m^3/s$ is utilised to circulate air near the ceiling of the container. Only two fans would be required in that case and the U/EI-EIL 454 becomes obsolete, two U/EI-EIL 715 are sufficient to meet the required ventilation volumetric flow rate.

In addition, the U/EI-EIL 715 can be mounted on the side walls when the U/EI-EIL 454 is excluded from the model. Mounting a fan on the side wall requires less effort than mounting one on the ceiling. The duct losses of both duct configurations are nearly identical. A fan mounted on the roof has high duct losses incurred by the rain cap. When the cooling fan is mounted on the side, high duct losses will be incurred by the 90° angle in the duct system which is necessary to ensure the cooling air flows from above over the engine cylinders.

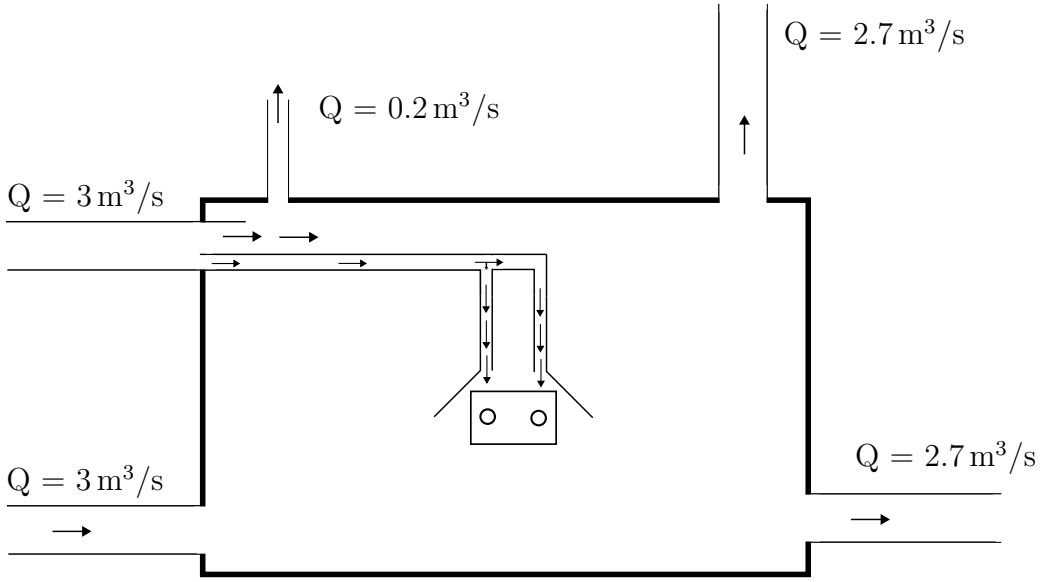

Figure 9.30: Not all air flowing through the inlet ventilation fan mounted on the ceiling must be pushed downwards. The fan may also be mounted on the upper part of the side wall such that part of the flow is directed over the engine and part of the air recirculates air near the ceiling.

9.6 Incidence risk test cell per year

The risk map can be iterated once more by including the recommendations stated above. The letters in the risk map stand for the following leak cases (iterated from Chap-

ter 7),

- A ⟶ crankcase leakage
- B ⟶ fuel injector leakage
- C ⟶ fuel pipe rupture
- D ⟶ wall crack
- E ⟶ intake manifold leakage
- F ⟶ exhaust manifold leakage
- G ⟶ leakage through valve

Table 9.4: Risk map of hydrogen leakages in the test cell container with precautions.

Likelihood \ Severity	1	2	3	4	5
1	E,F,G	D	C		
2	A	B			
3					
4					
5					

The severity of each case decreases since the room is compartmentalised as hydrogen cannot come into contact with ignition sources. A fuel pipe rupture, fuel injector leak, leak through the crankcase vent and wall crack should not lead to a deflagration and detonation and are all reduced to a green-zone. Especially a leakage in the crankcase vent should not impose a large hazard. The crankcase vent is mounted on the bottom of the engine and hydrogen may leak due to a loose connection. Hydrogen would leak with low momentum since the pressure is not high in the crankcase. A potential leak would be immediately disposed of due to the inclusion of the inlet fan and outlet duct near the floor of the container.

Furthermore, HyRAM includes a risk analysis model. The probability of a no ignition, test shutdown, deflagration and detonation can be estimated through the container parameters. The program assumes the room is well-ventilated and includes the necessary safety measures. Furthermore, the program assumes human errors do not occur, hence leaks due to loose connectors are neglected despite it in reality imposing the largest hazard (Hysafe, 2009). The program requires as input the dimensions of the test room, injection pressure, amount of pipes in the container, cylinders, compressors, container temperature, fluid temperature et cetera.

Two sets of cases are included, a strong leak with a mass flow rate of 2.69 g/s (gap diameter of 1.65 mm. The second case includes a leak with a mass flow rate of 0.0269 g/s, hence a leak which is one hundred times weaker than the worst case condition. The risk scenarios of the weak leak are displayed in Table 9.5.

Table 9.5: Risk assessment of a weak leak in the test cell ($\dot{m} = 0.0269$ g/s).

Scenario outcome	**Average events per year**	**Incidence per # years**	**Branch line probability**
No ignition	0.0084	119.02	10 %
Shutdown	0.076	13.23	90 %
Deflagration	0	0	0 %
Detonation	0	0	0 %

A probability of 90 % shutdown means 90 % of the time when a leak occurs, the leak is detected and hydrogen is disposed of successfully and the test set-up is shutdown in time. 10 % of the time the leak is not detected in this instance. HyRAM sets the probability of a hydrogen leak being detected by default at 90 %. The 90 - 10 percentage distribution is not based on any statistical data and is set arbitrarily. It may be noticed weak leaks do not entail a detonation or deflagration and thus do not impose a hazard as the consequence is always a no ignition or test shutdown scenario.

Table 9.6 displays the risk scenarios for a strong leak ($\dot{m} = 2.69$ g/s).

Table 9.6: Scenario outcomes and risk probability of a leak in the test cell for a strong leak ($\dot{m} = 2.69$ g/s).

Scenario outcome	**Average events per year**	**Incidence per # years**	**Branch line probability**
No ignition	1.1E-4	8,818	10 %
Shutdown	0.001	968	89.88 %
Deflagration	9.2E-7	1.09E6	0.08 %
Detonation	4.6E-7	2.2E6	0.04 %

The risk of a detonation each year is 4.6E-5 % according to the model, excluding the possibility of a human error. Nonetheless, a leak is most likely to occur due to a human error. A hydrogen leak will happen once in the coming 5 years according to the hydrogen safety experts.

Operatives must continuously follow the safety guidelines to minimise the risk. In April 2021, two researchers died when they opened the container door of a test cell with a hydrogen fuel cell test set-up inside. A leak caused hydrogen to accumulate in the test cell and was not disposed of well due to poor ventilation. When the researchers

opened the door it caused a spark which was sufficient to ignite the hydrogen-air cloud mixture.

Similarly in 2019 at a silicones plant in the United States four workers died. The plant was not ventilated well while simultaneously the hydrogen detectors were not functioning well either. The building exploded and the blast could be felt 30 km from the site [3].

[3] https://www.wsws.org/en/articles/2019/12/23/expl-d23.html [Retrieved 10.05.2021]

Chapter 10

Conclusion

The aim of the report is to design a test cell for the development of a retrofit hydrogen air-cooled piston engine. The test cell environment is divided into two separate 20-feet containers, one houses the control room and the other the test set-up.

A fan cools the engine from above which simultaneously ventilates part of the container. The incoming required cooling air velocity is estimated to be 15.97 m/s with induced-draught fans at maximum load conditions. In the test cell, forced-draught fans will be mounted which induce more turbulence and therefore enhance cooling. The required cooling velocity may therefore be slightly lower than the estimated value.

The major concerns in the test cell are the accumulation of heat and diffusion of hydrogen. The worst case scenario in the test cell is presumed to be a leak in the fuel injector with a gap of 1.65 mm and hydrogen mass flow rate of 2.69 g/s. Consequently, particles impose a large hazard as they may become charged due to friction with the ventilation fans and cause an ignition of a hydrogen-air cloud mixture.

The test cell requires a ventilation system of $3\,m^3/s$ to ensure the average hydrogen volume concentration in the test cell does not exceed 25 % of the lower explosive limit of hydrogen. The final design includes a total ventilation flow rate of $6\,m^3/s$ to maintain the test cell at adequate temperatures and to include a fail-safe system to successfully dispose of hydrogen. The current set-up includes three inlet fans and three outlet ducts. The outlets may not include exhaust fans since in the event of a leak both hydrogen and charged particles are consequently present in the outlet, which may entail a detonation. It is demonstrated heat and hydrogen are disposed of effectively and the probability of a detonation due to a hydrogen leak is low when the container is compartmentalised.

An effective ventilation system is not sufficient to minimise the risk, further safety considerations are required. For example, it must be ensured all the elements in the test cell are grounded, all elements are ATEX-3 protected, the fuel pipe includes a double wall, explosion vents are mounted on the ceiling et cetera. Furthermore, simulations of a detonation and deflagration process are still required to further minimise the risk.

The probability of a detonation is $4.6 \cdot 10^{-5}$ % when all safety considerations are included and no human error occurs. Nonetheless, a detonation is most likely to occur due to a human error, such as not mounting objects well.

A few limitations remain present since tests must be performed in a 20-feet container. The test cell is developed such that test experiments can be performed across the Netherlands. However, locations where one may test with hydrogen are limited. Further research is required regarding possible test locations in the Netherlands.

Chapter 11

Recommendations

The CFD analysis is a tool to comprehend the diffusion of hydrogen and warm air within an enclosed environment. The configuration of the test cell may change or the duct system may be altered. To ensure safety of the operatives during testing, additional steps must be defined. To be able to adapt to changes, the following recommendations must be complied to, to ensure a safe design and minimisation of detonation risk.

- One of the next steps should be researching the possible test locations in the Netherlands and accordingly the maximum allowed noise level. At the moment it is unknown for the collaborative group where tests with hydrogen combustion are allowed. Furthermore, the fan power might be restricted by the local noise regulations, which affects the flow field within the test cell container.

- Currently, the analysis assumes hydrogen is in gaseous state. The CFD results are not valid anymore if experiments are performed with liquid hydrogen. A liquid hydrogen leak will yield a different diffusion profile than a gaseous hydrogen leak despite liquid hydrogen evaporating rapidly. A second CFD analysis is required to model the diffusion of hydrogen in the test cell when one plans to experiment with liquid hydrogen.

- Setting up the organisational mitigation plans and adding inert gases such as helium or nitrogen to the test set-up are a substantial part of enhancing safety as well. The CFD analysis is a tool to provide an initial guess of the most optimal ventilation system but in itself is not sufficient to guarantee a safe test cell environment.

- The ducting system and fume hood are simplified in the CFD model, the flow field in the test cell container will therefore slightly differ. Careful consideration must be taken with assessing the flow field near the engine.

- Simulations of the detonation and deflagration process are still required. Through simulations in blastFoam it can be predicted when a detonation is most likely to occur and when a deflagration transitions into a detonation. Furthermore, the analysis predicts the minimum thickness of the fume hood for instance.

- The shock waves of the leak are not modelled very accurately since a unstructured mesh is utilised near the leak. The effects are expected to be negligible but one should remain careful that the diffusion of hydrogen may slightly differ from what the CFD simulations display.

- The effect of the rippled walls is accounted for through a constant roughness coefficient. The grooves on the ceiling of the container may hinder the outflow of hydrogen more than predicted in the CFD simulations and must be carefully monitored.

Bibliography

[Airbus Deutschland 2003] Airbus Deutschland: *Liquid Hydrogen Fuelled Aircraft - System Analysis*. In: *Cryoplane* (2003), p. 1–80

[Anderson 2011] Anderson, J.: *Fundamentals of Aerodynamics*. Vol. 6. Mcgraw-Hill Education International, 2011

[Biennal Report 2005] Biennal Report: *Hydrogen Fundamentals*. In: *Biennial Report on Hydrogen Safety* (2005), p. 1–9

[Blomqvist 2009] Blomqvist, C.: *Distribution of ventilation air and heat by buoyancy forces inside buildings - an experimental study*. Vol. Doctoral. 2009. – 55 pp.

[Brand et al. July 2003] Brand, J. ; Sampath, S. ; Shum, F. ; Bayt, R. L. ; Cohen, J.: *Potential use of hydrogen in air propulsion*. In: *AIAA\ICAS International Air and Space Symposium and Exposition: The Next 100 Years* (July 2003), p. 1–11

[Canan and Ibrahim 2019] Canan, A. ; Ibrahim, D.: *Review and evaluation of hydrogen production options for better environment*. In: *Journal of Cleaner Production* 218 (2019), p. 835–849

[Chen and Mao 2017] Chen, H. ; Mao, Z.: *The study on the results of hydrogen pipeline leakage accident of different factors*. In: *IOP Conference Series: Earth and Environmental Science* 64 (2017)

[CleanSky 2020] CleanSky: Hydrogen-powered aviation: A fact-based study of hydrogen technology, economics, and climate impact by 2050. 1 (2020)

[Dagdougui et al. 2018] Dagdougui, H. ; Sacile, R. ; Bersani, C. ; Ouammi, A.: Hydrogen Storage and Distribution: Implementation Scenarios. In: *Hydrogen Infrastructure for Energy Applications* (2018), Nr. Atex 137, p. 37–52

[Das 1990] Das, L. M.: *Hydrogen engines: A view of the past and a look into the future*. In: *International Journal of Hydrogen Energy* 15 (1990), p. 425–443

[Durbin and Malardier-Jugroot 2013] Durbin, D. J. ; Malardier-Jugroot, C.: *Review of hydrogen storage techniques for on board vehicle applications*. In: *International Journal of Hydrogen Energy* 38 (2013), p. 14595–14617

[F.R. et al. 2005] F.R., Schauer ; C.L., Miser ; K.C., Tucker ; R.P., Bradley ; J.L., Hoke: *Detonation initiation of hydrocarbon-air mixtures in a pulsed detonation engine.*. Vol. 1343. AIAA-paper, 2005

[Frijters 2020] Frijters, W.: A Flying Test Bed for Sustainable Aviation: A Literature Review. (2020)

[Gibson 1919] Gibson, A. H.: *The air cooling of petrol engines.* University college Dundee, 1919

[Green and Glasson 1992] Green, R. K. ; Glasson, N. D.: *High-pressure hydrogen injection for internal combustion engines.* In: *International Journal of Hydrogen Energy* 17 (1992), p. 895–901

[Haglind and Singh 2006] Haglind, Fredrik ; Singh, Riti: *Design of aero gas turbines using hydrogen.* In: *Journal of Engineering for Gas Turbines and Power* 128 (2006), p. 754–764

[Hagstrom and Siren 2000] Hagstrom, Kim H. ; Siren, Kai: *Calculation of room velocity using kinetic energy balance.* In: *ASHRAE Transactions* 106 (2000)

[Heinsohn 1991] Heinsohn, Robert J.: *Industrial ventilation: Engineering Principles.* New York : John Wiley & Sons, Inc., 1991

[Hübert et al. 2014] Hübert, T. ; Boon-Brett, L. ; Palmisano, V. ; Bader, M. A.: *Developments in gas sensor technology for hydrogen safety.* 2014

[Hysafe 2009] Hysafe: *HYSAFE – Safety of Hydrogen As an Energy Carrier Deliverable D113 Initial Guidance for Using Hydrogen in Confined Spaces -Results from InsHyde.* Framework, Sixth and Network, Programme, 2009. – 1–89 pp.

[Hysafe 2011] Hysafe: *Accidental Phenomena and Consequences - Release of Hydrogen.* (2011)

[Khandelwal et al. 2013] Khandelwal, B. ; Karakurt, A. ; Sekaran, P. R. ; Sethi, V. ; Singh, R.: *Hydrogen powered aircraft: The future of air transport.* In: *Progress in Aerospace Sciences* 60 (2013), p. 45–59. – URL `http://dx.doi.org/10.1016/j.paerosci.2012.12.002`

[Kuo. 1986] Kuo., K. K. Y.: *Principles of Combustion.* New york : John Wiley and Sons, 1986

[Lino Guzzella 2010] Lino Guzzella, Christopher H. O.: *Introduction to Modelling and Control of Internal Combustion Engine Systems.* 2010. – ISBN 9783642107740

[Lycoming Manual 2005] Lycoming Manual: *Operator ' s Manual HIO-360 & TIO-360 Series.* (2005)

[Magarajan et al. 2012] Magarajan, U ; R, Thundil Karuppa R. ; Elango, T: *Numerical Study on Heat Transfer of Internal Combustion Engine Cooling by Extended Fins Using CFD.* In: *Research journal of recent sciences* 1 (2012), p. 32–37

[Martyr and Plint 2012] Martyr, A. J. ; Plint, M. A.: *Engine testing*. Elsevier, 2012

[Merk 1958] Merk, H. J.: *The Macroscopic Equations for Simultaneous Heat and Mass Transfer in Isotropic, Continuous and Closed Systems*. Vol. 8:73-99. Appl. Sci. Res., 1958

[Mills and Coimbra 2015] Mills, A.F. ; Coimbra, C.F.M.: *Basic heat and mass transfer*. Vol. 3. Temporal Publishing LLC, 2015

[Molkov and Brennan 2011] Molkov, V. ; Brennan, S.: *Hydrogen properties, releases and dispersion*. In: *"HySafer"* (2011)

[Najjar 2013] Najjar, Y.S.H.: *Hydrogen safety: The road toward green technology*. 2013

[Nojoumi et al. 2009] Nojoumi, H. ; Dincer, I. ; Naterer, G. F.: *Greenhouse gas emissions assessment of hydrogen and kerosene-fueled aircraft propulsion*. In: *International Journal of Hydrogen Energy* 34 (2009), p. 1363–1369. – URL `http://dx.doi.org/10.1016/j.ijhydene.2008.11.017`

[Reddy Kummitha and Reddy 2017] Reddy Kummitha, O. ; Reddy, B. V.: *Thermal Analysis of cylinder block with fins for different materials using ANSYS*. In: *Materials Today: Proceedings* 4 (2017), Nr. 8, p. 8142–8148. – URL `https://doi.org/10.1016/j.matpr.2017.07.155`

[Rosen and Koohi-Fayegh 2016] Rosen, Marc A. ; Koohi-Fayegh, Seama: The prospects for hydrogen as an energy carrier: an overview of hydrogen energy and hydrogen energy systems. In: *Energy, Ecology and Environment* 1 (2016), Nr. 1, p. 10–29. – ISSN 23638338

[Sagar and Agarwal 2018] Sagar, S. M. ; Agarwal, A. K.: *Knocking behavior and emission characteristics of a port fuel injected hydrogen enriched compressed natural gas fueled spark ignition engine*. In: *Applied Thermal Engineering* 141 (2018), p. 42–50. – URL `https://doi.org/10.1016/j.applthermaleng.2018.05.102`

[Schefer et al. 2006] Schefer, R. W. ; Houf, W. G. ; San Marchi, C. ; Chernicoff, W. P. ; Englom, L.: *Characterization of leaks from compressed hydrogen dispensing systems and related components*. In: *International Journal of Hydrogen Energy* 31 (2006), p. 1247–1260

[Schey and Biermann 2020] Schey, O. W. ; Biermann, A. E.: *Heat dissipation from a finned cylinder at different fin plane and air-stream angles*. (2020)

[Smitkova et al. 2011] Smitkova, M. ; Janíček, F. ; Riccardi, J.: *Life cycle analysis of processes for hydrogen production*. In: *International Journal of Hydrogen Energy* 36 (2011), p. 7844–7851

[Sopena et al. 2010] Sopena, C. ; Diéguez, P. M. ; Sáinz, D. ; Urroz, J. C. ; Guelbenzu, E. ; Gandía, L. M.: *Conversion of a commercial spark ignition engine to run on hydrogen: Performance comparison using hydrogen and gasoline.* In: *International Journal of Hydrogen Energy* 35 (2010), p. 1420–1429

[Sutton and Gnoffo 1998] Sutton, K. ; Gnoffo, P. A.: *Multi-component Diffusion with Application to Computational Aerothermodynamics.* Vol. 98-2575. AIAA Paper, 1998

[Taira et al. 2015] Taira, Y ; Saburi, T ; Kubota, S ; Sugiyama, Y ; Matsuo, A: *Numerical investigation of hydrogen leakage from a high pressure tank and its explosion.* In: *International Conference on Hydrogen Safety* (2015), p. 1–11

[Van Den Berg 2007] Van Den Berg, M.: *Night noise guidelines for Europe.* In: *Turkish Acoustical Society - 36th International Congress and Exhibition on Noise Control Engineering, INTER-NOISE 2007 ISTANBUL* 7 (2007), p. 5016–5025

[Venetsanos et al. 2011] Venetsanos, A. G. ; Adams, P. ; Azkarate, I. ; Bengaouer, A. ; Brett, L. ; Carcassi, M. N. ; Engebø, A. ; Gallego, E. ; Gavrikov, A. I. ; Hansen, O. R. ; Hawksworth, S. ; Jordan, T. ; Kessler, A. ; Kumar, S. ; Molkov, V. ; Nilsen, S. ; Reinecke, E. ; Stöcklin, M. ; Schmidtchen, U. ; Teodorczyk, A. ; Tigreat, D. ; Versloot, N. H.: *On the use of hydrogen in confined spaces: Results from the internal project InsHyde.* In: *International Journal of Hydrogen Energy* 36 (2011), p. 2693–2699

[Verhelst et al. 2009] Verhelst, S. ; Maesschalck, P. ; Rombaut, N. ; Sierens, R.: *Increasing the power output of hydrogen internal combustion engines by means of supercharging and exhaust gas recirculation.* In: *International Journal of Hydrogen Energy* 34 (2009), p. 4406–4412. – URL `http://dx.doi.org/10.1016/j.ijhydene.2009.03.037`

[Wallner T. 2009] Wallner T., Miers S.: *Safety Considerations for Hydrogen Test Cells.* (2009)

[Walter 2001] Walter, Lanz: Module 1: Hydrogen Properties. In: *Hydrogen Fuel Cell Engines* (2001), p. 41

[Wang et al. 2019] Wang, Xi ; Sun, Bai gang ; Luo, Qing he: Energy and exergy analysis of a turbocharged hydrogen internal combustion engine. In: *International Journal of Hydrogen Energy* 44 (2019), Nr. 11, p. 5551–5563. – URL `https://doi.org/10.1016/j.ijhydene.2018.10.047`. – ISSN 03603199

[White et al. 2006] White, C. M. ; Steeper, R. R. ; Lutz, A. E.: *The hydrogen-fueled internal combustion engine: a technical review.* In: *International Journal of Hydrogen Energy* 31 (2006), Nr. 10, p. 1292–1305

[Yip et al. 2019] Yip, H. ; Srna, A. ; Yuen, A. C. Y. ; Kook, S. ; Taylor, R.A. ; Yeoh, G. H. ; Medwell, P. R. ; Chan, Q. N.: *A review of hydrogen direct injection for internal combustion engines: Towards carbon-free combustion.* In: *Applied Sciences (Switzerland)* 9 (2019), Nr. 22, p. 1–30

[Yu et al. 2013] Yu, J. ; Vuorinen, V. ; Kaario, O. ; Sarjovaara, T. ; Larmi, M.: *Visualization and analysis of the characteristics of transitional underexpanded jets.* In: *International Journal of Heat and Fluid Flow* 44 (2013), p. 140–154. – URL `http://dx.doi.org/10.1016/j.ijheatfluidflow.2013.05.015`

[Yüceil et al. 2000] Yüceil, K. B. ; Ötügen, M V. ; Arik, E.: *Underexpanded Sonic Jets : A PIV Study.* In: *10th International Symposium on Application of Laser Techniques to Fluid Mechanics, Lisbon, Portugal* (2000), Nr. January 2000

Appendix A: CFD Set-up & Processing

In this chapter the set-up of the CFD model is explained in conjunction with the case studies. A basis CFD model will be developed to which few alterations are made, subsequently in Chapter 8 the repercussions of these design changes are analysed through a sensitivity analysis. This ranges from alternating the inlet velocity to observing the influence on the flow field of varying the geometry of the engine and changing the shape of secondary elements such as the dynamometer.

A.1 Selecting the CFD software

The first step is to select the CFD software to simulate the energy balance and air flows. It has been previously mentioned ANSYS Fluent is chosen to perform the simulations with. ANSYS Fluent is chosen as the software package as it is the current industrial leading CFD software due to an easy to use GUI (graphical user interface). The alternative to ANSYS Fluent is OpenFoam, which receives a lot of affinity from accomplished aerodynamicists as it provides more freedom to the modeller and is equally powerful. However, the learning curve for OpenFoam is steeper than for ANSYS Fluent. As the experience of the modeller with CFD is limited, simulating the model through ANSYS Fluent is presumed to be more accessible. Subsequently, DesignModeler is a featured tool by ANSYS to design 3D CAD models with and is therefore utilised to developed a simplified model of the test cell.

Including every element in the test cell environment presented in Chapter 4 would yield an excessive amount of cells and immoderate computational time, withal the maximum amount of cells allowed with a student license is 512,000. Prior to developing the ANSYS-model one had to estimate through literature the approximate amount of required cells. The maximum cell count is presumed to not hinder the development of the CFD model. Rough estimates of the flow field are considered to be sufficient, detailed analysis of the flow field is superfluous. In addition, a sensitivity analysis is performed and presented in Appendix C, which proves that a grid size of approximately 300,000 cells is sufficient.

The exact rate of hydrogen diffusion is difficult to predict, the inlet cooling air velocity varies by changing the throttling settings, the inlet temperature varies as the

ambient conditions cannot be controlled et cetera. The aim is to be able to present recommendations to minimise the risk of a detonation, develop an efficient ventilation set-up and approximate the required engine cooling. A coarse analysis is sufficient to provide these recommendations and therefore detailed analysis is not necessary.

A.2 Pre-processing

The following step is to select the solvers, mesh the grid and define the boundary conditions in ANSYS Fluent.

A.2.1 CFD meshing

The grid composes of a mixed grid but primarily includes tetrahedron cells. A drawback of the tetrahedrons cells (unstructured grid) is the increase in computational time in comparison to hexahedron cells (structured grid). The benefit is the simplicity of meshing as it is less difficult to generate meshes of higher quality. Since a wide array of simulations will need to be performed with varying grids, developing a structured hexahedron grid is presumed to be more time intensive than generating the grid with tetrahedrons. A mesh with a larger concentration of hexahedron cells can potentially lead to a more efficient and higher quality mesh but is not attempted due to a time constraint.

A.2.2 Fluid & turbulence solver

In ANSYS Fluent one must select either a pressure- or density-based solver. The former is selected since a pressure based solver is recommended for incompressible flows by the ANSYS guidelines. Both solvers are able to solve for both incompressible and compressible flows[1]. Nonetheless, pressure-based solvers are still recommended for predominant incompressible flows. Furthermore, the gravity is set at $-9.806\,65\,\mathrm{m/s^2}$.

The following step is to select the fluid and turbulence models. The k-ϵ turbulence model solves the turbulence transport equation, turbulence generation as well as dissipation. The k-ϵ model is suitable to solve free flow regions while it is less accurate measuring the flow near walls. Hysafe (2011) explored various turbulence models and concluded the k-ϵ model, models hydrogen diffusion most accurately. Hysafe (2011) observed the standard model proposed by Lander and Spalding (= k-ϵ model), in contrary to other turbulence models, is able to accurately measure the effects of the turbulence energy, interaction with wind, buoyancy, transient sources with initial momentum and flow in complex geometries such as buildings. Therefore the aforementioned turbulence model is selected to model the diffusion of hydrogen with.

[1]The fluid zone near the hydrogen leak is compressible, since the pressure-based is able to solve for compressible flows as well, it should not raise any concern.

A few more options require to be selected within the k-ϵ solver. The scalable wall function is chosen instead of the standard wall function. The scalable wall function allows for rapid successive refinements as it will maintain the y^+-value automatically above 11.25 (the minimum required y^+-value). A feature which will be beneficial during the sensitivity analysis. The standard wall options requires each mesh to be checked whether the grid complies to the requirements of the wall function as the y^+-value is not automatically adjusted if the minimum value is not met.

A further distinction may be noticed between the standard and realisable model. The realisable model reformulates the turbulent viscosity factor C_μ and adjusts the second transport equation (the dissipation rate ϵ), which is derived from the transport mean-square vorticity fluctuation. The realisable model improves the capability of the solver to capture the mean flow of complex structures and flows characterised by recirculation, rotation, boundary flows and round jets. A drawback is that the realisable model is less stable than the standard turbulence model. Nonetheless, it is the recommended model when predicting secondary flows. The realisable model is selected at cost of stability and hence computational time as the circulation is relatively high within the test cell.

Fluid models must be appointed besides the turbulence model. The energy equation is enabled to predict the thermal load in the test cell container. The energy equation is enabled for both predicting the thermal load and diffusion of hydrogen in the test cell.

To proceed, a combustion model is set-up for the energy balance model. A non-premixed combustion process is selected in the species tab. The energy balance model includes four cylinders, each with a fuel and air inlet (as clarified in Figure 8.3). The combustion characteristics are set through the non-premixed combustion model. The maximum number of species, temperature of the inlet fuel and air, and operating pressure in the combustion chamber are defined. The combustion model is part of the simulation model despite the convective heat transfer being severely underestimated, as mentioned in Section 4.2.5. The error by not including the oil cooling and cooling fins is approximated in Section 6.6. The error can be compared to the CFD results by including the combustion model, thereby verifying the calculations in Section 6.6.

The non-premixed combustion model may be not selected if a leak must be modelled as otherwise Fluent instantly assumes the hydrogen-air mixture ignites. The hydrogen diffusion model utilises the same CAD model but a different species model. The fluid solvers, boundary conditions and cell zones do not differ between the two models. The sole difference is in selecting a different species model. A species transport is selected in the species tab instead of non-premixed combustion to model the diffusion of hydrogen. Withal, within cylinders the combustion process cannot be modelled. Therefore, the cylinders are set as heat sources with an intrinsic heat generation factor in W/m^3K. For a clear overview, all the input values are summarised in Section 8.1.3. A hydrogen-air mixture is selected in the species model. The composition of the mass fraction

percentages requires to be set for each boundary inlet and outlet of the test cell. For example, for boundary conditions of the inlet duct, every species mass fractions must be set to zero (H_2, H_2O etc.) except for oxygen, which is set to 0.23. Fluent assumes the inlet comprises of air when the oxygen mass fraction is set as 0.23 and computes the remaining percentage of nitrogen (0.77). The inlet boundary condition of the leakage includes a hydrogen mass fraction of 1. The next step is to set the boundary and cell zone conditions.

A.2.3 Boundary & cell zone conditions

In this section, the Dirichlet or Neumann conditions along with the cell zone conditions are elaborated upon. The cell zone conditions imply the fan zones and heat sources.

The model includes two inlets and two outlets. Both inlets are specified by a Dirichlet boundary condition with the total pressure set as zero. No work is generated at the two inlet ducts, the flow is set in motion by the internal ventilation fans near the entrance of the container. A total pressure change of zero is valid with no work being produced at the inlet. One has to specify the gauge total pressure rather than the total pressure in ANSYS Fluent. The gauge total pressure is the difference in total pressure across two boundaries. The total pressure in the inlet duct equals the total pressure of the environment if the gauge total pressure is set to zero. Furthermore, the temperature of the incoming air is set to 295 K to simulate the inlet conditions of the empirical method in Section 4.2.5.

The same condition for the gauge total pressure does not hold at the outlet ducts as the ventilation fans exert work and entail a total pressure increase. The gauge (static) pressure is set zero at the outlet. The gauge pressure is the difference in static pressure across the boundary. The downstream flow communicates with the upstream flow for subsonic flows. The static pressure in the outlet duct must equal the static pressure of the ambient air (Anderson, 2011). The two outlet boundary conditions comprise of a Dirichlet boundary condition with pressure gauge set zero.

The remaining boundary conditions to be set are the external walls of the ducts and container. Each wall is given a heat transfer coefficient of 25 W/m^2K and free stream temperature of 295 K. A heat transfer coefficient is an experimentally obtained value for natural convection in ambient air (Martyr and Plint, 2012).

Next, the cell zone conditions are determined. Each zone must either be set as a solid or fluid zone along with further specifications. A fluid zone entails a fluid flowing through the zone while a solid zone entails the material inside the zone is a solid material such as aluminium. For example, the engine must be set as a solid zone and the fan as a fluid zone.

Furthermore, some zones require further specifications. In each fan zone the '3D fan zone' option is enabled. In the '3D fan zone' the dimensions and pressure jumps of the fan can be defined. The input values are previously calculated in Section 4.2.5

while the dimensions of the fan of the U/EI-EIL 564 and U/EI-EIL 715 are provided by Induvac. The pressure jumps include the induced losses by the duct system and are included in the summary in Section 8.1.3.

With the 3D fan zones set, the heat sources must be defined, these include the four combustion chambers, dynamometer, exhaust pipe and two lamps. Heat sources only require one input parameter which is the source term in W/m^3. The temperatures of the exhaust pipe, lamp, dynamometer are determined through literature. For instance, on average the water-cooled dynamometer is expected to attain a temperature of 303 - 323 K. The heat generation in W/m^3K of the dynamometer can be determined as the dimensions are provided by the manufacturer [2]. The variables to estimate the heat generation are included in the summary in Section 8.1.3. A few zones do not require further specifications such as the engine block itself or the fluid zone of the container.

A.2.4 CFD solver

The solver settings are defined in Table A.1.

Table A.1: Solver settings in ANSYS Fluent.

Pressure-velocity coupling	
Scheme	Coupled
Spatial discretisation	
Gradient	Least square cell based
Pressure	Second order
Momentum	Second order upwind
Turbulent kinetic energy	Second order upwind
Turbulent dissipation rate	Second order upwind
O_2	Second order upwind
H_2O	Second order upwind
H_2	Second order upwind
Energy	Second order upwind

A second order upwind should in all instances be more accurate than a first order upwind scheme, at the cost of computational time. The following settings are suggested by ANSYS Fluent to obtain the most accurate results. Selecting a first order upwind scheme reduces the computational time and may be of interest when testing a wide array of different models with various ventilation set-ups. For the validation, verification and final design however a second order upwind scheme will always be selected.

[2] `https://www.taylordyno.com` [Retrieved 07.02.2021]

A.2.5 Simulation strategy

The simulation strategy comprises of setting the residuals and defining the time scale factor. Furthermore, some settings vary for each simulation or may vary during a simulation such as the under-relaxation factors. Under-relaxation factors reduce the pseudo time step of one of the transport equations or one of the equations (velocity, energy, species, ...).

The following phase is to run the simulation. A steady-state time solution will be selected instead of a transient solution as its computational cost is expensive. The aim is to discover poorly ventilated areas and to prevent the accumulation of hydrogen and heat, hence a steady-state solution provides sufficient information. ANSYS Fluent employs a pseudo transient solution, meaning it implements a pseudo transient time step and remains to have a (partially) physical meaning. Transient tendencies may be captured by pausing the simulation run a few times at various iterations and analyse the flow.

The first step in computing the grid is selecting a pseudo transient time step. A large pseudo transient time step entails rapid convergence with the risk of the solution diverging. A small pseudo transient time step entails slow convergence but provides for more stability. The ideal pseudo transient time step is one that converges rapidly but remains stable. The user consequently has the possibility to either directly specify the pseudo transient time step or use an automatic time scale factor. ANSYS determines the time step through heuristics with the automatic timescale factor, the timescale is automatically defined through a velocity and length scale.

Table A.2: Automatically defined time step in ANSYS Fluent.

$\mathbf{\Delta t_u}$	$\mathbf{\Delta t_p}$	$\mathbf{\Delta t_g}$	$\mathbf{\Delta t_r}$	$\mathbf{\Delta t_c}$	$\mathbf{\Delta t_v}$
$\frac{0.3L}{max(U_{bc},U_d)}$	$\frac{0.3L}{U_{dp}}$	$\sqrt{\frac{L}{g}}$	$\frac{0.1}{\omega}$	$\frac{0.3L}{max(U_{bc},U_d U_{dp},\bar{c})}$	$\frac{L^2}{v}$

With U_{bc} the maximum velocity at the boundary, U_d the maximum velocity in the flow field and U_{dp} the maximum induced velocity. The length scale L either equals L_v, the volumetric length scale or L_d, the domain length scale.

Fluent allows the user to select a conservative time scale factor, which selects the minimum of the six above defined time steps and smaller length scale, while the aggressive options selects the maximum time step and larger length scale. Furthermore, the user has the option to multiply or divide this pseudo transient time step, by default this factor equals one. This pseudo transient time step does not require to be constant along the entire simulation. The pseudo time steps, defined in Table A.2, are computed for each iteration.

Specific to CFD model of the test cell environment, transient effects will still be present even though the simulation solves for a steady-state solution. The combustion process will not reach a constant flow field and heat distribution, it will vary as long as the engine is running. In addition, the ventilation fans introduce turbulence and circulation through the room as the fans are continuously spinning. The steady-state solution will be periodic as the air currents will be ever-changing due to air circulation and turbulence.

ANSYS displays scaled residuals, between each iteration, the residual displays the difference in magnitude between each time step. Therefore, residuals will remain relatively large with larger time steps. It is expected the solution continues to oscillate once the solution has converged. the residuals should decrease and plateau when the pseudo transient time step or automatic timescale factor is scaled down once the solution has converged. Reducing the time step once the solution has converged and audit whether the residuals immediately decrease is an additional tool to verify the convergence of the solution.

For instance, assume the overall engine temperature varies between 690 K and 695 K. Setting the pseudo time step to 1, the temperature may differ by 0.001 K for each iteration. If the pseudo time step is reduced to 0.1, the difference in temperature between the two iterations should decrease as well, e.g. the temperature decreases by 0.0001 K per iteration. Therefore, reducing the pseudo time step when the solution has converged entails a decrease in the scaled residuals as well.

Generally, a decrease in residuals by three orders of magnitude (10^{-3}) may indicate convergence according to the ANSYS user's guide [3]. For the energy residual a decrease by six orders of magnitude is desired (10^{-6}).

A.3 Intermediate summary of the CFD set-up

This following list includes a summary of the CFD set-up chapter.

- ANSYS Fluent is selected instead of OpenFoam as the learning curve is presumed to be more gradual. Yet, the grid size in Fluent is limited by a student license. The maximum allowed amount of cells the grid may contain is 512,000. The limitation does not affect the analysis however.

- k-ϵ is the chosen turbulence model.

- The hydrogen diffusion model includes a species transport process while the energy balance model includes a combustion process. The user can only select one of the two aforementioned processes to be simulated at once. The combustion process cannot be enabled while simulating the diffusion of hydrogen as Fluent assumes a

[3] `https://www.afs.enea.it/project/neptunius/docs/fluent` [Retrieved 07.02.2021]

hydrogen-air mixture ignites spontaneously. Similarly, the energy balance model cannot include the species transport process as a hydrogen-air mixture does not ignite in that instance.

- The CAD model is simplified to reduce the computational cost of the simulation and to not exceed the maximum allowed cell count. A large part of the test set-up is not included in the model.

- The simulation will solve for a steady-state solution to minimise the computational cost. A transient solution may provide additional information but is presumed not to be cost beneficial. Fluent does employ a pseudo transient time step and therefore the simulation can be paused at a few iterations to capture transient tendencies.

Appendix B: ANSYS Mathematical Model Hydrogen Diffusion

ANSYS Fluent does not require an input of mathematical equations, one can simply select a model and subsequently the solver computes the equations. The underlying mathematical model is presented in this chapter to provide the reader with a deeper understanding of the hydrogen diffusion model. The species transport model computes Fick's law of diffusion by default.

B.1 Fick's law

Fick's law defines mass diffusion coefficients to compute the diffusion flux of a species. Laminar and turbulent flows entail different coefficients. The following model is implemented by ANSYS Fluent[1]. Not that Merk (1958); Sutton and Gnoffo (1998) propose the model Fluent utilises. The mass diffusion coefficients for a laminar flow may be computed through Equation B.1,

$$J_i = -\rho D_{i,m} \nabla Y_i - D_{T,i} \frac{\nabla T}{T}, \tag{B.1}$$

with $D_{i,\,m}$ the mass diffusion coefficient for species i, Y_i the mass fraction and $D_{T,\,i}$ Soret's thermal diffusion coefficient. Equation B.1 is only valid when $Y_i \ll 1$, excluding the carrier gas. The user must specify $D_{i,\,m}$ within ANSYS Fluent separately if Y_i is relatively large. The mass fraction of hydrogen within the test cell is low and therefore Equation B.1 can be included.

Equation B.1 is replaced by Equation B.2 when the flow is turbulent instead of laminar,

$$J_i = -\left(\rho D_{i,m} + \frac{\mu_t}{\mathrm{Sc}_t}\right) \nabla Y_i - D_{T,i} \frac{\nabla T}{T}, \tag{B.2}$$

with Sc_t the effective turbulent Schmidt number and μ_t the eddy viscosity. The Schmidt number can be determined through Equation B.3,

[1] `https://www.afs.enea.it/project/neptunius` [Retrieved 10.01.2021]

$$\mathrm{Sc}_t = \frac{\mu_t}{\rho D_t}, \tag{B.3}$$

with D_t the effective mass diffusion coefficient for turbulent flows. The mass diffusion coefficients can be altered but are by default defined by an empirical model included in ANSYS Fluent.

B.2 Maxwell-Stefan approach

ANSYS Fluent has the ability to model full multicomponent diffusion as well. The Maxwell-Stefan equations should be used when the mixture is non-dilute, hence when $\mathrm{Y}_i \ll 1$ is not valid anymore. The mass fraction (Y_i) of hydrogen may become significant in the test cell container for larger leakages. Therefore it might be interesting to compare the results of the Maxwell-Stefan equations to Fick's law, which is a generalised definition. The Maxwell-Stefan equations can be used to obtain the diffusive mass flux in multicomponent systems. The model is more comprehensive than Fick's law, Fick's law can be derived from Maxwell's theory. Fluent prefers Fick's law since the Maxwell-Stefan equation require the computation of a N^2 co-factor determinants of size (N - 1) X (N - 1) and one determinant of size N X N, with N the number of chemical species (Sutton and Gnoffo, 1998). It implies Fick's law has a lower computational cost than the Maxwell-Stefan equations.

The Maxwell-Stefan equation is as follows (Merk, 1958),

$$\sum_{\substack{j=1\\ j\neq i}}^{N} \frac{X_i X_j}{\mathcal{D}_{ij}} \left(\vec{V}_j - \vec{V}_i\right) = \vec{d}_i - \frac{\nabla T}{T} \sum_{\substack{j=1\\ j\neq i}}^{N} \frac{X_i X_j}{\mathcal{D}_{ij}} \left(\frac{D_{T,j}}{\rho_j} - \frac{D_{T,i}}{\rho_i}\right), \tag{B.4}$$

with X the mole fraction, $\vec{V}$ the diffusion velocity vector, $\vec{d_{\mathrm{i}}}$ a diffusion vector for mechanical effects, $\mathcal{D}_{ij}$ the binary mass diffusion coefficient and D_T the thermal diffusion coefficient. For an ideal gas the Maxwell diffusion coefficients equal the binary diffusion coefficients. When it is assumed the external force on each species is the same and the pressure diffusion is neglected, then

$$\vec{d_i} = \nabla X_i.$$

In addition, since the diffusive mass flux vector equals

$$\vec{J_i} = \rho_i \vec{V_i}$$

Equation B.4 can be simplified to,

$$\sum_{\substack{j=1\\ j\neq i}}^{N} \frac{X_i X_j}{\mathcal{D}_{ij}} \left(\frac{\vec{J_j}}{\rho_j} - \frac{\vec{J_i}}{\rho_i}\right) = \nabla X_i - \frac{\nabla T}{T} \sum_{\substack{j=1\\ j\neq i}}^{N} \frac{X_i X_j}{\mathcal{D}_{ij}} \left(\frac{D_{T,j}}{\rho_j} - \frac{D_{T,i}}{\rho_i}\right). \tag{B.5}$$

The diffusive mass flux vector $\vec{J}$ may then be obtained from Equation B.6,

$$\vec{J_i} = -\sum_{j=1}^{N-1} \rho D_{ij} \nabla Y_j - D_{T,i} \frac{\nabla T}{T}. \tag{B.6}$$

The other terms can then be defined as follows,

$$D_{ij} = [D] = [A]^{-1}[B] \tag{B.7}$$

$$A_{ii} = -\left(\frac{X_i}{\mathcal{D}_{iN}} \frac{M_w}{M_{w,N}} + \sum_{\substack{j=1 \\ j \neq i}}^{N} \frac{X_j}{\mathcal{D}_{ij}} \frac{M_w}{M_{w,i}} \right) \tag{B.8}$$

$$A_{ij} = X_i \left(\frac{1}{\mathcal{D}_{ij}} \frac{M_w}{M_{w,j}} - \frac{1}{\mathcal{D}_{iN}} \frac{M_w}{M_{w,N}} \right) \tag{B.9}$$

$$B_{ii} = -\left(X_i \frac{M_w}{M_{w,N}} + (1 - X_i) \frac{M_w}{M_{w,i}} \right) \tag{B.10}$$

$$B_{ij} = X_i \left(\frac{M_w}{M_{w,j}} - \frac{M_w}{M_{w,N}} \right) \tag{B.11}$$

Where A,B and D are (N - 1) X (N - 1) matrices with D the generalised Fick's law diffusion coefficient D_{ij}.

B.3 Mass diffusion coefficients

The mass diffusion coefficients require inputs for both models. The mass diffusion coefficient $D_{i,m}$ for Fick's law is a constant value for each species. Either the default input value is maintained or the input value is adjusted. The diffusion coefficient is maintained at the default value for all the simulations performed in this report if Fick's law is applied.

The binary mass diffusion coefficients are determined through a kinetic theory model included in ANSYS with the Maxwell-Stefan approach. The kinetic theory model utilises the following approach, the Lennard-Jones parameters (σ_i and $(\epsilon/k_B)_i$) must be defined for each species (Sutton and Gnoffo, 1998). σ_i is the characteristic length and $(\epsilon/k_B)_i$ is an energy parameter with k_B the Boltzmann constant. The solver in Fluent applies the Chapman-Enskog formula to compute the diffusion coefficients,

$$\mathcal{D}_{ij} = 0.00188 \frac{\left[T^3 \left(\frac{1}{M_{w,i}} + \frac{1}{M_{w,j}} \right) \right]^{1/2}}{p_{\text{abs}} \sigma_{ij}^2 \Omega_D}, \tag{B.12}$$

where p_{abs} is the absolute pressure, M_w the molecular weight and Ω_D the diffusion collision integral, which is a measure of the interaction between molecules in the system. Ω_D is a function of T_D^* and equals,

$$T_D^* = \frac{T}{(\epsilon/k_B)_{ij}} \tag{B.13}$$

,
where $(\epsilon/k_B)_{ij}$ is the geometric average of the mixture,

$$(\epsilon/k_B)_{ij} = \sqrt{(\epsilon/k_B)_i (\epsilon/k_B)_j}. \tag{B.14}$$

σ_{ij} is the arithmetic average of the individual σ for a binary mixture,

$$\sigma_{ij} = \frac{1}{2}(\sigma_i + \sigma_j). \tag{B.15}$$

Note that with Fickian diffusion the turbulent flows are computed with Equation B.2 and laminar flows with Equation B.1.

B.4 Thermal diffusion

Thermal diffusion is included in the model as some components in the container attain high temperatures, especially near the internal combustion engine. ANSYS Fluent includes a built-in model to determine the thermal diffusion through an empirical model. The empirical model is deduced from Kuo. (1986),

$$D_{T,i} = -2.59 \times 10^{-7} T^{0.659} \left[\frac{M_{w,i}^{0.511} X_i}{\sum_{i=1}^{N} M_{w,i}^{0.511} X_i} - Y_i \right] \cdot \left[\frac{\sum_{i=1}^{N} M_{u,i}^{0.511} X_i}{\sum_{i=1}^{N} M_{w,i}^{0.489} X_i} \right]. \tag{B.16}$$

The diffusion coefficient above is a form of Soret's diffusion coefficient due to which heavy molecules diffuse less rapidly than light molecules towards heated surfaces.

Appendix C: Velocity Profiles Mesh Refinement

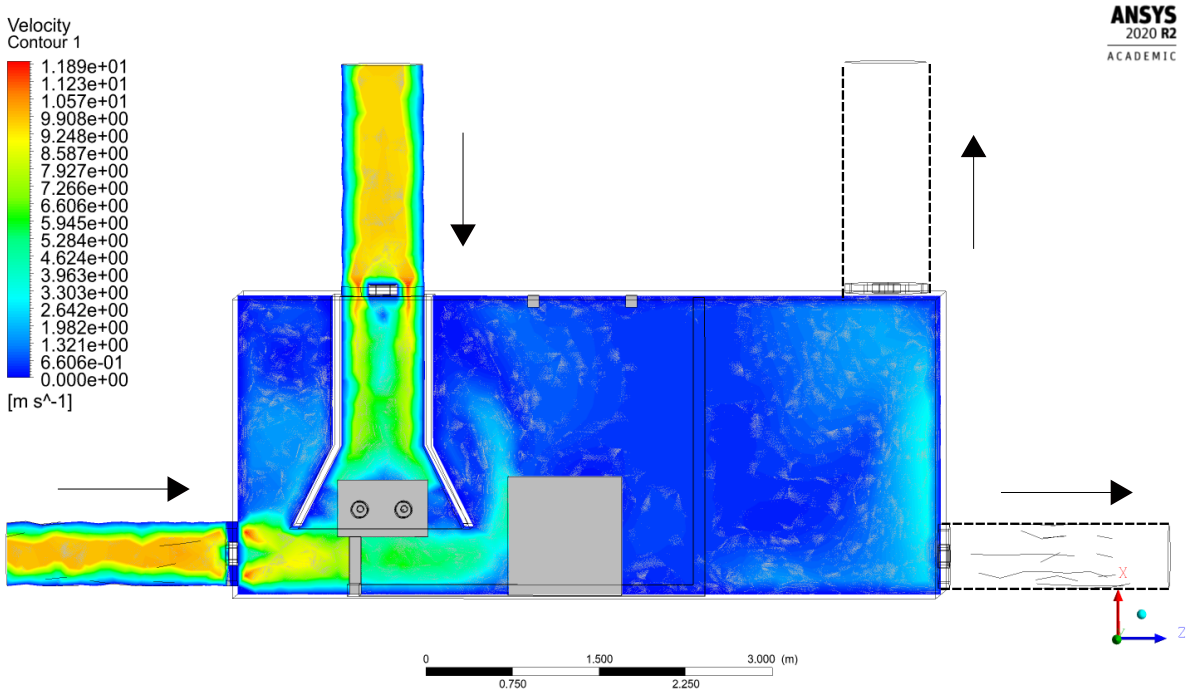

Figure C.1: Velocity profile of a mesh with ≈ 116,000 cells.

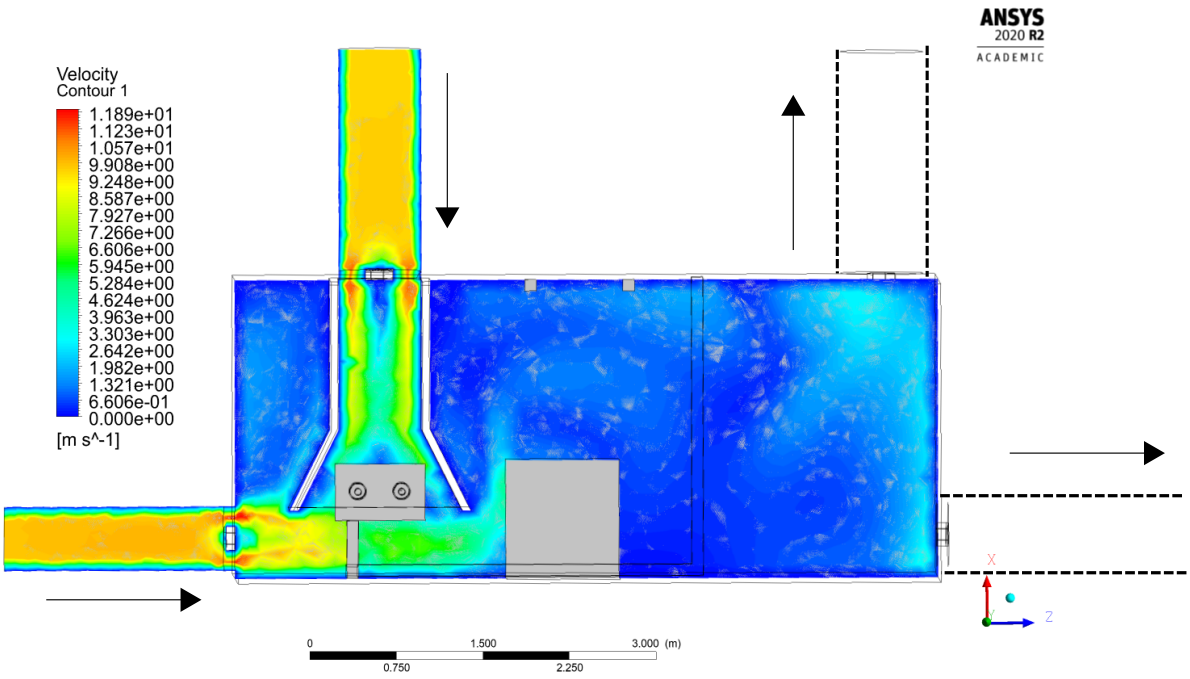

Figure C.2: Velocity profile of a mesh with ≈ 177,000 cells.

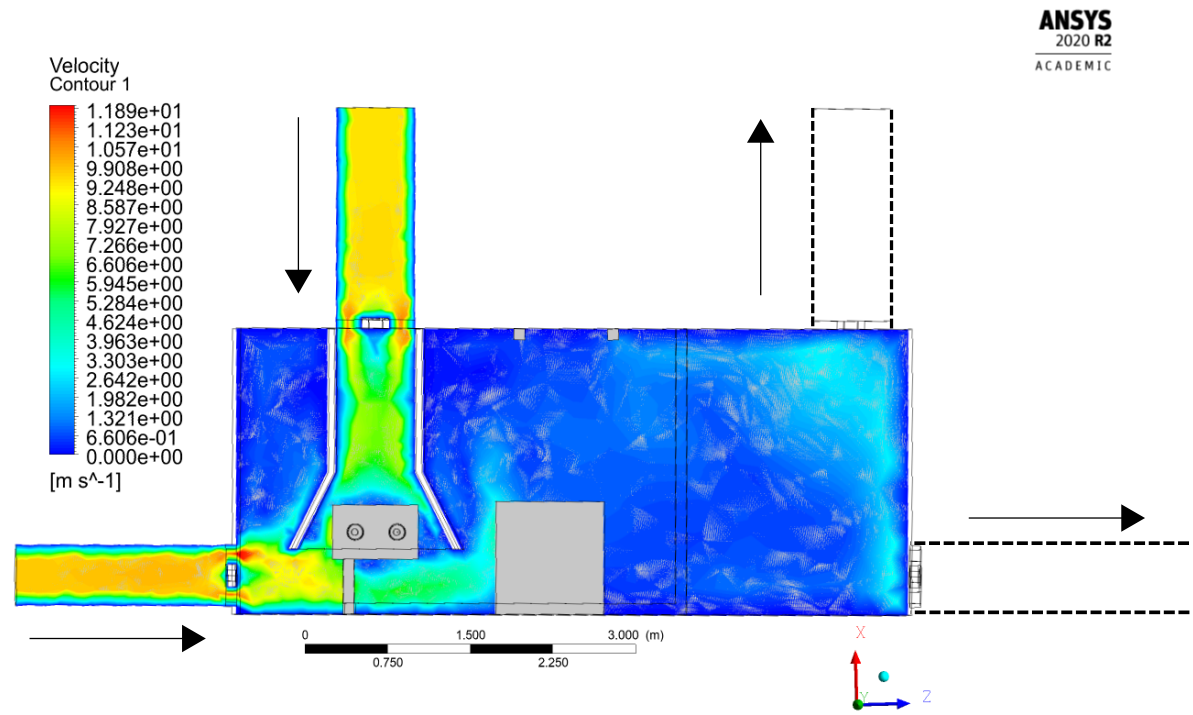

Figure C.3: Velocity profile of a mesh with ≈ 260,000 cells.

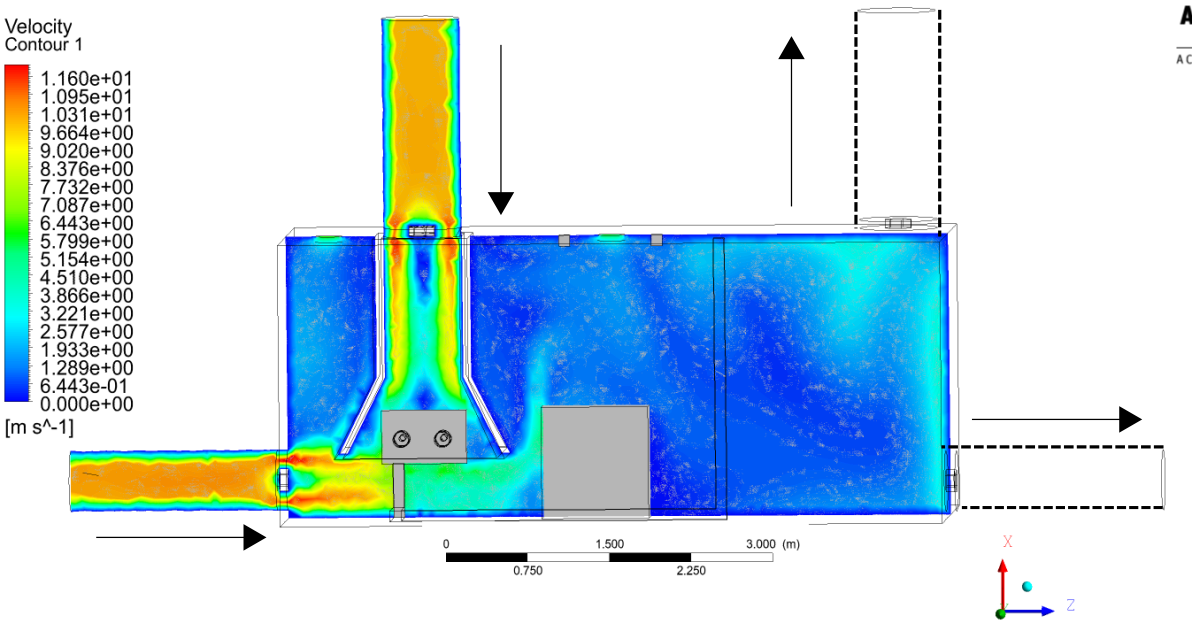

Figure C.4: Velocity profile of a mesh with ≈ 330,000 cells.

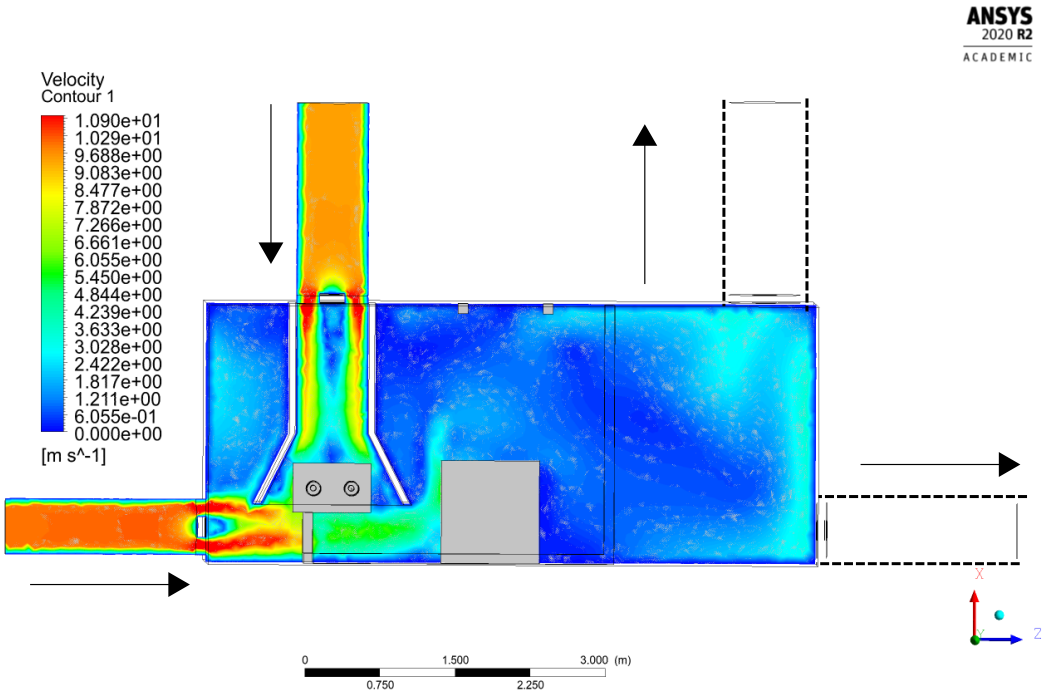

Figure C.5: Velocity profile of a mesh with ≈ 360,000 cells.

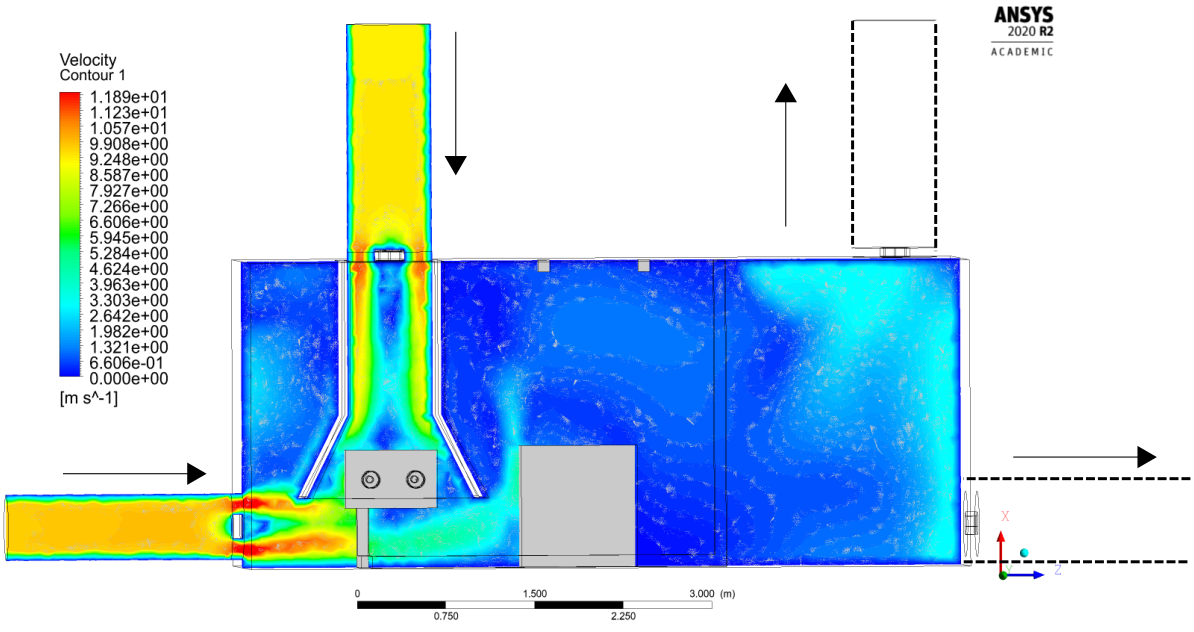

Figure C.6: Velocity profile of a mesh with ≈ 477,000 cells.